Ice Surface Temperature from Metop Infrared Atmospheric Sounding Interferometer

V 1.0

Validation Report

Response to EUMETSAT ITT No. 15/137

Authors:

Gorm Dybkjær, Jacob L. Høyer, Jörg Steinwagner,

Kristine Skovgaard Madsen and Rasmus Tonboe

Danish Meteorological Institute

June 2017

Abstract

Validation of Arctic and Antarctic Ice Surface Temperatures (IST) from Metop Infrared Atmospheric Sounding Interferometer (IASI). IASI IST is calculated using a Piece-Wise Linear Regression Cube algorithm ($PWLR^3$) that combines measurements from all IASI individual fields of view (IFOV) to perform retrievals in each IASI IFOV individually. This results in an IST product with a spatial resolution of approximately 12 km and with multiple daily data coverage in Polar Regions. Unlike existing IST products, e.g. OSISAF and NASA Thermal Infrared (TIR) clear-sky IST products, the IASI IST is an All-Sky surface temperature product. The IASI IST algorithm works on TIR data only, if a cloud test is passed, else a multi sensor passive microwave algorithm is enabled. IASI IST is validated for Arctic and Southern Ocean sea ice and Greenland and Antarctic land ice. The validation is stratified with respect to in situ instrument type, temperature, quality measures and other collocated information. For Arctic sea ice, the performance of the non-filtered IASI IST minus buoy air temperatures, is STD = 7.5 K and bias = 0.4 K and STD = 4.7 K and a bias of 1.1 K, for the best 10% data, based on filters using the IASI IST quality indicator. The error of the remaining data after filtering is approximately 1 K higher than existing TIR clear-sky algorithms, but with a smaller bias. The performance of non-filtered IASI IST temperatures for Greenland ice sheet surface temperatures is STD = 5.3 K and Bias = -0.8 K and STD = 3.8 K and Bias = 1.3 K, for the best 10% data. Better performance is found for the Antarctic Ice sheet.

Table of Content

Abstract **2**

Table of Content **3**

Abbreviation and Acronyms **5**

1 Introduction **6**

1.1 Background 6

1.2 Compliancy to commissioned work 7

1.3 Report structure 8

1.4 Reference Documents 8

2 Methodology **10**

2.1 IST satellite inter-comparison 10

2.2 Validation strategy 11

3 Data, In Situ **12**

4 Data, RS and NWP **15**

4.1 Metop-IASI IST 15

4.2 Metop-AVHRR IST 16

4.3 MODIS IST 16

4.4 Ice Concentration 16

4.5 NWP 17

5 Match-Up DB **18**

5.1 Match-up criteria's 18

5.2 The MUDB files 18

5.3 MUDB access 18

6 Theoretical considerations of uncertainties **20**

6.1 Vertical sampling of microwaves in snow and ice 20

6.2 The uncertainty budget for infrared radiometer data 21

7 Results **22**

7.1 Validation – Land IST 22

7.1.1 Special considerations for land IST 23

7.1.2 General validation statistics for Land Ice 23

7.1.3 Stratified temperature validation statistics 24

7.1.4 IASI cloud indicator vs PROMICE cloud calculation 36

7.1.5 Sampling effects 38
7.2 Validation – Sea IST 38
7.2.1 Special considerations for sea IST 39
7.2.2 General statistics for Sea Ice validation 39
7.2.3 Distribution of temperature differences 40
7.2.4 Relation to other matchup parameters 44
7.3 Satellite IST inter-comparison 47
7.3.1 Level 3 data 47
7.3.2 Satellite IST inter-comparison 47
7.3.3 Inter-comparison with ERA-Interim 53

8 Discussion 55

9 Recommendations 60

References 62

Appendix A: In situ data format 64

Appendix B: Match-Up data description 67

Appendix C: In situ data inventory 70

Appendix D: Land Ice supplementary figures 72

Appendix E: Sea Ice supplementary figures 121

E.2 Supporting figures for section 7.2.4 130

Appendix F: Satellite inter-comparison, including ERA-Interim 136

Appendix G: Look-Up table for General and filtered IASI IST performance 141

Abbreviation and Acronyms

AMRC	-	The Antarctic Meteorological Research Center
AMSU	-	Advanced Microwave Sounding Unit
AWS	-	Automatic Weather Station
AVHRR	-	Advanced Very High Resolution Radiometer
CDR	-	Climate Data Record
ECMWF	-	The European Centre for Medium-Range Weather Forecasts
GSFC	-	Goddard Space Flight Centre
IASI	-	Infrared Atmospheric Sounding Interferometer
IST	-	Ice Surface Temperature
KO	-	Kick-Off
LST	-	Land Surface Temperature
Metop	-	Meteorological Operational (EUMETSAT)
MHS	-	Microwave Humidity Sounder
MUDB	-	Match-Up Data Base
NASA	-	National Aeronautics and Space Administration (USA)
NH	-	Northern Hemisphere
NWP	-	Numerical Weather Prediction
PM	-	Progress Meeting
PMW	-	Passive Microwave
RS	-	Remote Sensing
TIR	-	Thermal Infra-Red
OSI SAF	-	Ocean and Sea Ice, Satellite Application Facility
SH	-	Southern Hemisphere
SST	-	Sea Surface Temperature
SoW	-	Statement of Work

1 Introduction

The objective for this report is to validate the land and sea Ice Surface Temperature (IST) product from the Infrared Atmospheric Sounding Interferometer (IASI) instrument on-board Metop satellites. The geographical focus of the study is the Arctic, but ice surfaces in the southern hemisphere are also addressed, but to a lesser extent.

The study is made up by three main parts:

1) Compilation of an in situ surface temperature datasets, relevant for the validation of IASI IST.
2) Collocation of IASI and in situ surface and air temperatures and auxiliary data with respect to space and time, in a Match-Up Data Base (MUDB).
3) Validation of IASI IST for Arctic and Southern Ocean sea ice and Greenland and Antarctic land ice.

The outcome of the study contribute to understanding the characteristics, strengths and weakness of the current IASI ice surface temperature product derived over sea and land ice-surfaces. A full scale validation of the IASI level-2 IST product is conducted; where also uncertainty issues of the validation process are addressed. The IASI IST will be inter-compared with other satellite IST products and surface and air temperature data from the operational and a re-analysis atmospheric model from ECMWF.

1.1 Background

Large scale monitoring of surface temperatures from satellites is important for two main reasons: 1) As stand-alone monitoring of current and climatological state of the earth surface, and 2) as input to physically based climate and short and medium range prediction models for the atmosphere, ocean and ice. Applications of remotely sensed sea and land surface temperatures are commonly acknowledged to improve the initial state of numerical models, but ice surface temperatures is a relatively novel satellite product and only few and non-operational attempts have been carried out in order to assimilate satellite IST into model systems (Rasmussen and Høyer, 2017; Kauker et al., 2015).

The prerequisite for using satellite based IST and other observations in model assimilation schemes, is knowledge of the observation uncertainty. Now, there are several issues that complicate the determination of satellite IST uncertainties. First of all, in situ observations are sparse in the Polar Regions because of pour accessibility and harsh conditions for sensitive instruments. Secondly, common in situ temperature observations in Polar Regions lack traceability for mainly two reasons. 1) A sensors vertical position relative to snow/ice/air surfaces is typically not constant during the instrument deployment period, due to snow precipitation and snow drift, and 2) sea ice deployed instruments are most often lost due to ice melt or ice deformation, thus making post calibration impossible.

To perform a thorough evaluation of the IASI IST product, the largest possible in situ data volume from several in situ platforms has been compiled and matched up with IASI IST data. Based on the match-up data set it has been possible to establish the IASI IST performance in various ice surface regimes, under various atmospheric and seasonal conditions.

The performance of the IASI IST compared to other satellite IST products is particular interesting because known satellite based IST monitoring systems are dependent on clear sky conditions, whereas the IASI IST product is an all sky algorithm.

1.2 Compliancy to commissioned work

The commissioned deliverables from the ITT are outlined in table 1.1, including the section and appendix in which the work is fulfilled.

Table 1.1 *Compliancy table, relating requirements from the ITT [RD-6] to this report.*

Deliverable	Response
Compile final report	This report
Compilation of in situ surface and air temperature data in NetCDF format for the area and time of interest	Chapter 3, Appendix A
Compilation of accompanying (NWP-temperature fields, IC, other IST data set in level-2 and 3) for data inter-comparison and stratification of validation results	Chapter 4
An inventory list describing the in situ data.	App. C
Quality control on all in situ data	Chapter 3
Dedicated MUDB for IASI IST vs. air and surface temperature data from various in situ data sources	Chapter 5, Appendix B
Estimate the uncertainty related to temporal and spatial sampling effects and surface inhomogeneity.	Chapter 6
Compile validation results for Land Ice using feasible and relevant filters	Section 7.1 Appendix D
Compile validation results for Sea Ice using feasible and relevant filters	Section 7.2 Appendix E

Minor deviations from proposed work have occurred. These are:

- The operational ECMWF IFS model replaces the proposed ERA-Interim in the level 2 MUDB, due to an assumed bias in surface and air temperature fields in the Arctic (see section 4.5).
- Temporal Match-Up constraint is 50 minutes, not 120 minutes, as discussed at PM1. This change has been made to reduce processing time on Match-Up production, by only allowing1 orbit per in situ measurement. This was necessary because changes to the MUDB required more re-runs of the entire MUDB.

At Kick-Off and Progress Meetings other „nice-to-have“-elements were discussed, if time allowed. These elements are not required in the Statement of Work [RD-6]:

- To establish an IASI footprint simulator to inter-compare IASI IST with AVHRR IST within identical fields of view. This has not been carried out.
- Add histograms of errors in validation plan. Done.
- Add temperature stratification in validation plan. Done.
- Add altitude stratification in validation plan. Partly done.
- It was not possible to acquire additional Antarctic in situ data from Australian Antarctic Service in time, as discussed at PM1.
- NWP wind history has been added to the MUDB.
- ‘OmC’ cloud information variable has been added to MUDB.

1.3 Report structure

This report is divided into eight chapters describing all from data collection to final discussions. Chapter 2 describes the overall methodology from collection of input data, match-up procedure to validation strategy. Description of the collected in situ data is given in chapter 3, and all other input data are described in chapter 4. The data match-up procedure is described in chapter 5; while all components of the MUDB is listed in appendix B. Chapter 6 treats some general uncertainty aspects of satellite IST measurements. Results from the full data set performance and stratified results are presented in Chapter 7. A discussion of the results is found in the last chapter.

1.4 Reference Documents

Table 1.2 *Internal EUMETSAT documents that have been used.*

No.	Document Title	Reference
RD-1	Validation Report for the OSI SAF High Latitude L2 Sea and Sea Ice Surface Temperature	SAF/OSI/CDOP2/DMI/SCI/RP/247
RD-2	Algorithm theoretical basis document for the OSI SAF Sea and Sea Ice Surface Temperature L2 pro-cessing chain	SAF/OSI/CDOP2/DMI/SCI/MA/223
RD-3	The Piece-wise linear regression	Hultberg and August, ITSC

		EUM/RSP/TEN/13/723383
RD-4	IASI Level-2: Product guide	EUM/OPS-EPS/MAN/04/0033
RD-5	IASI Level 2: Product Generation Specification	EPS.SYS.SPE.990013, v8C
RD-6	SOW Statement of Work. Ice Surface Temperature from Metop Infrared Atmospheric Sounding Interferometer	EUM/RSP/SOW/15/822812
RD-7	Algorithm Theoretical Basis Document for the OSI SAF Global Reprocessed Sea Ice Concentration Product	SAF/OSI/CDOP2/MET-Norway/SCI/MA/209

2 Methodology

To validate the level 2 IASI IST product, a combination of in-situ measurements, satellite and model data is used. The validation means is a Match-Up Data Base (MUDB) in which the IASI IST data are collocated with reference temperature data from in situ platforms and relevant auxiliary information from other Metop level 2 products; such as atmospheric water content and quality indicators. Also satellite ice concentration data are collocated with IASI IST data, as well as temperature and wind data from ECMWF operational NWP model (see description of MUDB in appendix B). The NWP data are included in the level 2 MUDB for inter-comparison purposes and other Metop level 2 products and sea ice concentration data are included for data filtering and stratification purposes. Now, the in situ measurements are considered the „truth", and the satellite products are compared to this using Standard Deviation (STD) and Bias. Qualitative considerations of uncertainties are made in chapter 6.

The performance of the IASI IST algorithm is stratified into homogenous states of the surface and atmosphere, by using the auxiliary data provided in the MUDB. This stratification is used to identify weaknesses and strengths of the IASI IST algorithm and subsequently to advise means to optimize product quality. This is seen in light of a trade-off between the best quality matchups and data volume is described.

This study is dependent on the quality of the applied in situ temperature observations. A description of the applied in situ data is given in chapter 3 and an estimate of their accuracy, by expert judgement, is available in Appendix C, along with other Meta information.

2.1 IST satellite inter-comparison

The IASI level 2 MUDB does not contain collocation with other satellite IST data. To inter-compare IASI IST with other satellite IST products and model data, a dedicated level 3 MUDB is generated. The spatial resolution of the level 3 grid is 0.05 degree. The temperature fields are obtained by aggregating the individual level 2 satellite IST data within 36 hours from the analysis time. The level 3 satellite data are subsequently grouped into larger areas for the actual inter-comparison with IASI IST. This is described in section 7.3.

Three other satellite IST products were selected for satellite IST inter-comparison, namely the OSI-205 product from EUMETSAT's OSI SAF and MODIS Terra and Aqua IST products (see chapter 4).

2.2 Validation strategy

A validation strategy was developed in the initial part of the project to be able to assess the performance of the IASI IST observations for the different regions and with the available satellite, in situ data and auxiliary data sets. The validation will include the following points:

- Satellite observations will be Matched-Up with in situ observations available in the DMI in situ database.
- Using the matchup database, comparisons between satellite surface temperatures will be carried out against in situ and NWP.
- Satellite time series will be compared at selected locations.
- Separate validation statistics for Skin Sea ice surface temperatures and Land ice surface temperatures and separately for each hemisphere.

The matchup database will be used to assess the IASI observations dependency to:

- Surface temperature
- Observation type
- Seasons
- Ice concentration
- Temporal homogeneity
- Spatial homogeneity
- Hemisphere and type of ice (land or sea)

To assess the actual performance of the IASI observations, all the contributing factors will have to be considered when interpreting on e.g. the satellite versus in situ differences. Including results from several other projects such as ESA FRM4STS, the uncertainty budget, including estimates of temporal and spatial sampling effects and in situ and satellite uncertainties are discussed.

The validation metrics that will be used to assess the differences are standard validation analysis numbers, such as:

- Standard deviation of differences
- Mean difference (Bias)
- Correlation between the two data sets
- Root mean square of differences
- Relation of the above measures with other data sets, e.g. ice concentration and quality indicators.

Following this strategy and deriving the metrics stated above should ensure a fair and objective validation of the IASI instrument and data product for all the four regions considered in this proposal.

3 Data, In Situ

In total, 136 stations, buoys and flights from 8 different in situ temperature sources over both northern and southern hemisphere land ice and sea ice have been collected, visually quality controlled and used for this study. This has resulted in a total of 373611 matchups relevant for validation and inter-comparison of level 2 IST from IASI (Table 3.1, Figure 3.1). Over land ice, the matchups include the approximately 16 closest satellite measuring points to each station for each satellite pass, to allow assessment of the spatial sampling error. For sea ice, in situ sources have been grouped in buoys measuring air temperature, buoys measuring surface temperature and flights measuring surface temperature, and only the closest satellite measuring point to each in-situ observation has been used. For the northern hemisphere, 7 buoys measured both air and surface temperature. For the southern hemisphere, no buoys available to this study measured surface temperatures, and the only surface temperature measurements available were made from airplane by the IceBridge program. The number of IceBridge matchups is limited, as we require the satellite and airplane paths to cross within one hour. For the northern hemisphere, the geographical distribution and data amount is considered to be acceptable for validation, except for a lack of sea ice observations from the eastern part of the Arctic Ocean. This could be mitigated by an extended study period, but this is out of reach in this project. For the southern hemisphere, data have been included as available, with limited data coverage in space and time.

The Arctic buoy data named ECMWF are in situ ice buoy data, retrieved from the MARS data archive at ECMWF. Land temperature data named WMO are temperature data from land-based Automatic Weather Stations, retrieved from the DMI GTS archive. All data are converted to a common netCDF format, as described in Appendix A, and provided as FTP pull by DMI (see section 5.3).

***Table 3.1** In situ data used in matchups, 2012. For this study, no sea ice surface temperature buoy data have been available from the southern hemisphere.*

		Number of stations/buoys/flights	Total number of matchups	Sources
Northern hemisphere	Land ice stations	10	334732	PROMICE, ARM, WMO
	Flights with surface temperatures over land ice	4	158	IceBridge
	Sea ice buoys with air and surface temperature	7	1254	
	Sea ice buoys with only air temperature	69	25014	ECMWF, IABP, NACOOS
	Sea ice buoys with only surface temperature	18	10998	
	Flights with surface temperature over sea ice	4	16	IceBridge
Southern hemisphere	Land ice stations	3	10140	AMRC, WMO
	Flights with surface tem-	12	694	IceBridge

	peratures over land ice			
	Flights with surface temperature over sea ice	10	39	IceBridge
Total		136	373611	

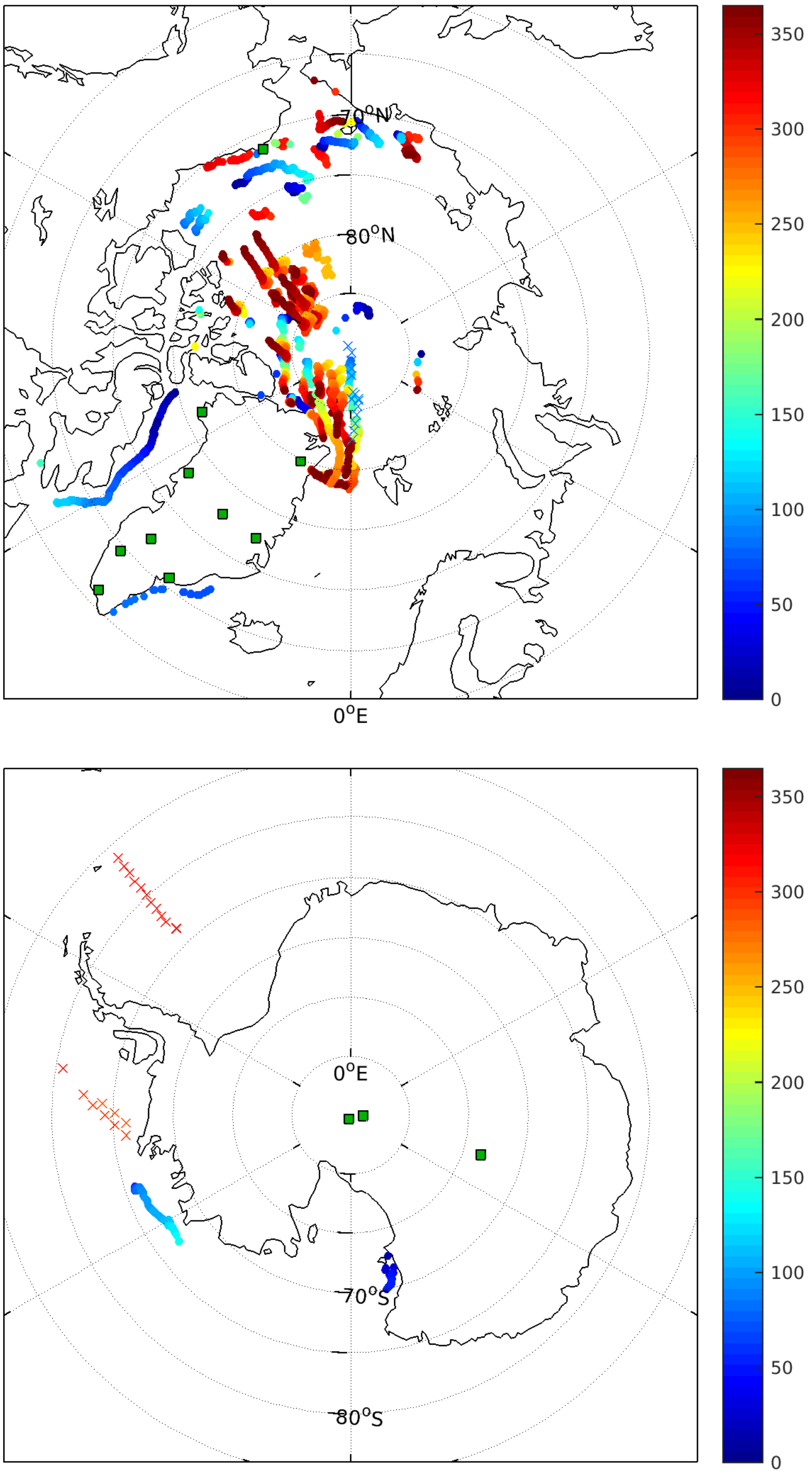

Figure 3.1 *Spatial distribution of matchup locations for land ice stations (green squares), sea ice observations from buoys (circles) and IceBridge flights (crosses), colour indicates day of year. Top: Northern hemisphere, bottom: Southern hemisphere.*

An overview of location, temporal sampling, continuation, air temperature sensor height, uncertainty of air temperature, surface temperature type, distribution statement and sea ice data filtering is provided in Appendix C. The temporal sampling in most cases resolves the diurnal cycle, and is thus assessed as adequate. The quality of air temperature observations has been assessed based on information available from the data providers, and based comparison with satellite data and other in situ data. For land stations, it is 0.5-1 K, and for sea ice buoys 1-3 K. The quality of surface temperatures is more varying, with the best quality available from in situ radiometer measurements and from the PROMICE radiation calculations for freezing conditions. SST/IST sensors and thermistors are very sensitive to snow cover, and thermistors also to direct sunlight. The quality of the flight radiometer observations has not been assessed in this study, but is expected to be 1-2 K.

4 Data, RS and NWP

One year of IASI IST data have been prepared for the match-up procedures. Beside the IASI IST data, several other data sets are compiled and included in either the level 2 or level 3 match-up procedures.

All included data sets are described here and table 4.1 gives an overview of the applied data sets.

Table 4.1 *Basic configurations of the three satellite products, the NWP data and the sea ice concentration data.*

Product	Product level	Spatial resolution Original/ level 3,4 grid	Level 2 File granule	Data Provider
Metop-A IASI +other level 2 prod.	2+3	~12 Km / 0.05 degree	3 min	EUMETSAT
Metop-A AVHRR IST, OSI 205	3	~1 km / 0.05 degree	3 min	EUMETSAT OSI-SAF/DMI
MODIS IST	3	~1 km / 0.05 degree	5 min	NASA-GSFC
ECMWF opr.	4	- / 0.5 degree	-	ECMWF
ERA-Interim, CDR	4	- / 0.5 degree	-	ECMWF
Ice Conc.	4	- / 25 km	-	OSI SAF

4.1 Metop-IASI IST

The IASI surface temperature algorithm is an all-sky retrieval algorithm. The algorithm is the Piece-Wise Linear Regression Cube algorithm (PWLR[3]) that combines the measurements from IASI Individual Fields Of View (IFOV) and collocated AMSU and MHS radiances to perform retrievals in each IASI IFOV individually. Only when a 3-step clear-sky procedure unanimous declares cloud free conditions, the IASI IST algorithm is based on Thermal Intra Red (TIR) data only, else Passive Microwave (PMW) data are included in the algorithm [RD-3][RD-5]. The surface temperature algorithm is trained using NWP data from the operational model at ECMWF (see section 4.5).

The IASI IFOV resolution is approximately 12 km, but the associated AMSU and MHS data are of coarser resolution, thus making the effective IST resolution larger than 12 km [RD 5].

The Metop IASI IST and associated data are provided by EUMETSAT for the purpose of this study. Data from 2012 and 2014 were provided, but only 2012 data are used in this validation report, and only Metop-A IASI data and water vapour data from the Metop MHS instrument. IASI IST and auxiliary data were delivered in HDF5 data formats.

Following IASI level 2 variables and auxiliary Metop information are provided and applied to the MUDB:

- Geolocation
- Satellite, Sun and view geometry
- Surface temperature (K)
- Quality indicator for surface temperature
- Water-vapour total column (mm)
- Quality indicator for water-vapour
- Predicted OBS-CALC assuming clear-sky in selected window channels; relates to cloud signal
- Average surface elevation within the field of view.

4.2 Metop-AVHRR IST

A level 3 inter-comparison between IASI and Metop AVHRR SST/IST is presented in section 7.3. In contrast to the Metop IASI IST, the AVHRR algorithm is a clear-sky algorithm, working entirely on TIR data, in a split window algorithm. The algorithm works within three temperature domains, cold, medium and warm, as suggested by Key et al. (Key et al., 1997). Calculations of algorithm coefficients is estimated from relations between modelled surface temperatures with modelled top-of-atmosphere brightness temperatures, determined from a radiative transfer model. The Metop AVHRR IST product was a preoperational version of the OSI-205 product that is documented and validated in the OSI SAF project (Dybkjær et. al., 2012, [RD-1]).

Only cloud free and ice contaminated data with and view angles less than 45 degrees and common data sanity checks are used. These data corresponds to quality levels „good“ and „best“ [RD-1]. The daily level 3 aggregation is described in section 7.3.

4.3 MODIS IST

From commitments in other projects, such as the ESA Globtemperature project, DMI has gained access to two MODIS products; MYD29 (Aqua) and MOD29 (Terra), respectively (Hall et al., 2004). The products are version 6 IST only (Hall, D. K. and G. A. Riggs. 2015, Riggs et al., 2006), prepared by the ESA Globtemperature project (Darren Ghent, pers. comm.). These satellite observations are originally level 2 TIR IST estimates. The algorithm uses a split-window technique and implemented as a simple regression Model [Hall et al., 2004] and retrievals are limited to clear-sky conditions. The daily level 3 aggregation is described in section 7.3.

4.4 Ice Concentration

Ice concentration (IC) data has been collocated with the IASI surface temperatures and added to the MUDB files for data stratification purposes. The IC data is the reprocessed OSISAF data set, OSI-409. The algorithm is a hybrid; a linear combination of two algorithms, the Bristol algorithm and the Bootstrap frequency mode algorithm [RD-7]. The IC data set is a daily level 4 product gridded to an equal area 12.5 km grid.

4.5 NWP

The operational deterministic NWP model from ECWMF (OPR) is added to the level 2 IASI MUDB files. According to Dee et al. (2011) AMSU data are being assimilated into the OPR model. Hence, NWP data sets are correlated to MW radiances that are input to the IASI IST algorithm.

In the proposal, ERA-Interim was suggested to be included in the IASI MUDB files, but several works have documented that the ERA-Interim has a warm bias in the Arctic (Lupkes et al., 2010 and Jakobson et al., 2012). On the other hand, the OPR data included in this investigation is used as training for the IASI IST algorithm (Dee and Uppala, 2009) and it is expected highly correlated with the IASI IST data. The inclusion of OPR data is thus of special interest for the IASI IST algorithm developers, for them to trace weakness and strengths of the training procedure.

The NWP data are resampled to a 0.5 degree grid. Skin and air temperatures and 10 m wind data are collocated with the IASI IST level 2 data. The temporal resolution of the NWP data is 1 hour.

Data from the reprocessed ERA-Interim data set from ECMWF is added to the level-3 satellite inter-comparison in section 7.3.

5 Match-Up DB

The Match-Up Data Base (MUDB) compiled for this project contains collocated in situ temperature measurements from ships, planes and drifting buoys and level 2 IASI IST and associated level 2 products from other Metop sensors (See data descriptions in section 4.1 and appendix B). The MUDB files are arranged as one file per in situ platform, thus covering up to 1 year of data in each file.

The MUDB files are sub-divided into 4 major groups, each covering a major area of interest: Land Ice and Sea Ice for both Northern and Southern Hemispheres.

5.1 Match-up criteria's

Match-Up of IASI IST observations with in situ temperature measurements comply with following spatial and temporal constraints:

- Position of in situ platform must be within 50 km of centre IASI pixel.
- Recording time of in situ measurement must be within 50 minutes of IASI level 2 segments.

5.2 The MUDB files

The MUDB files are space-separated text files with 53 columns. Only MUDB files from the automatic PROMICE weather stations are associated with an extra column (col. 54), containing in situ cloud information. All columns are described in APPENDIX B.

The filename convention is:

iasi_ist_matchup_<insitu input filename>_<matchup script filename>.txt

So, ***iasi_ist_matchup_IABP_TA_2011O_v1p3_nh.txt***, contains IASI Match-Up data from IABP buoy file ***IABP_TA_2011O***, using Match-Up script ***v1p3_nh***.

5.3 MUDB access

All MUDB files, all *in situ* input data and the associated meta data record, are available on DMI's ftp site, [ftp.dmi.dk](ftp.dmi.dk), in following catalogue structure:

- iasi_ist
  - docs
  - figures
    - land
    - sea
    - level3

- insitu
    - icebridge
    - land
    - sea
- mudb (removed, property of EUMETSAT)
    - icebridge
    - land
    - sea
    - level3

6 Theoretical considerations of uncertainties

The snow surface temperature is among the most important variables in the sea ice energy balance equation and it significantly affects the atmospheric boundary layer structure, the turbulent heat exchange and the ice growth rate. In addition, advanced thermodynamic ice models treat the temperature of the snow surface and snow-ice surface as vital parameters for the development of the sea ice in the model. The temperature gradient in the snow is affecting the measurement uncertainty of the buoys used for validation. The buoys may be measured at the surface (this is what we usually expect), they may be partially buried in the snow or they may be completely buried in the snow. Different types of buoys are measuring differently. The temperature gradients in the snow on sea ice may be about 100K/m and we usually expect a warm bias during winter for those buoys which are buried in the snow.

The surface temperature measured by infrared radiometers is a representation of the physical snow surface temperature. However, because of the large temperature gradients in the winter snow-pack, the snow surface temperature may be significantly different from the snow-ice interface temperature and the microwave effective temperature. The effective temperature ($Teff$, sometimes called the skin temperature), measured by microwave radiometers is an integrated temperature for a layer with a thickness which is proportional to the penetration depth. The microwave penetration and the temperature gradients in the snow give a warm bias during winter when measuring the ice surface temperature using microwave data.

6.1 Vertical sampling of microwaves in snow and ice

The microwave's penetration into the snow and sea ice is a function of attenuation and scattering. The attenuation in the snow is a function of the imaginary part of the dielectric constant, for the snow or ice sometimes called the loss. The loss is an order of magnitude larger for liquid water than for ice. This means that melt-water in the snow or liquid brine-pockets in the saline ice effectively block further penetration. The loss of melt water and saline brine is nearly the same for frequencies higher than about 10 GHz. The scattering is a function of frequency, the scatterer size and the permittivity contrast between the scatterer and the background and the extinction is the sum of the attenuation and the scattering. The extinction in snow and ice is higher for higher frequencies primarily because of scattering. The penetration into the snow and ice is therefore deeper at 6 GHz than at 89 GHz. The effective temperature is the integrated emitting layer temperature. At 6 GHz the penetration into the saline ice, i.e. the penetration depth, is a function of the ice temperature. This means that the penetration is deeper at colder temperatures and shallower at warmer temperatures.

The snow surface temperature and the air temperatures are prognostic variables in numerical weather prediction models. However, these model variables are poorly correlated with snow - ice interface temperature or the *Teff6v* because of the penetration through the snow cover and the steep temperature gradient in the snow layer in winter.

In general there are very few impurities or salts in glacier ice and snow and therefore the penetration of microwaves in glacier ice is primarily a function of scattering in the snow and firn and it is much deeper than for sea ice.

6.2 The uncertainty budget for infrared radiometer data

The largest source of uncertainty in infrared radiometer data is undetected clouds, i.e. when you are measuring the temperature of clouds when expecting to be measuring the surface temperature. This is a systematic uncertainty which normally results in a cold bias. Other uncertainty sources include the instrument noise, geo-location uncertainty, the ice emissivity uncertainty and the IST algorithm uncertainty. In addition to these uncertainties there is normally an uncertainty related to the quality level of the data (usually there are quality levels between 0 and 5, where 5 is the best.

- The uncertainty due to undetected clouds: this uncertainty is difficult to quantify but it normally results in a negative bias because clouds are normally colder than the Earth's surface. It can be included in the uncertainty budget as a global uncertainty based on the data quality levels (0-5).
- Instrument noise and how it propagates through the algorithm and affects the temperature estimate is a random uncertainty which is unlikely to be correlated temporally, spatially or with other uncertainty sources.
- The geolocation uncertainty is a random uncertainty related to the pointing accuracy of the sensor. Over sea ice it is a function of the sensor spatial resolution, pointing accuracy, sea ice concentration and the ice surface fraction temperature itself.
- The snow emissivity uncertainty is related to the spectral emissivity variability as a function of snow grain size and density. The snow emissivity is primarily a function of viewing angle. However, the magnitude of the emissivity variability with grain size and density depends on electromagnetic wavelength i.e. the channel and the spectral response function and angle.
- The algorithm uncertainty is the uncertainty in estimating the algorithm coefficients. This can be estimated when deriving the coefficients.

7 Results

All validation of IASI IST against in situ air and surface temperature measurements and inter-comparison with other satellite IST estimates, is presented in this chapter. The chapter is divided into 3 sections addressing land and sea ice validation for level 2 data and a satellite IST inter-comparison on level 3 data. These results are given in sections 7.1, 7.2 and 7.3, respectively. A look-up table for IASI IST performances for selected quality levels is given in Appendix G; i.e. validation of all data, best 33% and best 10% data, filtered by the IASI IST quality indicator is calculated.

7.1 Validation – Land IST

This section describes the validation results for Greenland and Antarctic ice sheets, from in situ location depicted in Figure 3.1.

Nine Automatic Weather Station (AWS) sites on Greenland are included, of which eight of them belong to the PROMICE network. The 'ninth' Greenland AWS station applied here is the Summit station from the DMI-GTS network. The PROMICE stations are located on the rim of the ice cap, whereas the Summit station is located in Central Greenland, at the ice cap Summit, at approximately 3200 m altitude. All Greenland sites measure air temperature at approximately 2 m (depending on snow depth) and PROMICE stations also estimate surface temperature from the outgoing long wave surface radiation and assuming black body radiation. Measurements are reliable and continuous. In total the NH land stations provided measurements for a maximum of 334732 matchups. Due to the well distributed and reliable observation network on the Greenland ice sheet, this area receives extra attention in this report.

For validation the IASI IST performance on the Antarctic ice sheet, three Automatic Weather Stations are applied: South Pole, Vostok and the AMRC station, Nico. The data are retrieved from the DMI-GTS network and they contribute with 10140 matchups (see Table 3.1. in Section 3).

Additionally to the AWS measurements, a few airborne radiometer measurement campaigns, from both Greenland and Antarctic ice sheets from the operation Ice-Bridge campaign (IB), are included. Over Greenland ice sheet there were 158 measurements and over Antarctica ice sheet there where 694 airborne measurements.

Many illustrations related to this section are placed in Appendix D and these figures are denoted D<*number*>, where number is a consecutive number.

7.1.1 Special considerations for land IST

From each PROMICE station cloud coverage is estimated from longwave-radiation/near-surface air temperature relationships. The PROMICE cloud data are compared with quality indices from the IASI level 2 data stream and IASI cloud indicator, *OmC*. This is discussed in Section 7.1.5.

7.1.2 General validation statistics for Land Ice

The basic performance of the IASI IST algorithm is tested against *in-situ* measurements and NWP data, stratified by hemisphere and temperature type, i.e. surface or air temperature. Table 7.1.1 gives an overview of the general performance of the IASI IST and stratified validation results for selected quality levels are calculated in Appendix G.

Northern Hemisphere IASI IST has a cold bias of -0.8 K compared with in-situ surface temperature measurements and -2.5 K compared with air temperature. Standard deviation of the error (STD) is 5.3 and 5.4 K, when compared with in situ air and surface temperature, respectively. The IASI IST has a slight positive bias of 0.3 K and a STD of 6.2 K, compared with NWP skin temperatures.

The cold bias between IASI IST and air temperature observations is partly explained by a physical cold biased surface and partly by a cold bias introduced by the non-detected clouds, as mentioned in chapter 5. This assumption is supported by the much smaller bias with surface temperatures. The air and surface temperature bias is also identified when comparing IASI IST with NWP for both NH and SH areas, as shown in table 7.1.1. However, it is remarkable that the STD values are significantly lower of the SH.

I large positive bias between IASI IST and air temperature on the SH is unexpected and remains unexplained. Note that there are no weather station measurements of skin temperatures on SH.; the 694 surface temperature match-ups are data from Operation IceBridge airplane campaigns (IB). IASI IST performs poorly against IB data, including a very low correlation coefficient.

Table 7.1.1 *General statistics from comparison between satellite IST vs in situ and NWP data. STD is the standard deviation of errors, r is the correlation and RMSE is the root mean square of the errors. Note that the only in situ surface temperatures from the SH are from the air-borne Operation Ice Bridge data program (IB).*

Parameter	Bias	STD	r	RMSE	Counts
Northern hemisphere					
IASI IST vs. aws air temp	-2.5 K	5.4 K	0.9	5.98 K	315140
IASI IST vs. aws surf temp	-0.8 K	5.3 K	0.9	5.36 K	298816
IASI IST vs. NWP air temp	-3.2 K	5.3 K	0.9	6.2 K	333885
IASI IST vs. NWP skin temp	0.3 K	6.2 K	0.9	6.2 K	333885
Southern hemisphere					
IASI IST vs. aws air temp	3.78	5.1	0.95	6.36	8889

IASI IST vs. IB surf temp	4.25	6.8	0.45	8.0	694
IASI IST vs. NWP air temp	-2.2	2.9	0.98	3.6	10790
IASI IST vs. NWP skin temp	-0.07	2.93	0.98	2.93	10774

Similar validation statistics between clear-sky satellite IST data and air temperatures from Summit AWS on the Greenland Ice Sheet has a Bias of -3.22 K and STD equal 3.14 K (Dybkjaer et al., 2012). I.e. traditional clear-sky satellite products have significant lower errors and comparable/higher bias for NH ice sheet, compared with the non-filtered all-sky IASI IST data.

In the subsequent sections, the validation will be stratified by available means and the IASI IST weaknesses in terms of, e.g. surface type and atmospheric state, will be identified.

7.1.3 Stratified temperature validation statistics

This section addresses validation of stratified datasets, in order to identify conditions where the IASI IST algorithm performs particularly good and bad.

First the IASI IST performance is evaluated for *intra-annual dependencies*. Figure 7.1.1 a and b show monthly average temperature bias and standard deviation for 2012, for NH and SH land station surface temperatures, respectively. Only few surface temperature data are available from SH and these data are IB radiometer data, and statistics from there is mainly shown for completeness.

For the NH, the IASI IST bias is generally low and negative over the course of the year; peaking in August, with a positive bias around 1 K. The standard deviation of the surface temperature error varies around 5 K within roughly one 1K and with minimum during summer and highest in November and December. With respect to both STD and Bias, the IASI IST performs best against in situ surface temperature measurements, during the period of light; from April to October.

The corresponding IASI IST evaluation against NWP surface temperatures is shown in Figure 7.1.2 *a* and *b*. The mean bias is relatively constant around 0 K for NH data. This is expected from the fact that the NWP data are used for training of the IASI surface temperature algorithm (see chapter 4). The standard deviation has minimum around 4.5 K during summer and worse during the dark period, up to 8 K. The IASI IST seems more successful for the summer month on the NH. The error statistics, for IASI IST vs NWP skin temperature, is significantly better for the SH, with nearly zero bias and a more or less constant standard deviation of 2-3 K. There appears no clear seasonal difference in the IASI IST performance against NWP data on the SH.

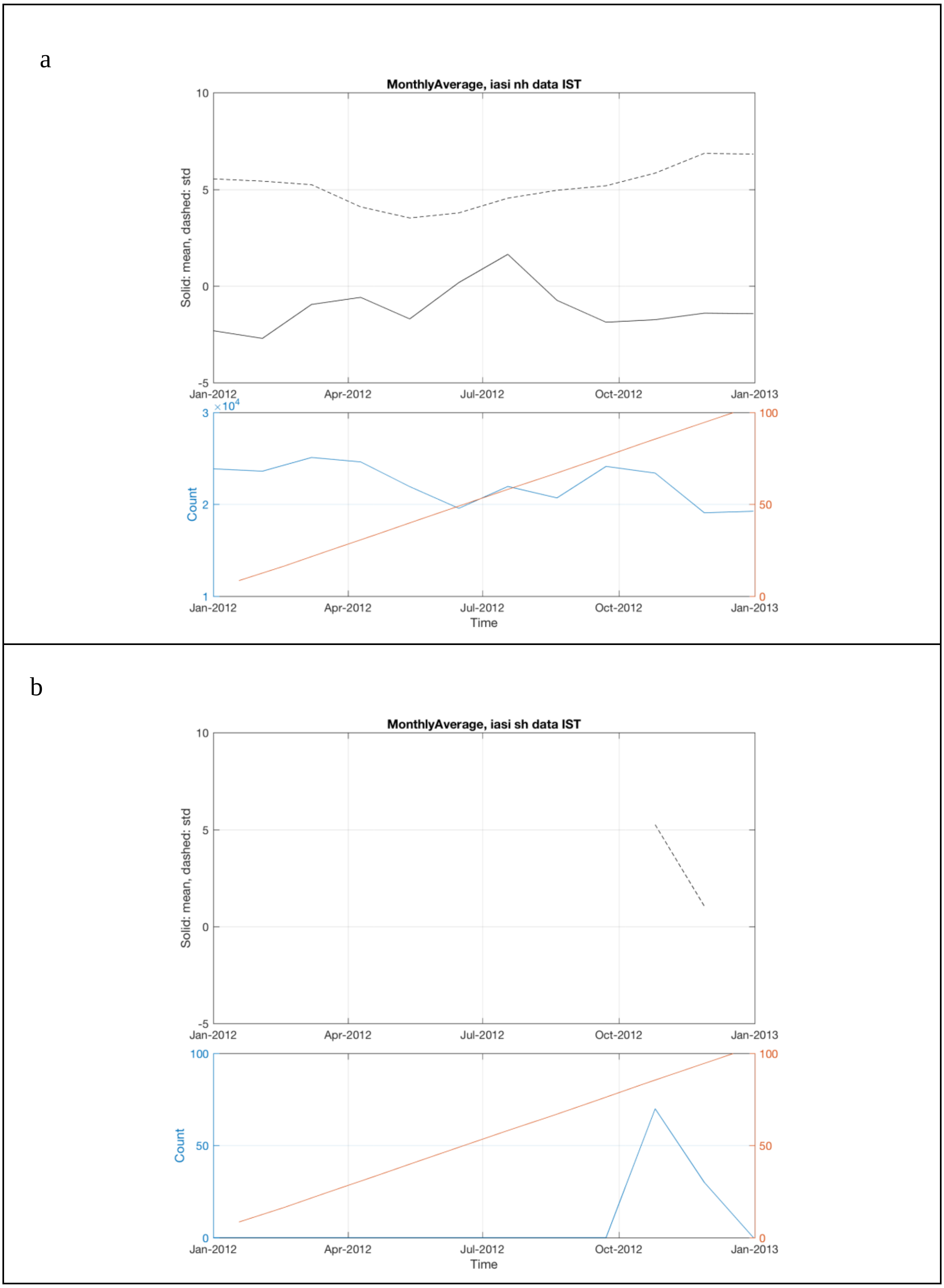

Figure 7.1.1 Inter-annual (monthly mean) error statistics for IASI IST – *in situ* Surface Temperature. *a) Upper panel: Solid: Monthly averaged temperature bias for NH IASI and station IST temperature measurements, dashed: standard deviation. Lower panel: Blue line: Number of counts used for averaging per monthly bin. Red line: relative amount of data. b) Upper panel: Solid: Monthly averaged temperature bias for SH satellite and station IST temperature measurements, dashed: standard deviation. Lower panel: Blue line: Number of counts used for averaging per monthly bin. Red line: relative amount of data.*

a

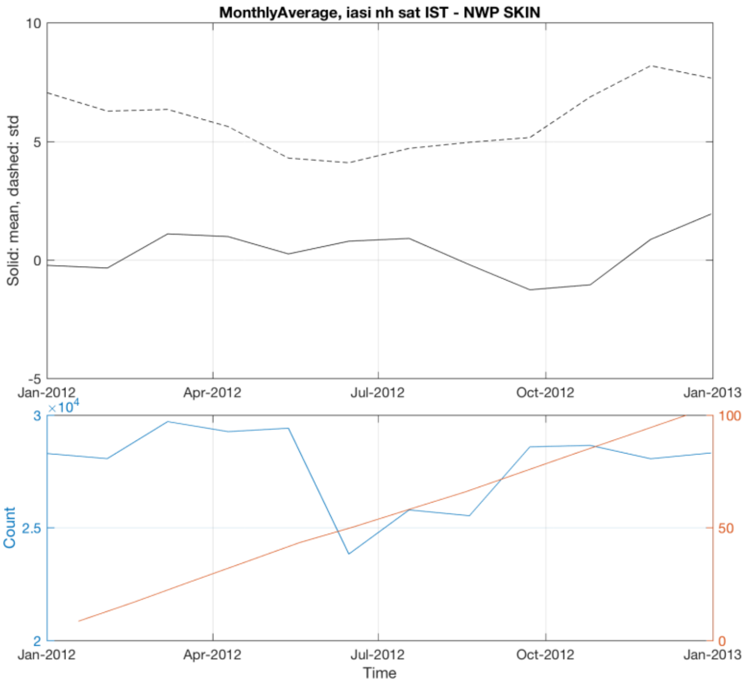

b

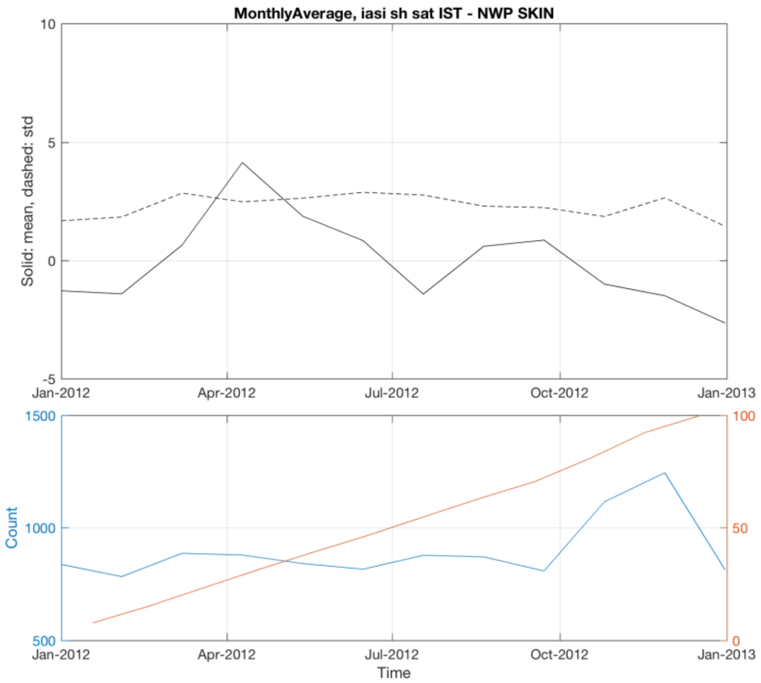

Figure 7.1.2 Inter-annual (monthly mean) error statistics for IASI IST – NWP Surface Temperature. *a) Upper panel: Solid: Monthly averaged temperature bias for NH for IASI IST and NWP SKIN temperatures, dashed: standard deviation. Lower panel: Blue line: Number of counts used for averaging per monthly bin. Red line: relative amount of data. b) Upper panel: Solid: Monthly averaged temperature bias for SH, dashed: standard deviation. Lower panel: Blue line: Number of counts used for averaging per monthly bin. Red line: relative amount of data.*

Looking at IASI IST performance against air and surface temperatures, as a function of distance to observation on the NH, an increasing STD from approximately 4 K to 6 K is revealed, going from 0 km to 70 km separation (D22 and figure 7.1.3, respectively). Bias seems almost unaffected by distance to observation. This dependency is nearly identical when comparing IASI IST to NWP surface and air temperatures (figure D6 and D23).

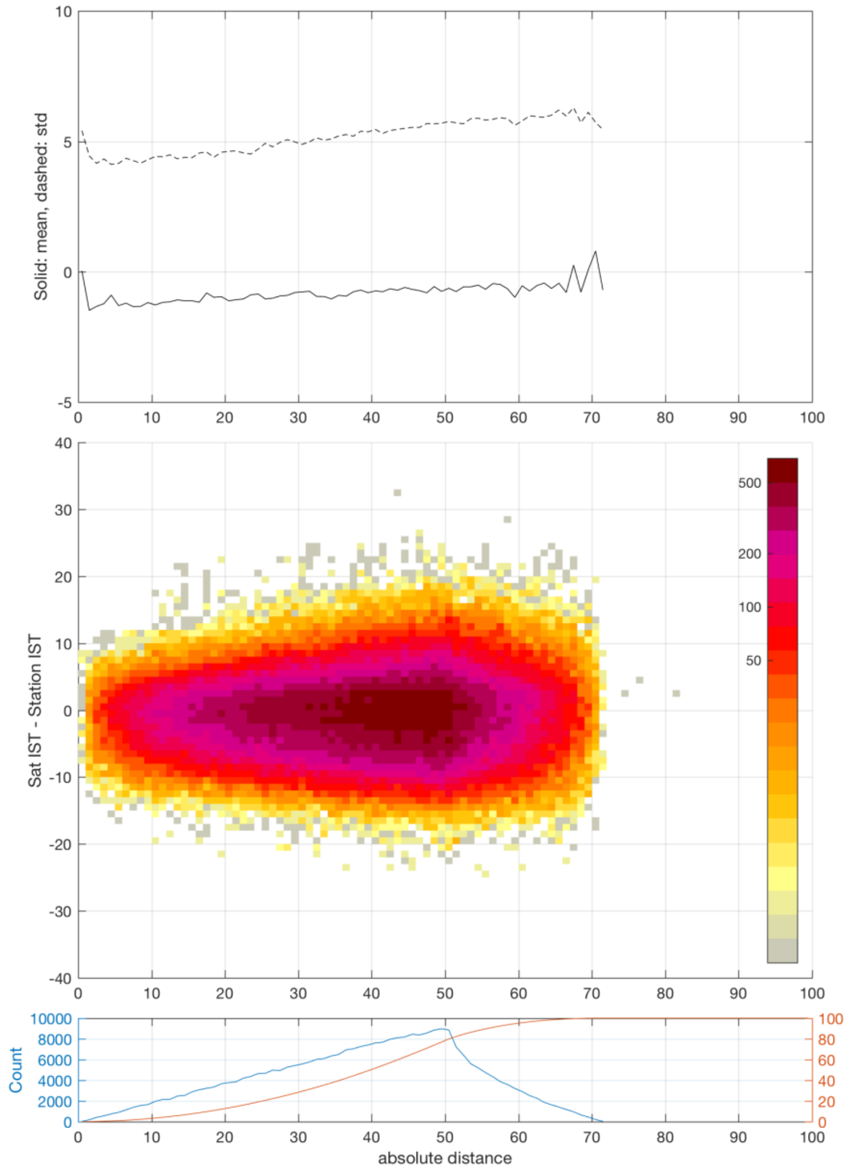

Figur 7.1.3 *Distribution and statistics on satellite IST – station IST differences as a function of absolute distance for the northern hemisphere. Top is mean (solid line) and standard deviation (dotted line), centre is a 2D histogram of the data distribution and bottom is data count per 1km bin for absolute distance (blue, left axis) and cumulated percentage of data count (red, right axis).*

This performance dependency with *distance to observation* is not seen in the SH data (figures D32 and D33). The absence of performance dependency to distance on SH may be explained by the relative positions of the AWS's on the Southern and Northern hemispheres. All PROMICE AWS's are positioned along the rim of the Greenland ice cap and they are therefore on a slope of the ice-cap, where the applied Southern Hemisphere AWS's are positioned on the high planes of the Antarctic ice cap. Consequently, moving away from a Greenland AWS will most likely results in changing altitude, whereas the altitude around the applied AWS positions on the Antarctic ice cap is more or less constant.

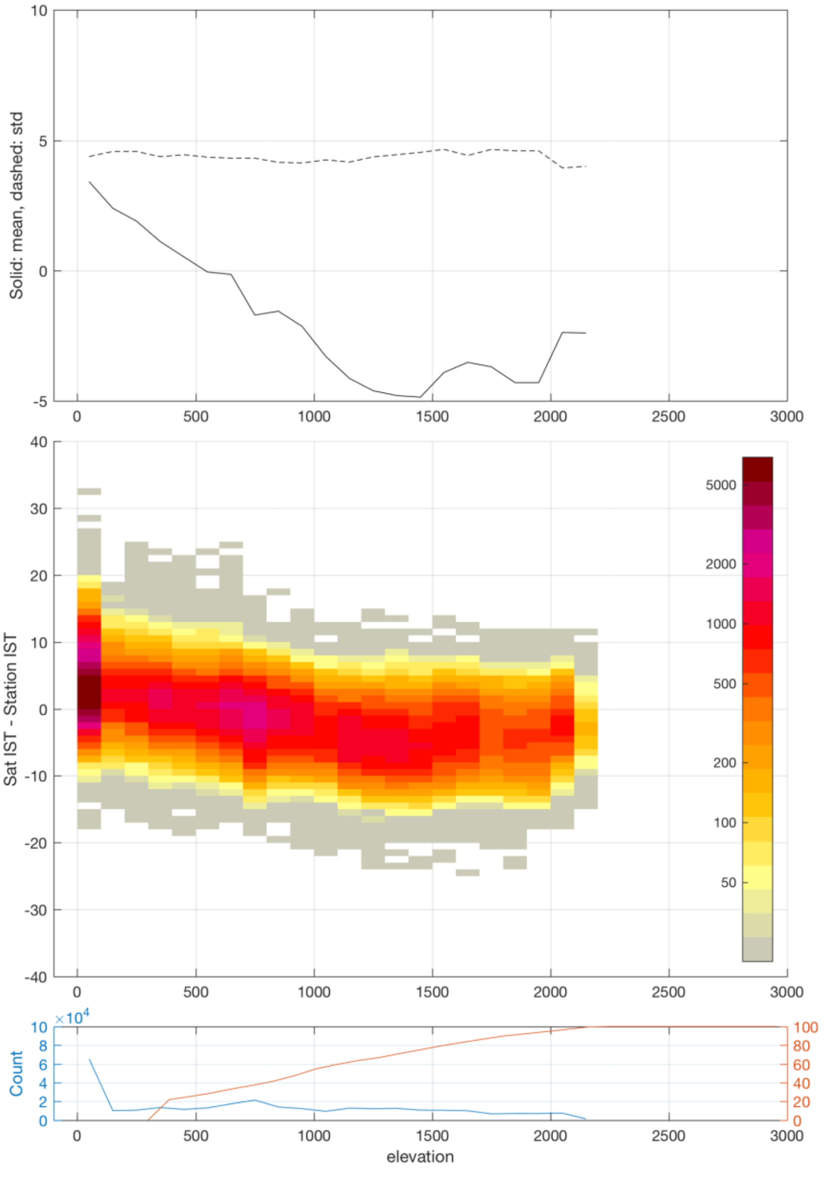

Figur 7.1.4 *Distribution and statistics on satellite IST – station IST differences as a function of elevation for the northern hemisphere. Top is mean (solid line) and standard deviation (dotted line), centre is a 2D histogram of the data distribution and bottom is data count per 100 m bin for elevation (blue, left axis) and cumulated percentage of data count (red, right axis).*

By plotting IASI IST performance against *elevation* a decreasing bias with increasing altitude is revealed. In figure 7.1.4, where IASI IST minus surface temperature observations is plotted against elevation, the bias drops to approximately -5 K from approximately 3 K, as elevation increases from sea level to ~2 km. The error seems invariant to altitude. The same is more or less the case when comparing with air temperature observations and with air and surface temperatures from NWP data (see D8, D24 and D25). No altitude dependencies of the IASI performance is found in the SH data, because of low variability in elevation around the applied SH AWS positions, as explained above.

From the IASI IST data stream we have collocated *water vapour* data (total column water in mm) from the MHS instrument on-board the Metop satellites. The influence of atmospheric water on error and bias related to surface temperature observations on NH is significant. However, for approximately half of all NH data the error is relatively constant, between 5 and 6 K and bias around -2 K (see figure 7.1.5). For wetter atmospheres, the STD seems to decrease with increasing atmospheric water content. The bias is best (closest to zero) at intermediate atmospheric water content. This pattern is also evident when comparing with air temperature observations and with both air and skin temperatures from NWP (see figures D26, D27 and D9, respectively).

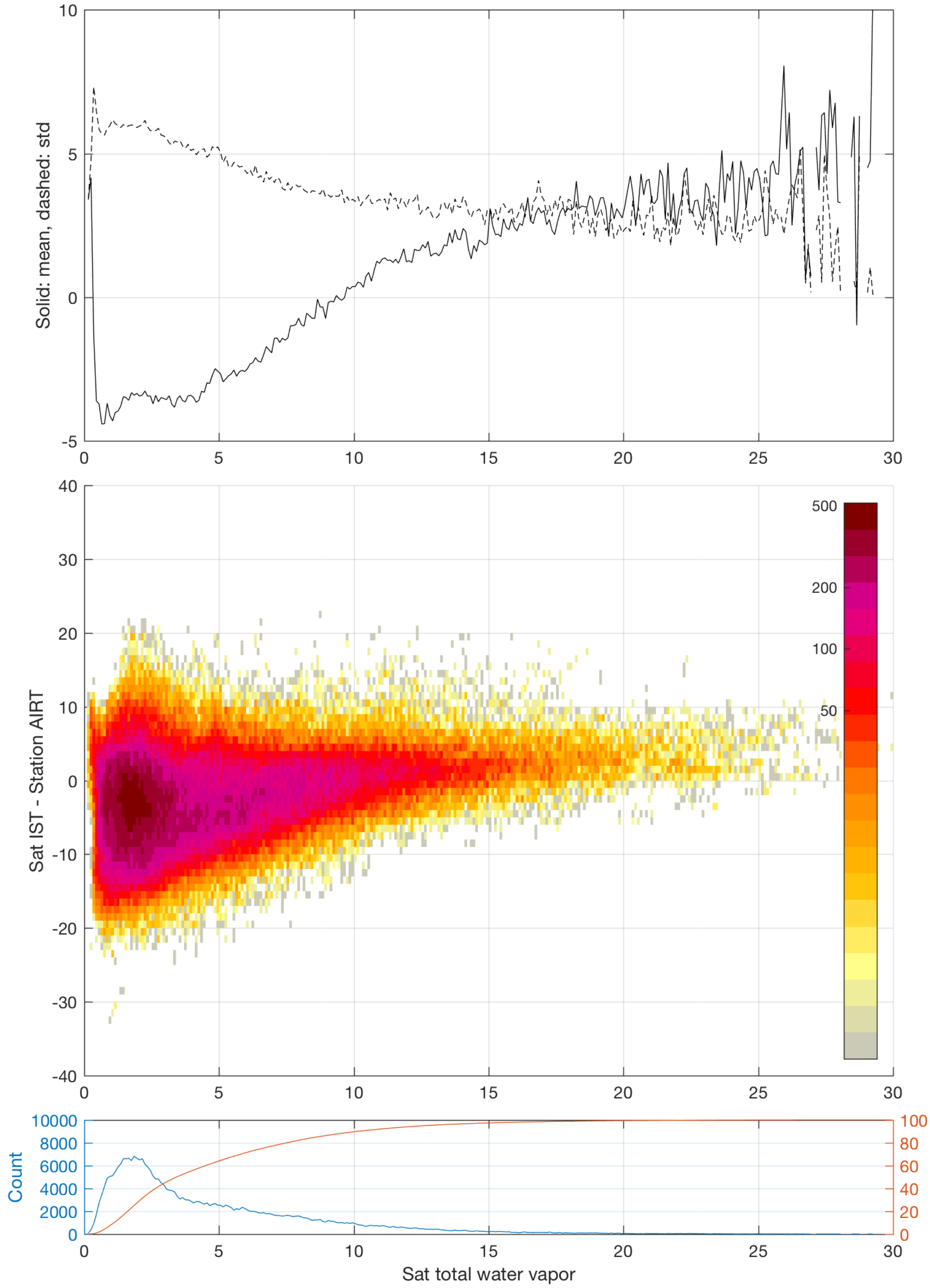

Solid: mean, dashed: std
Sat IST - Station AIRT
Count
Sat total water vapor
500
200
100
50

Figure 7.1.5 *Distribution and statistics of IASI IST and in situ surface temperature differences as a function of water vapour for the northern hemisphere (333926 matchups). Top is mean (solid line) and standard deviation (dotted line), centre is a 2D histogram of the data distribution and bottom is data count per 0.1 mm water vapour bin (blue, left axis) and cumulated percentage of data count (red, right axis).*

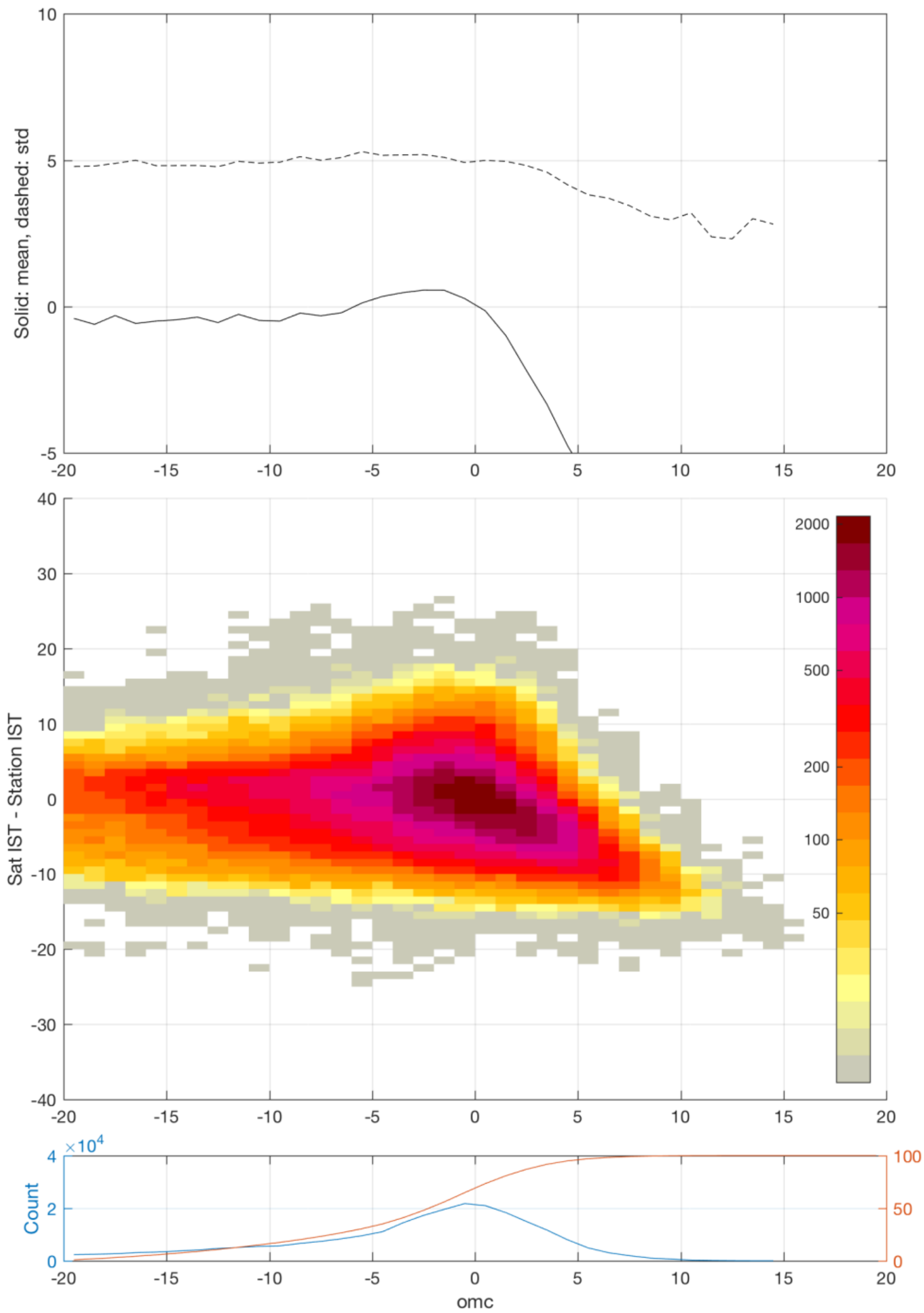

Figure 7.1.6 *Distribution and statistics of IASI IST and in situ temperature differences as a function of IASI OmC for the northern hemisphere (333926 matchups). Top is mean (solid line) and standard deviation (dotted line), centre is a*

2D histogram of the data distribution and bottom is data count per OmC unit bin (blue, left axis) and cumulated percentage of data count (red, right axis).

The corresponding validation data from the Antarctic land observations and NWP estimates are unfortunately very few and within narrow water vapour interval. Despite the pour data amount and low spread in the SH data, there seems to be less performance dependency related to the atmospheric water. Figures showing the IASI IST performance on the SH are D15, D16, D34 and D35.

The *OmC* variable that was provided in the IASI data stream (Observation minus Calculated) is the cloud index associated with the IASI IST algorithm. It is an indefinite index of which we have no knowledge, but it is expected to have an effect on the IASI performance, because it determines whether to apply the TIR or the PMW IST algorithms. The performance of IASI IST compared with surface temperature observations as a function of OmC is shown in figure 7.1.6. The associated error seems almost constant for all OmC values lower than zero, which includes approximately 70% of all match-ups. For positive OmC values the error drops. However, a marked dependency of IASI IST performance with OmC lies in the bias that drops drastically for positive OmC values. Corresponding error statistics for the SH is not unambiguous (see figures D17, D36 and D37).

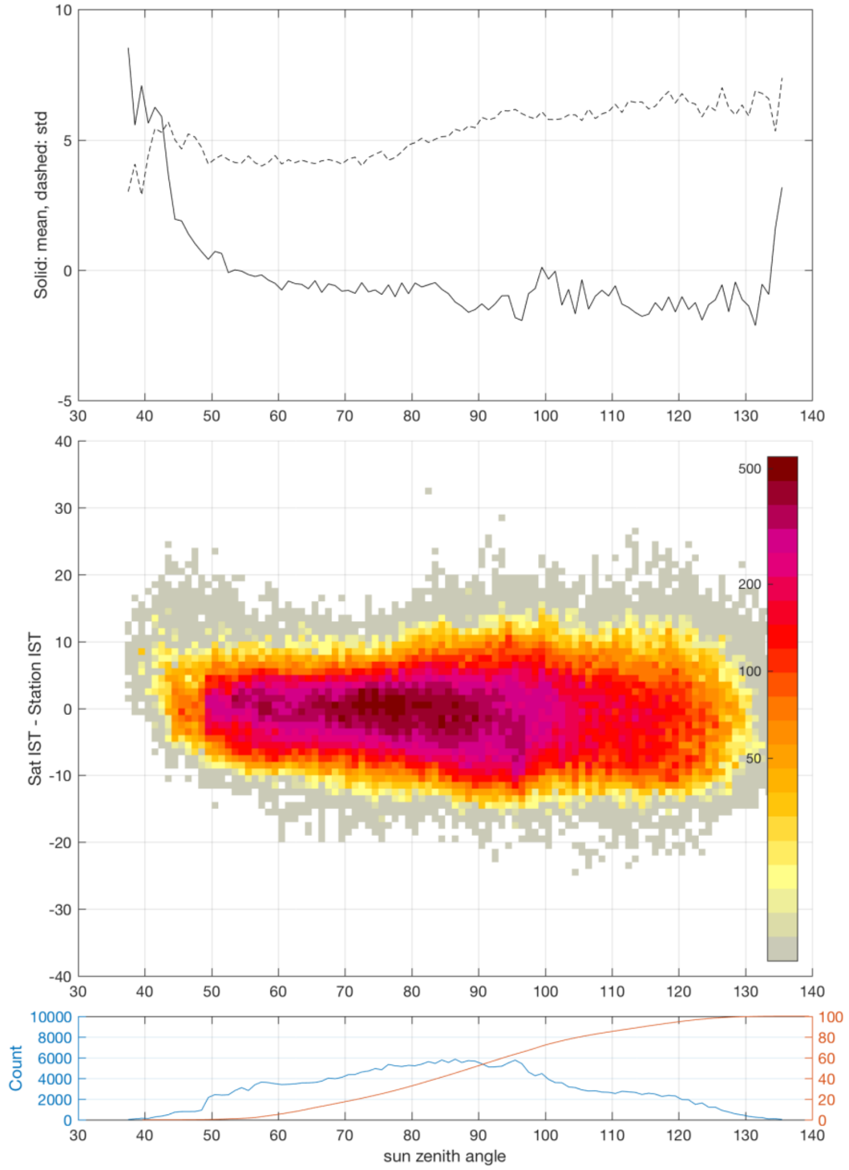

Figure 7.1.7 *Distribution and statistics on satellite IST – station IST differences as a function of sun zenith angle for the northern hemisphere. Top is mean (solid line) and standard deviation (dotted line), centre is a 2D histogram of the data distribution and bottom is data count per 1 degree bin for sun zenith angle (blue, left axis) and cumulated percentage of data count (red, right axis).*

Nearly all collocated land data on the NH are recorded for *sun-zenith angles* between 60 and 120 degrees. The sun-elevation ranges from day light to night time, over sun elevations at twilight, where the latter can be defined for sun elevation angles at 90 ±10 degrees. In figure 7.1.7 the IASI IST error relative to surface temperature observations on the NH show a daytime and night time performance regime that differ by approximately 2 K, where the best performance is during daytime (and summer). Bias seems generally less sensitive to sun-zenith angle. This day/night performance difference is the most robust signal across all stratified analysis performed here, i.e. for both NH and SH, and for air and surface temperature observation, including NWP data. Other validation statistics stratified by sun elevation are found in the Appendix D in figures D2, D10, D18, D19, D28 and D29. This is consistent with the intra-annual plots (figures 7.1.1 and 7.1.2), because the sun-zenith angle dependency is not only related to the time of day, but also highly related to the seasons, i.e. winter or summer.

Other satellite TIR IST products, like those used in section 7.3 (and described in chapter 4), normally show deteriorating performance with increasing *satellite zenith angle*. This is apparently not the case for IASI IST that show no dependency with satellite zenith angle, as illustrated in D3, D4, D11, D12, D20, D21, D30 and D31. Here, the errors and bias are plotted for IASI IST versus air and surface temperature observations and NWP data.

The IASI IST product is associated with a *quality indicator*. The quality indicator (qi) is an estimate of the absolute retrieval error compared with the ECWMF analysis [RD-3]. In order for the qi to work as a means to filter for best surface temperature quality data, it is crucial that the qi performance is reliable. The qi ranges from zero to indefinite, where 0 is the best quality. In figure 7.1.8 the temperature difference between satellite surface temperature and observed surface temperature is plotted as a function of the temperature quality index for the NH. The filtering process is now a bargain between maintaining data volume and data quality. For example, data with qi values less than 2 constitute only 10% of the data. For these data the IASI IST performance is STD = 4.5 K and Bias = 1 K. If half the data must be maintained after filtering (qi less than 2.5) the average STD rises to approximately 4.8 K. The corresponding performance for all data is STD = 5.3 K and Bias = -0.8 K (table 7.1.1 and Appendix G). It is worth noting that the qi works well as a quality indicator, as the IASI IST performance worsen with increasing qi. This is also valid when comparing IASI IST with air temperatures and NWP data on both NH and SH. However, the bias improves with increasing qi's when comparing IASI IST with air temperature observations on the SH and the IASI IST quality is not uniquely determined by the qi when comparing with SH surface temperatures. The latter is radiometer observations from Operation Ice Bridge only, from which validation results differ largely from validations against more conventional in situ measures. All temperature-error/qi distribution plots are found in Appendix D40-D47 and selected filtered validation results are calculated in the table in Appendix G.

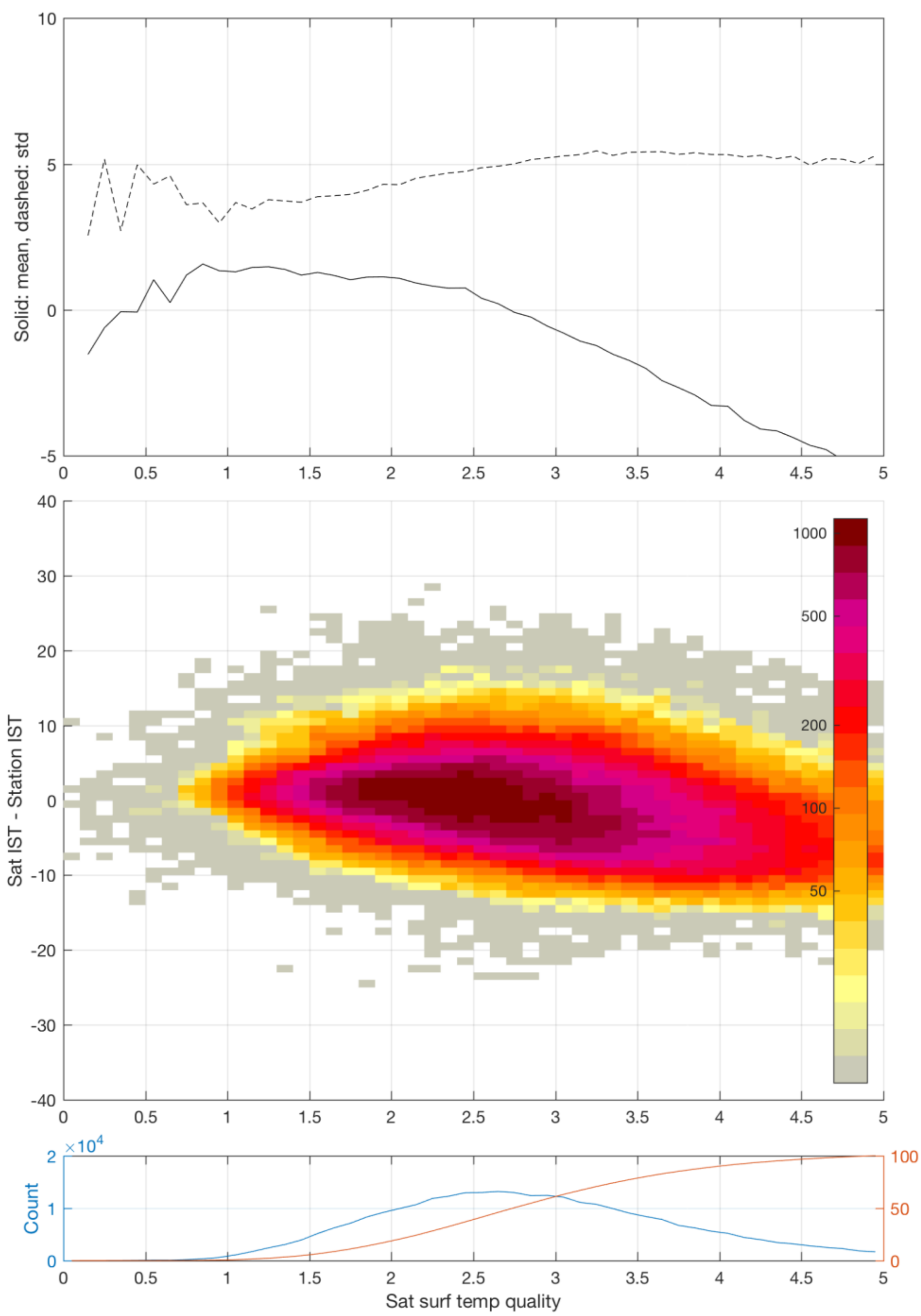

Figure 7.1.8 *Distribution and statistics on IASI IST and in situ surface temperature differences as a function of IASI individual temperature quality index for the northern hemisphere (333926 matchups).. Top is mean (solid line) and standard deviation (dotted line), centre is a 2D histogram of the data distribution and bottom is data count per quality index unit bin (blue, left axis) and cumulated percentage of data count (red, right axis).*

Generally for the Greenland ice cap, the IASI IST errors are lowest at cold conditions, whereas the bias is closest to zero for intermediate temperatures. This is the case when comparison against both observed air and surface temperatures (Appendix D48 and D49). The corresponding errors from the Antarctic ice sheet are generally low and smallest for intermediate temperatures (for the ice cap high planes), i.e. between -50 and -20. The bias acts, interestingly enough, very similar on both ice caps; being large and positive for low temperatures and approaching a cold bias of approximately -2 K, going towards 0 K.

7.1.4 IASI cloud indicator vs PROMICE cloud calculation

The figures 7.1.9, 7.1.10 and 7.1.11 show *OmC*, *the* IASI IST quality indicator and the error relative to observed surface temperatures as a function of the PROMICE cloud cover index, respectively. In figure 7.1.9 are in principle 2 measures of the same quantity and there seems to be a negative correlation between the two. However, the spread of the OmC is large and the corresponding correlation is low. The IASI IST quality indicator shows no correlation with the PROMICE cloud estimate. Finally, and in line with the latter, there is no relation between IASI IST error and the cloud cover estimated at the PROMICE stations, as it can be seen from figure 7.1.11.

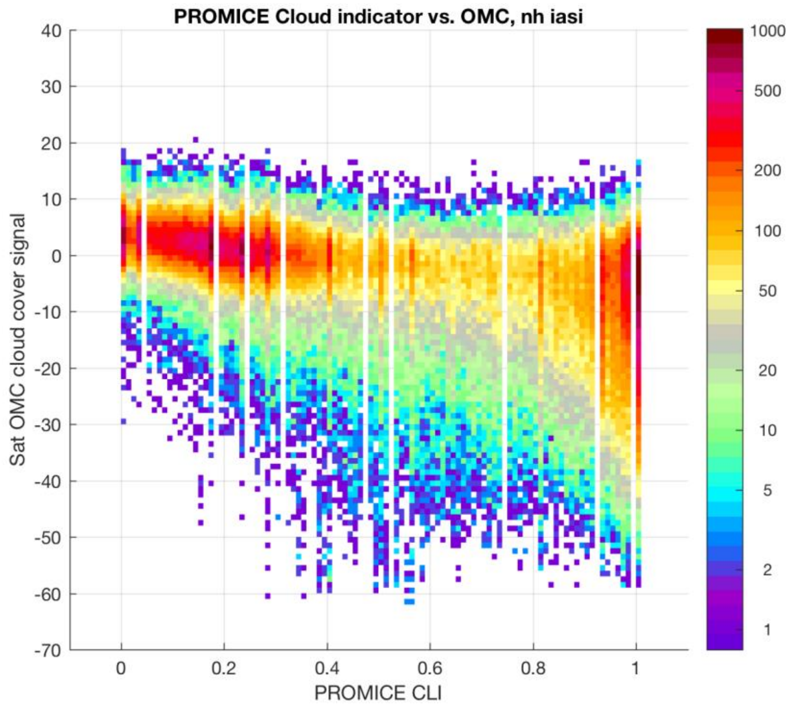

Figure 7.1.9 *2D-histogram showing the distribution of IASI OmC cloud cover signal as a function of PROMICE cloud index. Data set is from PROMICE stations only.*

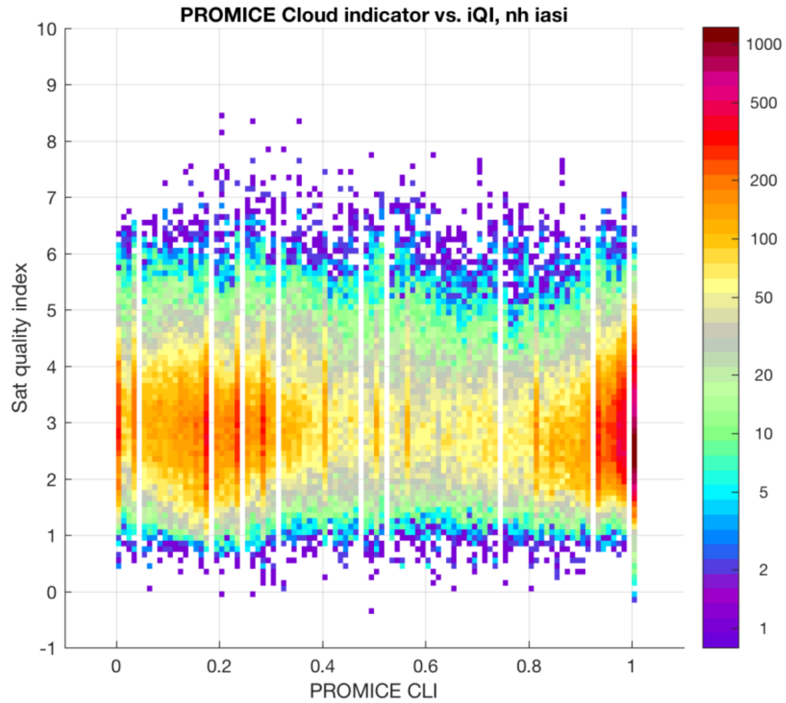

Figure 7.1.10 *2D-histogram showing the distribution of the IASI individual quality index as a function of PROMICE cloud index. Data set is from PROMICE stations only.*

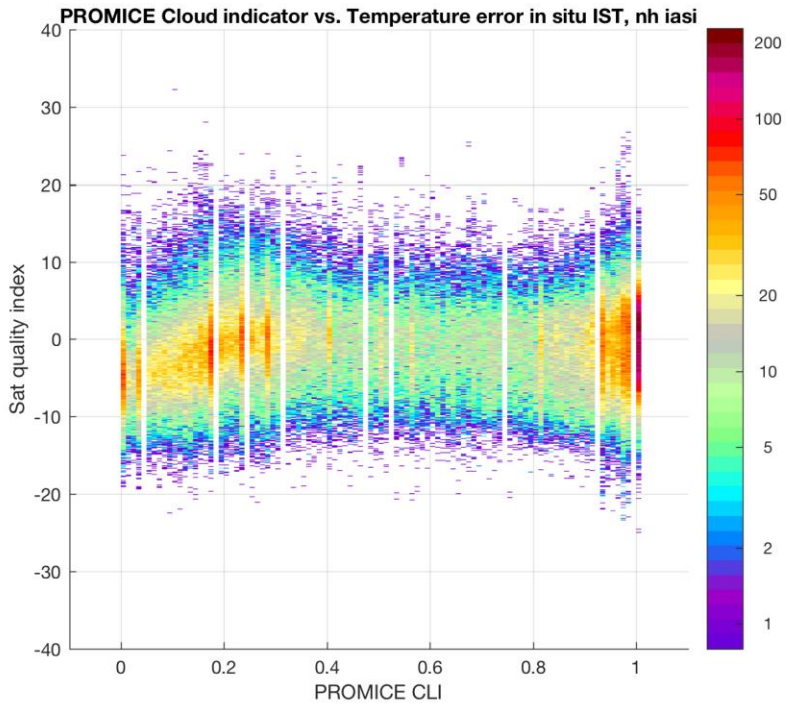

Figure 7.1.11 *2D-histogram showing the distribution of temperature error for IST as a function of PROMICE cloud index. Data set is from PROMICE stations only.*

7.1.5 Sampling effects

We have assessed the temperature error dependency with the time lag between the in-situ observation and the satellite measurement. It was expected to observe increasing error with increasing time difference. However, no performance dependency with temporal sampling was found within the matchup window of ±50 minutes. This is illustrated in figure 7.1.12 for the IASI IST difference with observed surface temperatures on the Greenland ice sheet and against the corresponding NWP skin temperatures in D39.

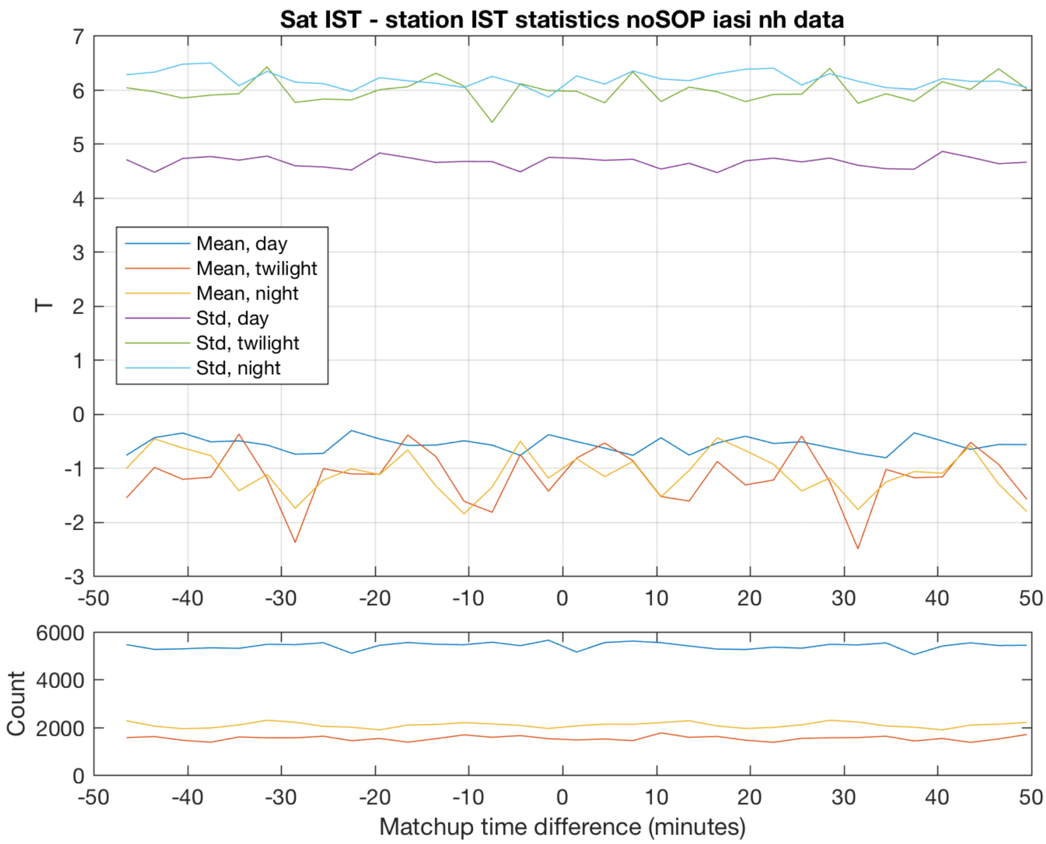

Figure 7.1.12 *Difference of IASI IST and station IST against the difference of the time of satellite measurement with the time of station measurement in minutes. Northern hemisphere data. Upper panel: purple, cyan and green lines are standard deviations for day, night and twilight, respectively. Blue, yellow and orange lines are the biases for day, night and twilight, respectively. Lower panel: Number of counts per minute bin.*

7.2 Validation – Sea IST

This section describes the validation of Arctic and Southern Ocean sea ice surface temperature, using in situ locations depicted in Figure 3.1.

7.2.1 Special considerations for sea IST

As described in chapter 3, the quality of the buoy surface temperature observations is lower than that of the buoy air temperature observations, and this affects the overall statistics when comparing to the satellite IST. Further, the amount of southern hemisphere observations is very limited. Therefore the emphasis in the following is on comparison with northern hemisphere buoy air temperature observations, with notes on southern hemisphere results where available.

Additionally to buoy measurements there were airborne measurements from the IceBridge project. These data are potentially very interesting for IST validation, because surface temperature recordings are from radiometer and thus a direct measure from the surface. However, the IceBridge data are very sensitive to surface properties over ocean, in particular in areas that are partly open water and ice. In chapter 6

7.2.2 General statistics for Sea Ice validation

General, non-stratified statistics of the comparison of IASI IST with air and surface in situ and model (NWP) temperatures are given in table 7.2.1. The buoy air temperatures show some differences to the satellite IST, with an overall root mean square difference of 7.5 K and a correlation of 75%. These data are stratified and further analysed in section 7.2.3. The buoy surface temperatures show even larger differences, possibly reflecting the lower data quality of the buoy surface temperature data, as described in section 3. The number of airborne skin temperature measurements is very limited due to the requirement of crossing flight and satellite passes, but for the northern hemisphere, the statistics are in line with the buoy statistics. For the southern hemisphere, a large bias is observed, but as shown in table 7.2.3 this is due to problems with daytime observations, and it is reduced to -0.8 K when using night time observations only.

In light of the relatively high bias and standard deviation between satellite and buoy data, the corresponding values to model data are noticeably better and with a very low bias. This is probably a reflection of the assimilation of IASI data in ECMWF's operational NWP model (see discussion in chapter 8).

It should also be noted that both ECMWF and IABP buoys are in the GTS data stream and thus likely used in the ECMWF model assimilation, post processing and/or validation system. This again is used to tune the algorithms for the IASI IST, so the buoys are not guaranteed to be independent of the IASI IST, and the error estimates even from the buoys could be a lower bound.

Table 7.2.1 *General comparison of satellite data with observations and NWP data*

Parameter	Bias	Standard deviation	Correlation	Root mean square diff.	Number of matchups
Northern hemisphere					
Sat IST - buoy air temp	0.4 K	7.5 K	0.75	7.5 K	26268
Sat IST - buoy surf temp	-7.7 K	8.9 K	0.53	11.8 K	12252
Sat IST - flight surf temp	3.6 K	3.3 K	0.82	4.8 K	16
Sat IST - NWP air temp	-0.6 K	2.8 K	0.96	2.9 K	34468
Sat IST - NWP skin temp	-0.3 K	2.9 K	0.96	2.9 K	34468

Southern hemisphere					
Sat IST - buoy air temp	-2.3 K	2.8 K	0.76	3.6 K	722
Sat IST - flight surf temp	6.2 K	9.0 K	0.15	10.8 K	39
Sat IST - NWP air temp	-0.9 K	2.5 K	0.73	2.6 K	722
Sat IST - NWP skin temp	-1.5 K	2.3 K	0.76	2.7 K	722

Validation statistics for clear-sky satellite IST from TIR data and air temperatures from Arctic buoys reveal Bias and STD of -2.76 K and 3.69 K, respectively (Dybkjaer et al., 2012). This means that traditional clear-sky satellite products have significant lower errors for NH, compared with the non-filtered all-sky IASI IST data.

7.2.3 Distribution of temperature differences

It has been investigated how the difference between in situ air and surface temperature and satellite IST relates to the temperatures themselves, the water vapour, the temperature and water vapour quality indicators, the OMC cloud indicator, time of the year, sun zenith angle and sea ice concentration, and how the difference between in situ air temperature and model IST relates to the temperature (Appendix E, figures E1-E14).

When assessing the difference between in situ air temperature and satellite IST as a function of the satellite temperature quality index, it is seen that the average quality index is close to 2, with 10% of the northern hemisphere data having a quality index of 1.4 or less (Figure 7.2.1, Appendix G). There is small bias and a standard deviation between satellite and in situ observations of ~3 K for a quality index below 1, rising to about 8 K for IASI IST with quality index higher than 2, for northern hemisphere sea ice. As seen from the 2D histogram in Figure 7.2.1 (left middle panel), the majority of data with quality index between approximately 0.5 and 3 show temperature errors less than 5 K, and could thus be considered good data, but there is also a relatively large amount of data with quality index between approximately 1.3 and 3.2 and temperature differences of up to 20 K in both directions, creating two “side lobes”. This will be investigated in the following.

The amount of southern hemisphere data is low, but the data indicate low STD and bias values with only little dependence on the quality index (figure 7.2.1 right).

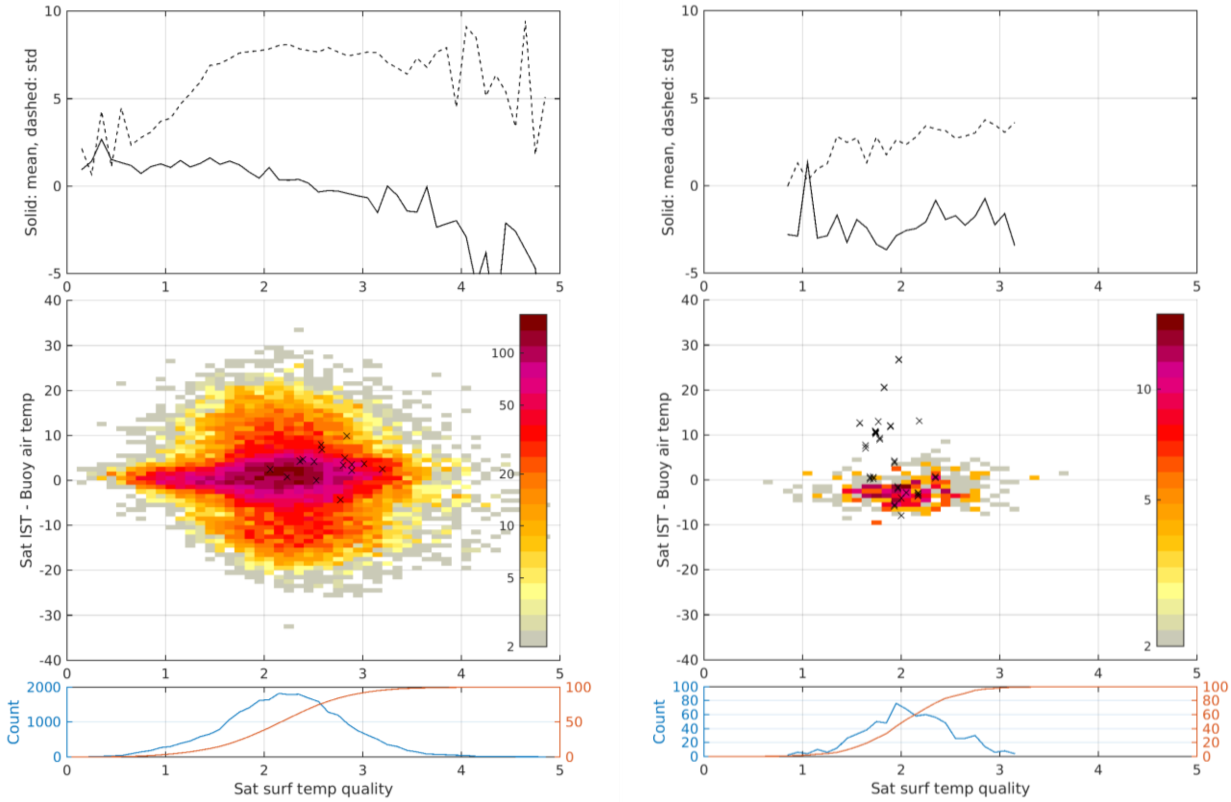

Figure 7.2.1 *Distribution and statistics on satellite IST – buoy air temperature differences as a function of the satellite surface temperature quality indicator for the northern hemisphere (left) and southern hemisphere (right). Top is mean (solid line) and standard deviation (dotted line), centre is a 2D histogram of the data distribution with black crosses showing airborne IST observations, bottom is data count per 0.1 quality indicator unit bin (blue, left axis) and cumulated percentage of data count (red, right axis).*

If specific causes for the high STD in NH data with temperature quality indicators between approximately 1.5 and 3 can be identified, it may be possible to retain the good data and only filter out the data with large errors, using other filtering means. For this analysis, the northern hemisphere sea ice data are grouped by the relation between buoy air temperature and satellite IST, and on the sun zenith angle ("daytime" for angles smaller than 90° and "night time", including the twilight period, for higher angle). I.e., during summer (with midnight sun), all data are denoted "daytime" and during the polar night, all data are denoted "night time". Similar analysis has been made of the buoy IST – satellite IST relationship (Appendix E, figure E15). Here, many of the buoy IST data are much warmer than the sat IST data, likely because of snow covered buoys. Especially, a data cluster with buoy IST around -16°C, with corresponding IASI IST between -20 and -40 C, worsen the validation statistics. These data have been traced to mainly two buoys deployed north of Canada. The buoy IST data are considered to be too snow affected to be used in the present state, and are thus not analysed further. See also discussion of uncertainties in chapter 6.

The highest density of daytime matchups have temperatures above -5°C (group 1, figure 7.2.2 top), and this small interval contains 10% of the total number of matchups (table 7.2.2). 12% of the matchups are daytime matchups with lower temperatures and a difference between temperatures of less than 5 K (group 2). A small but noticeable amount of data has buoy temperatures above -1°C and much colder satellite temperatures (group 3), likely due to cloud contamination. The "side lobe" containing satellite data that is more than 5 K colder than the in situ temperature is labelled group 4, and is also expected to contain satellite data affected by undetected clouds, while the “side lobe” with satellite data more than 5 K warmer than the in situ temperature is labelled group 5. It is noted that figure 7.2.2 show a clear separation of the “side lobe” data in group 4 and 5 from the “good” data in group 2.

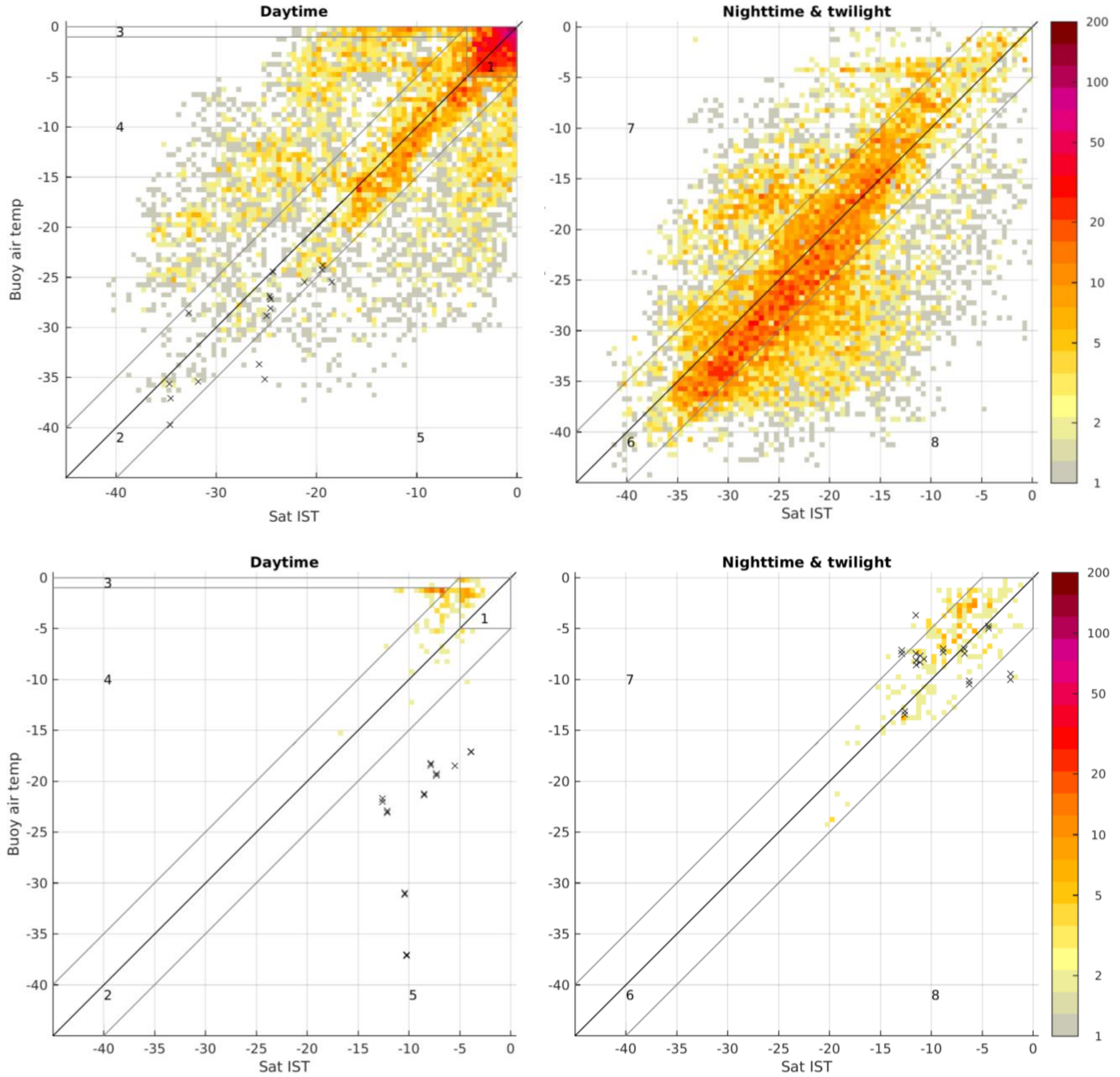

__Figure 7.2.2__ 2D histogram of the data distribution as a function of satellite IST and buoy air temperature for daytime observations (left) and night time (right), for the northern hemisphere (top) and southern hemisphere (bottom). Black crosses show matchups to airborne IST observations. The black line indicates a 1:1 relationship, and the grey lines define groupings. See text for explanation of group numbers.

*__Table 7.2.2__ Comparison of satellite data with northern hemisphere buoy air temperature measurements over sea ice, divided in groups.*First- and multi-year ice zones are defined in the text.*

Group	Description	Bias	STD	Correlation	% of all data selected
	All data	0.4 K		0.75	100
1	**Day, ≥ -5C**	**0.0 K**		0.28	10
2	**Day, good data < -5C**	**0.4 K**		0.93	12
3	Day, buoy close to melt	-11 K		0.24	1
4	Day, sat - buoy < -5C	-12 K		0.84	8
5	Day, sat - buoy > 5C	12 K		0.73	6
6	**Night, good data**	**0.5 K**		0.96	38
7	Night, sat - buoy < -5C	-9.7 K		0.87	10
8	Night, sat - buoy > 5C	10 K		0.75	14
	Marginal ice zone	3.7 K	6.1 K	0.32	6
	Ice covered region	0.1 K	7.5 K	0.73	94
	First year ice	-5.2 K	8.3 K	0.63	8*
	Multi-year ice	1.2 K	6.9 K	0.61	33*

Night time matchups are generally much colder, with most data in the range -40°C to -10°C. Here, all matchups with a difference between temperatures of less than 5 K are labelled group 6 (38% of the total dataset), with the "side lobe" containing satellite data that is more than 5 K colder than the in situ temperature is labelled group 7 and the "side lobe" with satellite data more than 5 K warmer than the in situ temperature is labelled group 8.

60% of the northern hemisphere data are in group 1, 2 and 6, and here satellite IST has a warm bias of about 0.5 K compared to the air temperatures, except in group 1, where the average bias is 0 K (table 7.2.2). The remaining groups show similar statistics, indicating that the two "side lobes" are of almost even weight and not very different from day to night.

In figure 7.2.2, matchups between airborne IST observations from IceBridge and satellite IST observations are marked with crosses. For the northern hemisphere, airborne data are only available during daytime, and show a warm bias of 3.6 K and a standard deviation of 3.2 K (Table 7.2.3). The IB data seem in general to be associated with large errors relative to IASI IST. This may be explained by foot-print differences between IB and IASI date, where the IB occasionally may measure water in leads or lower concentration sea ice areas, whereas the IASI data are large scale averages. This can explain unsystematic outliers. For that reason and because of the few IB observations, the IB data will not receive much attention here.

Of the southern hemisphere buoy data that are available, 82% are in group 1, 2 and 6, and almost all of the rest show a cold bias of the satellite IST (figure 7.2.2 bottom). For the IceBridge data, the number of observations is very limited, but the daytime matchups show a large warm bias of 14 K, while the night time data show a small negative bias of -0.8 K (figure 7.2.2, table 7.2.3).

Table 7.2.3 *Comparison of satellite data with airborne IST measurements over sea ice.*

Description	Bias	Standard deviation	Correlation	Root mean square diff.	Samples
Northern hemisphere, daytime	3.6 K	3.2 K	0.82	4.8 K	16

Southern hemisphere, daytime	14 K	5.5 K	0.53	15.3 K	18
Southern hemisphere, night time	-0.8 K	4.1 K	0.11	4.0 K	21

As an alternative to the split in groups, it is also possible to stratify the data according to ice concentration or type. 94% of all northern hemisphere matchups are from areas with at least 85% ice cover, showing almost neutral bias (table 7.2.2). The 6% data from the marginal ice zone (30-85% sea ice) show a larger positive bias, likely because the satellite measures a mixture of sea and ice surface temperatures.

To stratify by ice type, two zones characteristic of first year and multi-year sea ice were defined. The first year ice zone covers the southwestern Beaufort Sea and the East Siberian Sea from 150W to 45E and 70N to 77N. The multiyear ice zone covers the area north of Greenland and Canada, from 10W to 160W and 83N to 90N. 8% of the total northern hemisphere dataset is in this define first year ice zone, showing a cold bias of -5.2K (table 7.2.2). 33% of the matchups were inside the defined multiyear zone, showing a warm bias of 1.2 K and a standard deviation of 6.9 K. Generally there are large performance differences between the analysed ice types.

7.2.4 Relation to other matchup parameters

As described in section 7.2.3, data can be split in 8 groups, with the best data quality in group 1, 2 and 6. However, this splitting is only possible when validation data is available. Here, it is investigated if it is possible to make a similar filtering according to auxiliary parameters in the IASI IST MU files. The parameters in the MU data stream are: water vapour, satellite temperature quality, water vapour quality, OmC cloud indicator, month of the year, ice concentration, satellite zenith angle, and sun zenith angle. Figure 7.2.3 shows the histograms of the data distribution as a function of month of the year for all data and for the individual groups. Similar figures for all parameters are shown in Appendix E16 to E25. The relation with temporal and spatial matchup difference is investigated in similar fashion, also shown in Appendix E.

Looking at the *seasonal distribution*, there is a minimum of observations in June and July, with most data in October-December (figure 7.2.3). This is likely due to the deployment plan for buoys, with most deployments in the early fall, the general rather short life expectancy for sea ice buoys, and the melt-out of buoys in especially in summer. The distribution on daytime and night time observations reflect the polar night and polar day. The daytime observations show most group 1 data (above -5°C) in May – September, and when taking the overall data distribution into account, the peak is in June – August. The cold but good data in group 2 peak in May, where the temperatures are still low and the sun is up almost all the time. The group 3 data also show a clear peak in May. This is noticeable, since one could expect buoys to be close to melt-out all summer, but the total data amount is small. The group 4 data (daylight satellite observation much colder than in-situ observation, likely due to undetected clouds) peak in March and April, with 57% of the overall data count in April falling in this category. In March, 74% of the data are in group 4 or 7 (night time satellite observation much colder than in-situ observation). We speculate that the cloud mask has difficulties detecting the fog that often occurs over sea ice when the sun starts to rise in the spring, but this needs further investigation out of scope of this study. The group 5 data has a large peak in September, when there are still many openings in the sea ice, and many observations are available. In September, 40% of the data is in group 5 or 8. Supplementing this, the night time observations show a small tendency for more very cold satellite data (group 7) in December and January, when it is completely dark and the cloud detection is most difficult, and group 8 has most data in October and November, likely related to remaining openings in the sea ice. The data with small deviations show an almost even distribution in October – February, taking the total amount of data into account.

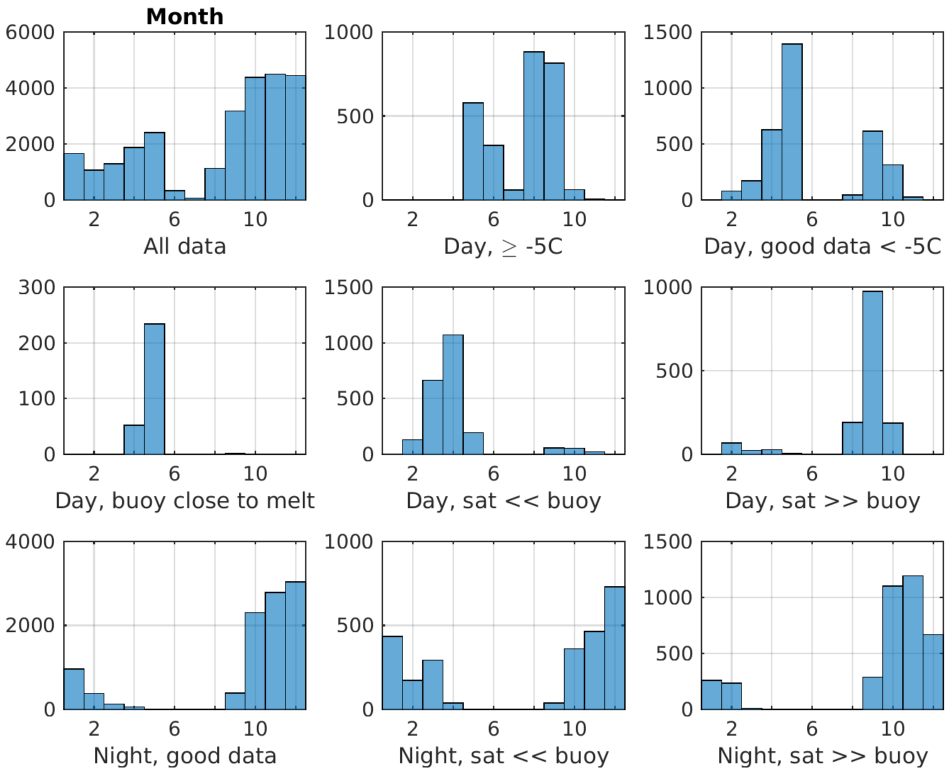

Figure 7.2.3 *Histograms of the data distribution as a function of month of the year for northern hemisphere sea ice matchups to buoy atmospheric temperatures. Top left shows all data, the following show distributions for the eight groups defined in figure 7.2.2.*

For the *water vapour (WV)*, almost all data with a value higher than 5-8 are either good data or daytime data where the satellite temperatures are at least 5 degrees warmer than the buoy data (figure E16). A filter requiring total column water vapour of at least 8 would thus remove date from the "cold side lobe" in group 3, 4 and 7. Unfortunately, it would also remove most data in group 2 (good daytime matchups with temperature errors smaller than -5°C) and 6 (good night time matchups), since the cold atmosphere also tends to be dry. With respect to temperature error (STD) there seems to be no easy means to filter good data from bad, using water vapour threshold, but with a tendency towards smaller STD for increasing WV. With respect to bias, the algorithm performs neutral at dry atmospheres with total column water vapour around 2 mm, both for SH and NH data (Appendix E4). However, the best 10% data filtered by WV quality has STD values around 3 K and WV quality seems to have a large effect on the IASI IST performance (E5). Data from the SH seem unaffected by WV quality (E5). The histograms for the errors against WV indicator are plotted in Appendix E18.

The distribution of errors (IASI IST - air temperatures) indicates that there is no easy filtering of good data, using the satellite *temperature quality indicator*, and still retaining the large data amounts (figure 7.2.1). The histograms for temperature quality indicator for all 8 groups from figure 7.2.2 are plotted in Appendix E17. In section 7.2.3, it was noted that for temperature quality indicator values of less than ~1.4, ~90% of the data set would be removed and one will be left with a group of data with small bias and low standard deviation. When comparing IASI with surface temperatures, the STD seems more or less constant, whereas the Bias worsens with increasing quality indicator value (Appendix E13).

The *OMC cloud indicator* has also been pre-filtered to remove outliers (Appendix E19). Here, the good but cold data from group 2 and 6 have a quite sharp distribution with a peak at -3 to -1 and few data below -10, but so does the cold biased data in group 4 and 7. The other groups, including group 1, have a distribution with a heavy cold tail and many data with OMC down to -20. In Appendix E6 it is clearer that OmC has only limited effect on the STD on both NH and SH. However, the OmC has an apparent large positive effect on the bias of the IASI IST data, where errors associated with large negative OmC have bias around 3, going towards zero bias for OmC approaching 0.

Far the most IST validation data for sea ice are for concentrations above 85%. This is seen in Appendix E21 that displays the error distribution in the 8 temperature zones. The marginal ice zone data (sea ice concentration between 30% and 85%) are mostly located in group 1 (both satellite and buoy temperatures within -5°C to 0°C) and group 5 (satellite IST much warmer than buoy air temperatures). In Appendix E10, the associated error statistics show improved performance going from 90% to 100% ice cover for NH and rather noisy statistics for lower ice concentrations. Despite poor data coverage from SH sea ice, the IASI IST performance there is much better that for NH sea ice.

The error distribution of the 8 temperature zones against *the satellite zenith angle* show discrete spikes between 0° and 60° according to the satellite orbit geometry, with increasing data amounts towards high orbit angles (Appendix E22). Group 2 shows a shaper increase than most of the other groups, but no clear separation can be made.

Most error data have *sun zenith angle* between 65° and 125°, with the most frequent sun zenith angle around 108° for the NH data (Appendix E23). Some patterns exist, e.g. group 3 where the buoy temperature is close to melt tend to have sun zenith angles below 80°, and there seem to be a tendency for more bad data from group 4, 5, 7 and 8 in the twilight zone with sun zenith angles from 80° to 100°. However, group 2 also has a peak in this range. Systematic distribution of errors related to sun-zenith angles are difficult to depict, because this dependency includes both seasonal issues, as well as diurnal illumination issues. However, from Appendix E9 the largest errors are around twilight and the bias is smallest during dark hours on the NH. The corresponding statistics for the SH show no performance dependency for illumination.

The temporal matchup differences show discrete spikes, related to the satellite orbit geometry (Appendix E24). The *spatial distance* between observation and centre IASI pixel position, shows the most frequent occurrence around 14 km, with a tail towards 60 km (Appendix E25). No clear data distribution patterns are seen in distribution for neither temporal stratification nor the spatial stratification in the 8 temperature zones.

7.3 Satellite IST inter-comparison

The inter-comparison of IASI IST observations against in situ observations can only be performed for regions and periods where in situ data are available. Satellites have much larger coverage than the in situ observations and vital information can therefore be gained from comparing different satellite products against each other.

7.3.1 Level 3 data

Daily level 3 aggregated satellite fields were generated from the level 2 observations described in sections 4.1-4.3 by averaging the individual level-2 satellite products within 36 hours from the central analysis time on a regular 0.05 degree latitude and longitude grid. The aggregation also included quality control on the different products. Only Modis observations with a good sea ice surface temperature quality flag were allowed. In addition, IASI IST observations with a quality indicator for skin observation above 3 were discarded. Finally, only Metop AVHRR SST/IST observations classified as cloud free by the PPS cloud mask were included in the processing (for more details on the level 3 aggregation, see Rasmussen and Høyer, 2017).

For this study, the daily aggregated level 3 satellite products were further averaged for spatial equal area regions of ~110x110 km throughout the Arctic. The positions of the averaging regions are shown in figure 7.3.1

7.3.2 Satellite IST inter-comparison

The corresponding surface temperature time series of the different satellite products are shown in figure 7.3.2 for selected regions that were ice covered for most of the time. Note that the Metop AVHRR may appear warm during periods where the averaging regions includes both ice and open waters, such as July to September in the region from 70^{o}N. This is probably a consequence of this product including both SST and IST and MIZ observations, whereas the other products only include IST observations.

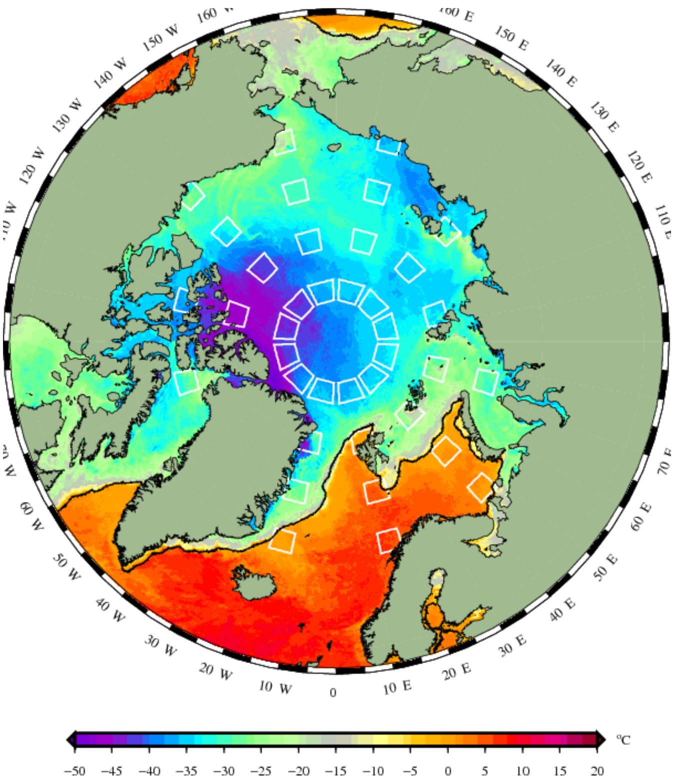

Figure 7.3.1 *Level 3 inter-comparison areas in white overlaid on a L4 SST/IST example from March. The sea ice concentration of 15 percent is the black contour.*

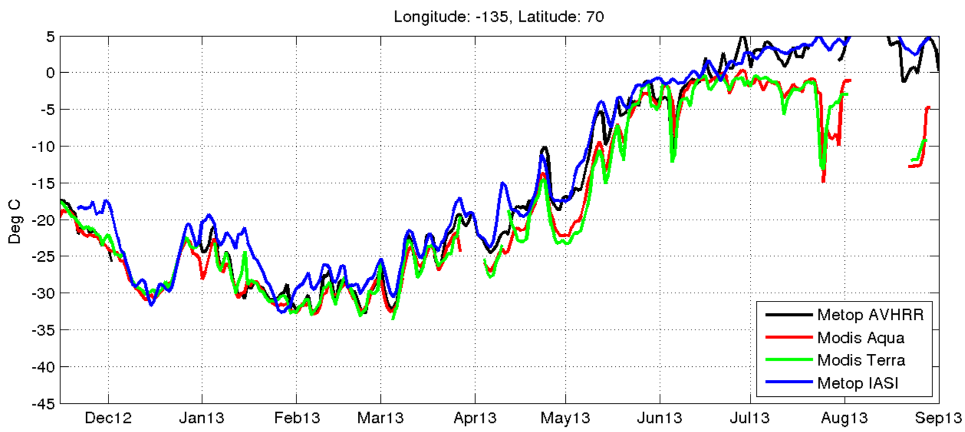

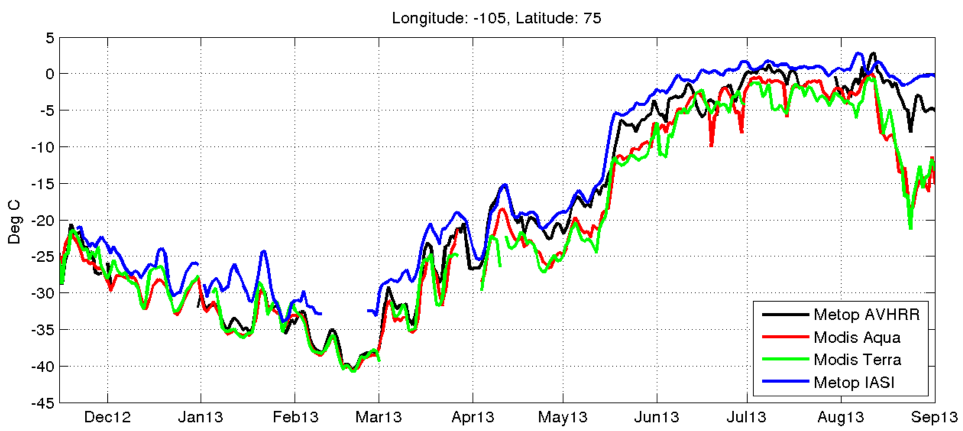

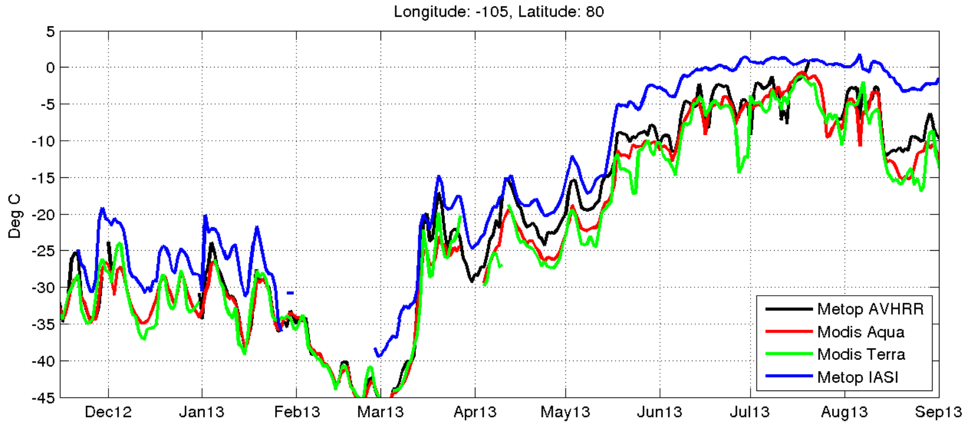
Longitude: -105, Latitude: 80
Deg C
Dec12
Jan13
Feb13
Mar13
Apr13
May13
Jun13
Jul13
Aug13
Sep13
Metop AVHRR
Modis Aqua
Modis Terra
Metop IASI

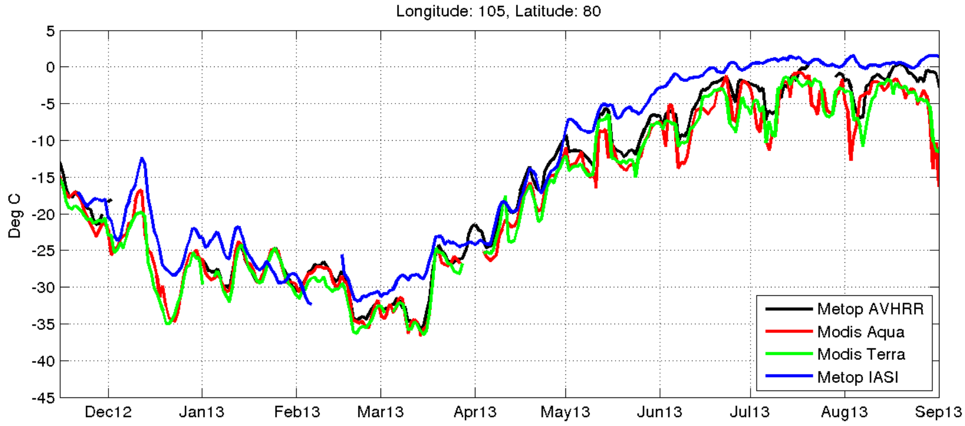
Longitude: 105, Latitude: 80
Deg C
Dec12
Jan13
Feb13
Mar13
Apr13
May13
Jun13
Jul13
Aug13
Sep13
Metop AVHRR
Modis Aqua
Modis Terra
Metop IASI

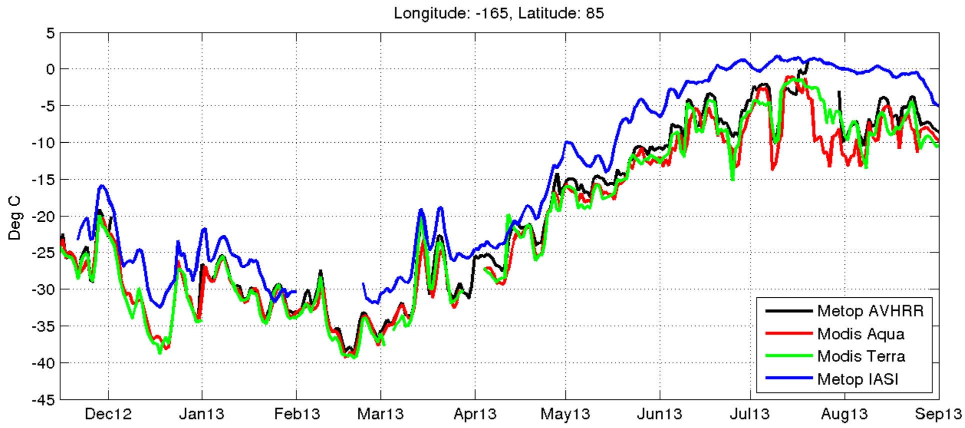
Longitude: -165, Latitude: 85
Deg C
Dec12
Jan13
Feb13
Mar13
Apr13
May13
Jun13
Jul13
Aug13
Sep13
Metop AVHRR
Modis Aqua
Modis Terra
Metop IASI

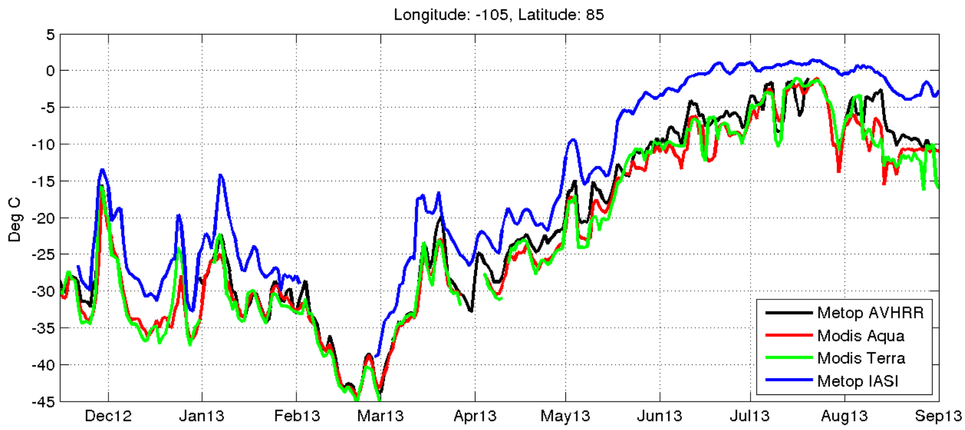
Longitude: -105, Latitude: 85
Deg C
Dec12
Jan13
Feb13
Mar13
Apr13
May13
Jun13
Jul13
Aug13
Sep13
Metop AVHRR
Modis Aqua
Modis Terra
Metop IASI

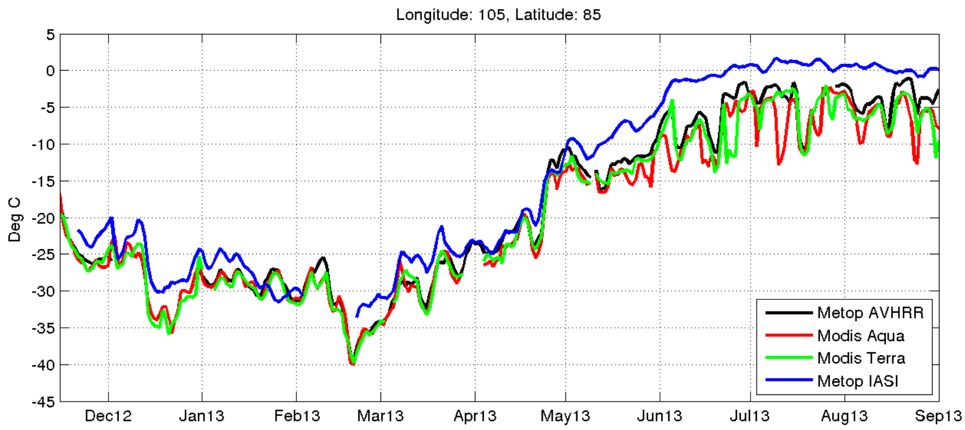

Figure 7.3.2 *Averaged Surface temperature from selected regions in figure 7.3.1. The central positions of the regions are listed in the title of each figure.*

The figures show the variations in the IST with time scales of several days. Maximum temperatures are typically reached in July and August and minimum temperatures in February. In general, all the satellite products agree on the temporal variability induced by weather events with a tendency for the IASI variability to be smaller than the Infrared satellite products. The figures also show that the IASI product displays a higher temperature for the major part of the time, compared to the purely infrared 1 km products from Metop AVHRR and Modis. An offset is evident during all seasons and occasionally exceeding 5C.

The average numbers when comparing the IASI time series against the other products are shown in table 7.3.1

Table 7.3.1 *Inter-comparison statistics of daily level 3 products for all averaging regions and for each latitude steps.*

Products	Latitude North	Number of matches	Bias	Standard deviation	Correla-tion	Root mean square diff.
IASI - Metop AVHRR	All	1425	2.8K	2.4K	0.98	3.7K
IASI – Modis Aqua	All	1585	4.5K	3.1K	0.97	5.4K
IASI – Modis Terra	All	1540	4.3K	3.0K	0.97	5.2K
IASI - Metop AVHRR	70	248	1.4K	2.1K	0.99	2.6K
IASI – Modis Aqua	70	257	3.7K	3.3K	0.97	4.9K
IASI – Modis Terra	70	246	3.6K	3.3K	0.97	4.9K
IASI - Metop AVHRR	75	491	2.4K	2.3K	0.98	3.3K
IASI – Modis Aqua	75	549	3.9K	3.1K	0.97	5.0K
IASI – Modis Terra	75	533	4.0K	3.1K	0.97	5.1K
IASI - Metop AVHRR	80	459	3.3K	2.3K	0.98	4.0K
IASI – Modis Aqua	80	521	4.9K	3.0K	0.97	5.7K
IASI – Modis Terra	80	507	4.5K	2.7K	0.98	5.2K
IASI - Metop AVHRR	85	227	4.3K	2.3K	0.98	4.9K
IASI – Modis Aqua	85	258	5.8K	2.8K	0.98	6.4K
IASI – Modis Terra	85	254	-5.4K	2.4K	0.98	6.0K

The table shows a latitudinal dependency of the performance of the IASI product, compared to the other products. The bias and standard deviation numbers are also shown in figure 7.3.3 as a function of central latitude for the averaging regions.

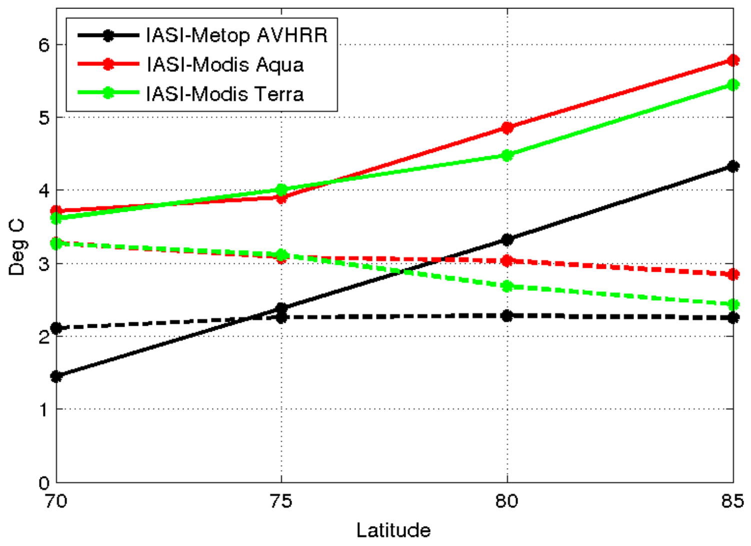

Figure 7.3.3 *Latitudinal bias (solid) and standard deviation (dashed) of the differences, when L3 IASI is compared against the other satellite L3 IR products*

The table and figure clearly show that linear latitudinal trends are seen in all the IASI inter-comparisons, with the IASI being about 2-3 degrees warmer biased at very high latitudes (85^{o}N) than at 70^{o}N compared against the other products. The standard deviations of the differences are slightly decreasing poleward for the comparison with Modis products. This points towards smaller variability for the Modis products Pole wards. The standard deviations for the IASI-Metop AVHRR comparisons do not show any latitudinal behaviour.

Note that the smallest differences, both in terms of bias and STD, in the inter-comparisons are obtained when IASI is compared against the Metop AVHRR. One explanation for the relatively good agreement could be that these instruments are placed on the same satellite, which would reduce any temporal sampling effects that might be included in the other comparisons.

Scatter plots of the L3 regionally averaged IASI IST L3 observations against the other IR products are shown in figure 7.3.4 to assess the IASI relative performance as a function of temperature.

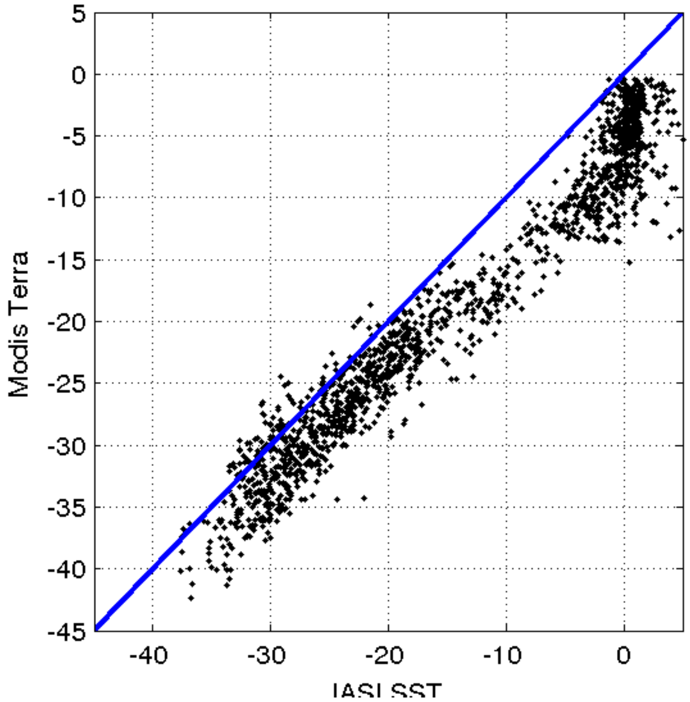

Modis Terra
IASI SST
5
0
-5
-10
-15
-20
-25
-30
-35
-40
-45
-40
-30
-20
-10
0

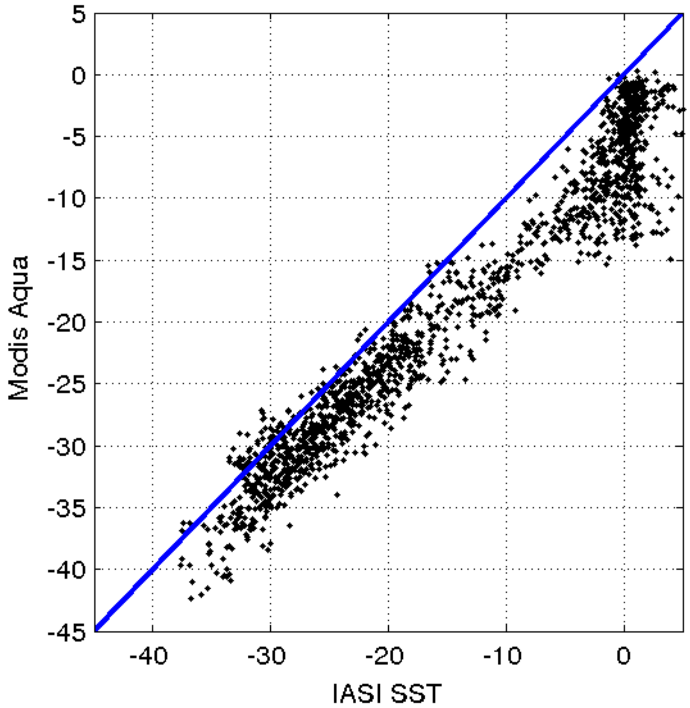

Modis Aqua
IASI SST
5
0
-5
-10
-15
-20
-25
-30
-35
-40
-45
-40
-30
-20
-10
0

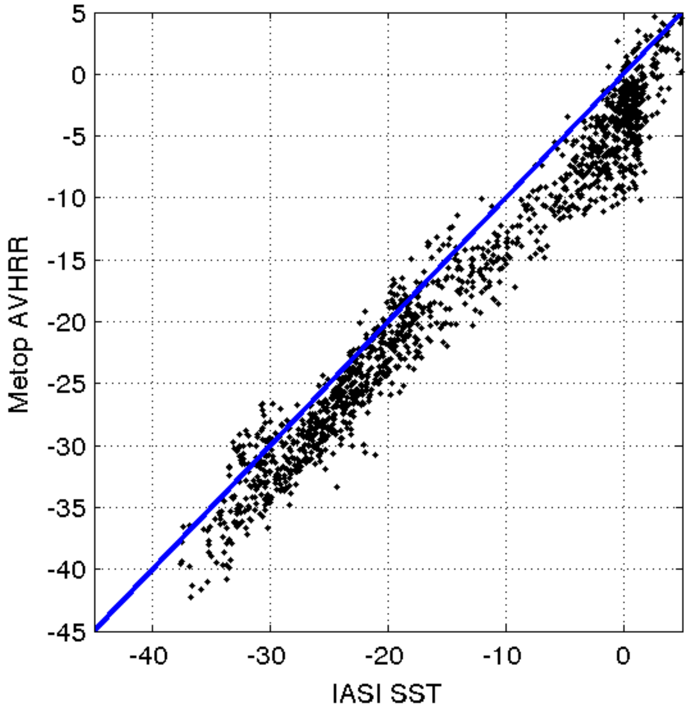

Figure 7.3.4 *Scatterplots of the L3 observations from IASI against Modis Terra (top), Modis Aqua (middle) and AVHRR (bottom). The blue lines indicate the 1:1 relationship.*

The figures show a characteristic behaviour, with a constant warm IASI for cold temperatures and a significantly warmer IASI product for IST warmer than -15°C. This pattern is seen in the inter-comparisons, which may indicate that it is can be ascribed to the IASI product or to general differences between IASI and pure IR retrievals.

In general, the level 3 inter-comparisons show that the IASI product is highly correlated with the AVHRR and Modis satellite products. There is a positive difference for all the inter-comparisons with IASI being 2-5°C warmer than the other satellite products. The variability of IASI IST is low compared to all 3 TIR products for temperatures warmer than ~7 C, thus supporting a suspicion that IASI IST is having issues when the snow is warm and wet. It is not unusual for PMW algorithm to have troubles dealing with wet snow, as discussed in chapter 6.

A warm offset (IASI relative to the other products) is present for all surface temperatures and increases with latitude. The standard deviation of the differences shows little latitudinal dependency, but there are indications that an elevated variability is found for IASI temperature around 0°C.

7.3.3 Inter-comparison with ERA-Interim

Inter-comparisons between the level-3 satellite products and the corresponding ERA-Interim T2m have also been performed for a few manually selected regions. These regions have been selected based upon an expert judgement with the aim of covering different types of atmospheric and sea ice conditions, from multiyear packed sea ice to first year level ice and for different atmospheric regimes. The figure below shows an example of the different surface temperature products for the Lincoln Sea, where the four satellite IST products are shown and where the ERA-Interim T2m has also been included.

Note that the ERA-Interim values are temporal snapshots and not averages as for the satellite products, which may explain the larger variability. It is interesting to note that the IAST IST values show a significantly better agreement with the ERA-Interim T2m value than with the other IR satellite IST products. This is a general feature for most of the regions and for periods with full ice cover. See Appendix F for more figures.

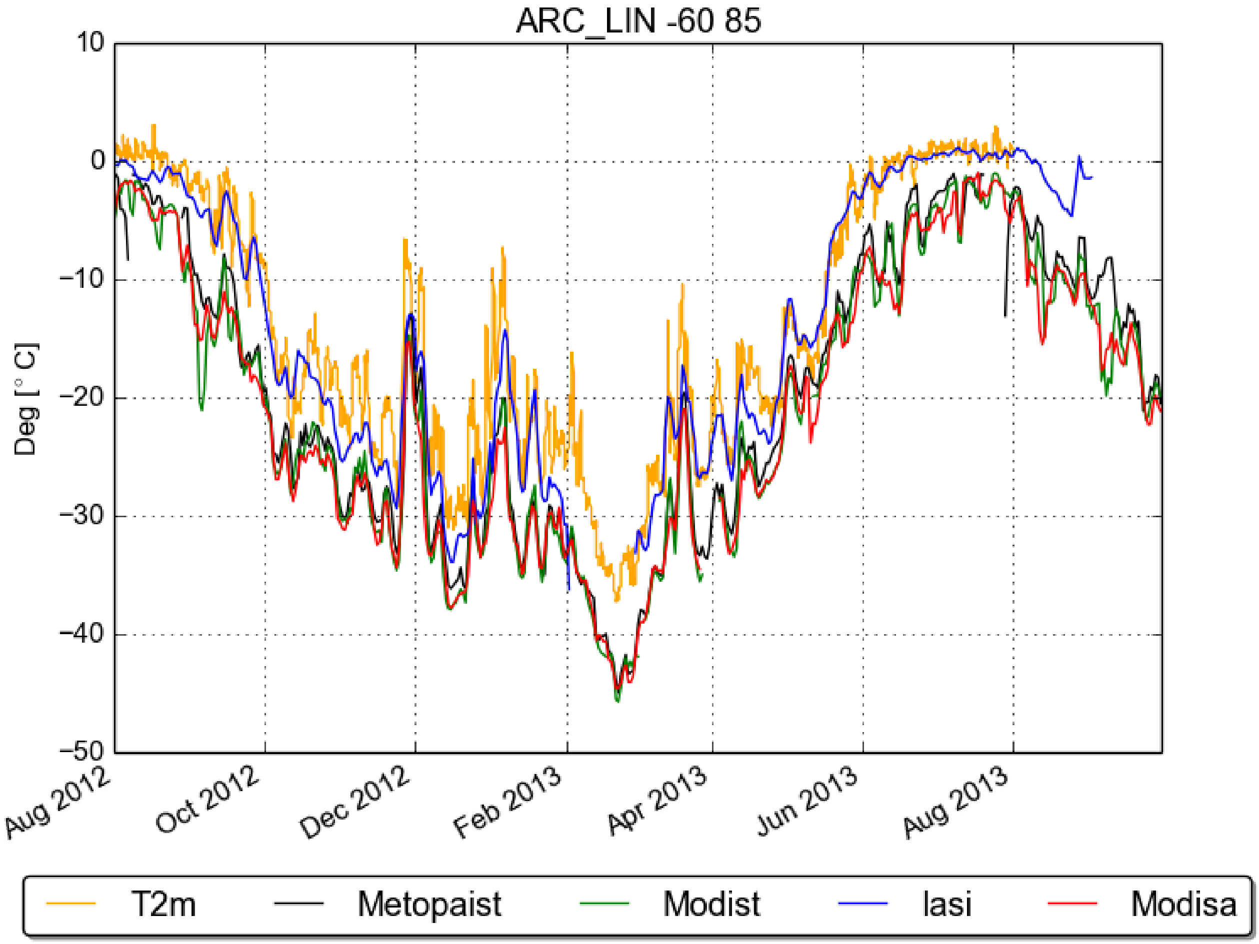

Figure 7.3.5 *Averaged satellite surface temperature and T2m from ERA-Interim from a region in the Lincoln Sea. The central positions (longitude, latitude) of the regions are listed in the title of the figure. T2m is the 3 hourly snapshot from the ERA-Interim and Metopaist is the Metop AVHRR SST/IST product.*

8 Discussion

The all-sky IASI IST product can become an important complementary contribution to existing clear-sky IST products and their applications in physical ice, ocean and atmosphere models. From this validation of the IASI IST performance, it appears that traditional Thermal Infrared IST algorithms perform better than the IASI IST, compared with in situ observations, however, TIR IST products tend to be cold biased in contrast to the IASI IST that seems to perform almost un-biased compared with reliable surface temperature observations. The low bias of the IASI IST product is likely a result of successful algorithm training, where cold biases of TIR IST data are caused by the contribution of cold cloud-top temperatures from un-detected clouds.

It was anticipated that IASI IST errors are larger than errors of TIR IST products, because passive microwave data measure an integrated temperature of a certain snow depth, rather than the actual snow surface skin temperature. The ability of the IASI IST algorithm to measure short term temperature variations and extreme warm and cold surface temperatures is therefore poor, by definition.

The study also reveals that large data volumes of reliable in situ surface temperature observations for 2012 are available from the rim of the Greenland ice sheet, from the PROMICE data set. These data are therefore very valuable for this study, and even more so, because these data are not assimilated in the NWP data that are used for training of the IASI algorithm. Consequently, we have more confidence in the Greenland ice sheet validation results and they have received more attention in this report compared with the Arctic sea ice temperature validation.

The IASI IST performance is evaluated for a wide range of environmental, spatial and temporal dependencies. The general IASI IST dependencies are identified and the results reveal that performance varies from sea ice to land ice and between the two hemispheres. In gross numbers, the IASI IST performs best against Southern Hemisphere sea ice air temperatures and worst against Northern Hemisphere Sea ice surface temperatures. This is, however, not a conclusion that should be drawn from this work, because the data volume of the SH sea ice observations is small and the representativeness is likely to be weak. Moreover, as discussed in chapter 6, the NH sea ice surface temperature measurements may be unreliable, which is substantiated from the fact that IASI IST apparently performs better against air temperatures than against surface temperatures. The conclusions based on SH surface temperature or SH sea ice air temperatures must therefore be drawn carefully, due to poor data coverage or possible weak representativeness.

From the validation table in Appendix G it is clear that the IASI IST performs well against NWP data; i.e. nearly un-biased and with relative small errors, except for the performance on the Greenland ice sheet, where errors are nearly 100 percent larger than elsewhere. A high consistency with NWP data is anticipated, because this data set is used for training of the IASI IST algorithm. The larger errors against NWP data from the Greenland ice sheet may originate from the fact that the NWP analysis for the ice sheet area is based on in situ observations from the coastal areas and not from level ice cap surfaces, thus not providing representative data for the ice cap environment for the analysis. This is in contrast to the Antarctic ice sheet air temperature NWP analysis that is produced from assimilation of the same observations used for validation in this report.

The IASI IST performance is generally worsened with higher product quality indicator values. It is possible to filter out bad quality IST data using this indicator, but at the expense of large amounts of data.

This work has identified a wide range of dependencies between product quality and other variables. The most interesting relations from chapter 7 are listed here, based on both the level 2 and level 3 match-up data:

Sea Ice:

- Level 3 analysis: IASI IST bias increases Poleward from 70 N, meaning that IASI IST becomes warmer northwards, relatively to TIR IST products. A direct latitude dependent bias is not identified in the level 2 analysis. To explain this we look into conditions that are generally different at high latitudes from the conditions at lower latitudes. At high latitudes one will generally observe lower atmospheric Water Vapour content, colder absolute temperatures, higher Sea Ice Concentration and higher sun zenith angles. From the level-2 data analysis there is no simple explanation for a latitudinal bias dependency, because higher SIC, decreasing WV content and increasing sun zenith angles seems to result in colder bias, whereas only decreasing air temperature can explain an increasing positive bias of IASI IST at higher latitudes.
- Level 3 analysis: Low variability of IASI temperatures warmer than approximately -7 C. It seems that IASI IST reaches a saturation temperature of ~0 C too early in spring, when TIR algorithms still estimate cold ice surfaces. The ERA-Interim temperatures are in agreement with the warm IASI IST, and thus confirming a well-documented positive bias of ERA-Interim in the Arctic.
- Level 3 analysis: Low diurnal and short-term variability, relative to TIR IST data, is observed. This reflects the nature of an algorithm that uses microwave sensors.
- Level 2 analysis: IASI IST is negatively biased at very dry atmosphere and positively biased at moister atmospheres for NH sea ice. The errors are also significantly smaller when the satellite data derived water vapour estimate is of high quality. No such dependency is observed for SH sea ice.
- Level 2 analysis: There seems to be no significant inter-annual IASI IST error dependency, but a cold bias during spring and a warm bias during freeze up is observed.
- Level 2 analysis: By increasing sea ice cover from 90 to 100% , representing approximately 90 % of all NH sea ice data in the match-up data set, the error is reduced and bias changes from large positive to approximately zero bias, thus indicating that the algorithm is not tuned for mixed ice and water areas.
- Level 2 analysis: A cold bias of -5.2 K is estimated from first year ice, whereas multiyear ice show a warm bias of 1.2 K and smaller errors. Properties of FYI and MYI generally differ in snow thickness and properties as well as ice thickness. These are properties that affect the PMW signal significantly and hence the estimated surface temperature, if the algorithm is not tunes specifically for the ice type in the field of view.
- Level 2 analysis: The IASI IST error is nearly independent of the absolute temperature, but bias drops rapidly from approximately 5 K at –30 C to -10 K at -15 C, thus making IASI relative warmer with decreasing absolute temperatures. This bias dependency on the

absolute temperature can be an effect from a tuning procedure that is not sufficiently stratified, as it apparently does not handle the full temperature range well.

Land Ice:

- IASI IST performance against NWP data is significantly better for SH land ice than for NH land ice, most likely due to more homogeneous conditions around SH observations sites compared with the Greenland observing locations. It is also likely that the inclusion of the Antarctic observations in the IASI algorithm training data set is causing high consistency between the data sets.
- IASI IST performs best against in situ surface temperature measurements during summer and during day light hours over Greenland, but not significant better during summer over Antarctica. The cloud test that determines the choice of algorithm performs best during daylight, which is likely to cause best IASI IST performance during light hours.
- IASI IST is warm biased for cold absolute temperatures, for both Greenland and Antarctic ice caps and compared with both surface and air temperature observations. This is also valid compared with NWP temperatures. This indicates that the algorithm training procedure is not representing the full temperature range in which it operates.
- Performance seems to be independent of time sampling of the collocated observation and satellite data. Both bias and STD are invariant inside the ±50 minutes in which the time collocation is done. At first sight this is surprising, because there is a clear temporal sampling dependency for TIR IST data, documented elsewhere. The reason for this is likely caused by the PMW algorithm that measures vertically integrated snow temperatures, to a depth where temperatures are nearly invariant to short term variations and temperature changes are delayed relative to temperature changes on the surface.
- IASI IST performs best at intermediate humid atmospheres. Errors are highest and bias is largest (negative) at very dry atmospheres. At intermediate total column WV (~10mm) the bias is zero and the error reaches its lowest level. Large errors at dry atmospheres can be a result of the fact that all MW channels usually are separable by atmospheric water content, but in dry atmospheres they are much alike and thus the PMW signatures from different bands are less pronounced. This will result in a very sensitive algorithm in dry atmospheres.
- Bias drops at positive OmC Values – i.e. IASI IST gets cold for positive OmC values and increasingly colder with higher OmC.
- There is an elevation dependent bias for the NH IASI IST. Large positive bias is seen for data at sea level, decreasing to a large negative bias at ~1500 m altitude. This effect is likely to be associated with increasing bias for humid atmospheres, which occurs at sea level. The elevation range for SH data is small and these data can neither confirm nor reject a similar elevation dependency on the Antarctic ice cap.
- The IASI IST difference from observations increases with increasing distance to observation for the Greenland ice cap data. No dependency with collocation distance is seen in the SH data. This is probably related to relative inhomogeneous areas around the Greenland land station, compared with the Antarctic land stations.

In general, the observed trends and dependencies of the IASI IST with environmental variables are more pronounced and robust when compared with land ice observations, as is the case when compared with sea ice temperature observations. There are mainly two reasons for this, namely less spatial homogeneity for the sea ice surfaces than for ice cap surfaces, caused by varying sea ice concentrations and not the least unreliably in situ surface measurements from drifting buoys. The unreliability of surface measurements from drifting buoys are mentioned in chapter 6 and illustrated in figure 8.1. Here, four Arctic drifters from the acknowledged Surface Velocity Program (SVP), are deployed within a few meters of each other's, on Arctic fast ice.

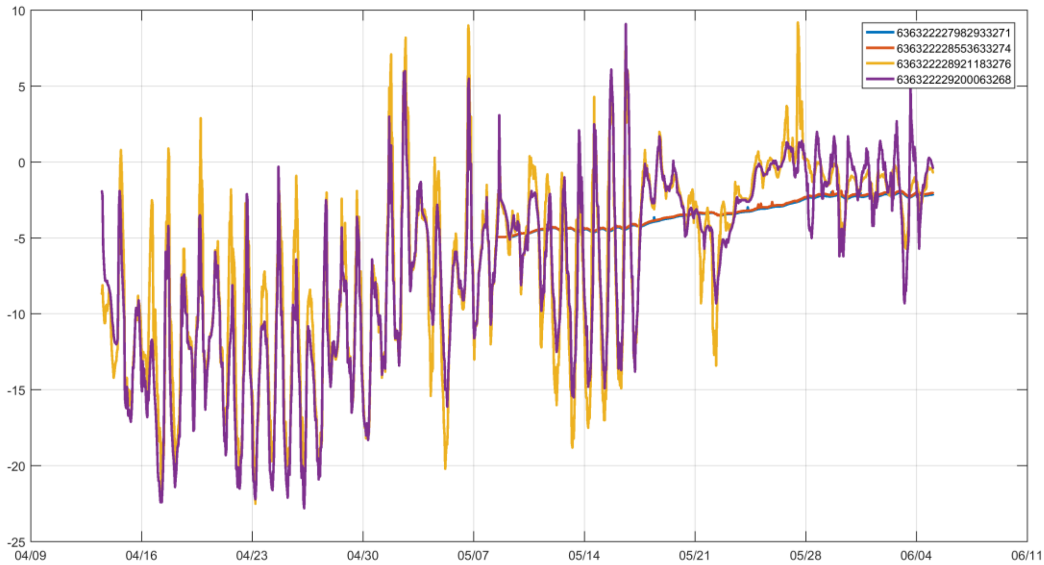

Figure 8.1 *Four identical SVN buoys deployed within a few meters on fast ice in Ingle Field Bredning in 2017. The blue and red curves (2 flat and coinciding curves warmer than -5 C) were deployed in January, with sensors partly covered by snow during the displayed period of time. The yellow and purple curves show temperatures from buoys deployed on April 12, with sensors at the snow surface until a ~10 cm snow fall occurred on May 19. and subsequent redistribution by snow drift.*

The blue and red curves (2 coinciding flat curves) show data from buoys deployed end of January 2017 and the yellow and purple curves show temperatures from buoys deployed on April 12, 2017. Two features are relevant to mark here, 1) The 2 buoys deployed in January show hardly any diurnal variability, due to snow covering the sensors, and 2) the two buoys deployed in April can differ by up to 8 degrees, due to shadows/sun effects and snow fall and drifting snow. The figure shows that four identical in situ devices in perfect working order within a few meters of each other's, can record temperatures that deviate by more than 10 K.

The issues regarding observation reliability unquestionably play a major role in the IASI IST sea ice performance statistics for the Northern Hemisphere. In order to break down the errors into observation errors and algorithm inability more work is needed. However, the error statistics for NH sea ice, as printed in Appendix G, suggest that the IASI IST quality is not adequate for ingestion in ocean and ice models, as per recommendations from Stammer et al. (2007). Here a RMSE of 4 K is recommended as threshold accuracy for IST assimilation. Based on the fact that very large sampling errors on the in situ observations are present we cannot conclude the exact error of IASI IST. A model assimilation study, using IASI IST, can reveal the true value of IASI IST in physical models.

As mentioned earlier, we have much higher faith in the surface and air temperature records from the PROMICE data records from the Greenland ice sheet and here the IASI IST performance is significantly better than for NH sea ice and improving with simple thresholding of the IST quality indicator and bringing the accuracy within threshold precision required by Stammer et al. (2007).

The results in this report also indicate that algorithm improvements can be obtained if the algorithm tuning can grasp a wider range of environmental variability.

The results presented and the considerations made here have led to a number of recommendations to improve the IASI IST algorithm, but it remains to be investigated whether these improvements can bring the product quality to a level requested for data assimilation. In any case, the IASI IST product is an interesting complementary product for existing TIR algorithms and the IASI IST should be tested as input to a mixed TIR/MW IST product and the effect in a level 4 product should subsequently be evaluated.

9 Recommendations

A minimum quality is required in order for the IASI IST to be used in numerical modelling. In a position paper from EUMETSAT, concerning model requirements, Stammer et al. (2007) mentioned that a Root Mean Square Error of 4 K is the threshold accuracy for using IST measurements in data assimilation.

In order to comply with a given threshold accuracy, distributed uncertainties must necessarily be associated with the product. The complete error budget must therefore be defined and calculated for the IASI IST product, based on the concept outlined in Chapter 6.

A range of dependencies between product accuracy and environment are documented in chapter 7 and discussed in chapter 8. These relations should be part of an uncertainties algorithm on their respective scales; e.g. dependencies for ice type and concentration, time of the year and the temperature it-selves have high impact on sea ice uncertainty. Elevation and atmospheric water vapour, has shown to be particular important for ice caps uncertainties.

It was discussed that new and more stratified algorithm training configurations should also be addressed, based on the documented dependencies, weaknesses and strength between the IASI IST product and environmental variables.

The recommendations for future developments on the IASI IST product are:

1) Define new algorithm training configuration oriented towards the identified algorithm weak spots; e.g.:
   a) Sea Ice: ice type, ice concentration, season, latitude
   b) Ice cap: Atmospheric water vapour, elevation, season,
2) Develop a complete uncertainty algorithm
   a) Provide distributed STD and BIAS estimates with the IASI IST product
3) Special issues to investigate closer
   a) The latitude dependent bias observed in the level-3 analysis
   b) The apparent lack of variability of IASI IST temperatures > -7 K in the level-3 analysis)
   c) Large errors at dry atmosphere
   d) Consider why SH sea ice performs better than NH sea ice.
   e) Consider why IASI – NWP generally match better for the SH than for NH.

The IASI surface temperature quality indicator (QI) that comes with the level 2 data stream has proved to work well as a means to filter out the largest errors, but often at the expense of large volumes of good data. A thorough review of the QI values against other environmental variables should be analysed further and more systematic, than attempted in chapter 7.2.3 and 7.2.4. In this way it may be possible to get a handle on good data that otherwise are filtered out by their QI value. However, a well-functioning uncertainty algorithm should be able to cope with that, and the uncertainties them-selves should be the single means for data filtering.

Finally, it is also recommended to flag the algorithm choice for future product versions, i.e. flag if the cloud tests activate the pure TIR algorithm rather than the mixed TIR and PMW algorithm. It is interesting to evaluate the effect of applying PMW data in the surface temperature estimate, because of large penetration depth of PWM data in snow and ice.

References

Collins, N., G. Theurich, C. DeLuca, M. Suarez, Trayanov A, V. Balaji, P. Li, W. Yang, and C. Hill. Design and implementation fo components in the earth system modeling framework. International Journal of High Performance Computing Applications, 19(3), 2004. doi: doi:10.1177/1094342005056120.

Dee, D. P., S. M. Uppalaa, . J.-N. Thepauta and F. Vitarta. The ERA-Interim reanalysis: configuration and performance of the data assimilation system. Q. J. R. Meteorol. Soc. 137: 553–597, April 2011 A.

Dybkjær, G., R. Tonboe, and J. Høyer, 2012: Arctic surface temperatures from Metop AVHRR compared to in situ ocean and land data, Ocean Sci. Discuss., 9, 1009–1043, 2012, www.ocean-sci.net/8/959/2012/, doi: 10.5194/os-8-959-2012

Hall, D.K., J. Key, K.A. Casey, G.A. Riggs and D. Cavalieri, 2004: "Sea ice surface temperature product from the Moderate Resolution Imaging Spectroradiometer (MODIS),"IEEE Transactions on Geoscience and Remote Sensing, 42:1076-1087.

Hall, D. K. and G. A. Riggs. 2015. MODIS/Aqua Sea Ice Extent 5-Min L2 Swath 1km, Version 6. [Indicate subset used]. Boulder, Colorado USA. NASA National Snow and Ice Data Center Distributed Active Archive Center. DOI: http://dx.doi.org/10.5067/MODIS/MYD29.006.

Jakobson, E., T. Vihma, T. Palo, L. Jakobson, H. Keernik, and J. Jaagus (2012), Validation of atmospheric reanalyses over the central Arctic Ocean, Geophys. Res. Lett., 39, L10802, doi:10.1029/2012GL051591.

Kauker, F., T. Kaminski , R. Ricker , L. Toudal-Pedersen , G. Dybkjaer , C. Melsheimer , S. Eastwood , H. Sumata , M. Karcher and R. Gerdes. Seasonal sea ice predictions for the Arctic based on assimilation of remotely sensed observations. The Cryosphere Discuss., 9, 5521–5554, 2015, doi:10.5194/tcd-9-5521-2015

Key, J. R., Collins, J. B., Fowler, C., and Stone, R. S. High-Latitude Surface Temperature Estimates from Thermal Satellite Data. Remote Sens. Environ., 61, 302–309, 1997.

Lüpkes, C., T. Vihma, E. Jakobson, G. König-Langlo, and A. Tetzlaff (2010), Meteorological observa-tions from ship cruises during summer to the central Arctic: A comparison with reanalysis data, Geophys. Res. Lett., 37, L09810, doi:10.1029/2010GL042724.

Rasmussen, Till.A.S. and Jacob L. Høyer. Assimilation of sea ice surface temperatures in a coupled ocean and sea ice model. Globtemperature user case No. 3 Del. 3.1, 2017

Riggs, George A., Dorothy K Hall, and Vincent V Salomonson. Modis sea ice products user guide to collection 5. NSIDC: Boulder, CO, USA, 2006.

SVP. http://www.metocean.com/products/metocean-systems/current-monitoring/svp

Stammer, D., Johanessen, J., LeTraon, P.-Y., Minnett, P., Roquet, H., and Srokosz, M.: Requirements for Ocean Observations Rel-evant to post-EPS, EUMETSAT Position Paper: AEG Ocean To-pography and Ocean Imaging, 10 January 2007, version 3, 2007.

Appendix A: In situ data format

In situ data files are available by FTP: ftp.dmi.dk/iasi_ist

In total, 134 date files are available in netCDF format with uniform structure. An example of the structure is outlined here, for the PROMICE station Upernavik Upper Station.

```
netcdf PROMICE_UPE_U_2009H {
dimensions:
    obs = UNLIMITED ; // (52968 currently)
    trajectory = 1 ;
    strlen = 9 ;
    termistor_level = 8 ;
variables:
    int trajectory_index(obs) ;
        trajectory_index:long_name = "which trajectory this obs belongs to" ;
        trajectory_index:instance_dimension = "trajectory" ;
    char call_sign(trajectory, strlen) ;
        call_sign:long_name = "Trajectory ID string" ;
        call_sign:cf_role = "trajectory_id" ;
    double time(obs) ;
        time:long_name = "time" ;
        time:standard_name = "time" ;
        time:units = "days since 1970-01-01 00:00:00" ;
        time:axis = "T" ;
    float lat(obs) ;
        lat:long_name = "latitude" ;
        lat:standard_name = "latitude" ;
        lat:units = "degrees_north" ;
    float lon(obs) ;
        lon:long_name = "longitude" ;
        lon:standard_name = "longitude" ;
        lon:units = "degrees_east" ;
    float TA(obs) ;
        TA:long_name = "Air temperature at mast_height (2.7 m when no snow is present)" ;
        TA:standard_name = "air_temperature" ;
        TA:units = "Celsius" ;
        TA:_FillValue = -999.f ;
        TA:coordinates = "time lat lon" ;
    float PR(obs) ;
        PR:long_name = "Air pressure at mast_height (2.7 m when no snow is present)" ;
        PR:standard_name = "air_pressure_at_sea_level" ;
        PR:units = "Pa" ;
        PR:_FillValue = -999.f ;
        PR:coordinates = "time lat lon" ;
    float HUR(obs) ;
        HUR:long_name = "Relative humidity at mast_height (2.7 m when no snow is present)" ;
        HUR:standard_name = "relative_humidity" ;
        HUR:units = "1" ;
        HUR:_FillValue = -999.f ;
        HUR:coordinates = "time lat lon" ;
    float FF(obs) ;
        FF:long_name = "Mean wind speed at 40 cm above mast_height" ;
        FF:standard_name = "wind_speed" ;
        FF:units = "m s-1" ;
        FF:_FillValue = -999.f ;
        FF:coordinates = "time lat lon" ;
    float DD(obs) ;
        DD:long_name = "Wind direction at 40 cm above mast height" ;
        DD:standard_name = "wind_from_direction" ;
        DD:units = "degree" ;
        DD:_FillValue = -999.f ;
        DD:coordinates = "time lat lon" ;
```

```
    float LWd(obs) ;
        LWd:long_name = "Surface longwave radiation downwards at 10 cm above mast_height" ;
        LWd:standard_name = "surface_downwelling_longwave_flux_in_air" ;
        LWd:units = "W m-2" ;
        LWd:_FillValue = -999.f ;
        LWd:coordinates = "time lat lon" ;
    float LWu(obs) ;
        LWu:long_name = "Surface longwave radiation upwards at 10 cm above mast_height" ;
        LWu:standard_name = "surface_upwelling_longwave_flux_in_air" ;
        LWu:units = "W m-2" ;
        LWu:_FillValue = -999.f ;
        LWu:coordinates = "time lat lon" ;
    float SWd(obs) ;
        SWd:long_name = "Surface shortwave radiation downwards at 10 cm above mast_height" ;
        SWd:standard_name = "surface_downwelling_shortwave_flux_in_air" ;
        SWd:units = "W m-2" ;
        SWd:_FillValue = -999.f ;
        SWd:coordinates = "time lat lon" ;
    float SWu(obs) ;
        SWu:long_name = "Surface shortwave radiation upwards at 10 cm above mast_height" ;
        SWu:standard_name = "surface_upwelling_shortwave_flux_in_air" ;
        SWu:units = "W m-2" ;
        SWu:_FillValue = -999.f ;
        SWu:coordinates = "time lat lon" ;
    float IST(obs, termistor_level) ;
        IST:long_name = "Ice Temperature from thermistors, depth: 1,2,3,4,5,6,7 and 10 m depth at installation " ;
        IST:standard_name = "ice_temperature" ;
        IST:units = "Celsius" ;
        IST:_FillValue = -999.f ;
        IST:coordinates = "time lat lon" ;
    float mast_height(obs) ;
        mast_height:long_name = "Height of sensor boom (2.7 m when no snow is present)" ;
        mast_height:standard_name = ;
        mast_height:units = "m" ;
        mast_height:_FillValue = -999.f ;
        mast_height:coordinates = "time lat lon" ;
    float IT(obs) ;
        IT:long_name = "Surface Snow Temperature calculated from radiation assuming black body. Standard deviation = 0.5C" ;
        IT:standard_name = "surface_temperature" ;
        IT:units = "Celsius" ;
        IT:_FillValue = -999.f ;
        IT:coordinates = "time lat lon" ;
    float CL(obs) ;
        CL:long_name = "Cloud cover fraction estimated from longwave radiation / near-surface air temperature relations" ;
        CL:standard_name = ;
        CL:units = "1" ;
        CL:_FillValue = -999.f ;
        CL:coordinates = "time lat lon" ;
    float Albedo(obs) ;
        Albedo:long_name = "Surface albedo calculated when solar radiation hits the sensor at angles larger than 20 degrees" ;
        Albedo:standard_name = ;
        Albedo:units = "1" ;
        Albedo:_FillValue = -999.f ;
        Albedo:coordinates = "time lat lon" ;

// global attributes:
        :featureType = "trajectory" ;
        :title = "PROMICE Automatic Weather Station Data" ;
        :abstract = "Near-surface meteorological data from stations on the Greenland Ice Sheet" ;
        :institution = "Geological Survey of Denmark and Greenland (GEUS)" ;
        :contact = "DVA (at) geus.dk" ;
        :PI_name = "Dirk Van As" ;
        :Conventions = "CF-1.6" ;
        :activity_type = " " ;
        :topiccategory = "ClimatologyMeteorologyAtmosphere" ;
        :keywords = "Atmospheric and land ice Observation Temperature Pressure" ;
        :gcmd_keywords = "Atmosphere > Atmospheric Pressure > Surface Pressure\n",
          "Atmosphere > Atmospheric Temperature > Surface Air Temperature\n",
          "Cryosphere > Snow/Ice > Snow/Ice Temperature" ;
        :project_name = "ACCESS" ;
```

```
        :area = "Northern Hemisphere" ;
        :product_name = "PROMICE" ;
        :distribution_statement = "Free with acknowledgements" ;
        :history = "2016-04-11 Inclusion in EUSTACE dataset, reformatting and visual quality control, pne@dmi.dk\n",
          "Thermistor data included, but not quality controlled. May contain errors!" ;
        :southernmost_latitude = "72.89.f" ;
        :northernmost_latitude = "72.89.f" ;
        :westernmost_longitude = "-53.55.f" ;
        :easternmost_longitude = "-53.55.f" ;
        :start_date = "2009-08-18 00:00:00 UTC" ;
        :stop_date = "2015-09-02 23:00:00 UTC" ;
        :original_file_name = "UPE_U_hour_v02.txt" ;
}
```

Appendix B: Match-Up data description

The Match-Up data files are organised as 1 file per in situ platform. Each file contains 53* columns with the information listed here:

(* PROMICE MU data contains 54 columns, see below)

- col: 1+2 buoy date and time as: yyy-mm-dd hh:mm:ss
- col: 3 buoy latitude
- col: 4 buoy longitude
- col: 5 buoy skin temperature (K)
- col: 6 buoy air temperature (K)
- col: 7 buoy air pressure (hpa)
- col: 8+9 satellite date and time as: yyy-mm-dd hh:mm:ss (time from central scanline)
- col: 10 satellite latitude
- col: 11 satellite longitude
- col: 12 satellite surface temperature
- col: 13 satellite surface temperature quality
- col: 14 satellite total column water vapour (mm)
- col: 15 satellite total column water vapour quality
- col: 16 Cloud cover signal. Predicted Observation Minus Calculated assuming clear-sky (see PW3.README).
- col: 17 satellite land fraction inside pixel (percent, from)
- col: 18 elevation in meters
- col: 19 sun zenith angle
- col: 20 satellite zenith angle = scan angle
- col: 21 distance in km between buoy position and satellite coordinate
- col: 22 absolute time difference (minutes) between buoy time stamp and satellite time stamp
- col: 23 ice concentration in per cent (osisaf) - closest to in situ observation
- col: 24+25 nwp date and time as: yyy-mm-dd hh:mm:ss of NWP prognosis closest to in situ observation (see prognosis length below)
- col: 26 nwp latitude
- col: 27 nwp longitude
- col: 28 nwp skin temperature (K)
- col: 29 nwp air temperature (K)
- col: 30 nwp wind speed in 10m closest nwptime minus 3hours

(sqrt(Ucomponent*Ucomponent+Vcomponent*Vcomponent))

- col: 31 nwp wind speed in 10m closest nwptime minus 2hours (sqrt(Ucomponent*Ucomponent+Vcomponent*Vcomponent))
- col: 32 nwp wind speed in 10m closest nwptime minus 1hours (sqrt(Ucomponent*Ucomponent+Vcomponent*Vcomponent))
- col: 33 nwp wind speed in 10m closest nwptime (sqrt(Ucomponent*Ucomponent+Vcomponent*Vcomponent))
- col: 34 nwp wind speed in 10m closest nwptime plus 1hours (sqrt(Ucomponent*Ucomponent+Vcomponent*Vcomponent))
- col: 35 nwp wind speed in 10m closest nwptime plus 2hours (sqrt(Ucomponent*Ucomponent+Vcomponent*Vcomponent))
- col: 36 nwp wind speed in 10m closest nwptime plus 3hours (sqrt(Ucomponent*Ucomponent+Vcomponent*Vcomponent))
- col: 37 The prognosis length of the closest (in time) NWP data.
- col: 38 absolute time difference (minutes) between NWP time stamp and satellite time stamp.
- col: 39 satellite surface temperature, average area value (matrix is defined by 'dslice', 3x3)
- col: 40 satellite surface temperature, max area value (matrix is defined by 'dslice', 3x3)
- col: 41 satellite surface temperature, min area value (matrix is defined by 'dslice', 3x3)
- col: 42 satellite surface temperature, std area value (matrix is defined by 'dslice', 3x3)
- col: 43 satellite surface temperature quality, average area value (matrix is defined by 'dslice', 3x3)
- col: 44 satellite surface temperature quality, max area value (matrix is defined by 'dslice', 3x3)
- col: 45 satellite surface temperature quality, min area value (matrix is defined by 'dslice', 3x3)

- col: 46 satellite surface temperature quality, std area value (matrix is defined by 'dslice', 3x3)
- col: 47 Cloud cover signal (OMC), average area value (matrix is defined by 'dslice', 3x3)
- col: 48 Cloud cover signal (OMC), max area value (matrix is defined by 'dslice', 3x3)
- col: 49 Cloud cover signal (OMC), min area value (matrix is defined by 'dslice', 3x3)
- col: 50 Cloud cover signal (OMC), std area value (matrix is defined by 'dslice' 3x3)
- col: 51 Input insitu filename
- col: 52 Input iasi ist filename
- col: 53 Input nwp filename
- col: 54 Cloud cover fraction estimated from longwave radiation / near-surface air temperature relations (COL 54 - ONLY FOR PROMICE DATA)

Appendix C: In situ data inventory

Table C1 *Data inventory for in situ and airborne observations, 2012.*

Name of dataset	Location	Temporal resolution	Ongoing	Air temperature sensor height	Uncertainty of air temperature	Surface temperature	Distribution
AMRC	Antarctica	10 minutes	Yes	3 m - may vary with snow cover	AWS quality, assessed to 0.5C	-	Free with acknowledgements
ARM	Alaska	1 minute	Yes	2 m	AWS quality, assessed to 1C	Radiometer	Free with acknowledgements
ECMWF dribu	Arctic and Antarctic sea ice	Varying hours - days	Yes	About 1.5 m	AWS quality, assessed to 1.5C	SST sensor	Contact ECMWF
IceBridge IAKST1B and IAKMET1B	Arctic and Antarctic land and sea ice	0.1 – 1 second	Yes, until launch of IceSat-2	-	-	Radiometer (airborne)	Free with acknowledgements
IABP	Arctic sea ice	1 hour	Yes	Unknown	Assessed to 1C	Unknown	Free
NAACOS	Arctic sea ice	6 hour	No	Close to surface	Median of top 5 thermistor sensors, no radiation shield, assessed to 3C	Thermistor	Contact DMI
PROMICE	Greenland	1 hour	Yes	0-2.7 m, varies with snow cover	AWS quality, assessed to 0.5C	Calculated from radiation	Free with acknowledgements
WMO, GTS weather station	Greenland and Antarctica	3 hour	Yes	Assumed 2 m	AWS quality, not assessed	-	Free

Table C2 *Data filters for sea ice in situ and airborne observations.*

Matchup column number (see Appendix B)	Parameter	Limits
17	Land fraction	≤ 1%
18	Elevation	≤ 10 m
5, 6, 12	In-situ and satellite temperature	≤ 0°C
23	Ice concentration	≥ 30%
7	Air pressure	Northern hemisphere: ≥ 980 hPa Southern hemisphere ≥ 940 hPa
13	Satellite surface temperature quality	≥ 0
15	Satellite total column water vapour quality	0 to 4
16	OMC Cloud cover signal	-40 to 10

Appendix D: Land Ice supplementary figures

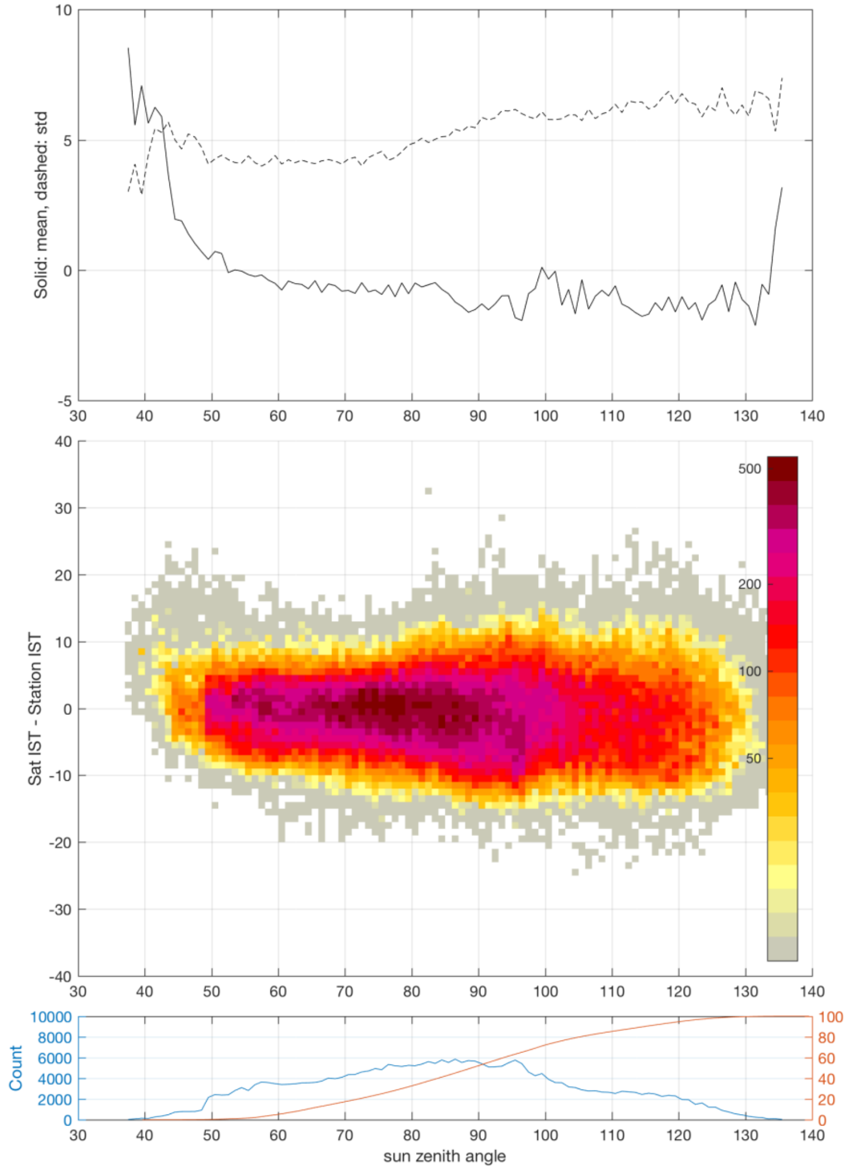

Figure D1 *Distribution and statistics on satellite IST – station IST differences as a function of sun zenith angle for the northern hemisphere. Top is mean (solid line) and standard deviation (dotted line), centre is a 2D histogram of the data distribution and bottom is data count per 1 degree bin for sun zenith angle (blue, left axis) and cumulated percentage of data count (red, right axis).*

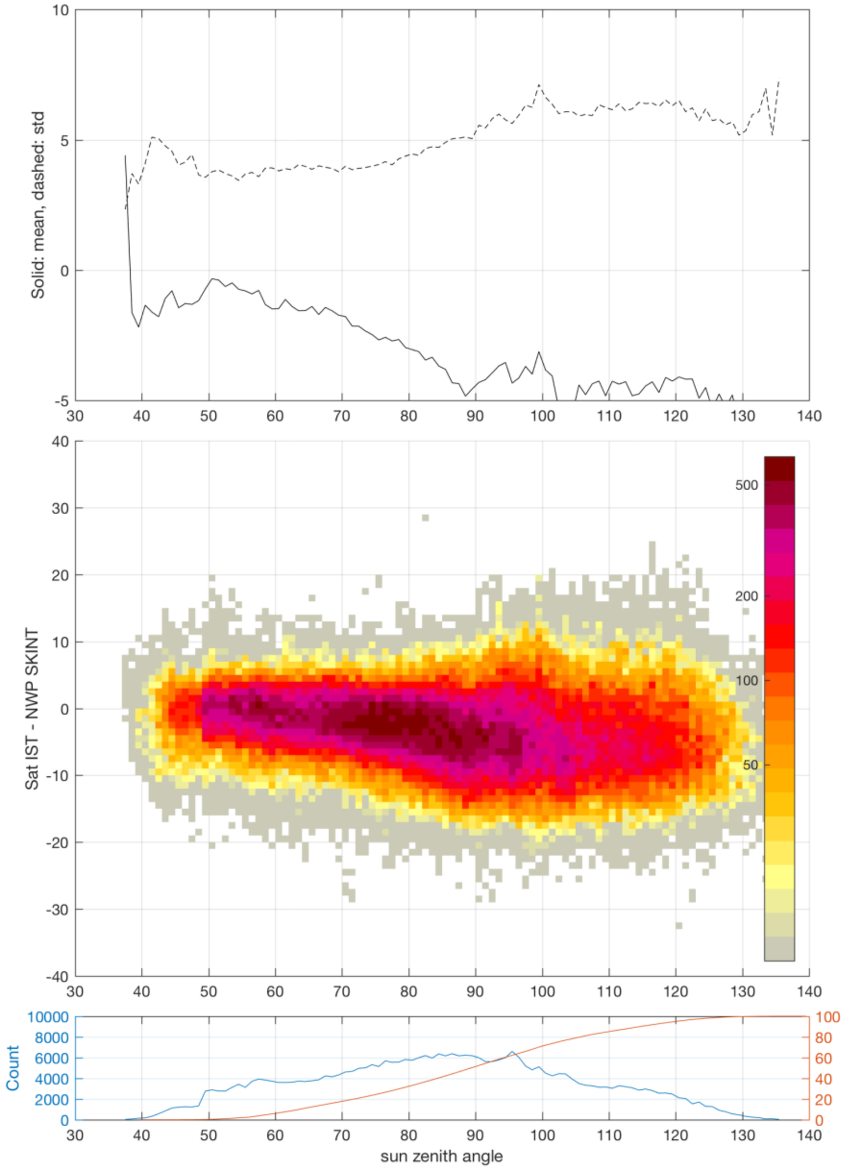

Figure D2 *Distribution and statistics on satellite IST – NWP SKIN temperature differences as a function of sun zenith angle for the northern hemisphere. Top is mean (solid line) and standard deviation (dotted line), centre is a 2D histogram of the data distribution and bottom is data count per 1 degree bin for sun zenith angle (blue, left axis) and cumulated percentage of data count (red, right axis).*

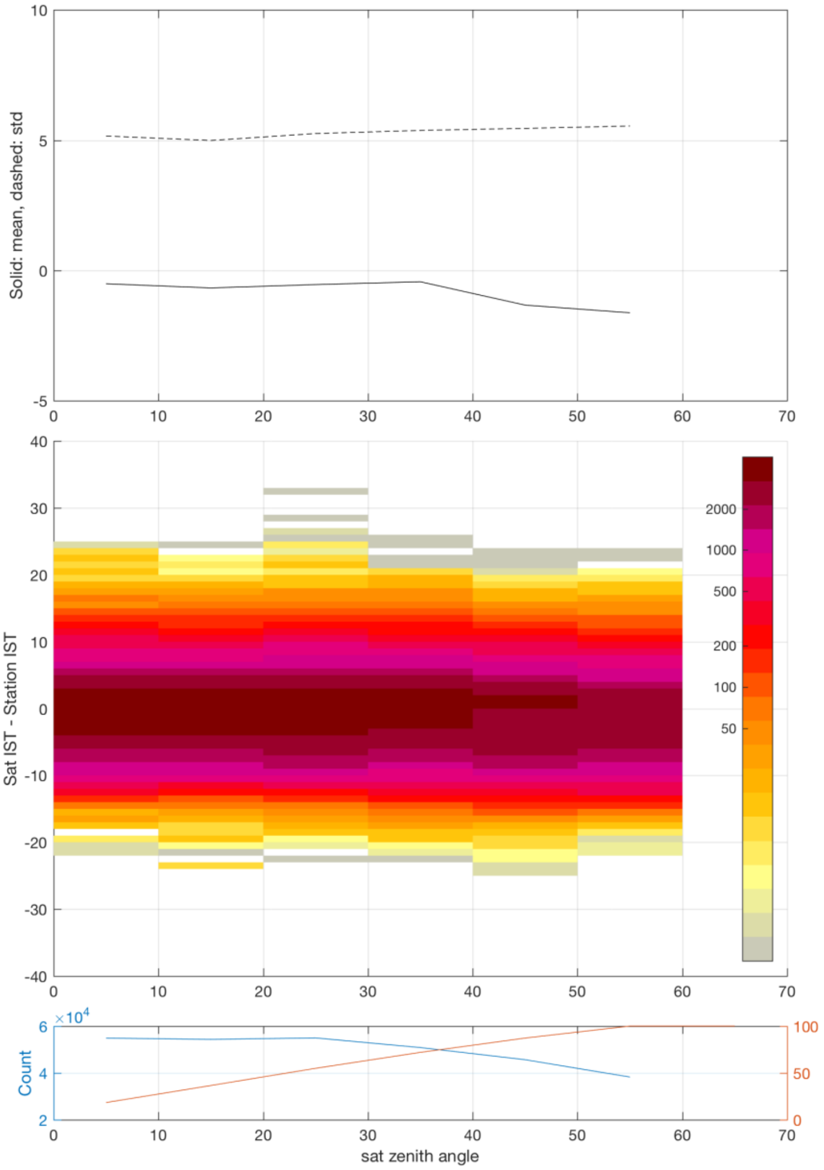

Figure D3 *Distribution and statistics on satellite IST – station IST differences as a function of satellite zenith angle for the northern hemisphere. Top is mean (solid line) and standard deviation (dotted line), centre is a 2D histogram of the data distribution and bottom is data count per 10 degree bin for sun zenith angle (blue, left axis) and cumulated percentage of data count (red, right axis).*

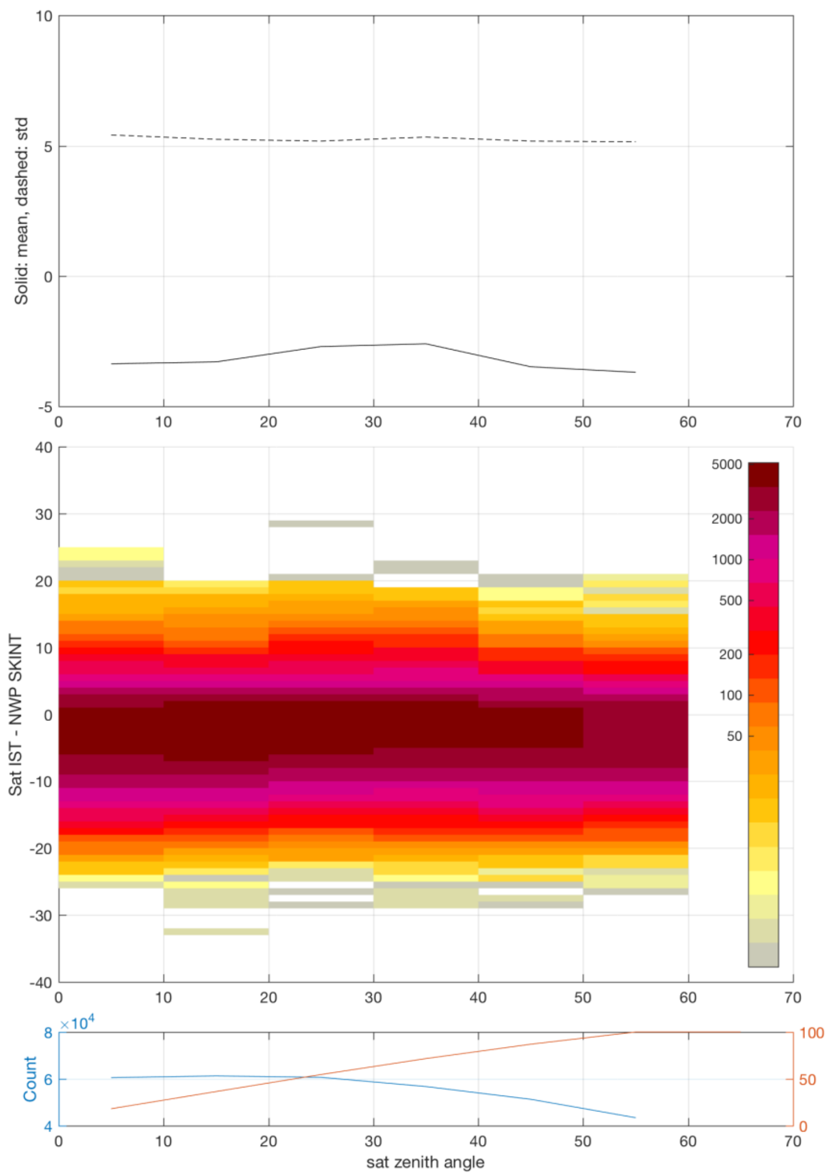

Figure D4 *Distribution and statistics on satellite IST – NWP SKIN temperature differences as a function of satellite zenith angle for the northern hemisphere. Top is mean (solid line) and standard deviation (dotted line), centre is a 2D histogram of the data distribution and bottom is data count per 10 degree bin for satellite zenith angle (blue, left axis) and cumulated percentage of data count (red, right axis).*

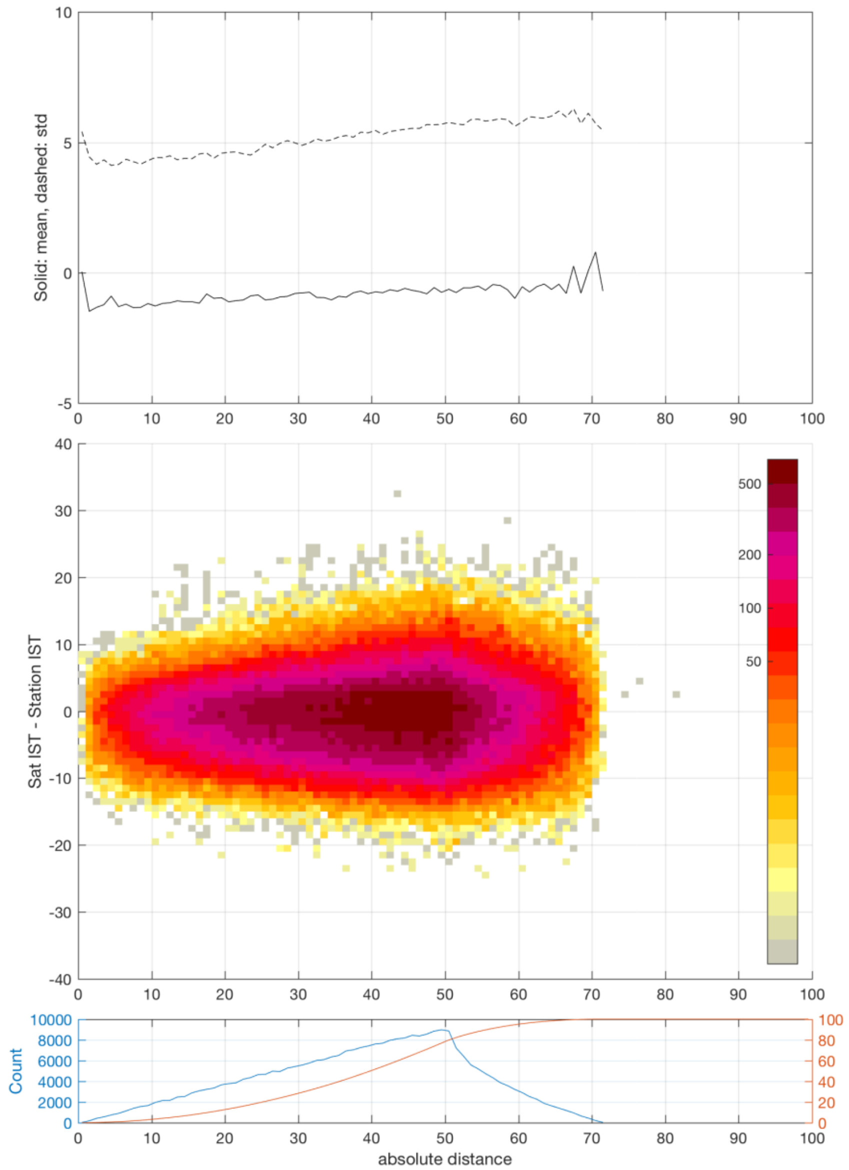

Figure D5 *Distribution and statistics on satellite IST – station IST differences as a function of absolute distance for the northern hemisphere. Top is mean (solid line) and standard deviation (dotted line), centre is a 2D histogram of the data distribution and bottom is data count per 1km bin for absolute distance (blue, left axis) and cumulated percentage of data count (red, right axis).*

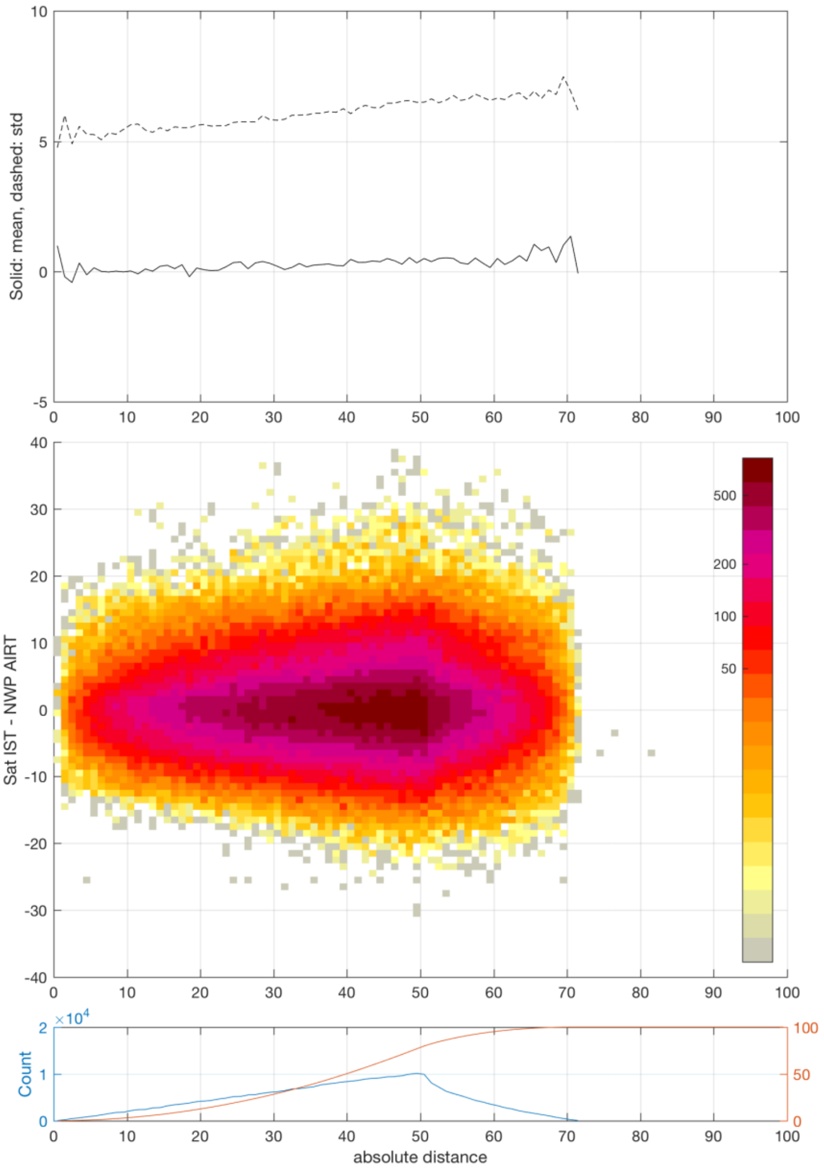

Figure D6 *Distribution and statistics on satellite IST – NWP SKIN temperature differences as a function of absolute distance for the northern hemisphere. Top is mean (solid line) and standard deviation (dotted line), centre is a 2D histogram of the data distribution and bottom is data count per 1km bin for absolute distance (blue, left axis) and cumulated percentage of data count (red, right axis).*

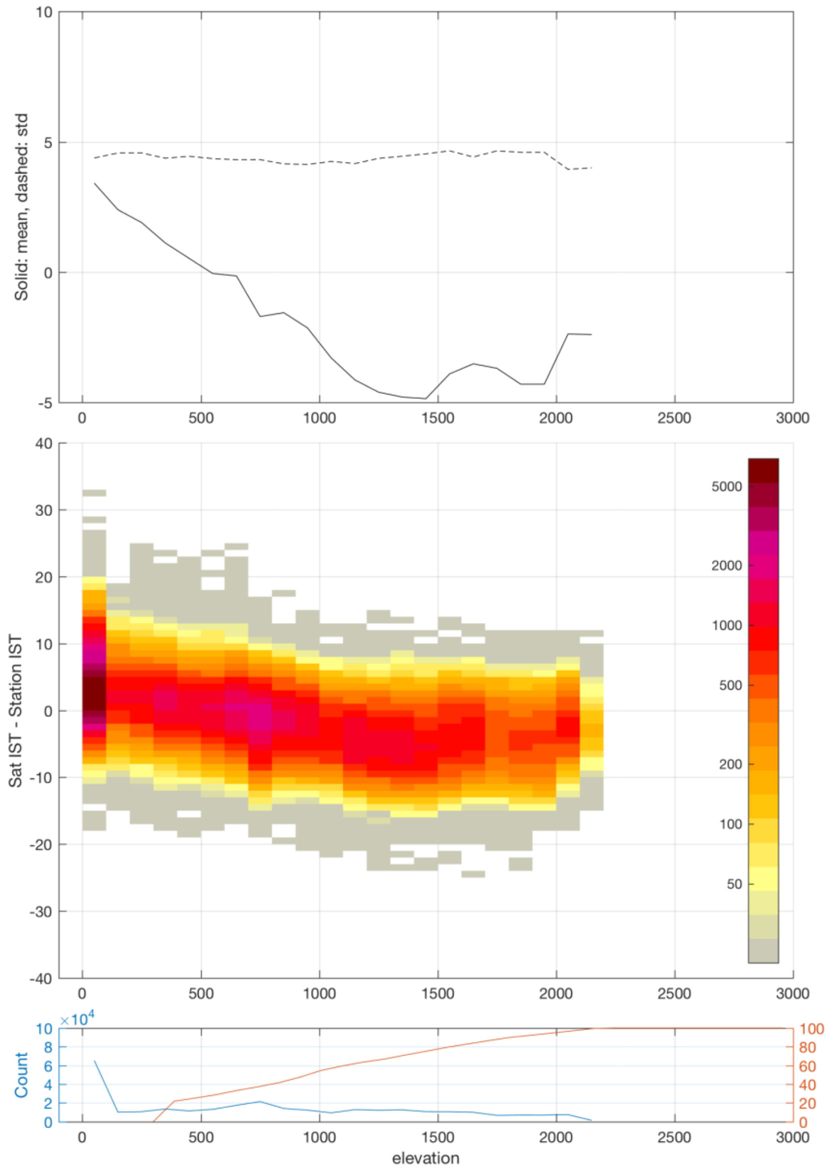

Figure D7 *Distribution and statistics on satellite IST – station IST differences as a function of elevation for the northern hemisphere. Top is mean (solid line) and standard deviation (dotted line), centre is a 2D histogram of the data distribution and bottom is data count per 100 m bin for elevation (blue, left axis) and cumulated percentage of data count (red, right axis).*

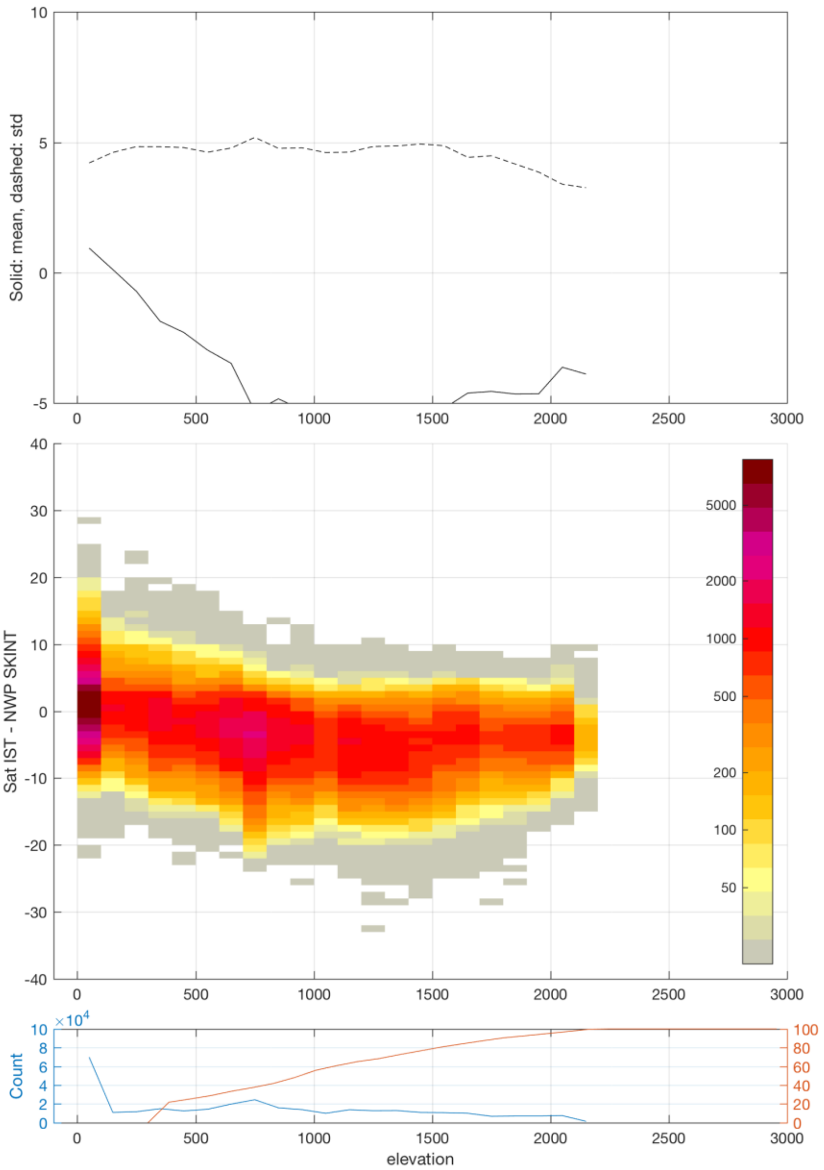

Figure D8 *Distribution and statistics on satellite IST – NWP SKIN temperature differences as a function of elevation for the northern hemisphere. Top is mean (solid line) and standard deviation (dotted line), centre is a 2D histogram of* the data distribution and bottom is data count per 100 m bin for elevation (blue, left axis) and cumulated percentage of data count (red, right axis).*

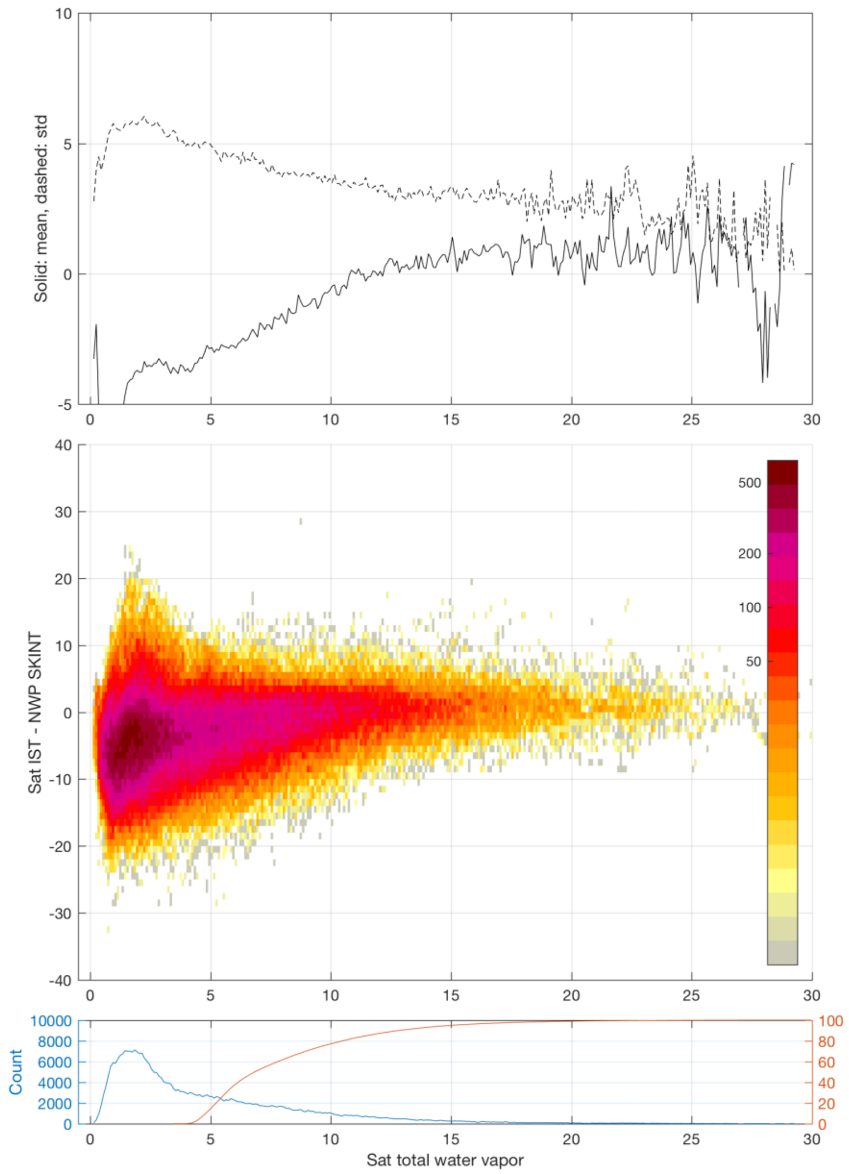

Figure D9 *Distribution and statistics on satellite IST – NWP SKIN temperature differences as a function of water vapor for the northern hemisphere. Top is mean (solid line) and standard deviation (dotted line), centre is a 2D histogram of the data distribution and bottom is data count per 0.1mm bin for water vapour (blue, left axis) and cumulated percentage of data count (red, right axis).*

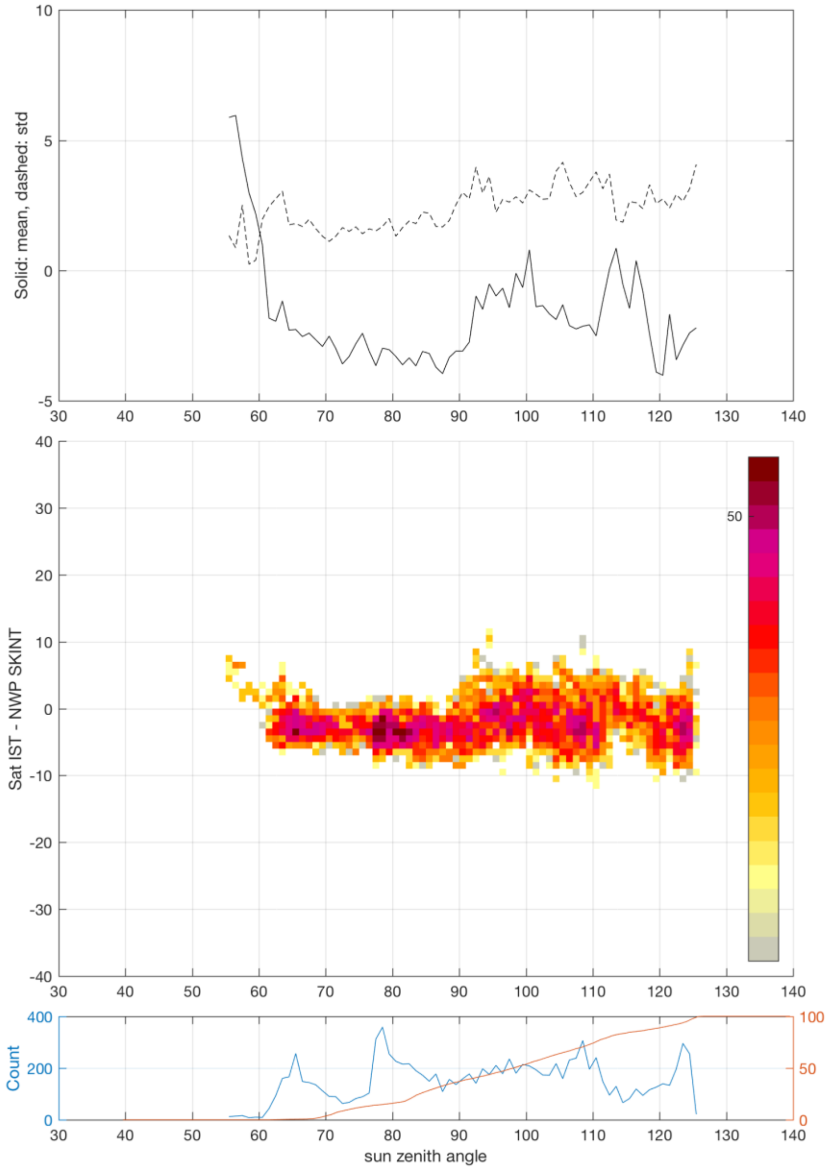

Figure D10 *Distribution and statistics on satellite IST – NWP SKIN temperature differences as a function of sun zenith angle for the southern hemisphere. Top is mean (solid line) and standard deviation (dotted line), centre is a 2D histogram of the data distribution and bottom is data count per 1 degree bin for sun zenith angle (blue, left axis) and cumulated percentage of data count (red, right axis).*

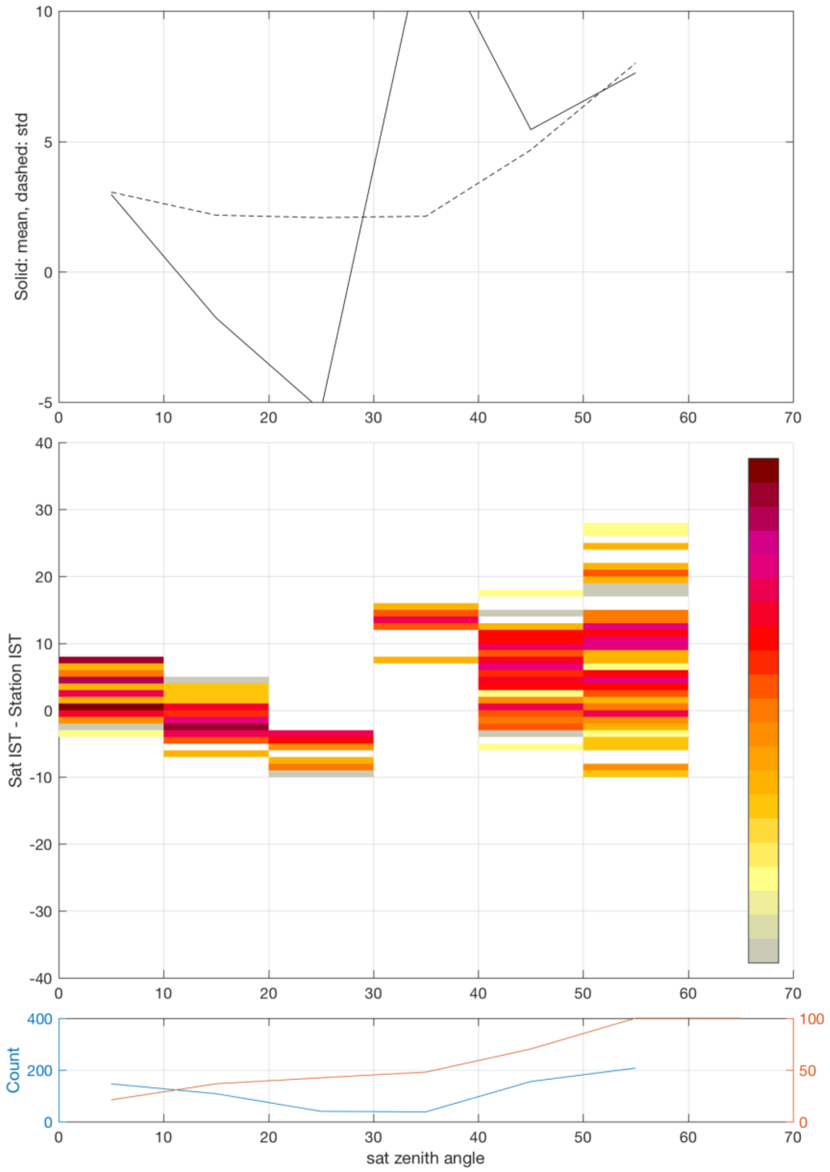

Figure D11 *Distribution and statistics on satellite IST – station IST differences as a function of satellite zenith angle for the southern hemisphere. Top is mean (solid line) and standard deviation (dotted line), centre is a 2D histogram of the data distribution and bottom is data count per 10 degree bin for sun zenith angle (blue, left axis) and cumulated percentage of data count (red, right axis).*

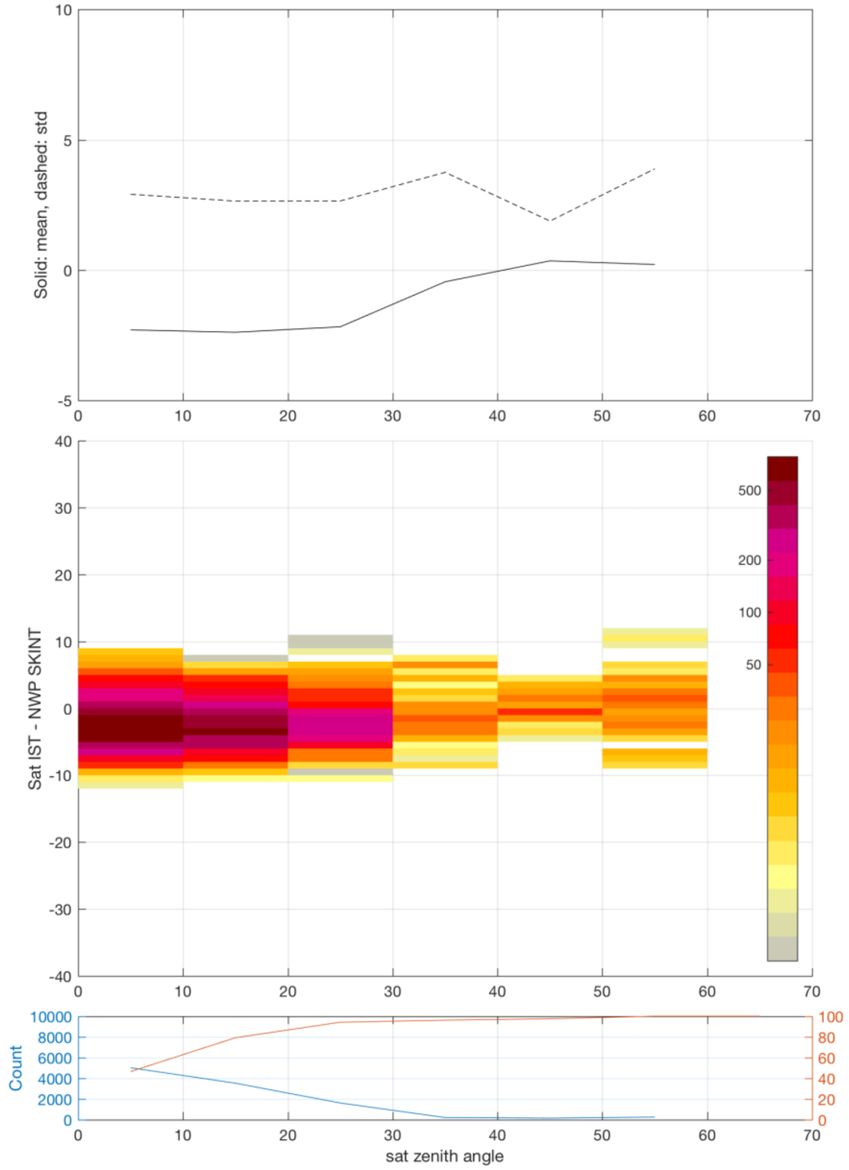

Figure D12 *Distribution and statistics on satellite IST – NWP SKIN temperature differences as a function of satellite zenith angle for the southern hemisphere. Top is mean (solid line) and standard deviation (dotted line), centre is a 2D histogram of the data distribution and bottom is data count per 10 degree bin for sun zenith angle (blue, left axis) and cumulated percentage of data count (red, right axis).*

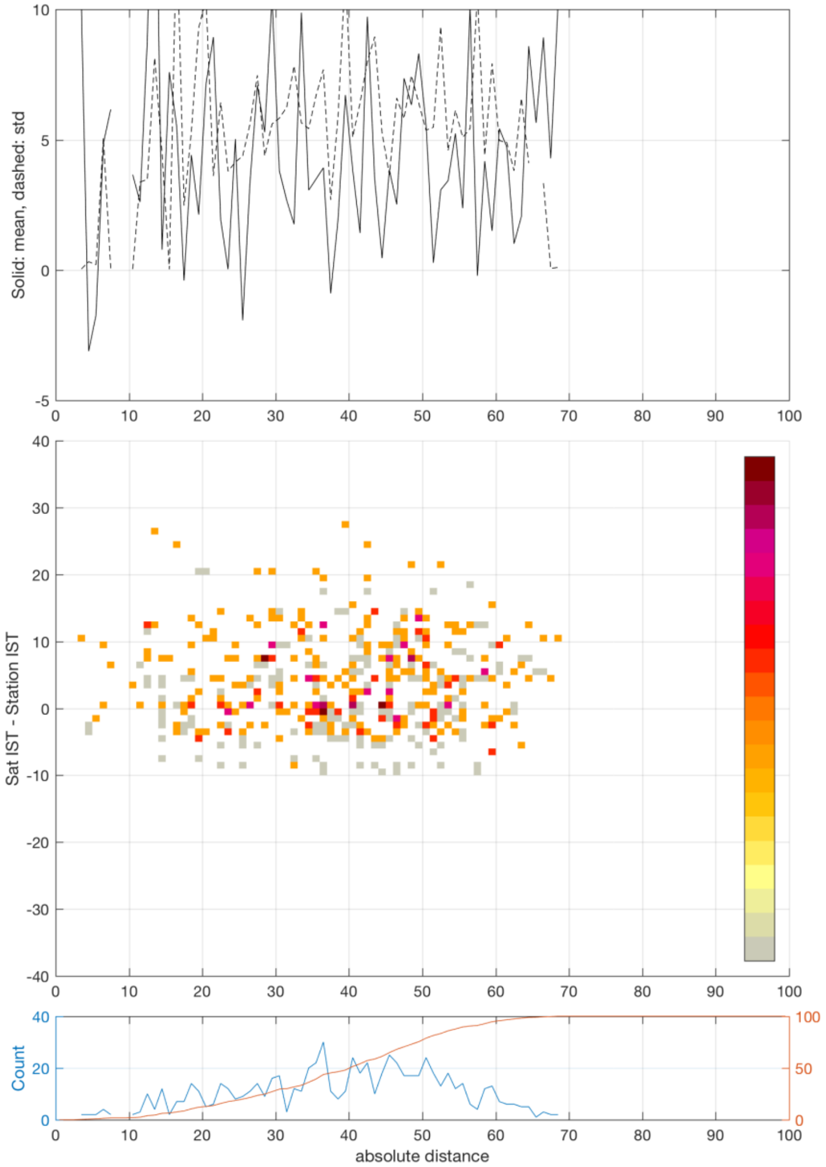

Figure D13 *Distribution and statistics on satellite IST – station IST differences as a function of absolute distance for the southern hemisphere. Top is mean (solid line) and standard deviation (dotted line), centre is a 2D histogram of the data distribution and bottom is data count per 1km bin for absolute distance (blue, left axis) and cumulated percentage of data count (red, right axis).*

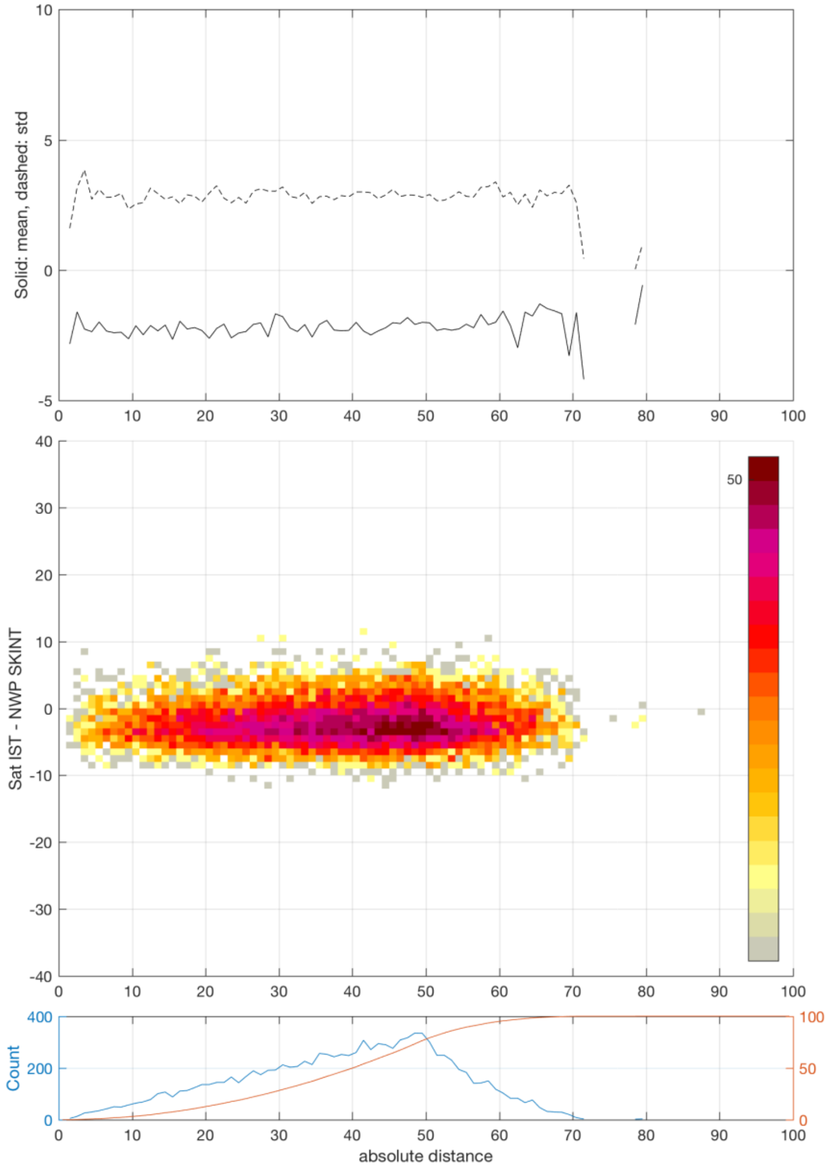

Figure D14 *Distribution and statistics on satellite IST – NWP SKIN temperature differences as a function of absolute distance for the southern hemisphere. Top is mean (solid line) and standard deviation (dotted line), centre is a 2D histogram of the data distribution and bottom is data count per 1km bin for absolute distance (blue, left axis) and cumulated percentage of data count (red, right axis).*

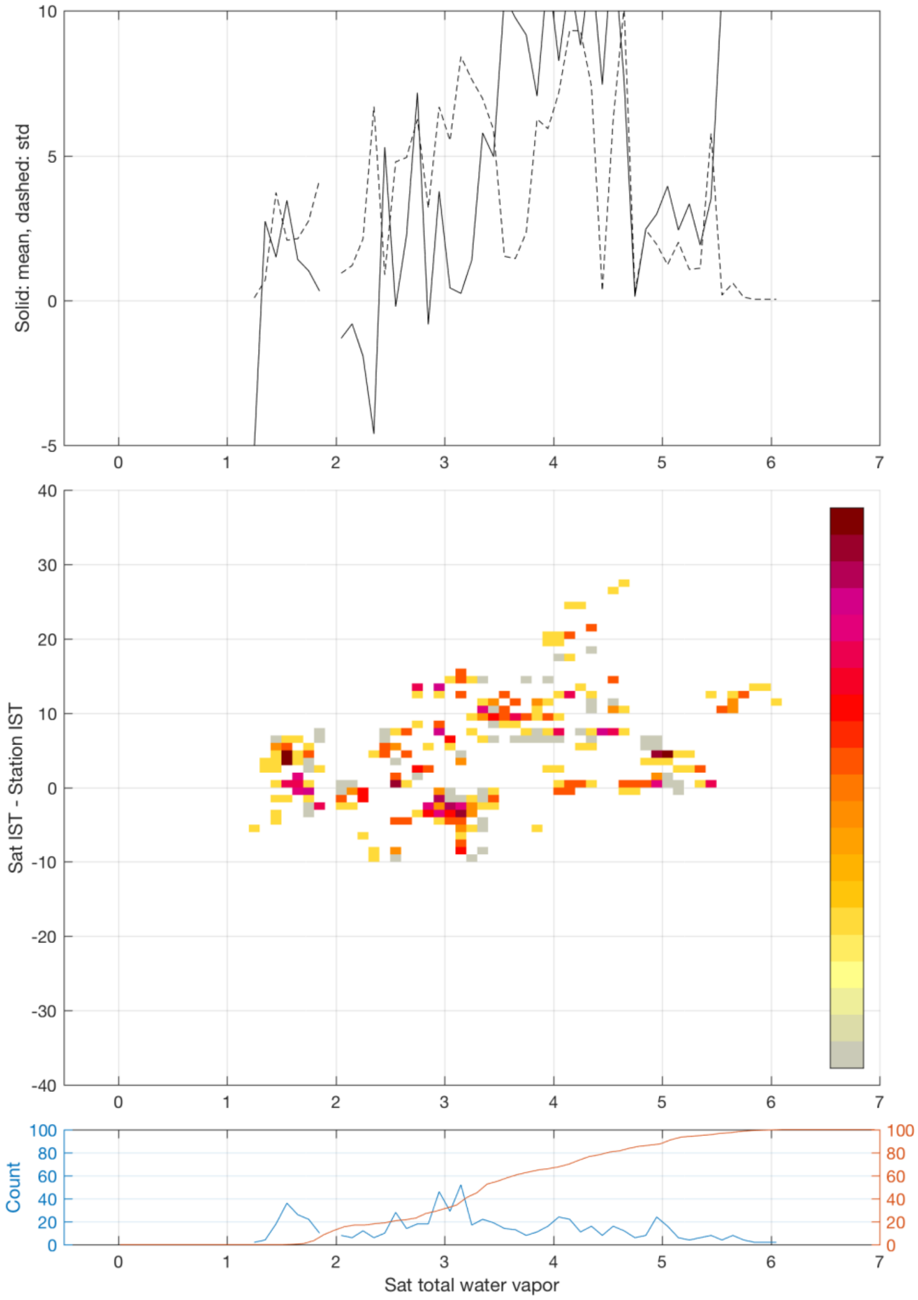

Figure D15 *Distribution and statistics on satellite IST – station IST temperature differences as a function of water vapour for the southern hemisphere. Top is mean (solid line) and standard deviation (dotted line), centre is a 2D histogram of the data distribution and bottom is data count per 0.1mm bin for water vapour (blue, left axis) and cumulated percentage of data count (red, right axis*

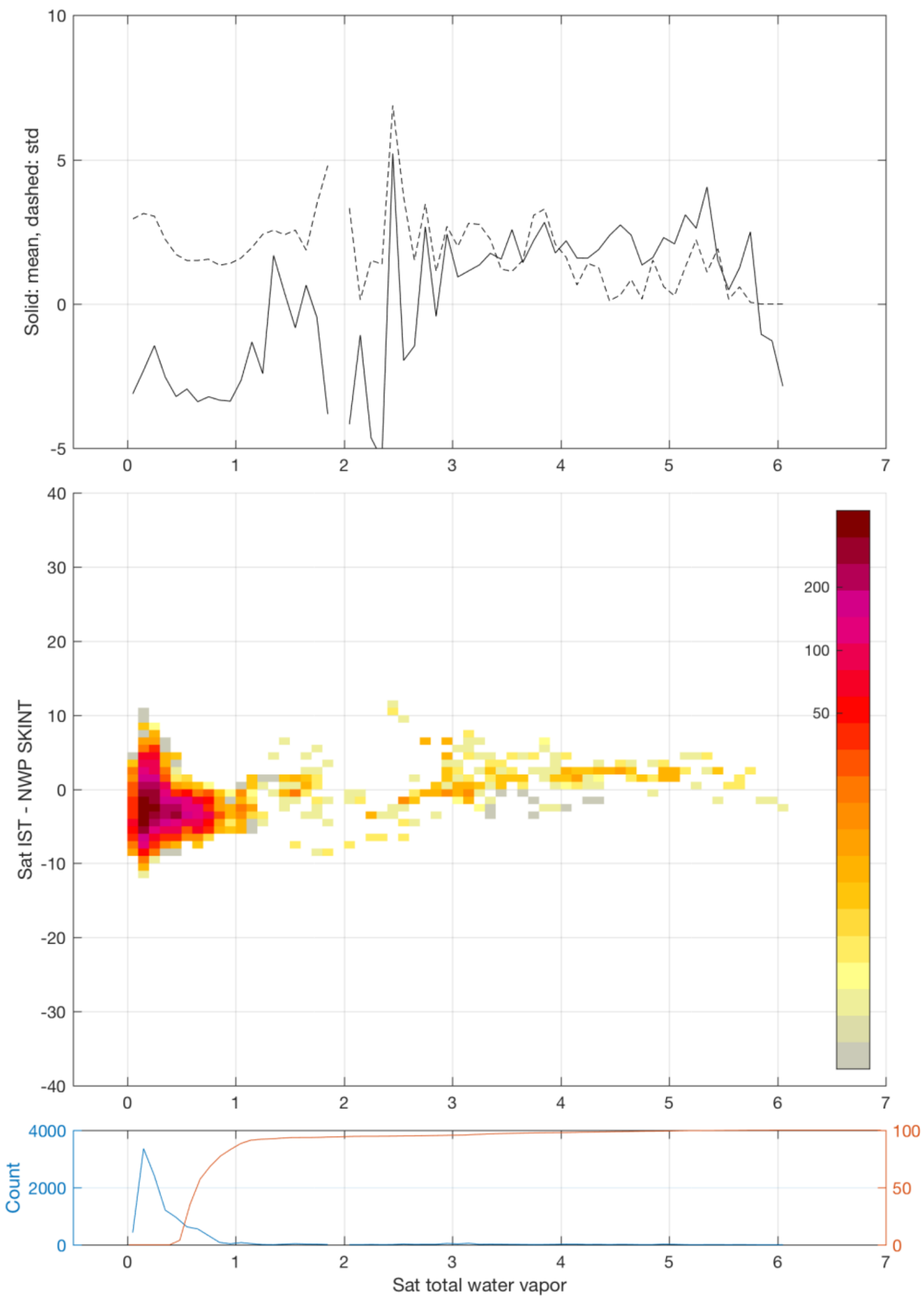

Figure D16 *Distribution and statistics on satellite IST – NWP SKIN temperature differences as a function of water vapour for the southern hemisphere. Top is mean (solid line) and standard deviation (dotted line), centre is a 2D histogram of the data distribution and bottom is data count per 0.1mm bin for water vapour (blue, left axis) and cumulated percentage of data count (red, right axis)*

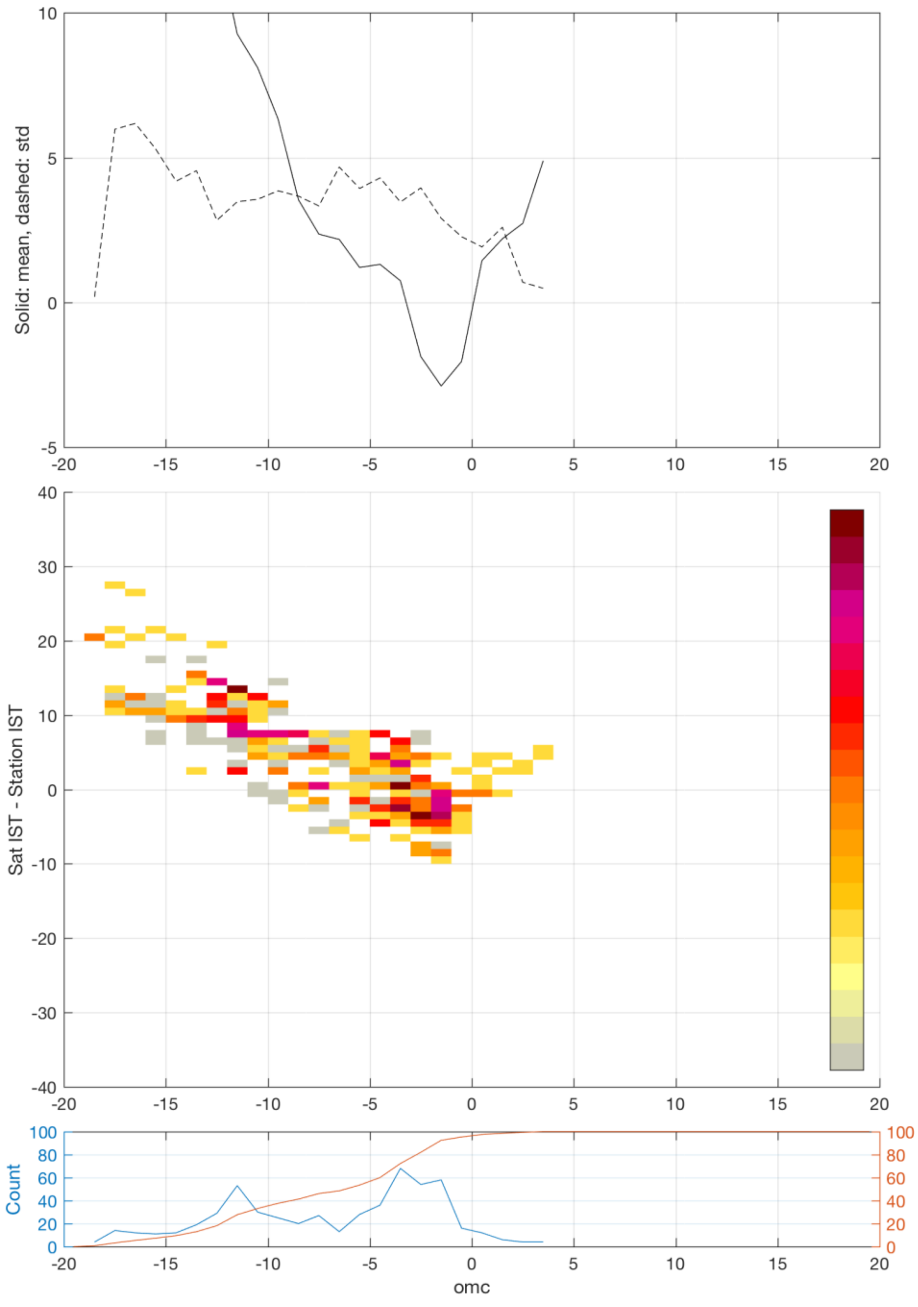

Figure D17 *Distribution and statistics on satellite IST – station IST differences as a function of OmC for the southern hemisphere. Top is mean (solid line) and standard deviation (dotted line), centre is a 2D histogram of the data distribu-*

tion and bottom is data count per 1 OmC unit bin (blue, left axis) and cumulated percentage of data count (red, right axis).

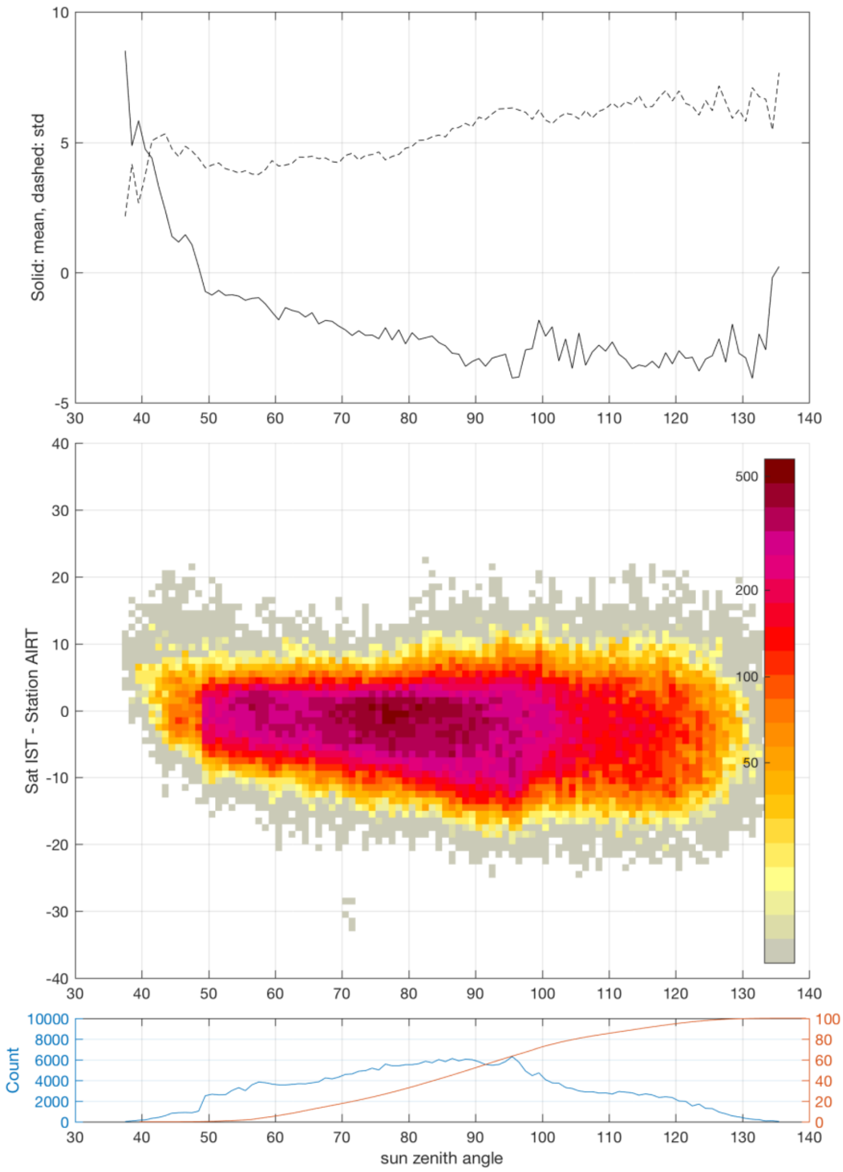

Figure D18 *Distribution and statistics on satellite IST – station AIRT temperature differences as a function of sun zenith angle for the northern hemisphere. Top is mean (solid line) and standard deviation (dotted line), centre is a 2D histogram of the data distribution and bottom is data count per 1 degree bin for sun zenith angle (blue, left axis) and cumulated percentage of data count (red, right axis).*

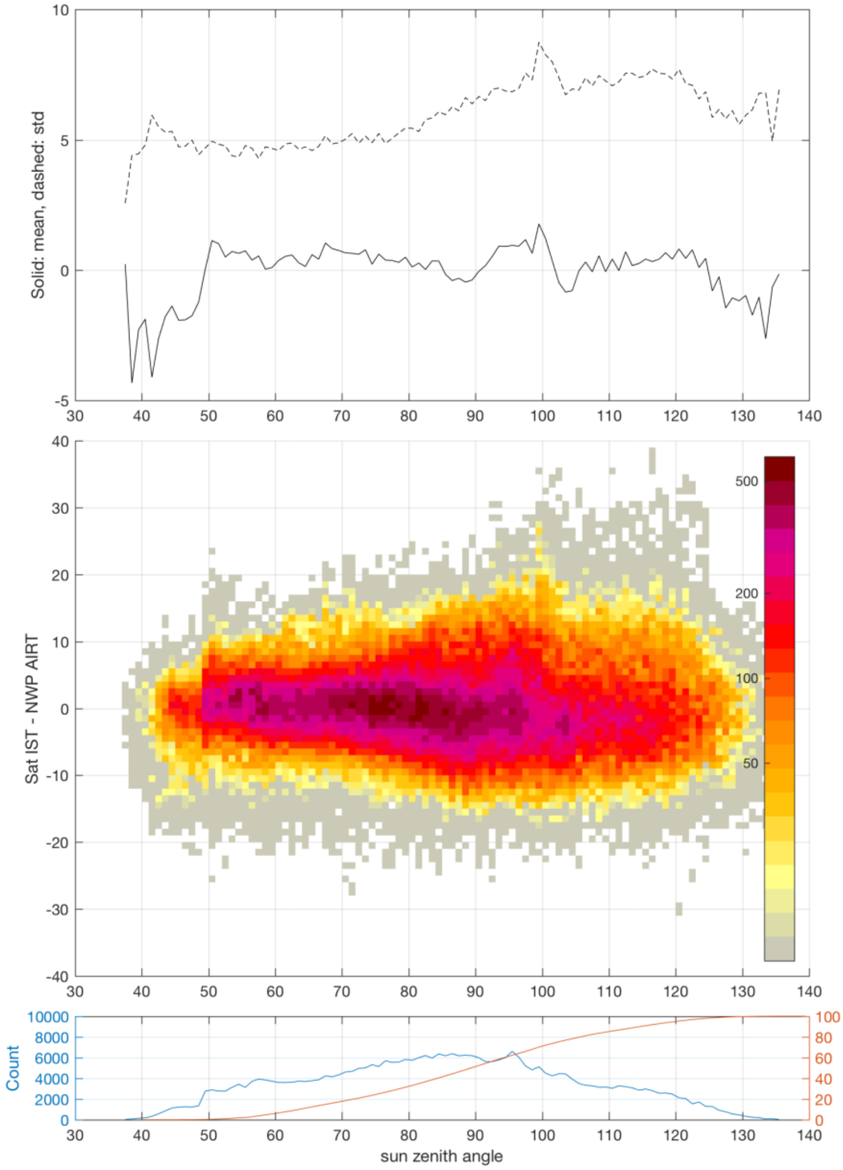

Figure D19 *Distribution and statistics on satellite IST – NWP AIRT temperature differences as a function of sun zenith angle for the northern hemisphere. Top is mean (solid line) and standard deviation (dotted line), centre is a 2D histogram of the data distribution and bottom is data count per 1 degree bin for sun zenith angle (blue, left axis) and cumulated percentage of data count (red, right axis).*

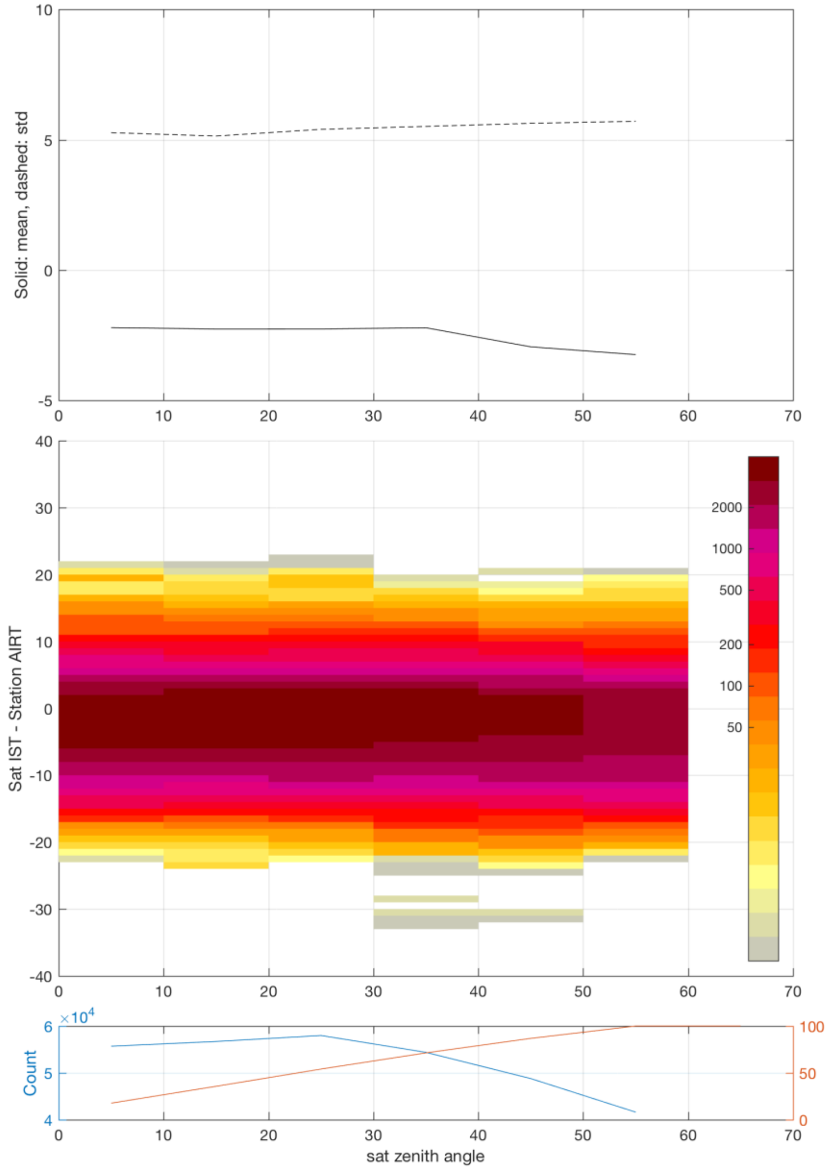

Figure D20 *Distribution and statistics on satellite IST – station AIRT temperature differences as a function of satellite zenith angle for the northern hemisphere. Top is mean (solid line) and standard deviation (dotted line), centre is a 2D histogram of the data distribution and bottom is data count per 10 degree bin for sun zenith angle (blue, left axis) and cumulated percentage of data count (red, right axis).*

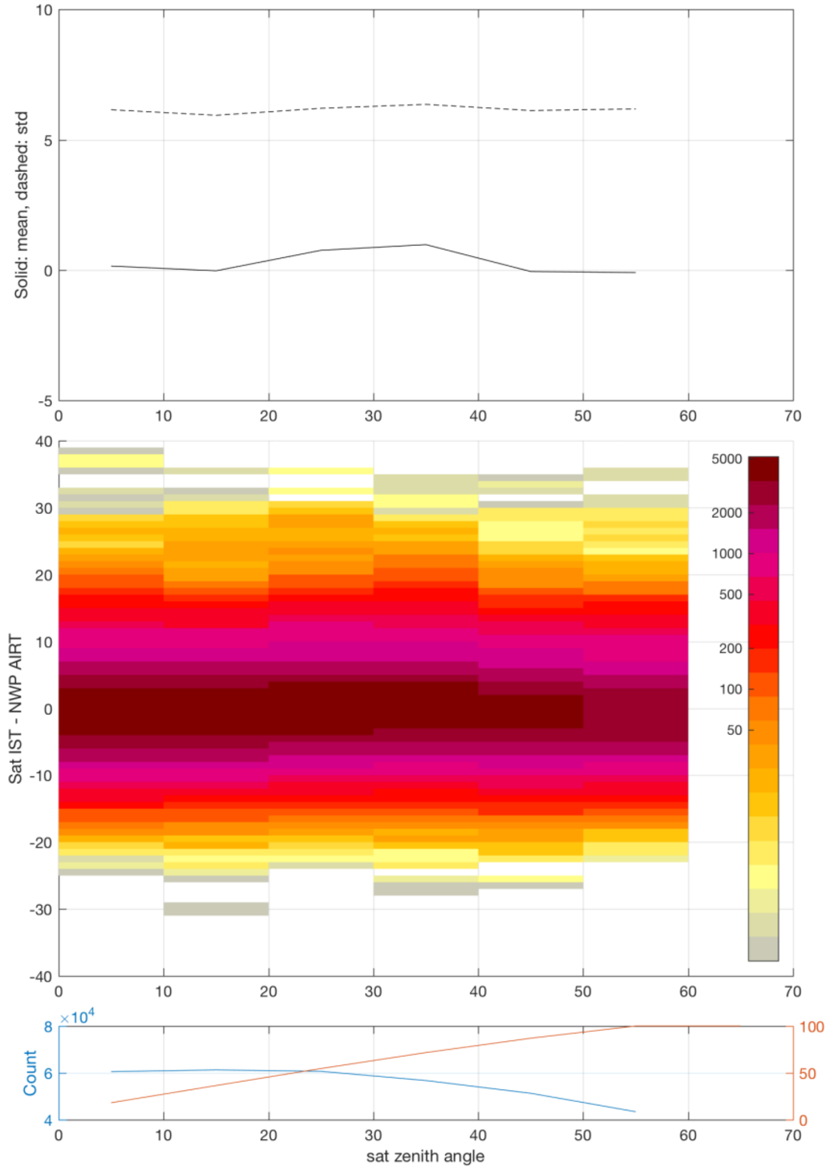

Figure D21 *Distribution and statistics on satellite IST – NWP AIRT temperature differences as a function of satellite zenith angle for the northern hemisphere. Top is mean (solid line) and standard deviation (dotted line), centre is a 2D histogram of the data distribution and bottom is data count per 10 degree bin for satellite zenith angle (blue, left axis) and cumulated percentage of data count (red, right axis).*

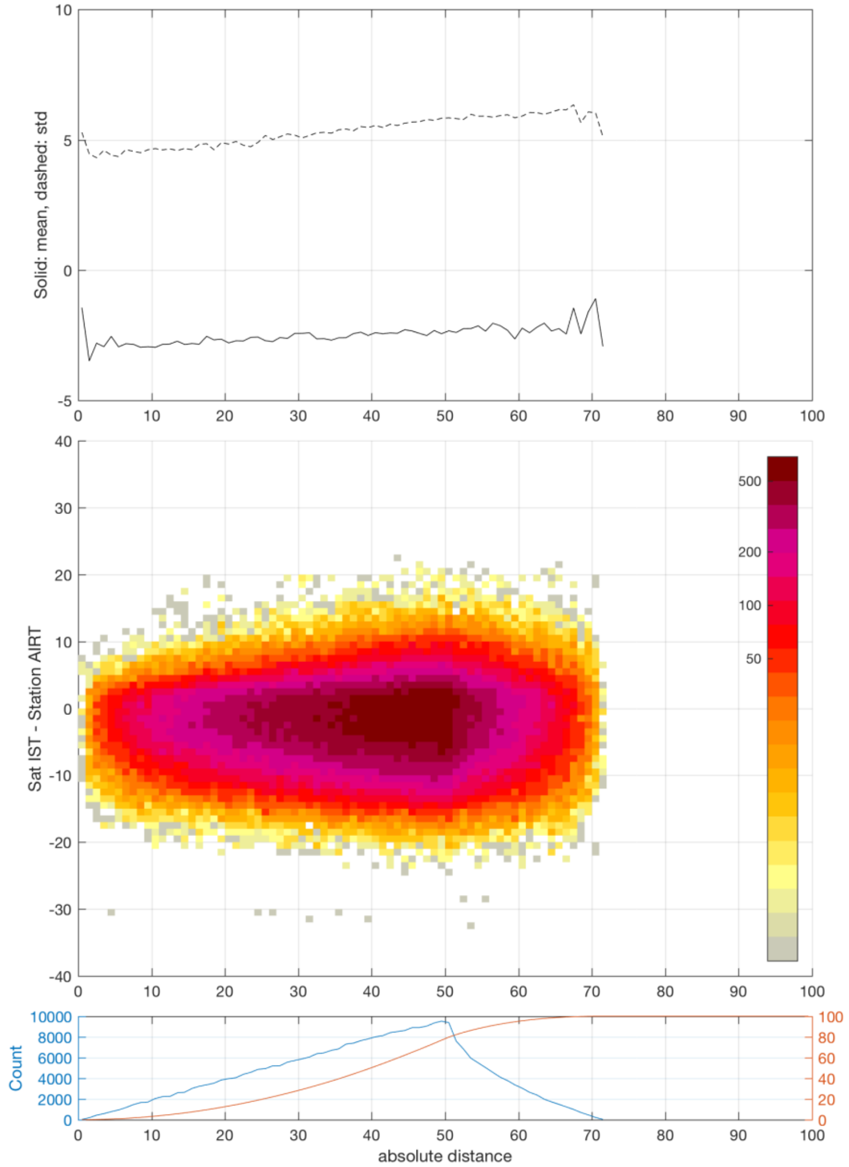

Figure D22 *Distribution and statistics on satellite IST – station AIRT temperature differences as a function of absolute distance for the northern hemisphere. Top is mean (solid line) and standard deviation (dotted line), centre is a 2D histogram of the data distribution and bottom is data count per 1 km bin for absolute distance (blue, left axis) and cumulated percentage of data count (red, right axis).*

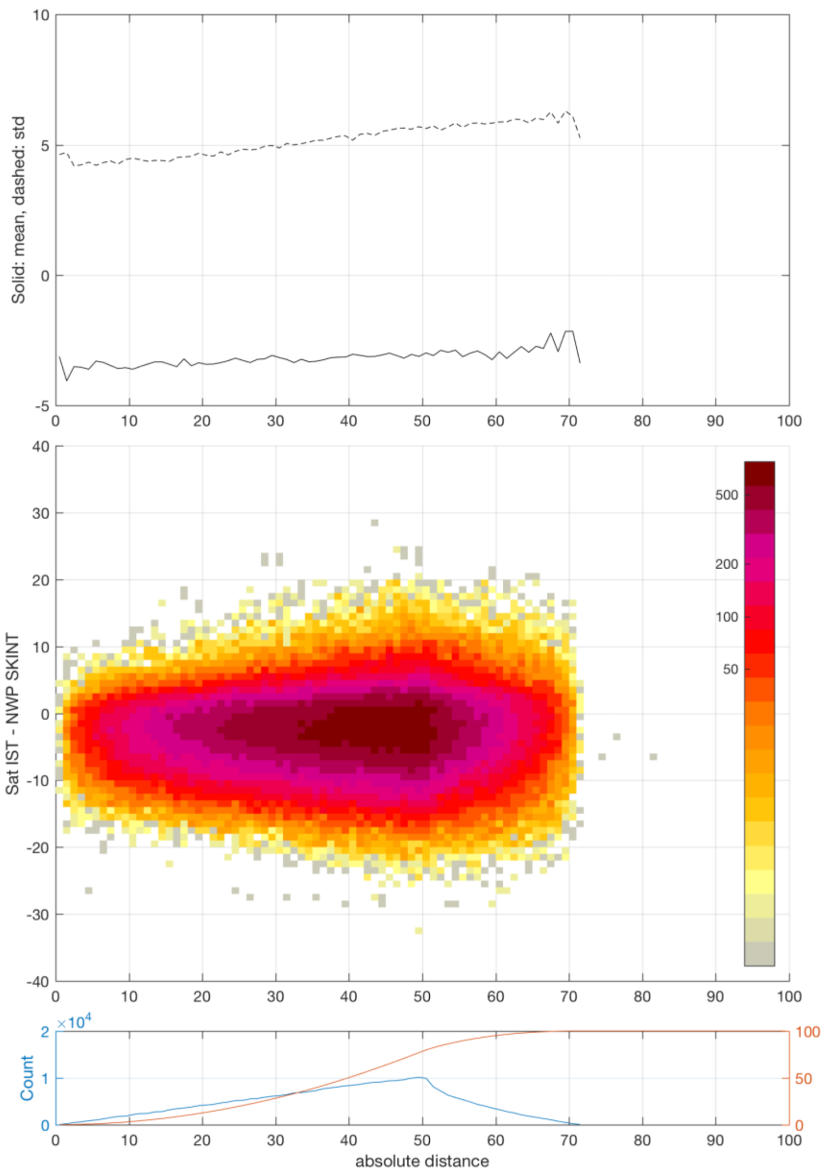

Figure D23 *Distribution and statistics on satellite IST – NWP AIRT temperature differences as a function of absolute distance for the northern hemisphere. Top is mean (solid line) and standard deviation (dotted line), centre is a 2D histogram of the data distribution and bottom is data count per 1 km bin for absolute distance (blue, left axis) and cumulated percentage of data count (red, right axis).*

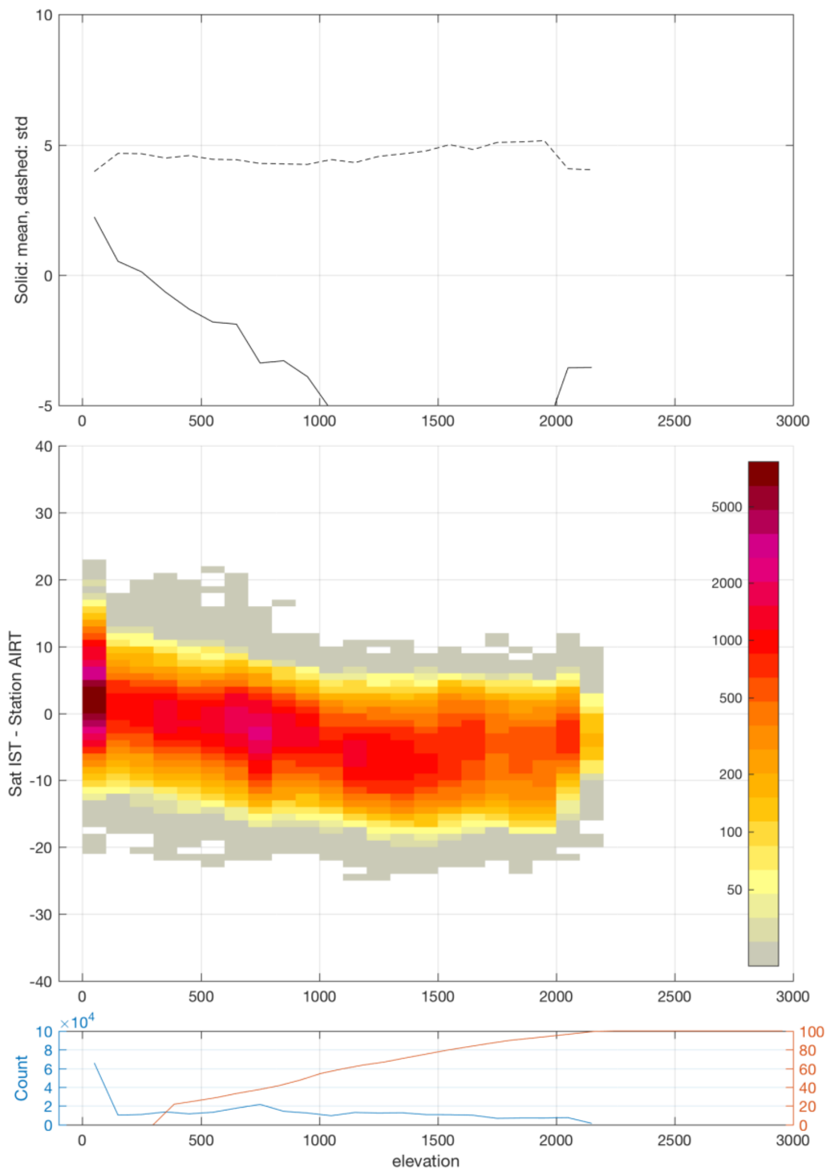

Figure D24 *Distribution and statistics on satellite IST – station AIRT temperature differences as a function of elevation for the northern hemisphere. Top is mean (solid line) and standard deviation (dotted line), centre is a 2D histogram of the data distribution and bottom is data count per 100 m bin for elevation (blue, left axis) and cumulated percentage of data count (red, right axis).*

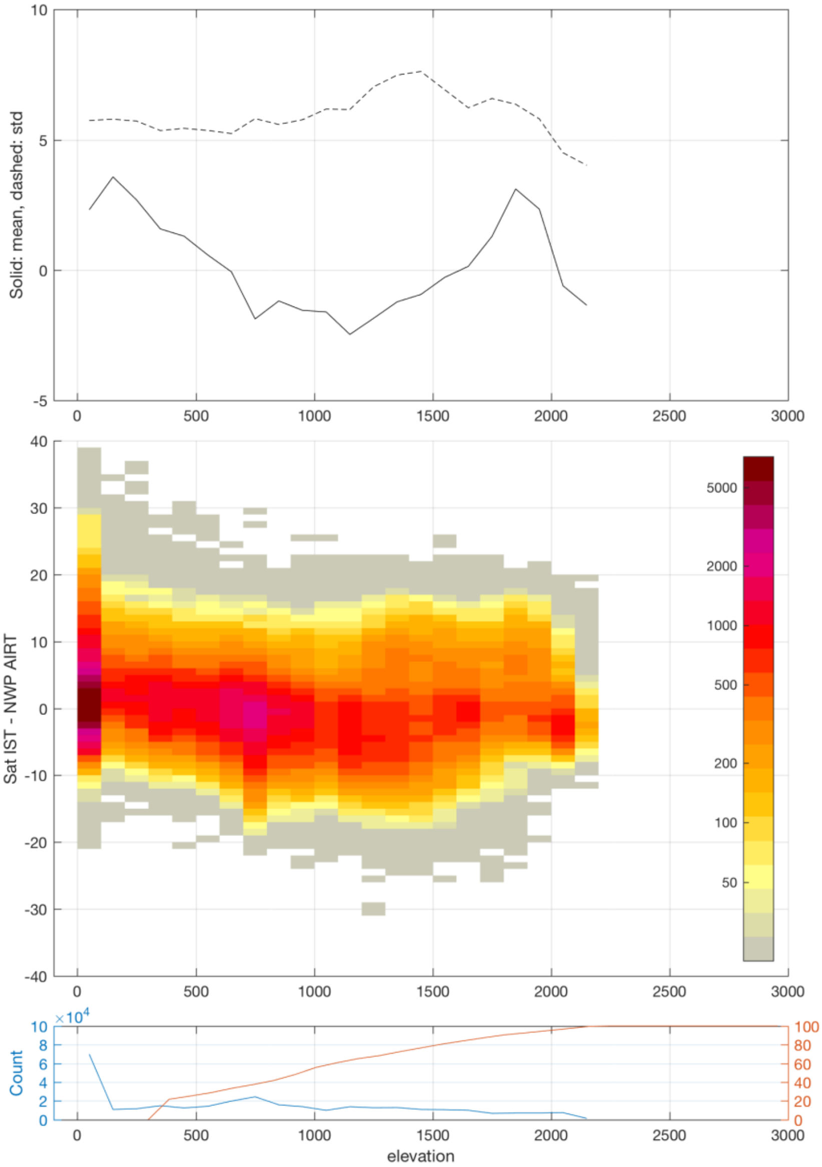

Figure D25 *Distribution and statistics on satellite IST – NWP AIRT temperature differences as a function of elevation for the northern hemisphere. Top is mean (solid line) and standard deviation (dotted line), centre is a 2D histogram of the data distribution and bottom is data count per 100 m bin for elevation (blue, left axis) and cumulated percentage of data count (red, right axis).*

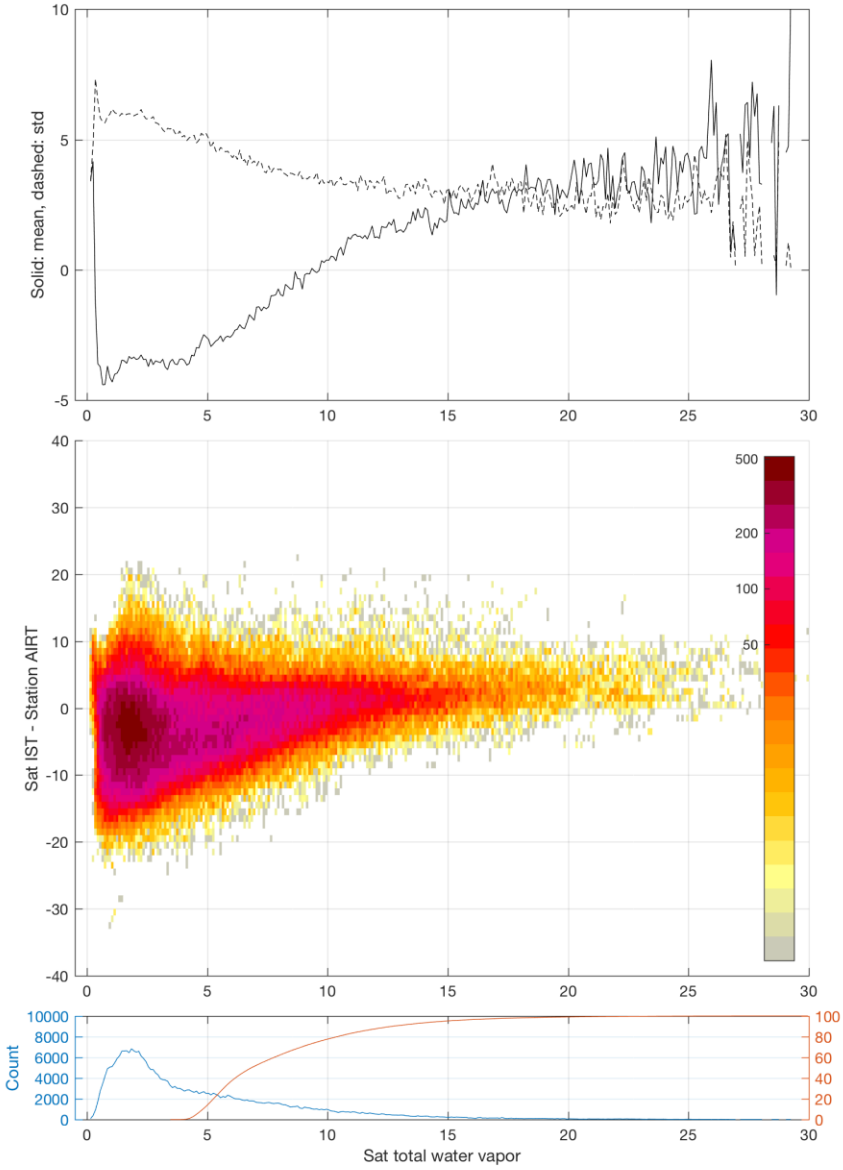

Figure D26 *Distribution and statistics on satellite IST – station AIRT temperature differences as a function of water vapour for the northern hemisphere. Top is mean (solid line) and standard deviation (dotted line), centre is a 2D histogram of the data distribution and bottom is data count per 0.1 mm bin for water vapour (blue, left axis) and cumulated percentage of data count (red, right axis).*

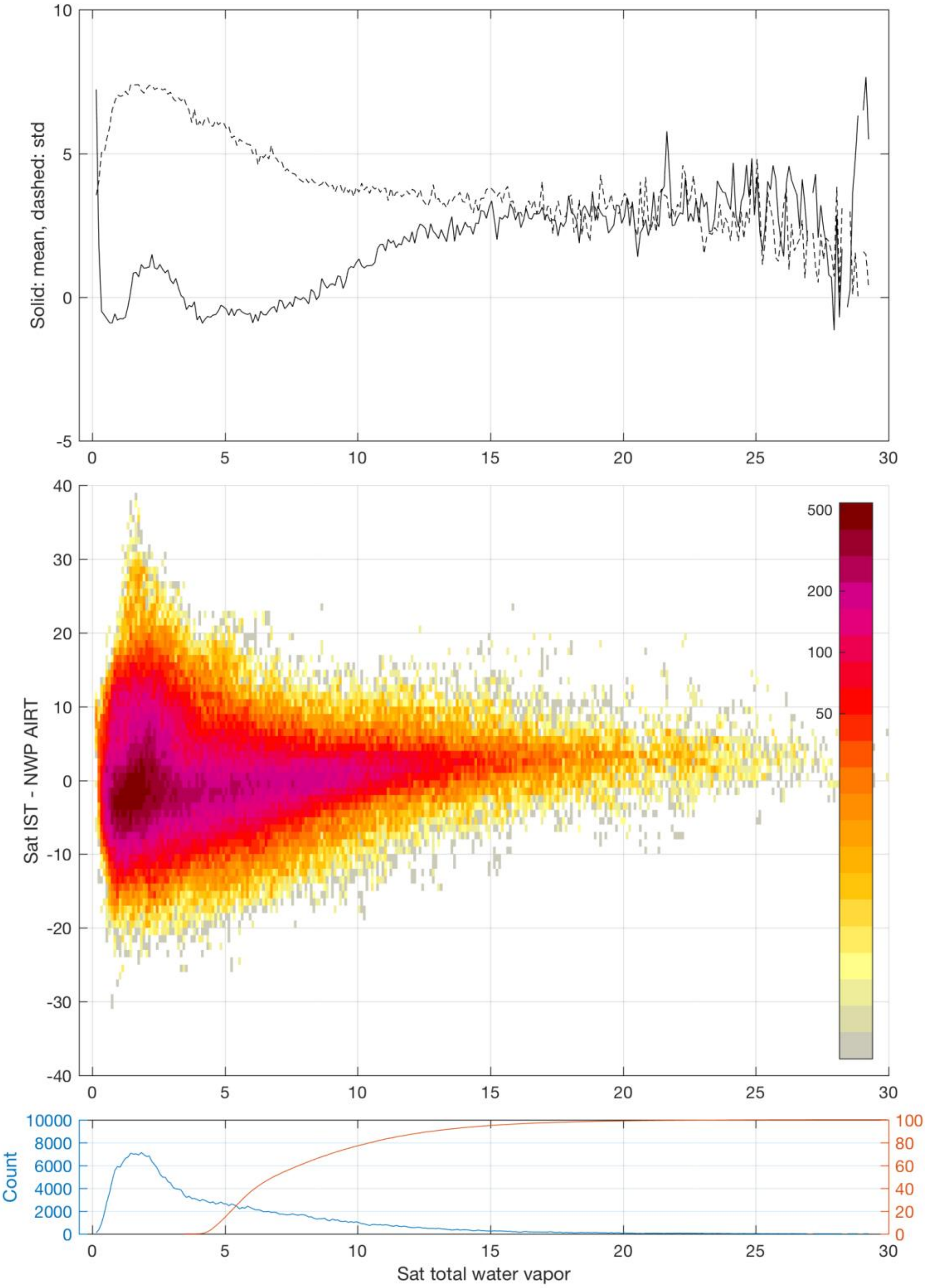

Figure D27 *Distribution and statistics on satellite IST – NWP AIRT temperature differences as a function of water vapour for the northern hemisphere. Top is mean (solid line) and standard deviation (dotted line), centre is a 2D histogram of the data distribution and bottom is data count per 0.1 mm bin for water vapour (blue, left axis) and cumulated percentage of data count (red, right axis).*

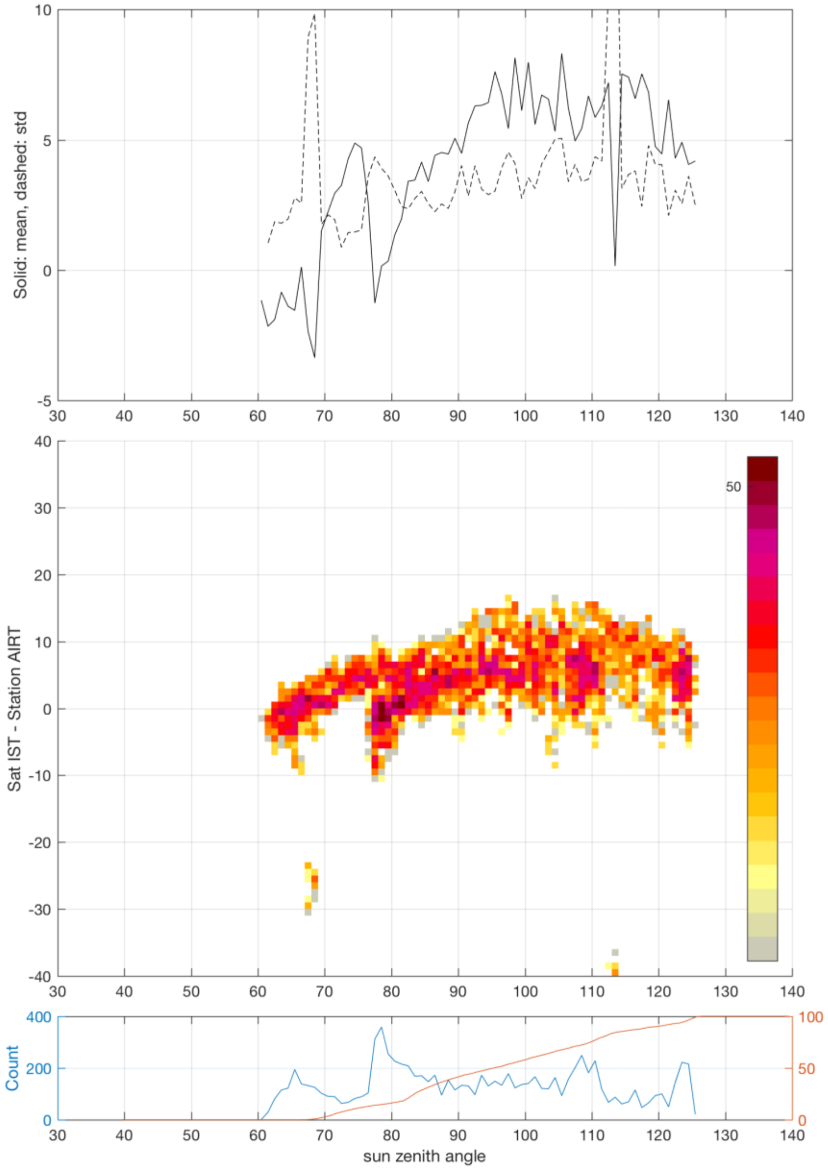

Figure D28 *Distribution and statistics on satellite IST – station AIRT temperature differences as a function of sun zenith angle for the southern hemisphere. Top is mean (solid line) and standard deviation (dotted line), centre is a 2D histogram of the data distribution and bottom is data count per 1 degree bin for sun zenith angle (blue, left axis) and cumulated percentage of data count (red, right axis).*

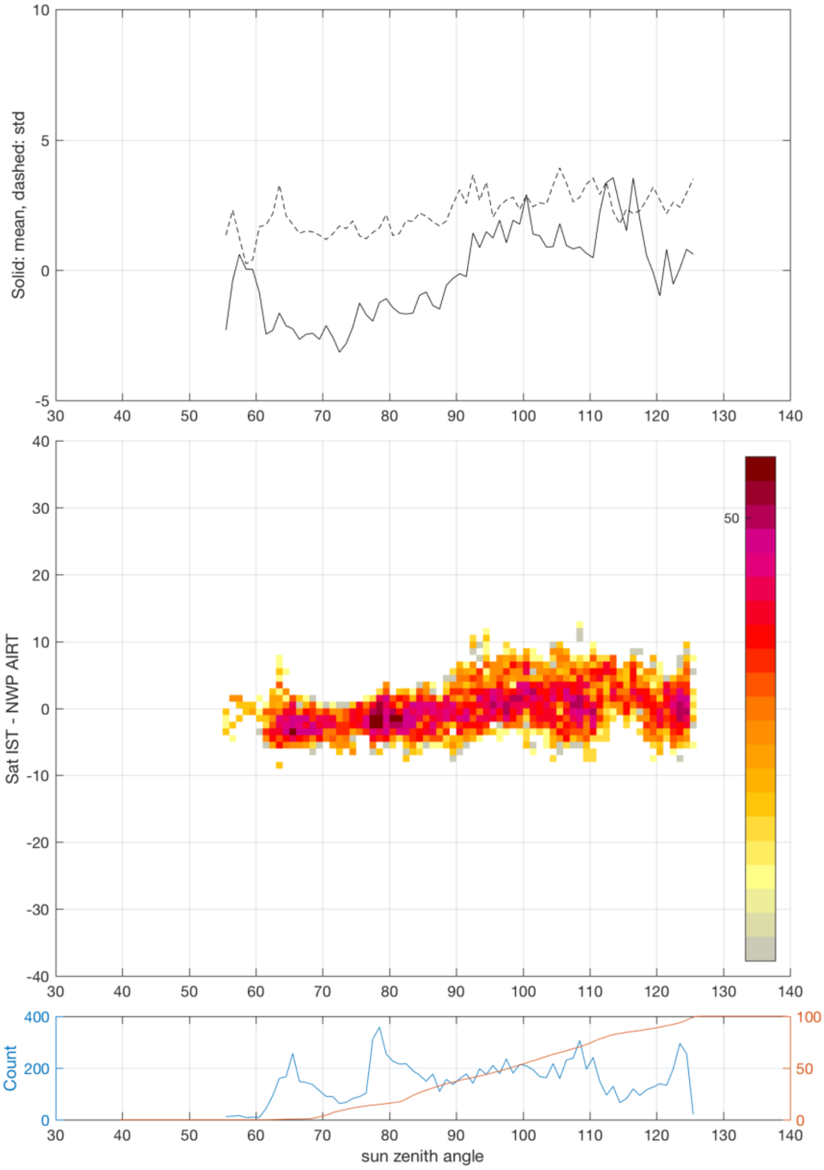

Figure D29 *Distribution and statistics on satellite IST – NWP AIRT temperature differences as a function of sun zenith angle for the southern hemisphere. Top is mean (solid line) and standard deviation (dotted line), centre is a 2D histogram of the data distribution and bottom is data count per 1 degree bin for sun zenith angle (blue, left axis) and cumulated percentage of data count (red, right axis).*

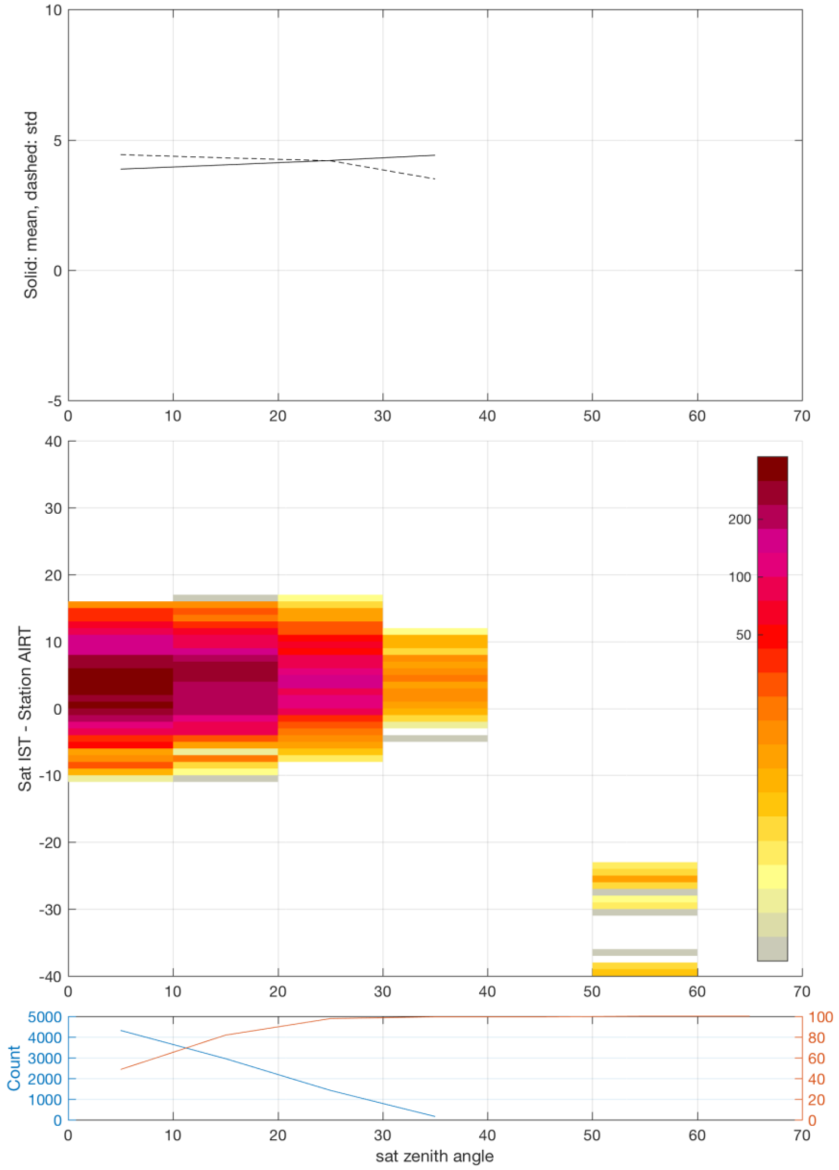

Figure D30 *Distribution and statistics on satellite IST – station AIRT temperature differences as a function of satellite zenith angle for the southern hemisphere. Top is mean (solid line) and standard deviation (dotted line), centre is a 2D histogram of the data distribution and bottom is data count per 10 degree bin for sun zenith angle (blue, left axis) and cumulated percentage of data count (red, right axis).*

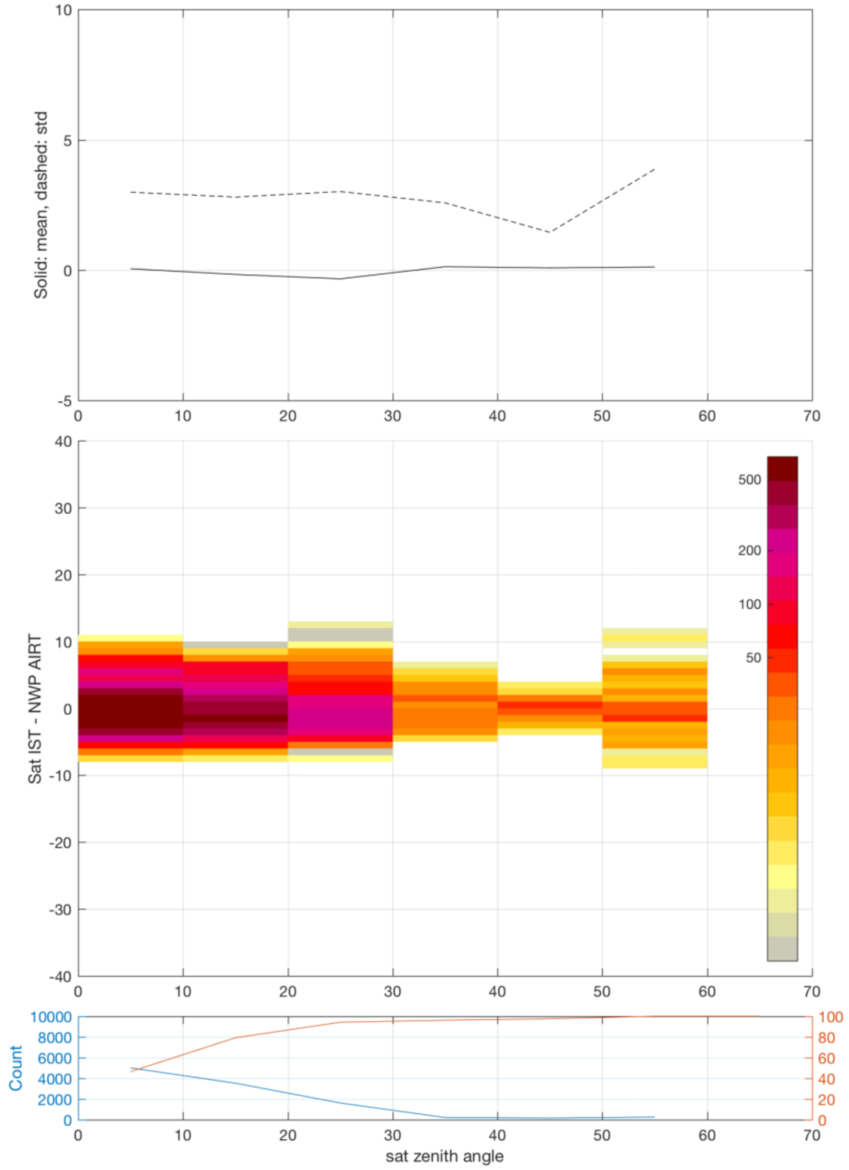

Figure D31 *Distribution and statistics on satellite IST – NWP AIRT temperature differences as a function of satellite zenith angle for the southern hemisphere. Top is mean (solid line) and standard deviation (dotted line), centre is a 2D histogram of the data distribution and bottom is data count per 10 degree bin for satellite zenith angle (blue, left axis) and cumulated percentage of data count (red, right axis).*

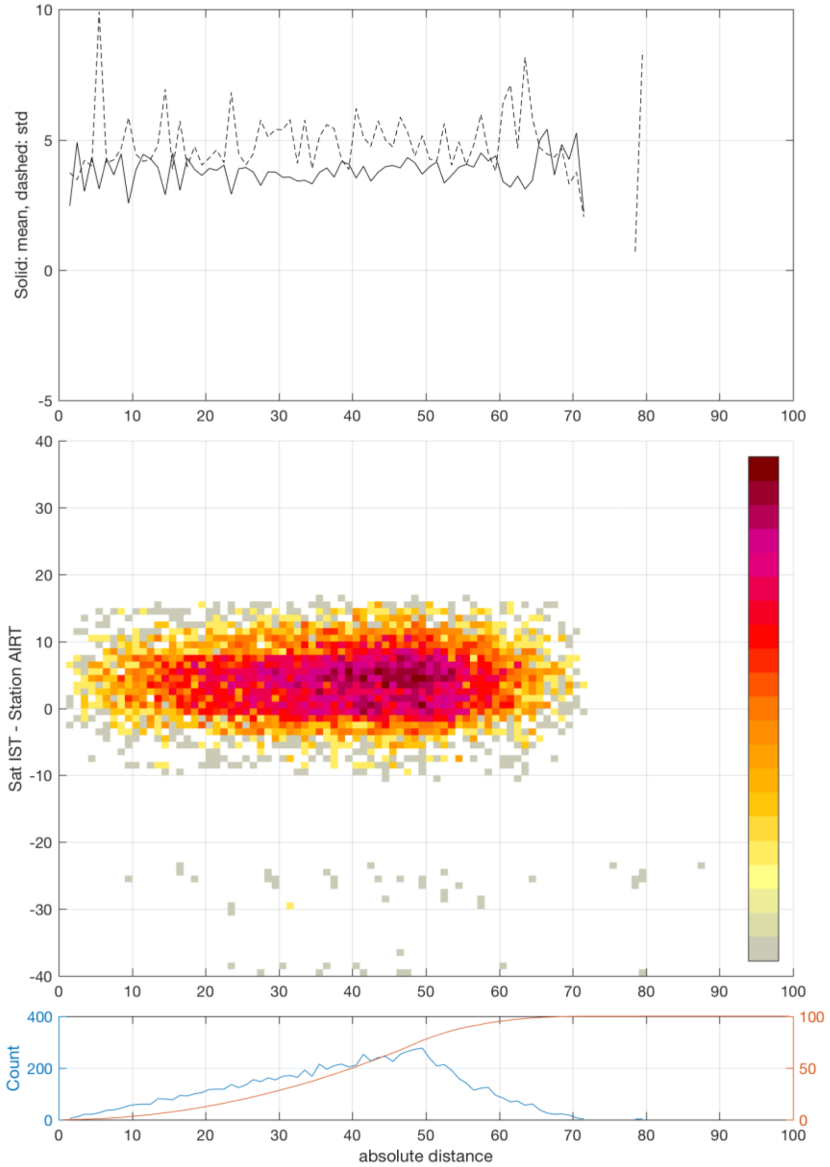

Figure D32 *Distribution and statistics on satellite IST – station AIRT temperature differences as a function of absolute distance for the southern hemisphere. Top is mean (solid line) and standard deviation (dotted line), centre is a 2D histogram of the data distribution and bottom is data count per 1 km bin for absolute distance (blue, left axis) and cumulated percentage of data count (red, right axis).*

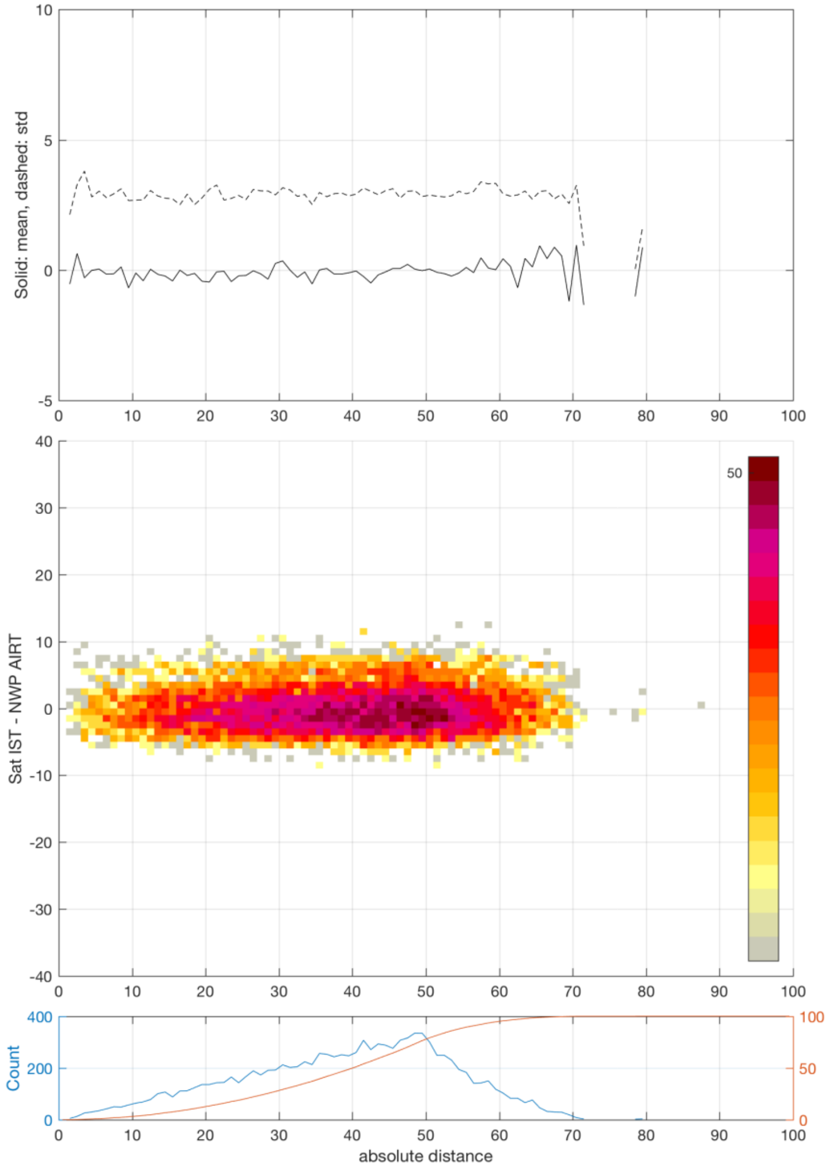

Figure D33 *Distribution and statistics on satellite IST – NWP AIRT temperature differences as a function of absolute distance for the southern hemisphere. Top is mean (solid line) and standard deviation (dotted line), centre is a 2D histogram of the data distribution and bottom is data count per 1 km bin for absolute distance (blue, left axis) and cumulated percentage of data count (red, right axis).*

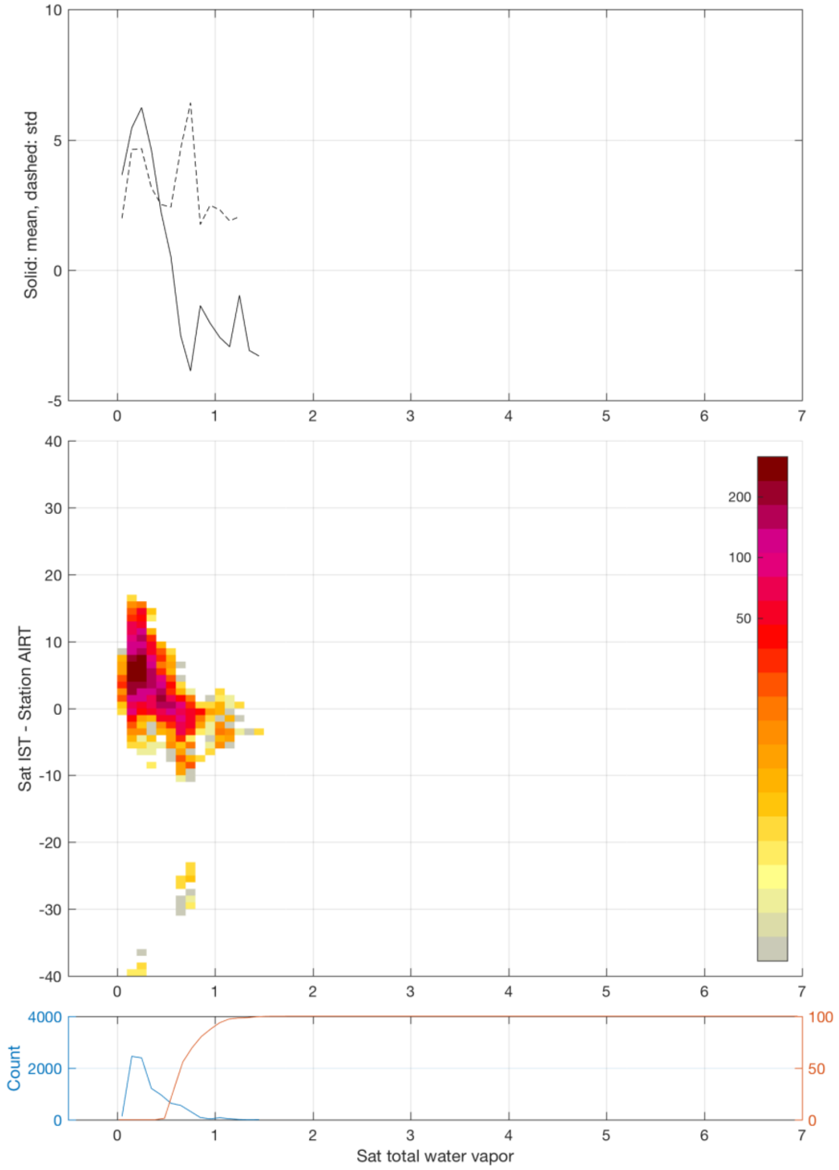

Figure D34 *Distribution and statistics on satellite IST – station AIRT temperature differences as a function of water vapour for the southern hemisphere. Top is mean (solid line) and standard deviation (dotted line), centre is a 2D histogram of the data distribution and bottom is data count per 0.1 mm bin for water vapour (blue, left axis) and cumulated percentage of data count (red, right axis).*

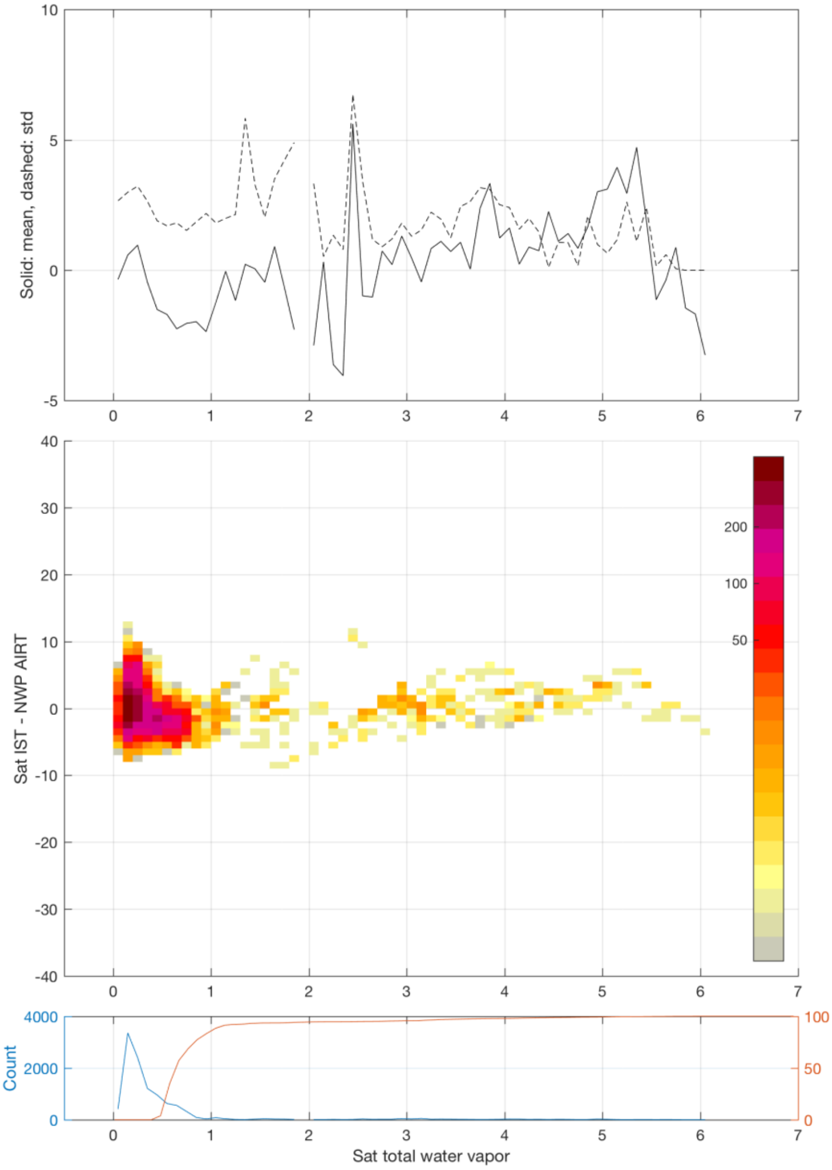

Figure D35 *Distribution and statistics on satellite IST – NWP AIRT temperature differences as a function of water vapour for the southern hemisphere. Top is mean (solid line) and standard deviation (dotted line), centre is a 2D histogram of the data distribution and bottom is data count per 0.1 mm bin for water vapour (blue, left axis) and cumulated percentage of data count (red, right axis).*

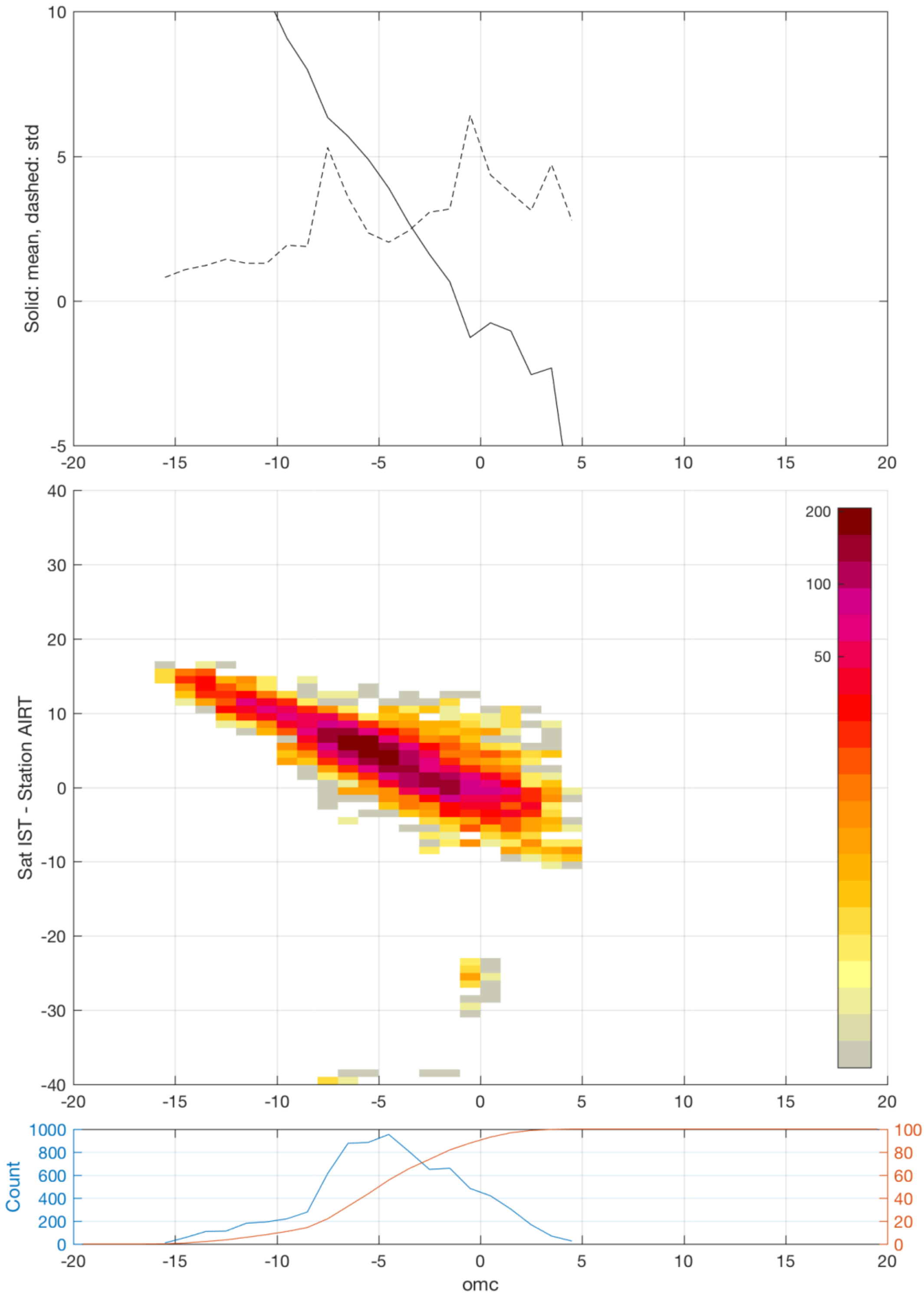

Figure D36 *Distribution and statistics on satellite IST – station AIRT temperature differences as a function of OmC for the southern hemisphere. Top is mean (solid line) and standard deviation (dotted line), centre is a 2D histogram of the data distribution and bottom is data count per 0.1 OmC unit bin (blue, left axis) and cumulated percentage of data count (red, right axis).*

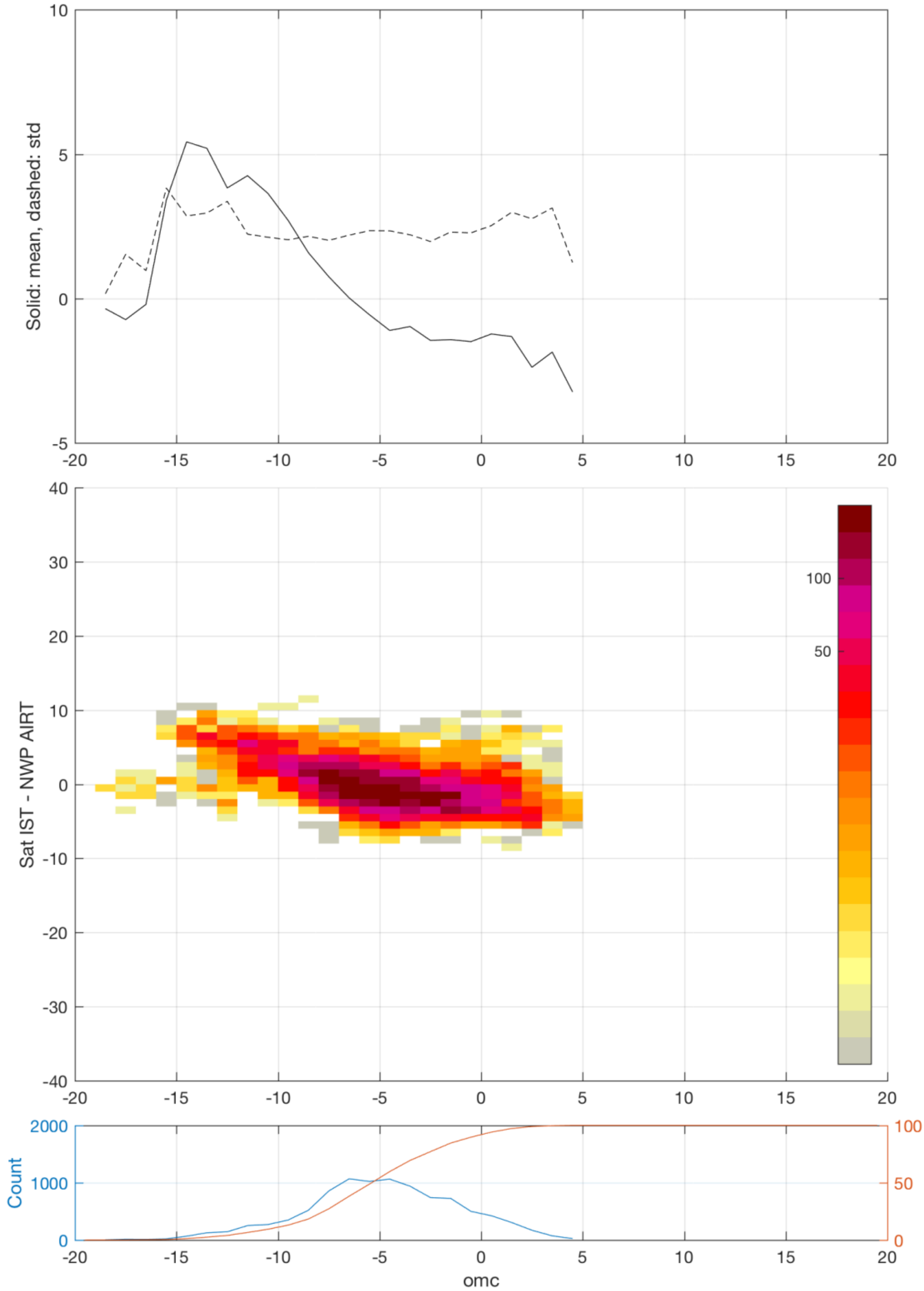

Figure D37 Distribution and statistics on satellite IST – NWP AIRT temperature differences as a function of OmC for the southern hemisphere. Top is mean (solid line) and standard deviation (dotted line), centre is a 2D histogram of the data distribution and bottom is data count per 0.1 OmC unit bin (blue, left axis) and cumulated percentage of data count (red, right axis).

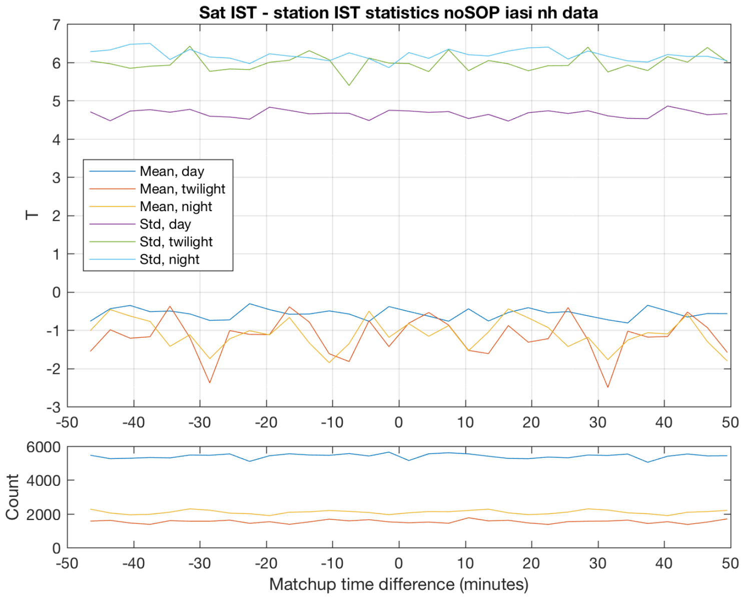

Figure D38 *Difference of IASI IST and station IST against the difference of the time of satellite measurement with the time of station measurement in minutes. Northern hemisphere data. Upper panel: purple, cyan and green lines are standard deviations for day, night and twilight, respectively. blue, yellow and orange lines are the biases for day, night and twilight, respectively. Lower panel: Number of counts per minute bin.*

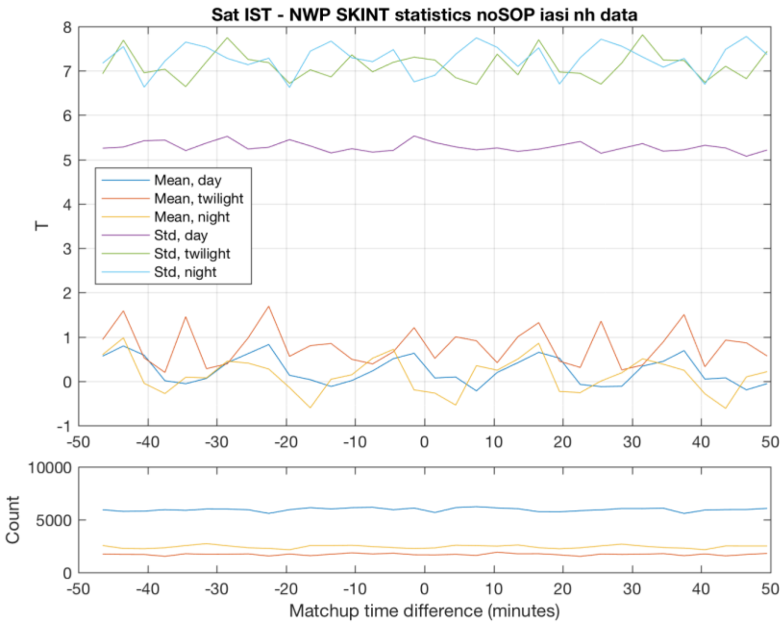

Figure D39 *Difference of IASI IST and NWP SKIN temperature against the difference of the time of satellite measurement with the time of station measurement in minutes. Northern hemisphere data. Upper panel: purple, cyan and green lines are standard deviations for day, night and twilight, respectively. blue, yellow and orange lines are the biases for-*

day, night and twilight, respectively. Lower panel: Number of counts per minute bin.

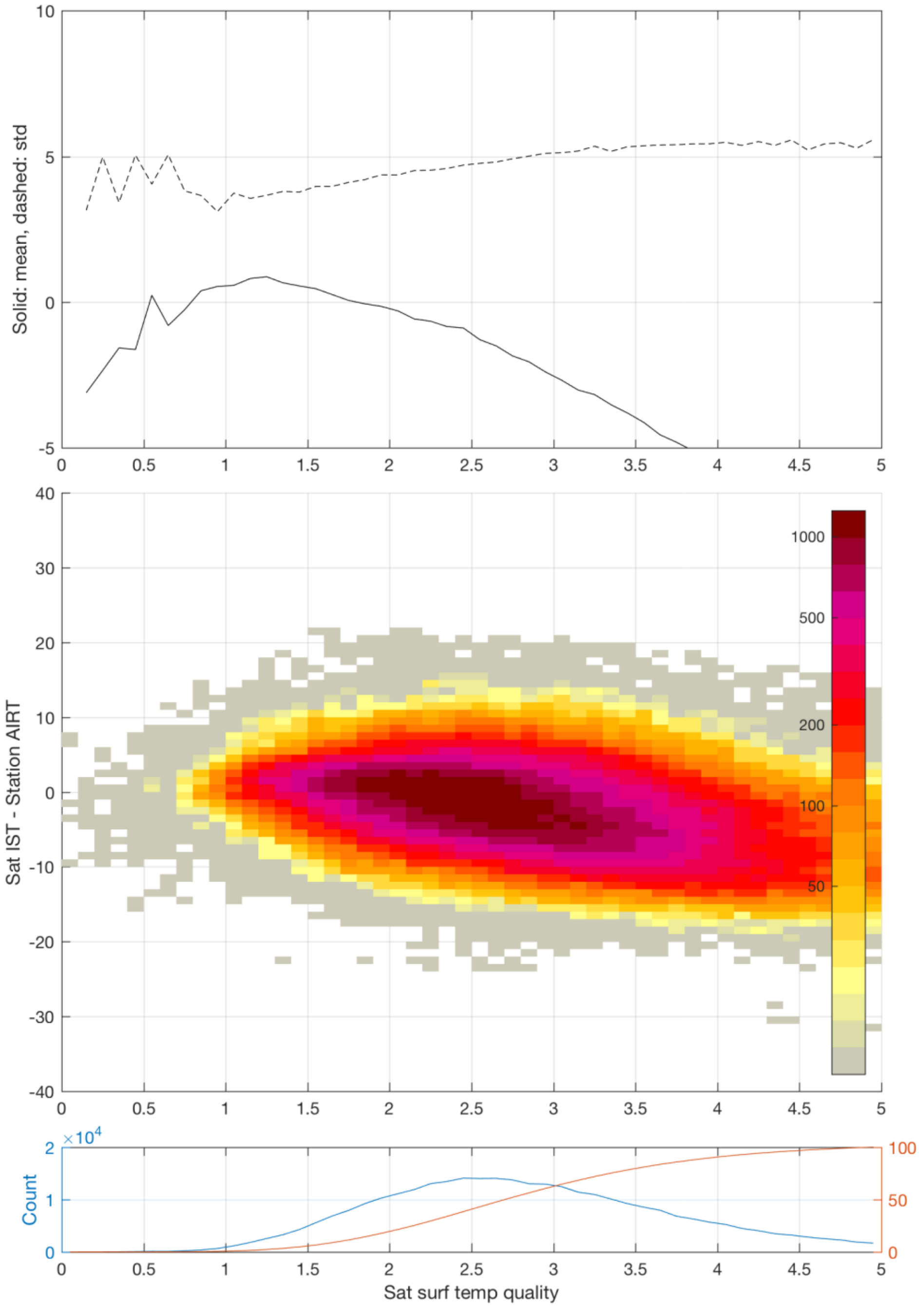

Figure D40 *Difference of IASI IST and AIR temperature observation against IASI temperature quality indicator. Northern hemisphere data. Top panel is mean (solid line) and standard deviation (dotted line), centre panel is a 2D histogram of the data distribution and bottom panel is data counts, absolute and relative accumulated.*

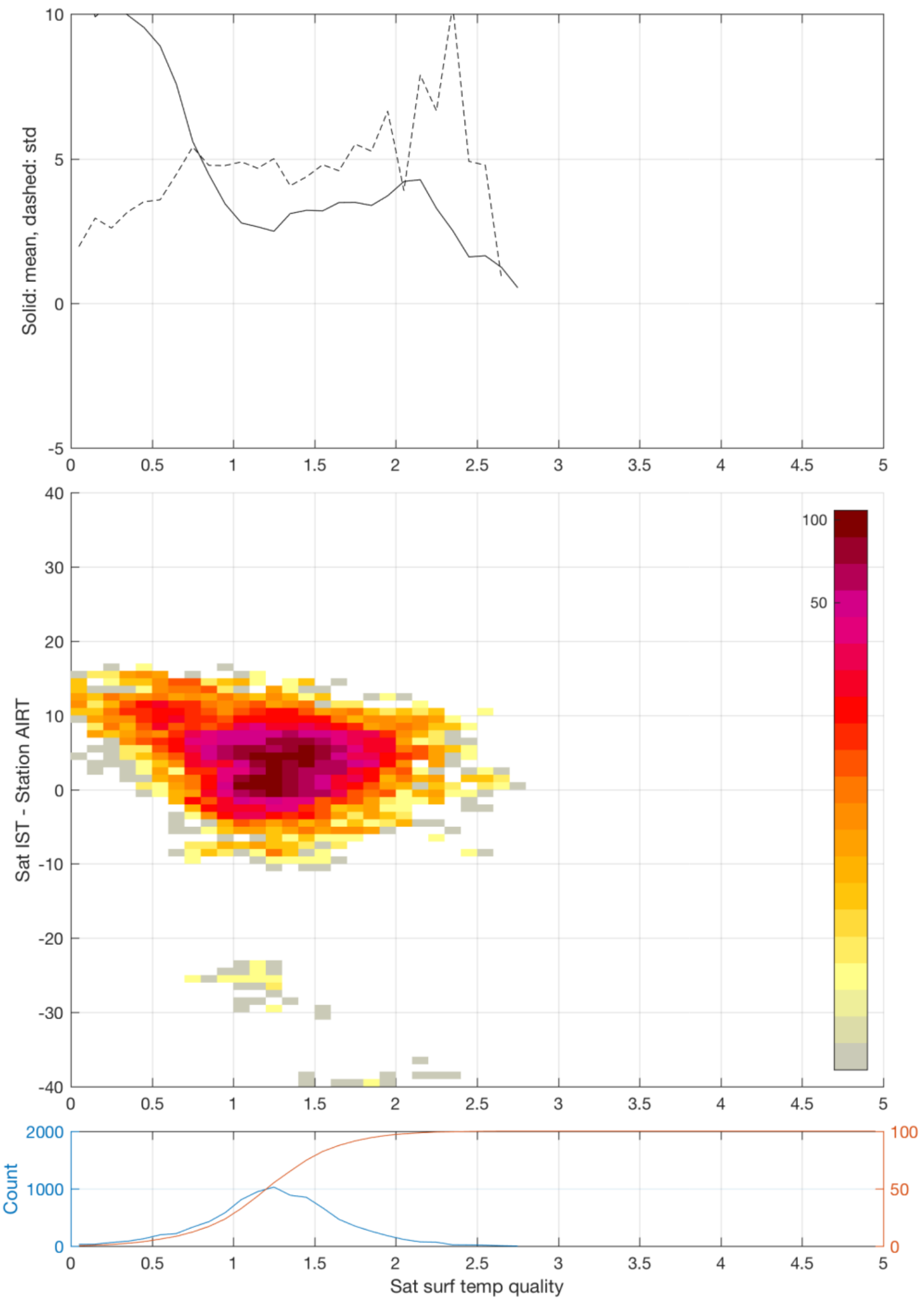

Figure D41 *Difference of IASI IST and AIR temperature observation against IASI temperature quality indicator. Southern hemisphere data. Top panel is mean (solid line) and standard deviation (dotted line), centre panel is a 2D histogram of the data distribution and bottom panel is data counts, absolute and relative accumulated.*

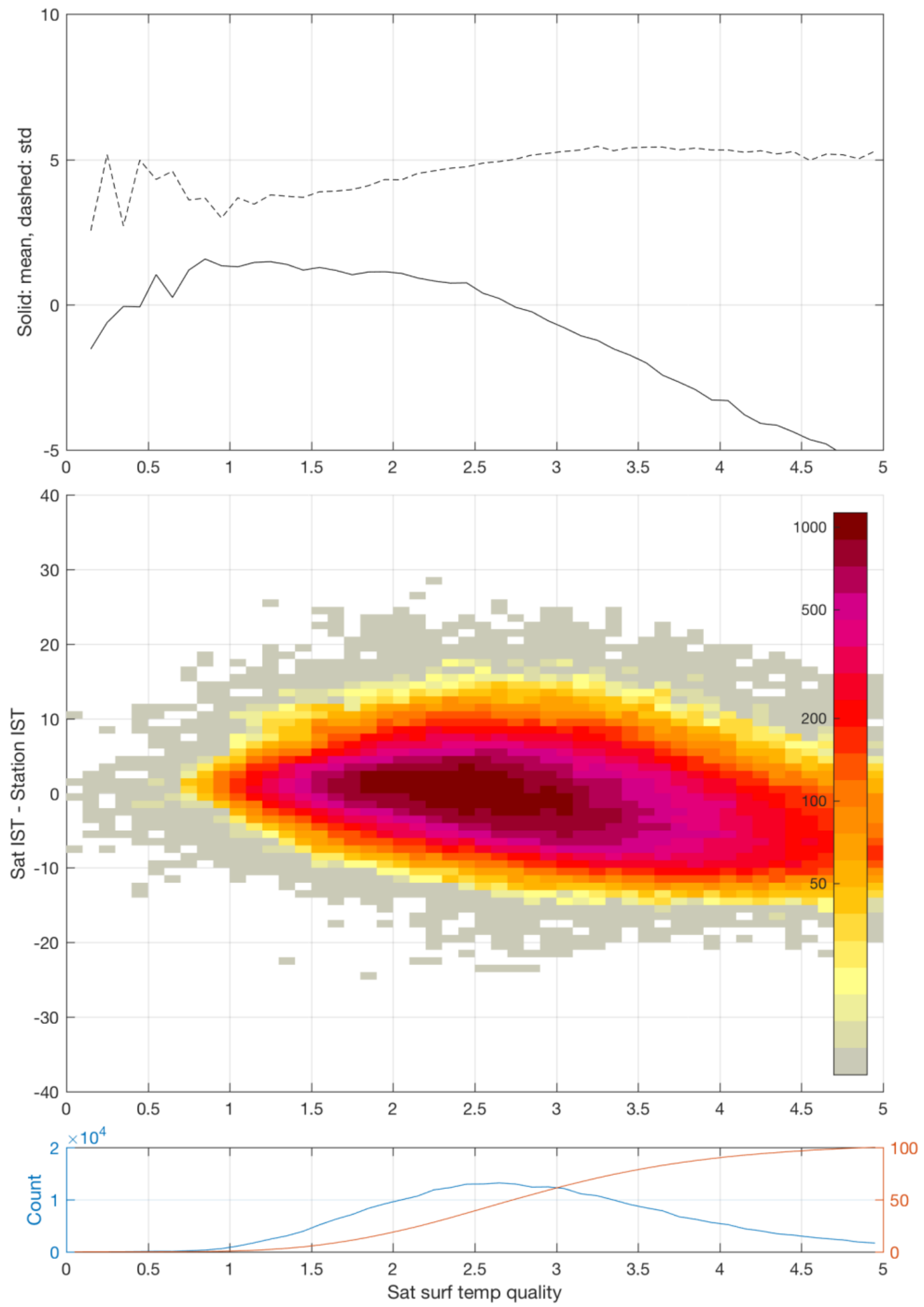

Figure D42 *Difference of IASI IST and SKIN temperature observation against IASI temperature quality indicator. Northern hemisphere data. Top panel is mean (solid line) and standard deviation (dotted line), centre panel is a 2D histogram of the data distribution and bottom panel is data counts, absolute and relative accumulated.*

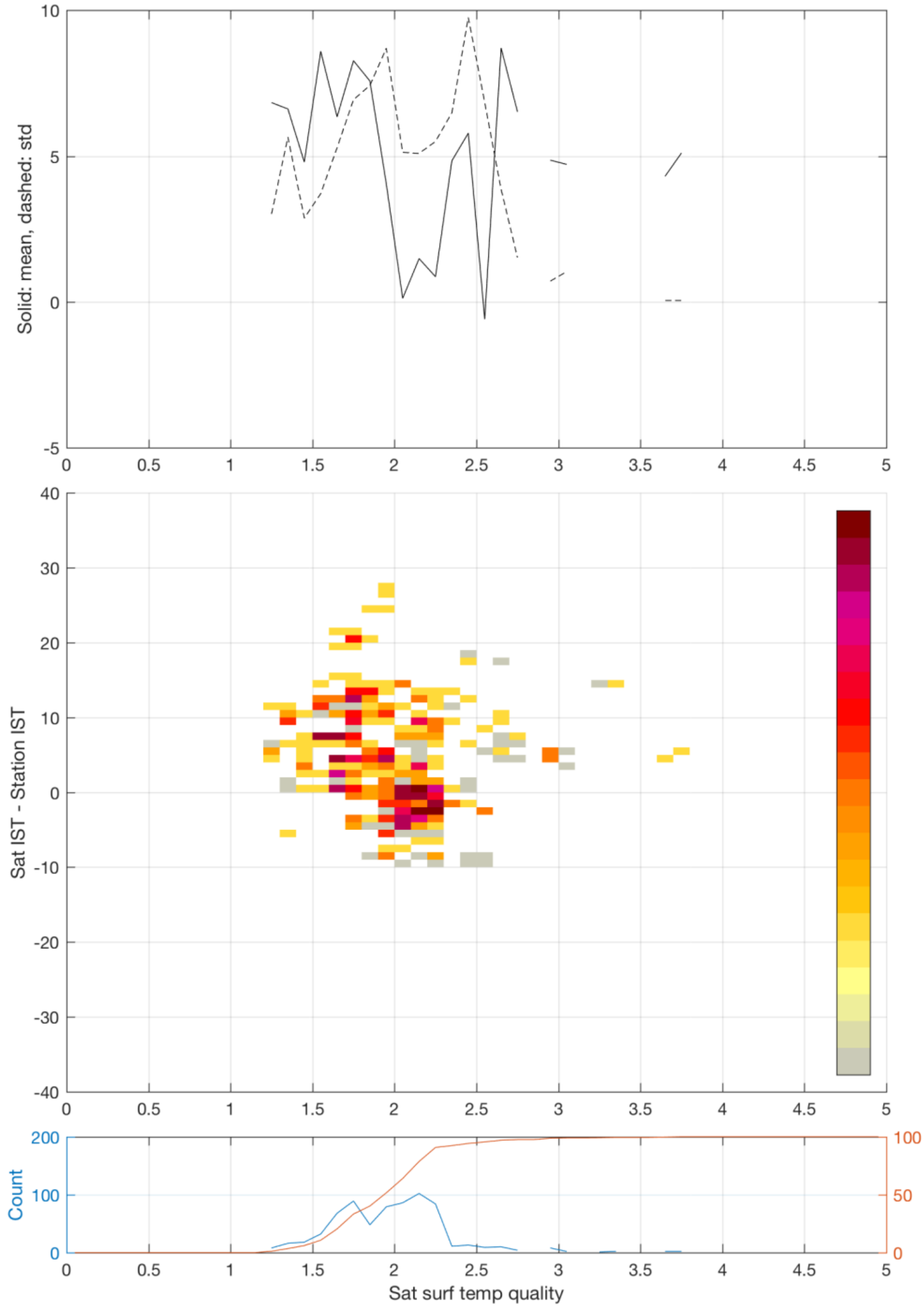

Figure D43 *Difference of IASI IST and SKIN temperature observation against IASI temperature quality indicator. Southern hemisphere data. Top panel is mean (solid line) and standard deviation (dotted line), centre panel is a 2D histogram of the data distribution and bottom panel is data counts, absolute and relative accumulated.*

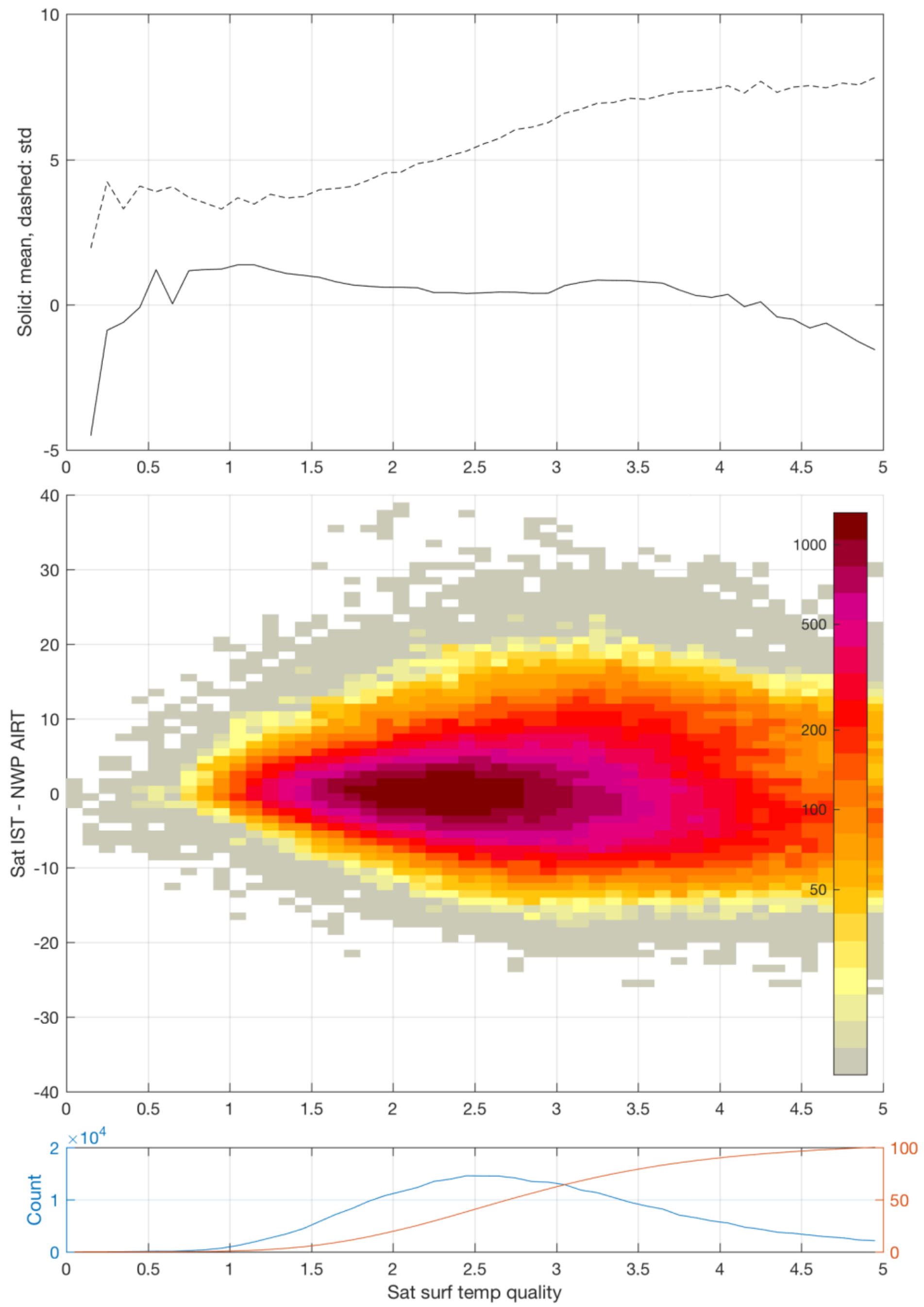

Figure D44 *Difference of IASI IST and NWP AIR temperature against IASI temperature quality indicator. Northern hemisphere data. Top panel is mean (solid line) and standard deviation (dotted line), centre panel is a 2D histogram of the data distribution and bottom panel is data counts, absolute and relative accumulated.*

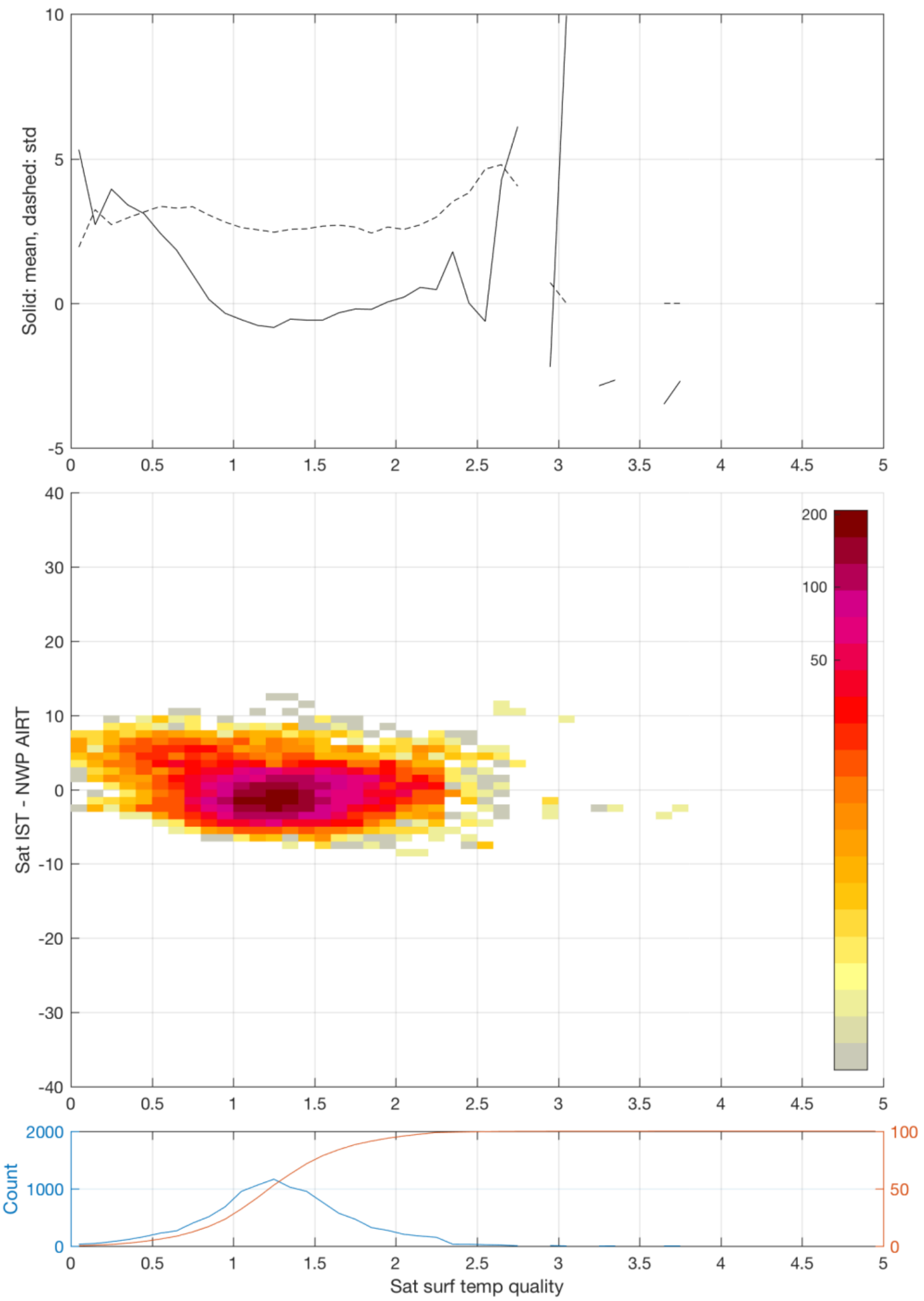

Figure D45 *Difference of IASI IST and NWP AIR temperature against IASI temperature quality indicator. Southern hemisphere data. Top panel is mean (solid line) and standard deviation (dotted line), centre panel is a 2D histogram of the data distribution and bottom panel is data counts, absolute and relative accumulated.*

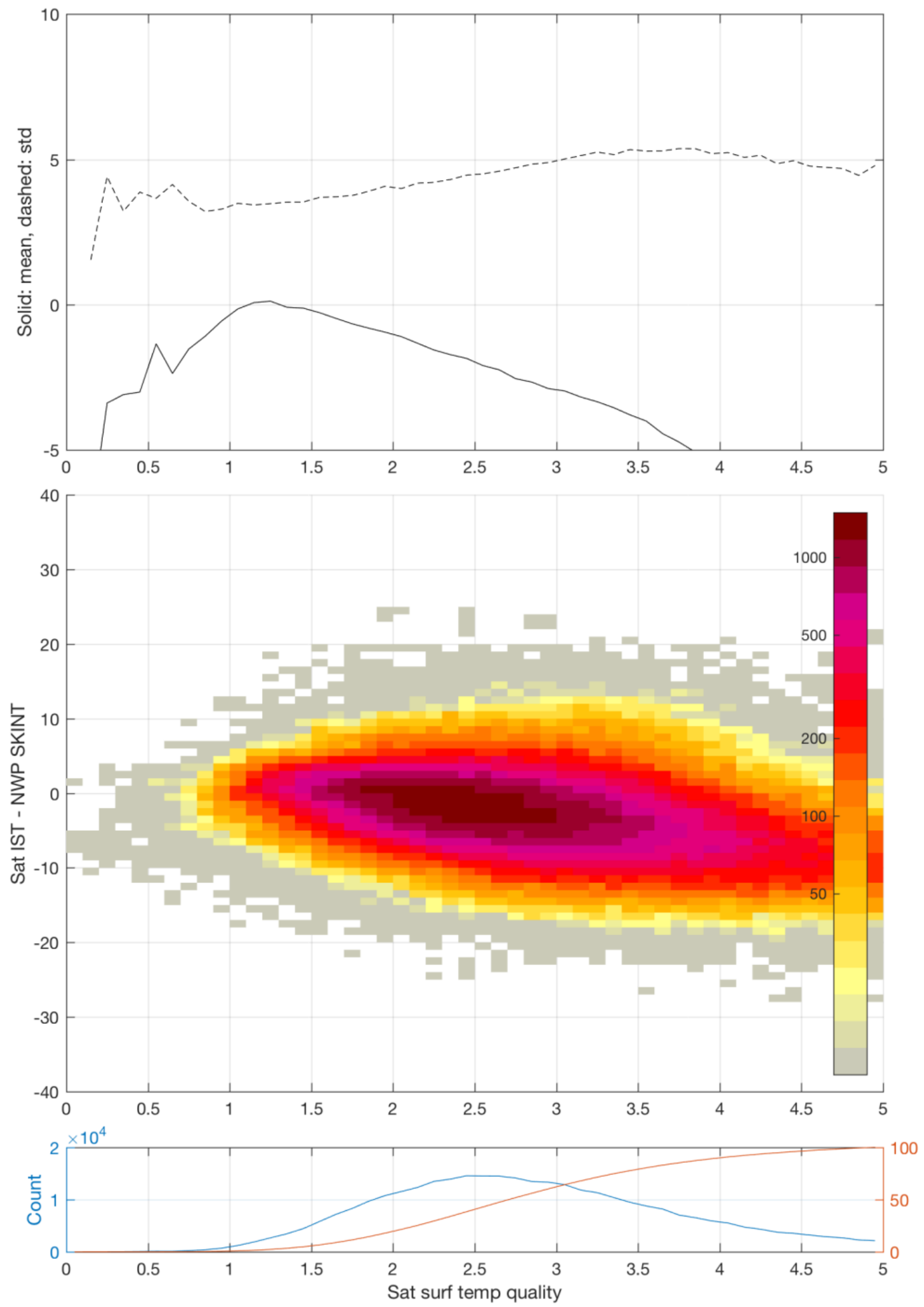

Figure D46 *Difference of IASI IST and NWP SKIN temperature against IASI temperature quality indicator. Norther hemisphere data. Top panel is mean (solid line) and standard deviation (dotted line), centre panel is a 2D histogram of the data distribution and bottom panel is data counts, absolute and relative accumulated.*

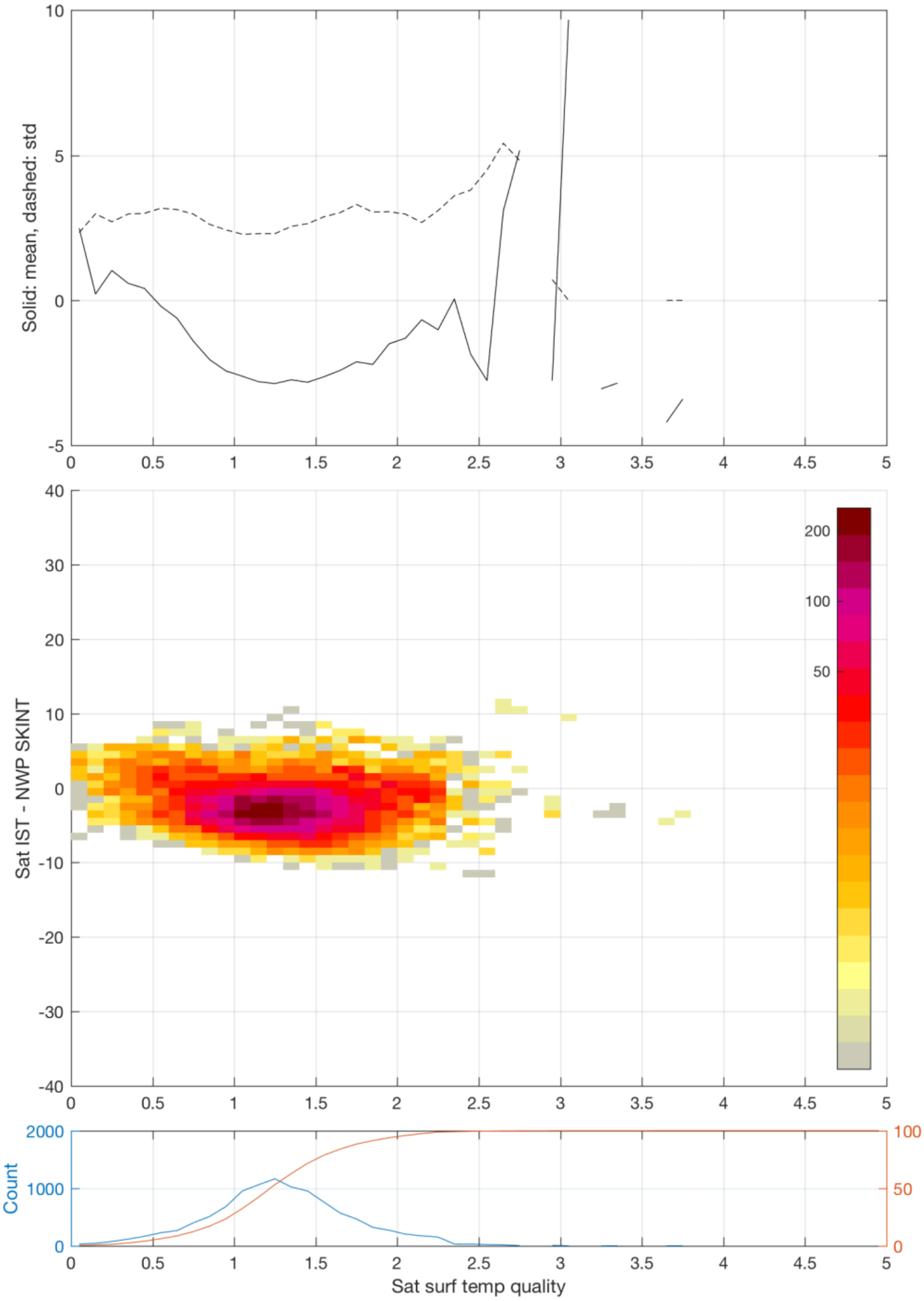

Figure D47 *Difference of IASI IST and NWP SKIN temperature against IASI temperature quality indicator. Southern Hemisphere data. Top panel is mean (solid line) and standard deviation (dotted line), centre panel is a 2D histogram of the data distribution and bottom panel is data counts, absolute and relative accumulated.*

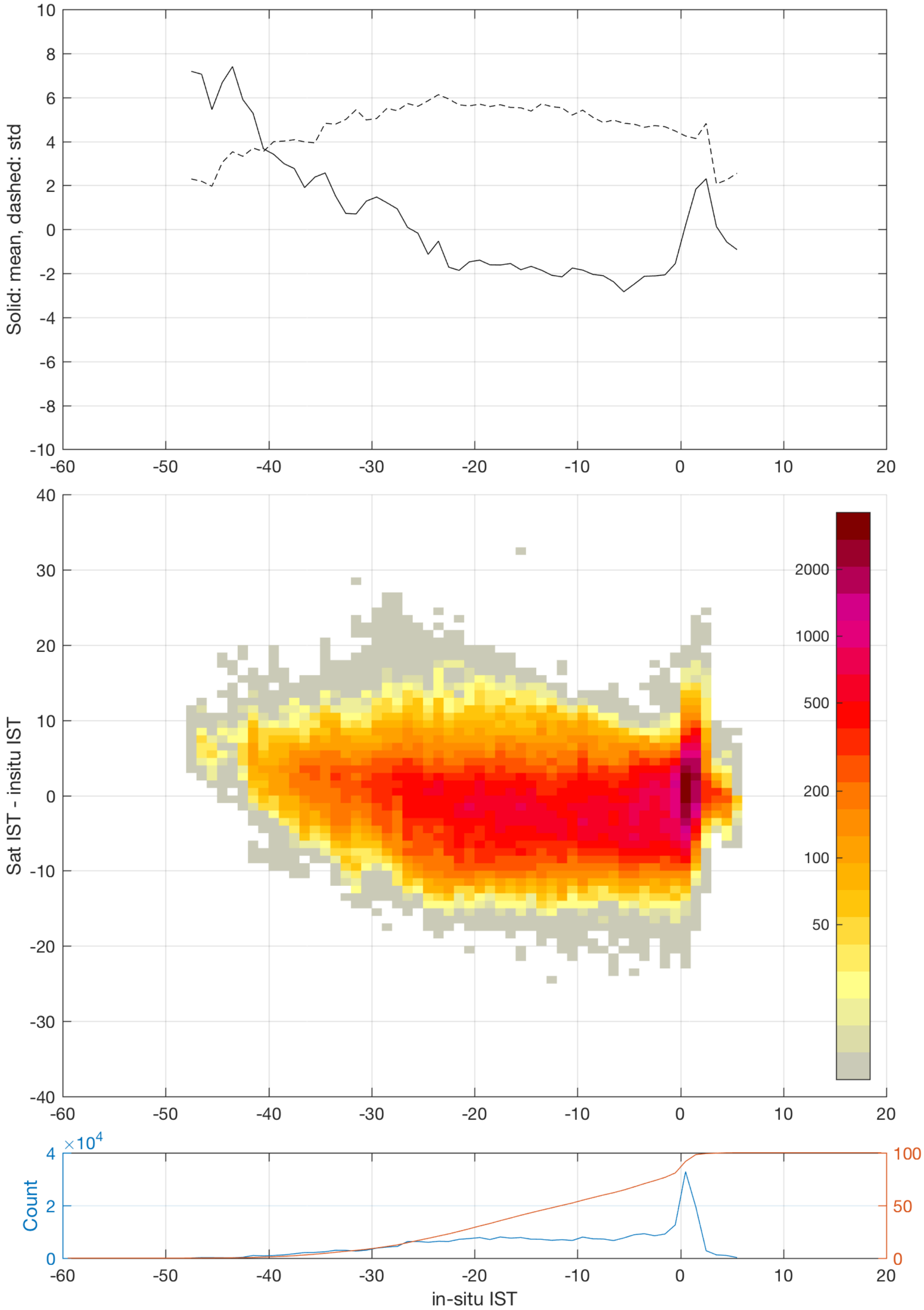

***Figure D48** Difference of IASI IST and surface temperature observations as a function of the surface temperature observation. Northern Hemisphere data. Top panel is mean (solid line) and standard deviation (dotted line), centre panel is a 2D histogram of the data distribution and bottom panel is data counts, absolute and relative accumulated*

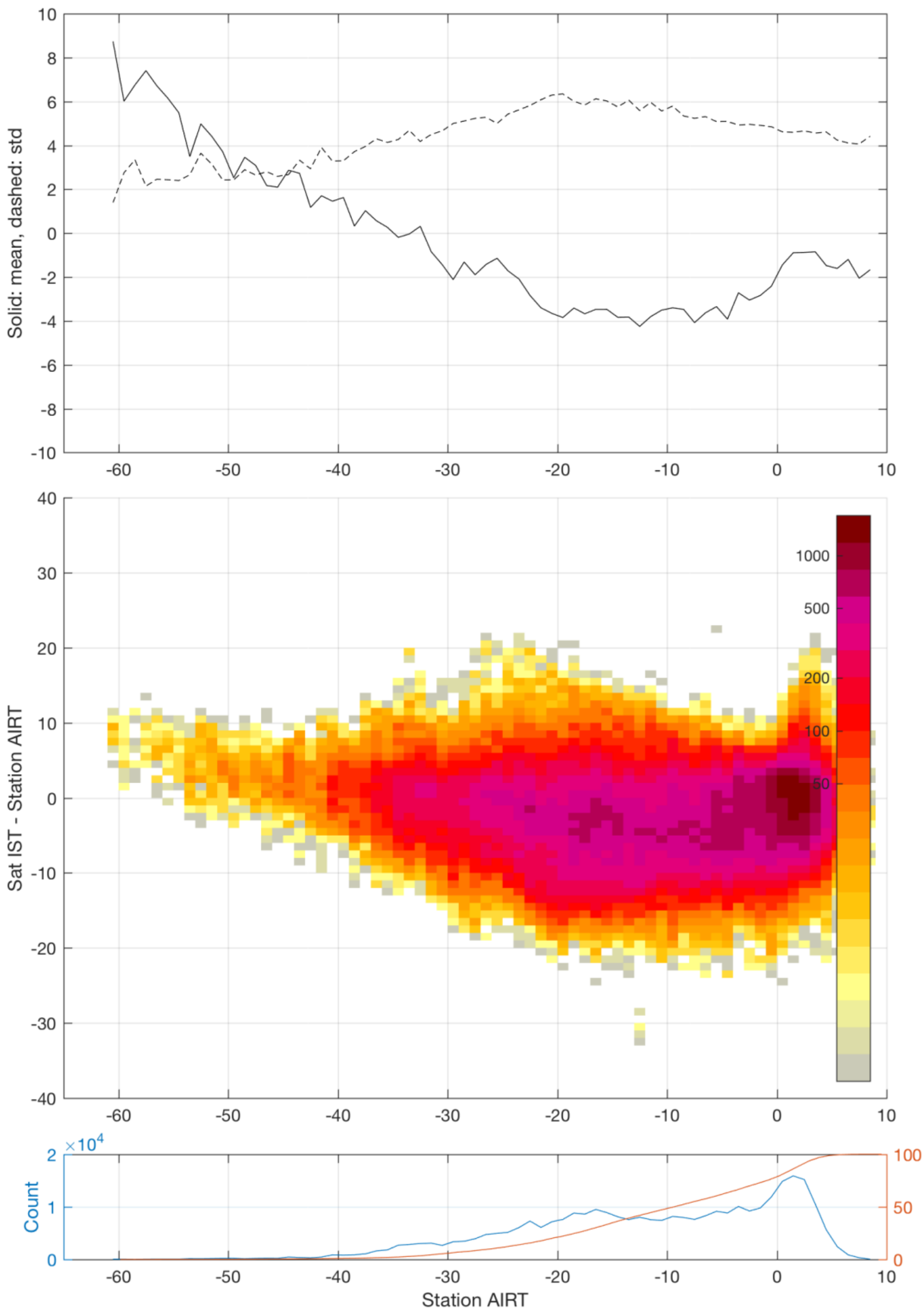

Figure D49 *Difference of IASI IST and air temperature observations as a function of the air temperature observation. Northern Hemisphere data. Top panel is mean (solid line) and standard deviation (dotted line), centre panel is a 2D histogram of the data distribution and bottom panel is data counts, absolute and relative accumulated*

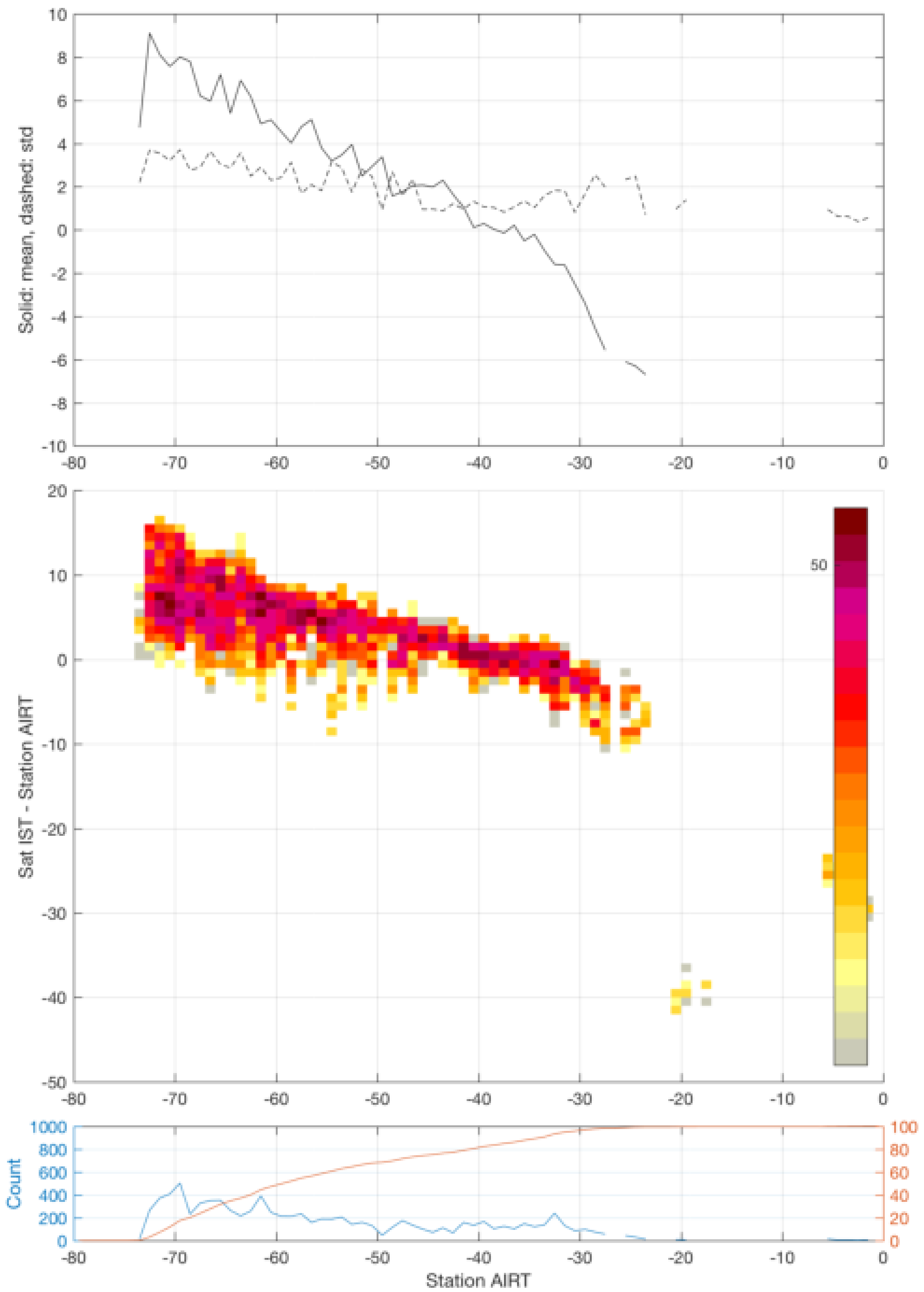

Figure D50 *Difference of IASI IST and air temperature observations as a function of the air temperature observation. Southern Hemisphere data. Top panel is mean (solid line) and standard deviation (dotted line), centre panel is a 2D histogram of the data distribution and bottom panel is data counts, absolute and relative accumulated*

Appendix E: Sea Ice supplementary figures

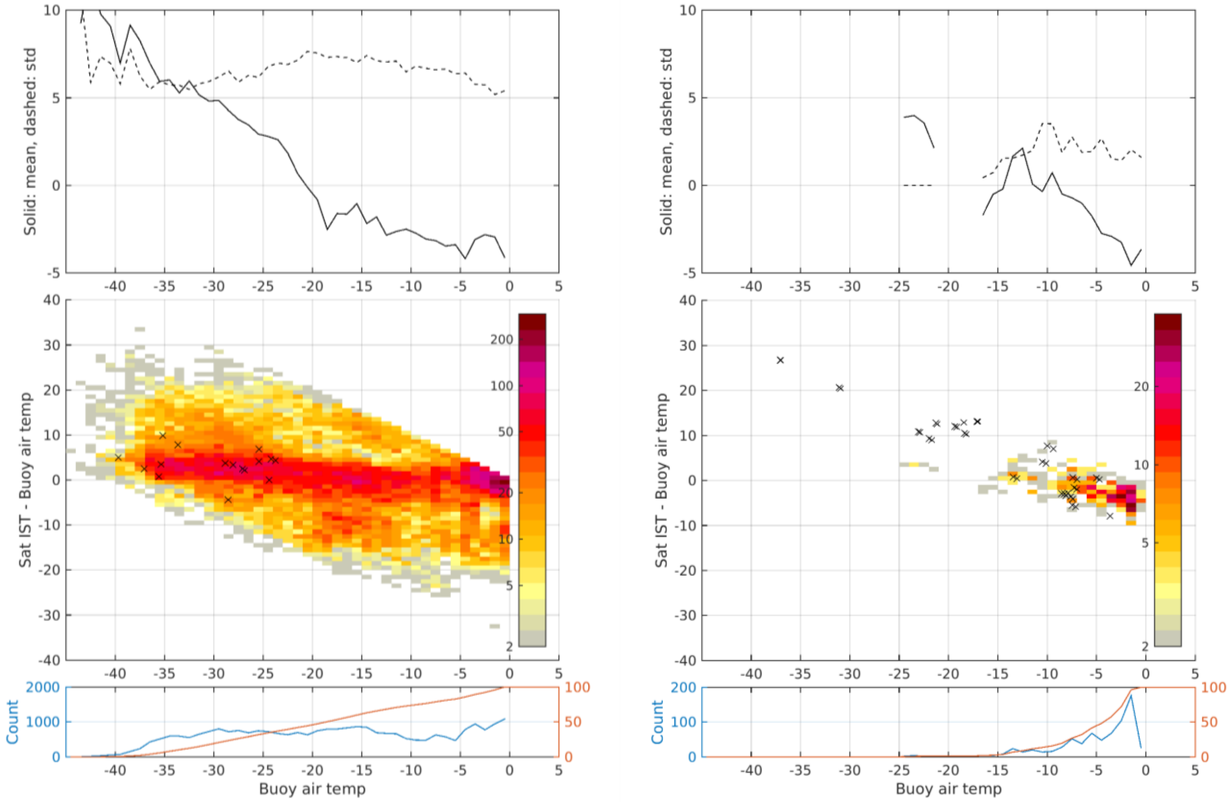

Figure E1 *Distribution and statistics on satellite IST – buoy air temperature differences as a function of the buoy air temperature for the northern hemisphere (left) and southern hemisphere (right). Top is mean (solid line) and standard deviation (dotted line), centre is a 2D histogram of the data distribution with black crosses showing airborne IST observations and bottom is data count per 1°C bin (blue, left axis) and cumulated percentage of data count (red, right axis).*

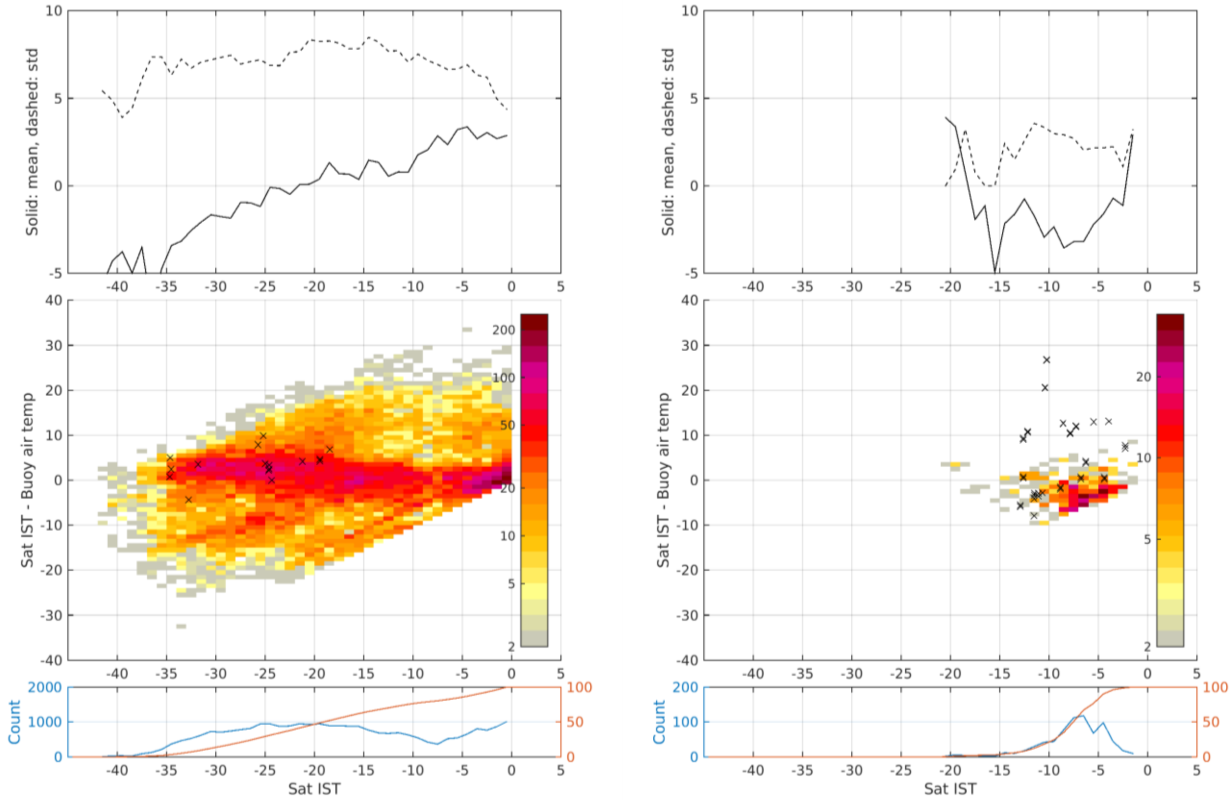

Figure E2 *Distribution and statistics on satellite IST – buoy air temperature differences as a function of the satellite IST for the northern hemisphere (left) and southern hemisphere (right). Top is mean (solid line) and standard deviation (dotted line), centre is a 2D histogram of the data distribution with black crosses showing airborne IST observations and bottom is data count per 1°C bin (blue, left axis) and cumulated percentage of data count (red, right axis).*

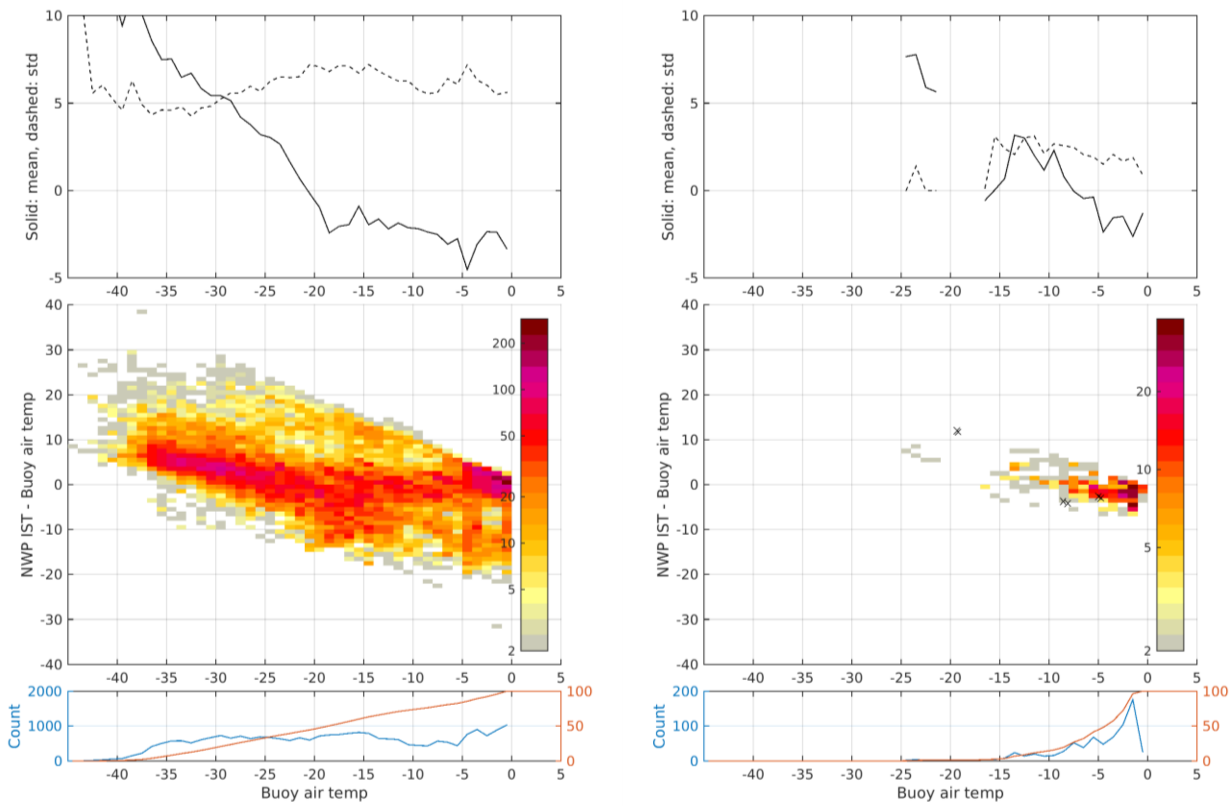

Figure E3 *Distribution and statistics on Era Interim IST – buoy air temperature differences as a function of the buoy air temperature for the northern hemisphere (left) and southern hemisphere (right). Top is mean (solid line) and stand-*

ard deviation (dotted line), centre is a 2D histogram of the data distribution with black crosses showing airborne IST observation and bottom is data count per 1°C bin (blue, left axis) and cumulated percentage of data count (red, right axis).

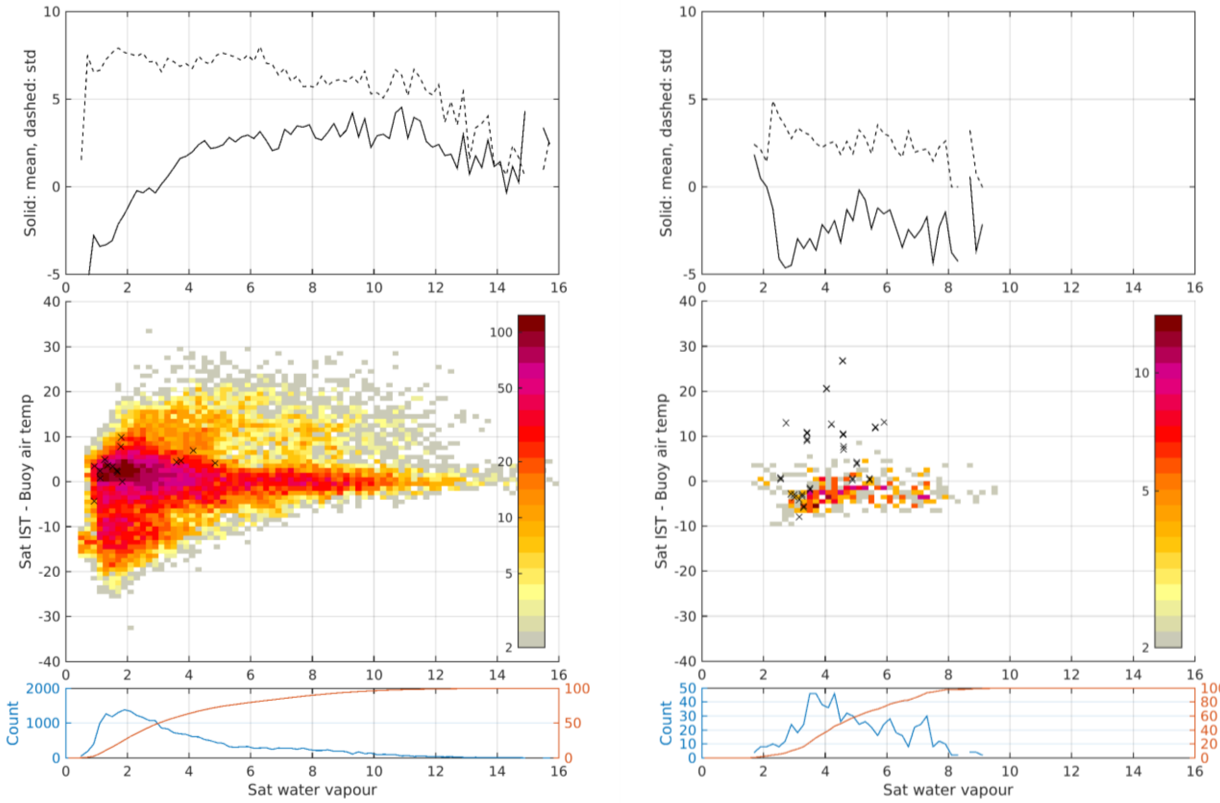

Figure E4 *Distribution and statistics on satellite IST – buoy air temperature differences as a function of total column water vapour (mm) for the northern hemisphere (left) and southern hemisphere (right). Top is mean (solid line) and standard deviation (dotted line), centre is a 2D histogram of the data distribution with black crosses showing airborne IST observations and bottom is data count per 0.2 mm bin (blue, left axis) and cumulated percentage of data count (red, right axis).*

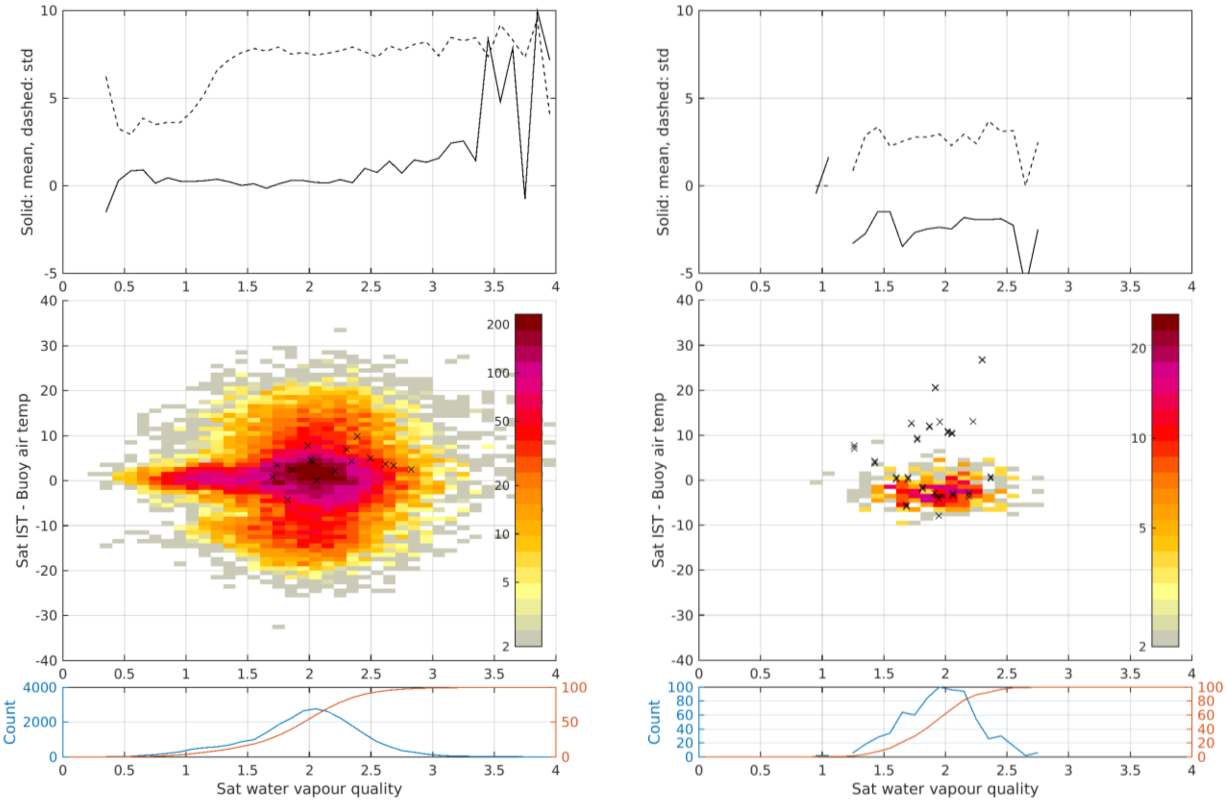

Figure E5 *Distribution and statistics on satellite IST – buoy air temperature differences as a function of water vapour quality index for the northern hemisphere (left) and southern hemisphere (right). Top is mean (solid line) and standard deviation (dotted line), centre is a 2D histogram of the data distribution with black crosses showing airborne IST observations and bottom is data count per 0.1 quality indicator unit bin (blue, left axis) and cumulated percentage of data count (red, right axis).*

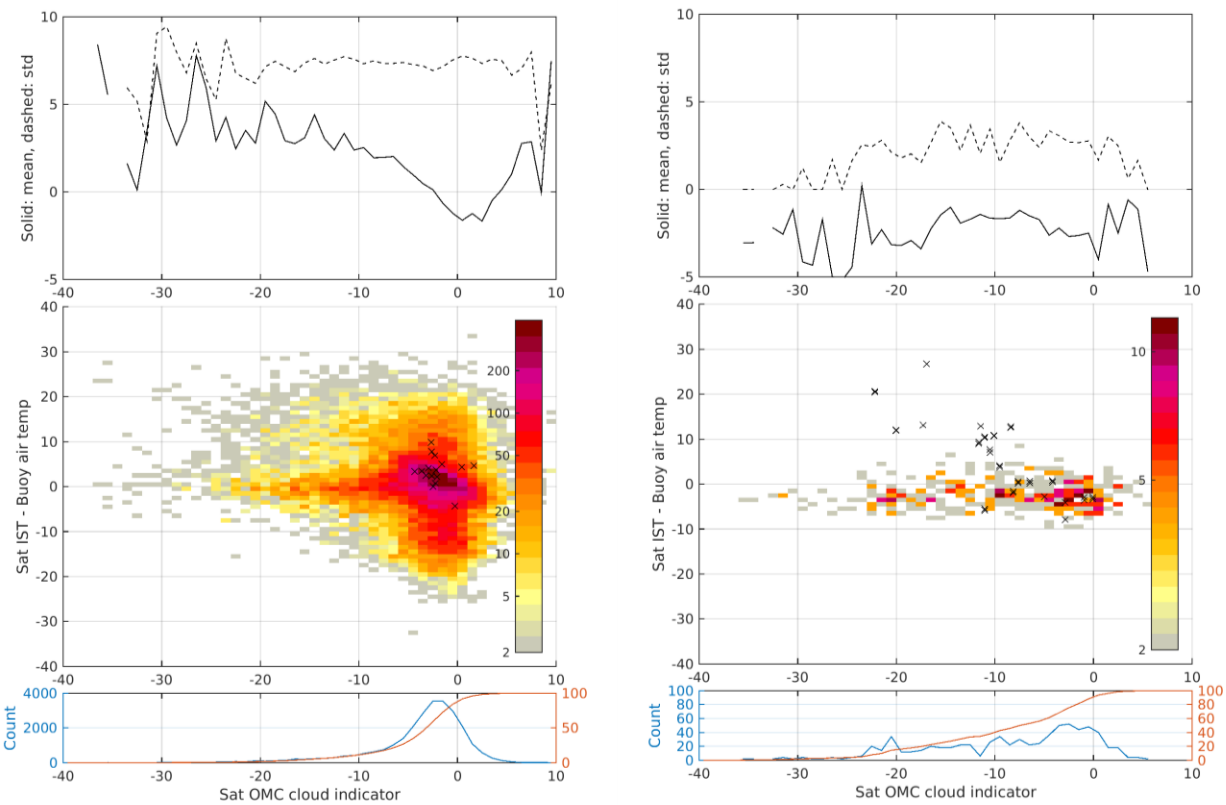

Figure E6 *Distribution and statistics on satellite IST – buoy air temperature differences as a function of OMC cloud indicator for the northern hemisphere (left) and southern hemisphere (right). Top is mean (solid line) and standard deviation (dotted line), centre is a 2D histogram of the data distribution with black crosses showing airborne IST observations and bottom is data count per 1 OMC indicator unit bin (blue, left axis) and cumulated percentage of data count (red, right axis).*

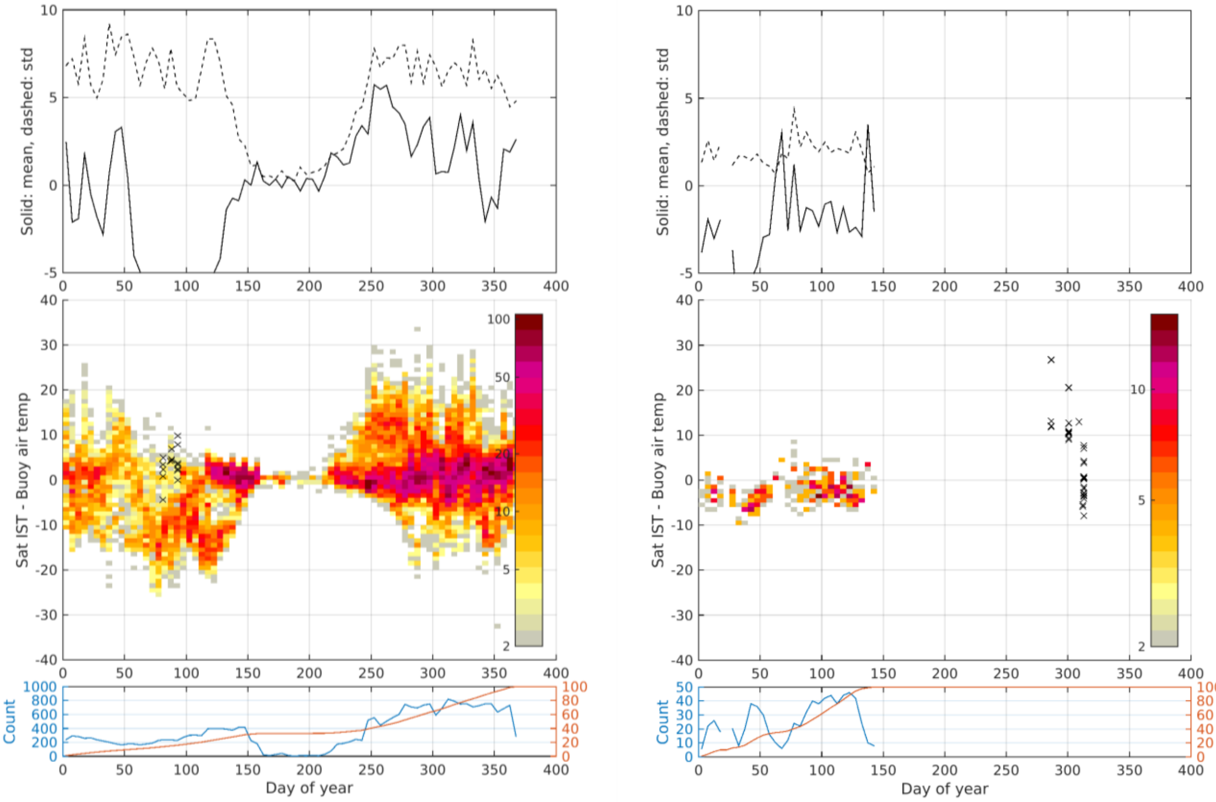

Figure E7 *Distribution and statistics on satellite IST – buoy air temperature differences as a function of time of the year (days) for the northern hemisphere (left) and southern hemisphere (right). Top is mean (solid line) and standard deviation (dotted line), centre is a 2D histogram of the data distribution with black crosses showing airborne IST observations and bottom is data count per 5 day bin (blue, left axis) and cumulated percentage of data count (red, right axis).*

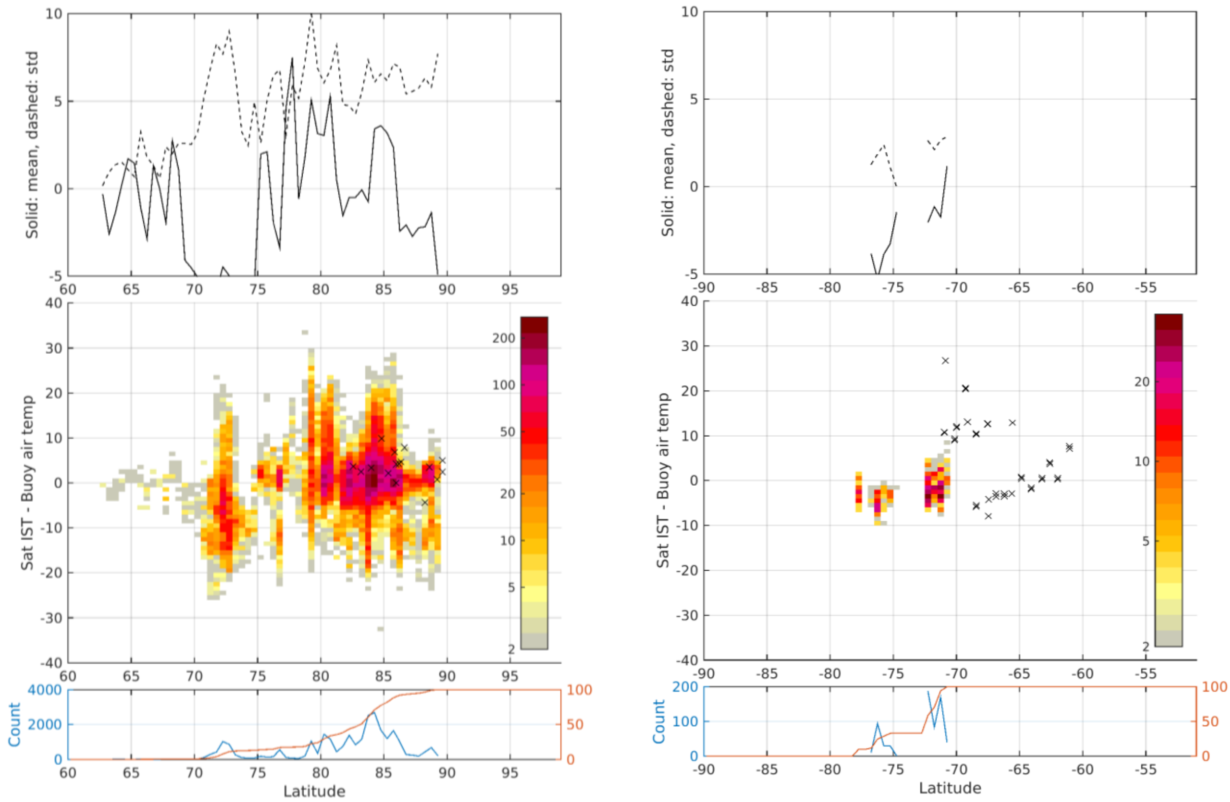

Figure E8 *Distribution and statistics on satellite IST – buoy air temperature differences as a function of latitude for the northern hemisphere (left) and southern hemisphere (right). Top is mean (solid line) and standard deviation (dotted line), centre is a 2D histogram of the data distribution with black crosses showing airborne IST observations and bottom is data count per 0.5 degree bin (blue, left axis) and cumulated percentage of data count (red, right axis).*

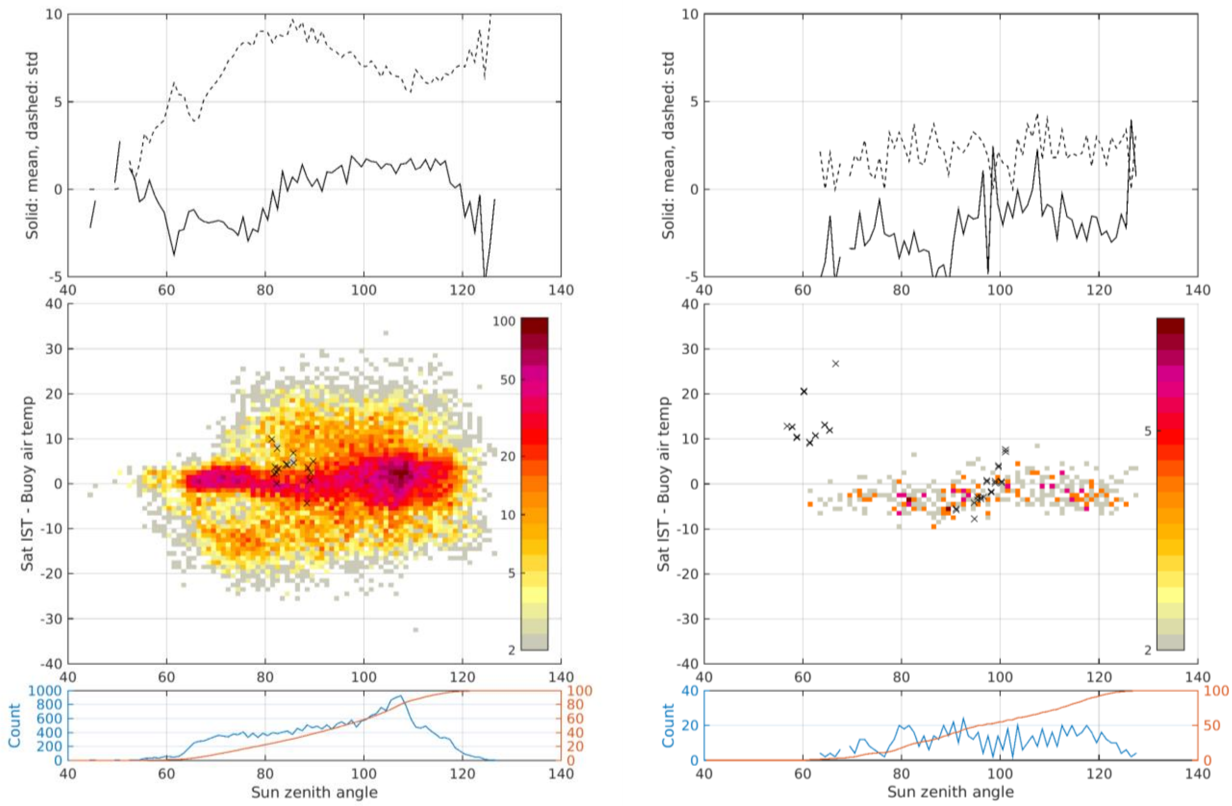

Figure E9 *Distribution and statistics on satellite IST – buoy air temperature differences as a function of sun zenith angle (degrees) for the northern hemisphere (left) and southern hemisphere (right). Top is mean (solid line) and stand-*

ard deviation (dotted line), centre is a 2D histogram of the data distribution with black crosses showing airborne IST observations and bottom is data count per 1° bin (blue, left axis) and cumulated percentage of data count (red, right axis).

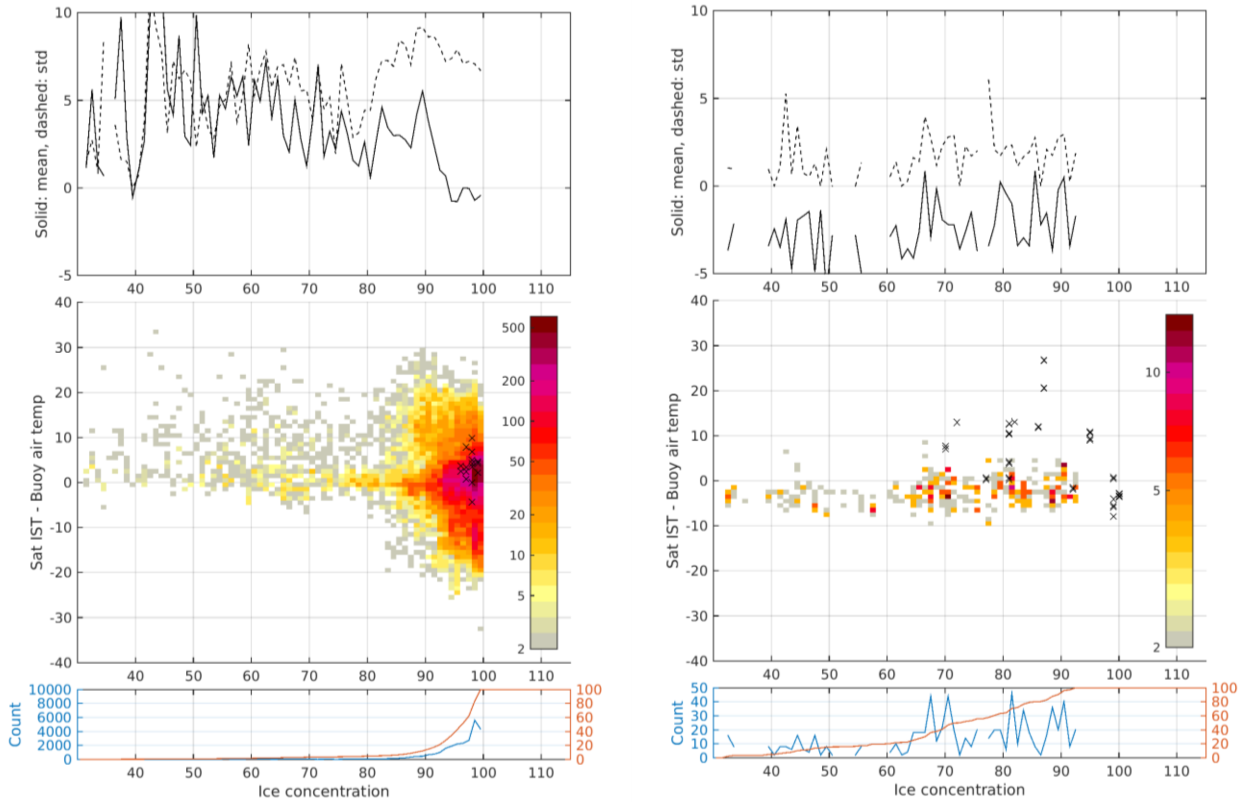

Figure E10 *Distribution and statistics on satellite IST – buoy air temperature differences as a function of sea ice concentration (%) for the northern hemisphere (left) and southern hemisphere (right). Top is mean (solid line) and standard deviation (dotted line), centre is a 2D histogram of the data distribution with black crosses showing airborne IST observations and bottom is data count per 1% bin (blue, left axis) and cumulated percentage of data count (red, right axis).*

Supplementary 3-panel plots for buoy skin temperature (no southern hemisphere data available):

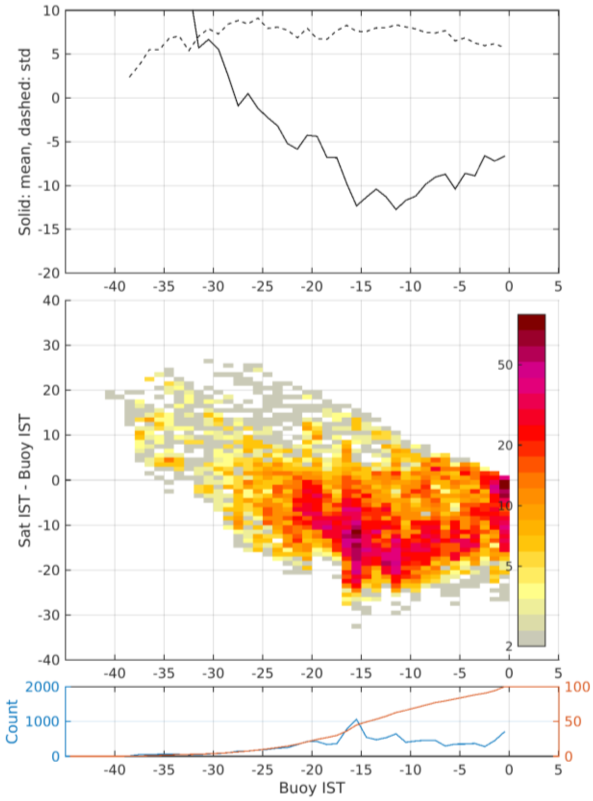

Figure E11 *Distribution and statistics on satellite IST – buoy IST differences as a function of the buoy IST for the northern hemisphere. Top is mean (solid line) and standard deviation (dotted line), centre is a 2D histogram of the data distribution and bottom is data count per 0.1 quality indicator unit bin (blue, left axis) and cumulated percentage of data count (red, right axis).*

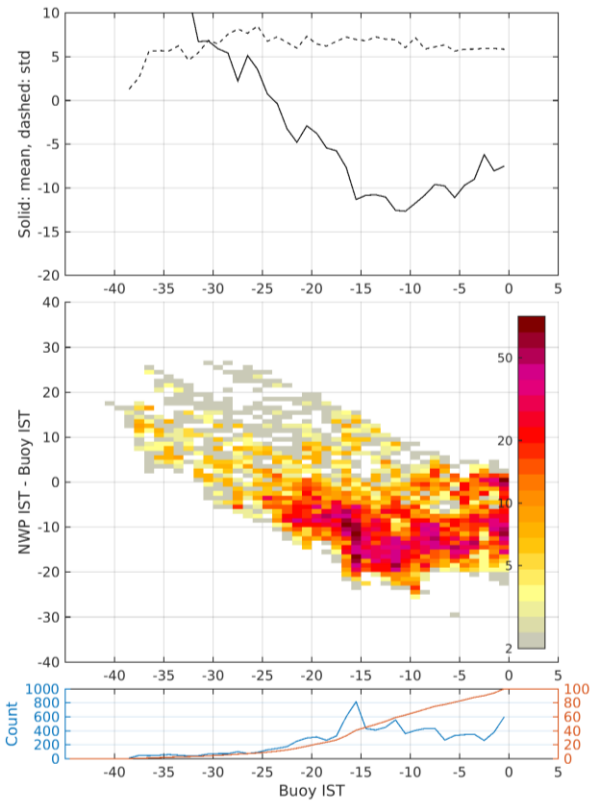

Figure E12 *Distribution and statistics on Era Interim IST – buoy IST differences as a function of the buoy IST for the northern hemisphere. Top is mean (solid line) and standard deviation (dotted line), centre is a 2D histogram of the data* *distribution and bottom is data count per 0.1 quality indicator unit bin (blue, left axis) and cumulated percentage of data count (red, right axis).*

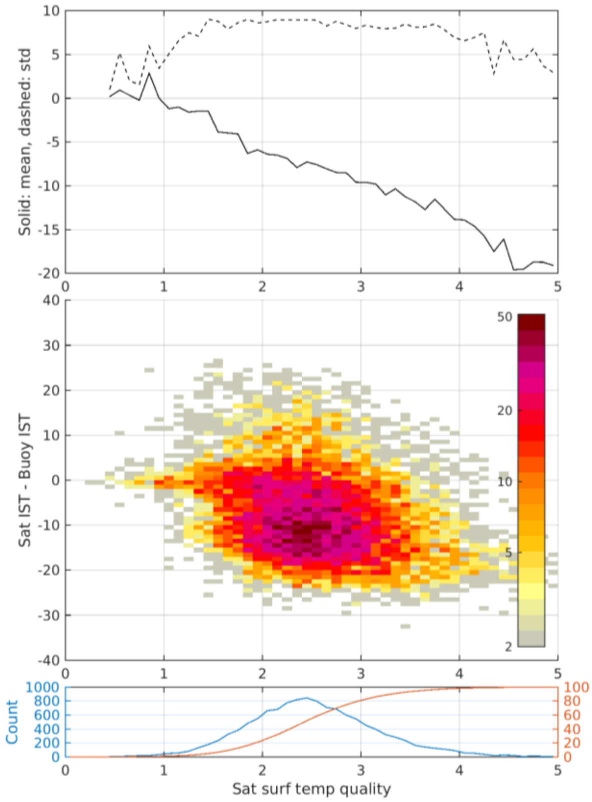

Figure E13 *Distribution and statistics on satellite IST – buoy IST differences as a function of the satellite surface temperature quality indicator for the northern hemisphere. Top is mean (solid line) and standard deviation (dotted line), centre is a 2D histogram of the data distribution and bottom is data count per 0.1 quality indicator unit bin (blue, left axis) and cumulated percentage of data count (red, right axis).*

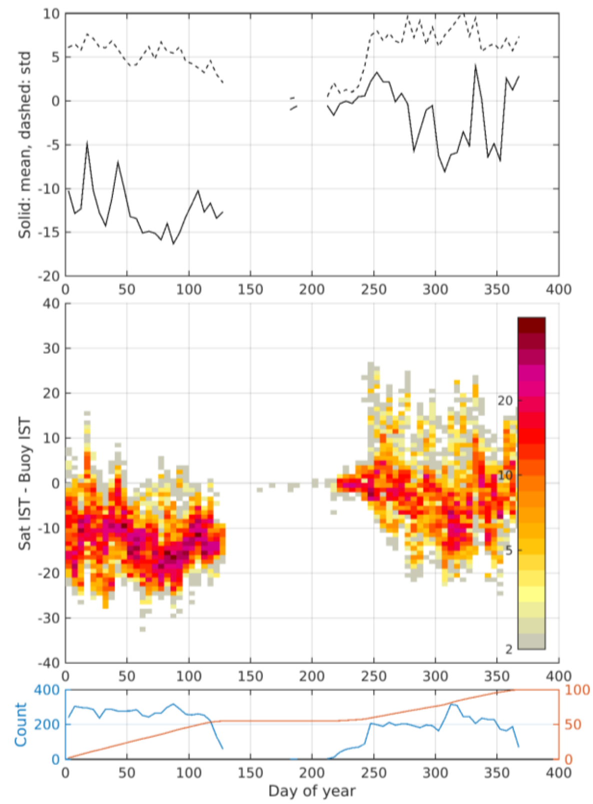

Figure E14 Distribution and statistics on satellite IST – buoy IST differences as a function of time of the year (days) for the northern hemisphere. Top is mean (solid line) and standard deviation (dotted line), centre is a 2D histogram of the data distribution and bottom is data count per 5 day bin (blue, left axis) and cumulated percentage of data count (red, right axis).

Supplementary 2D data distribution plots for buoy skin temperature:

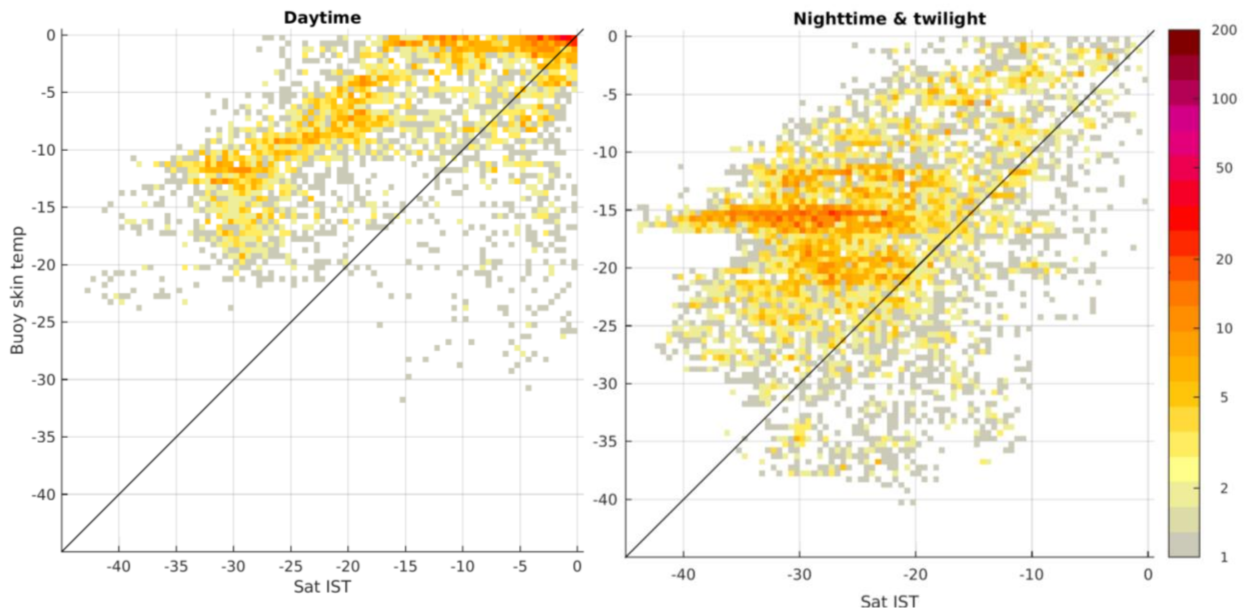

Figure E15 *2D histogram of the data distribution as a function of satellite IST and buoy IST for daytime observations (left) and night time (right), for the northern hemisphere. The black line indicates a 1:1 relationship.*

E.2 Supporting figures for section 7.2.4

Histogram plots for each of the eight categories described in figure 7.2.2:

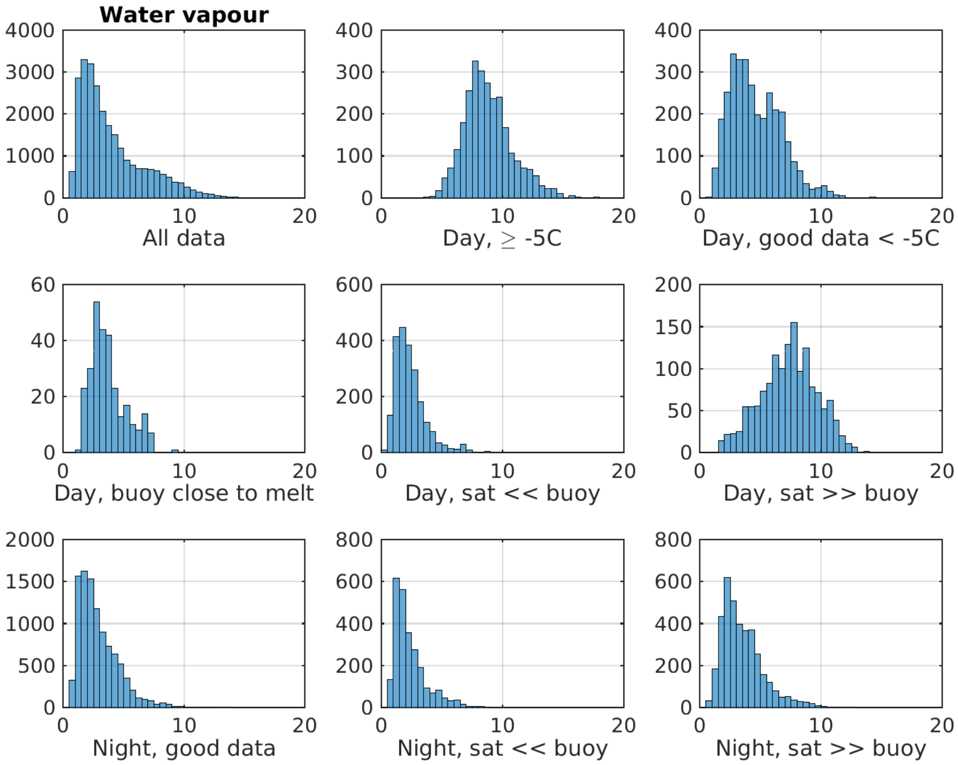

Figure E16 *Histograms of the data distribution as a function of water vapour for northern hemisphere sea ice match-ups to buoy atmospheric temperatures. Top left shows all data, the following show distributions for the eight groups defined in figure 7.2.2.*

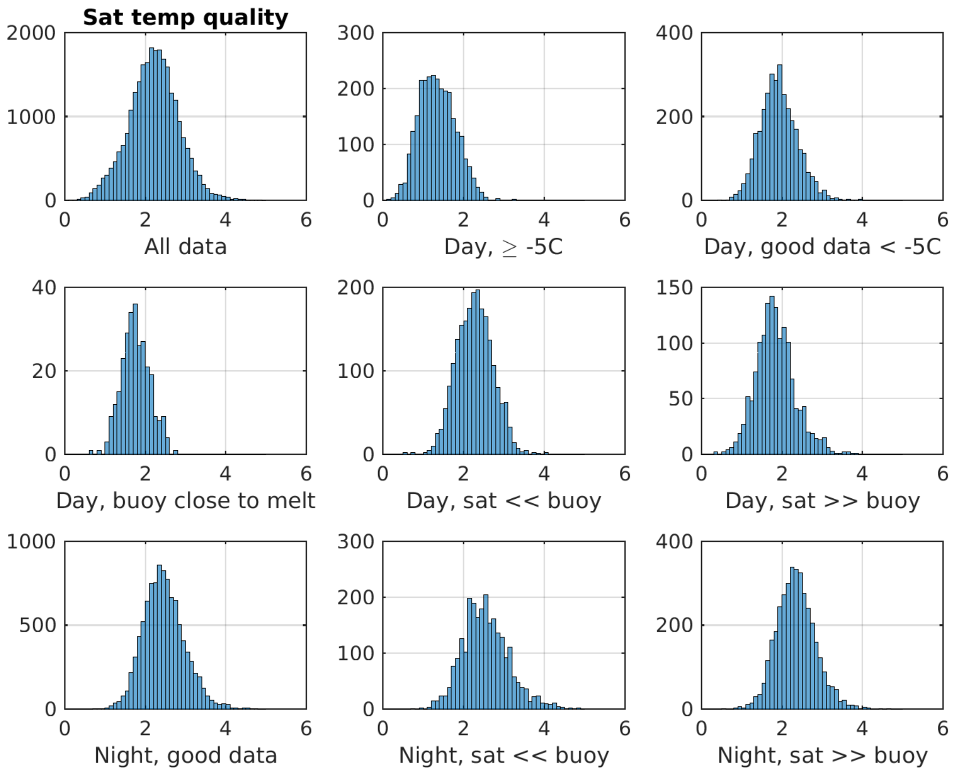

Figure E17 *as figure E16 but for satellite temperature quality.*

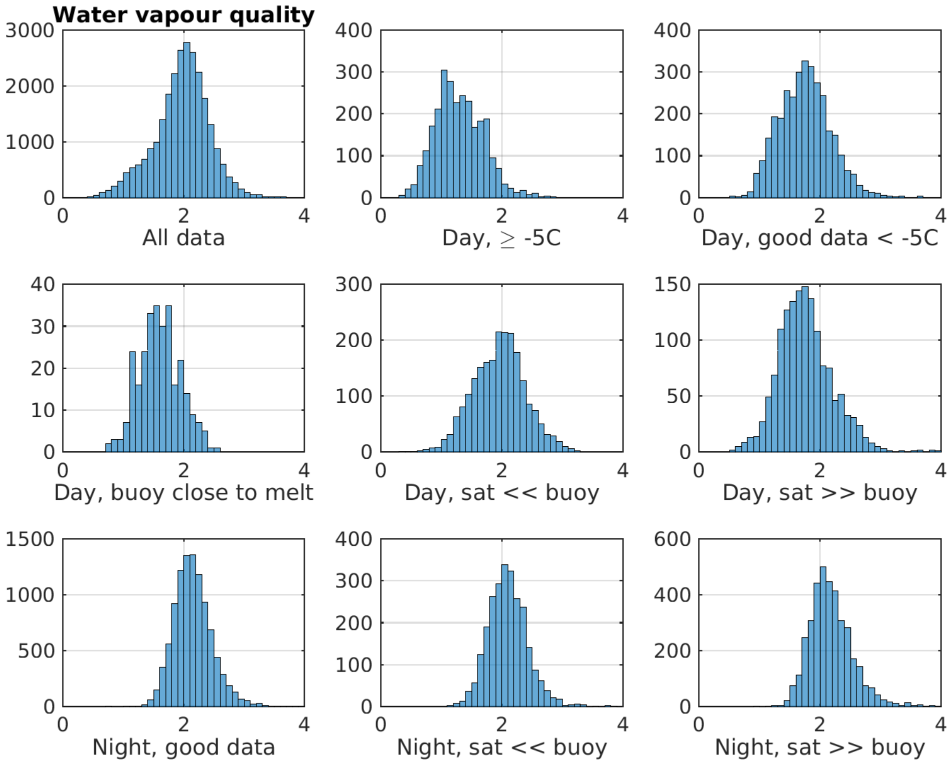

Figure E18 *as figure E16 but for water vapour quality.*

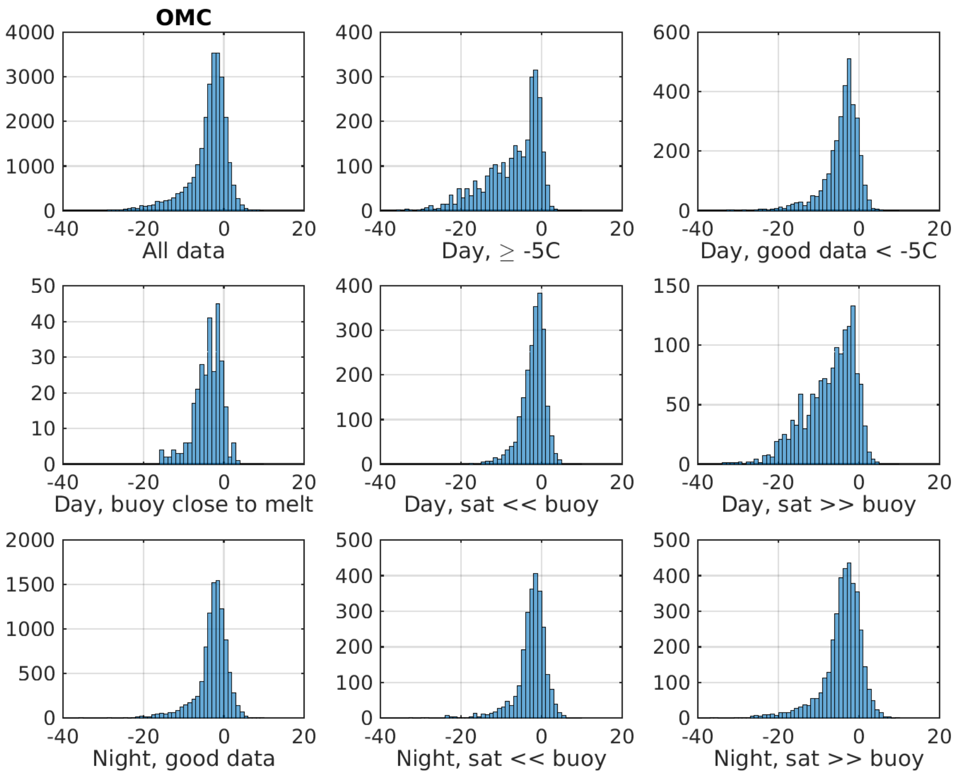

Figure E19 *as figure E16 but for OMC cloud indicator.*

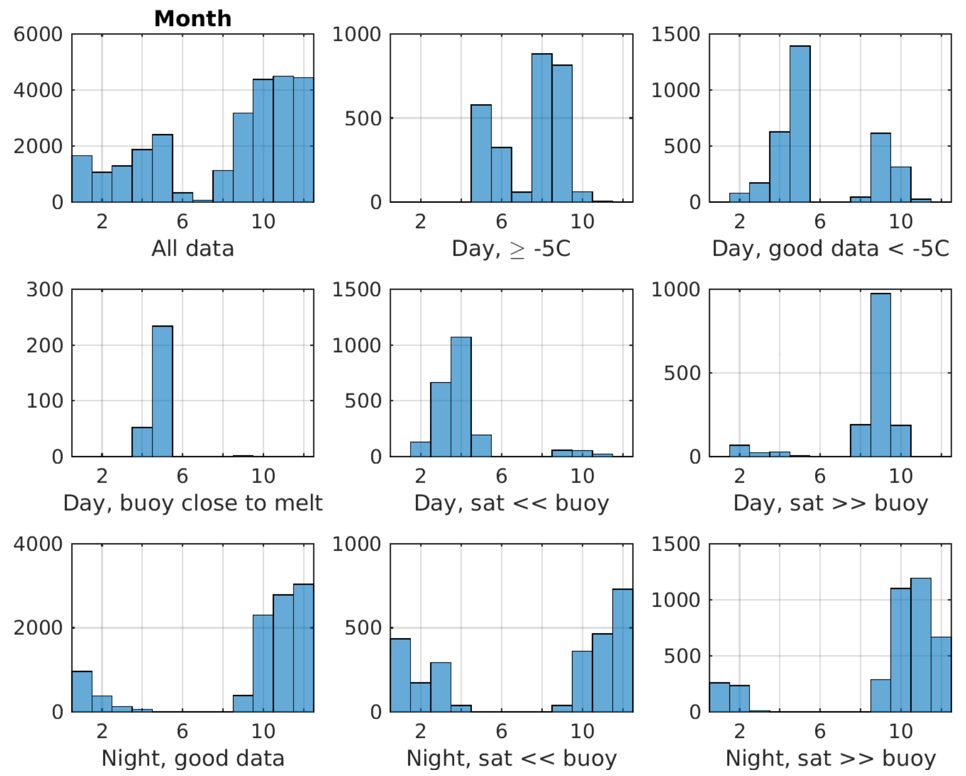

Figure E20 *as figure E16 but for month of the year (this is a copy of figure 7.2.3, included for completeness).*

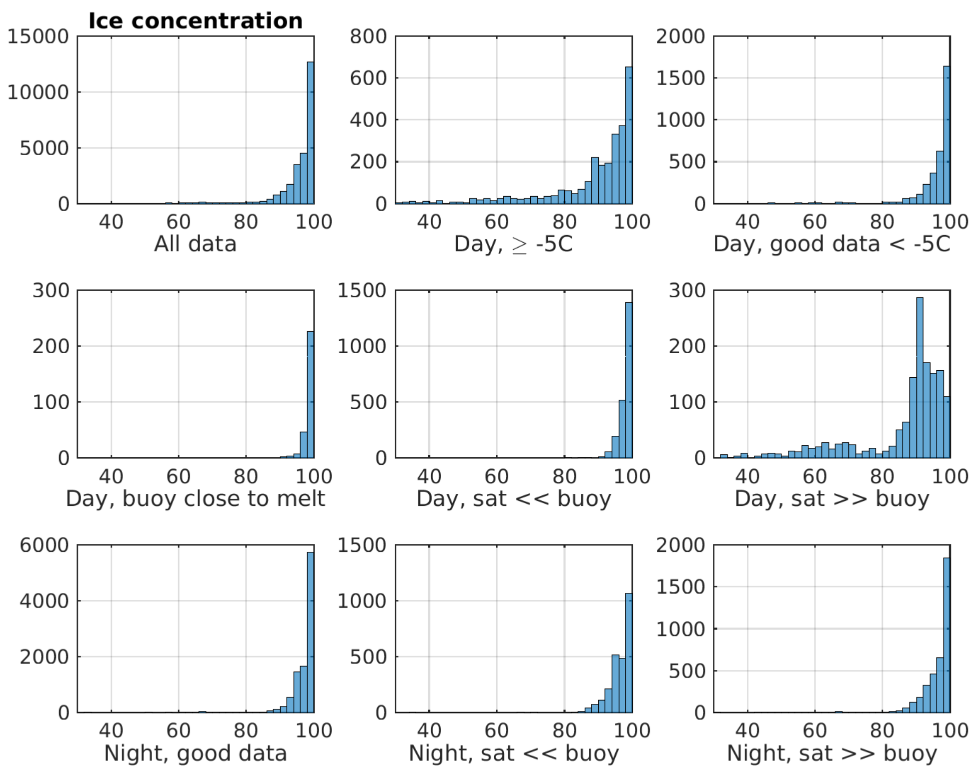

Figure E21 *as figure E16 but for sea ice concentration.*

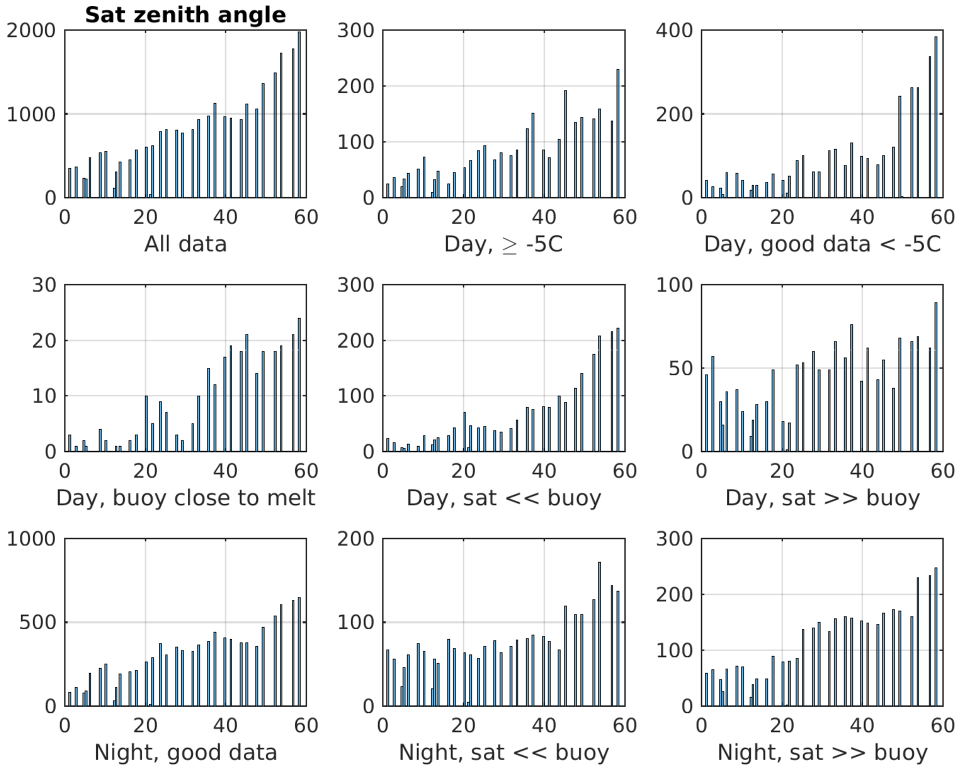

Figure E22 *as figure E16 but for satellite zenith angle.*

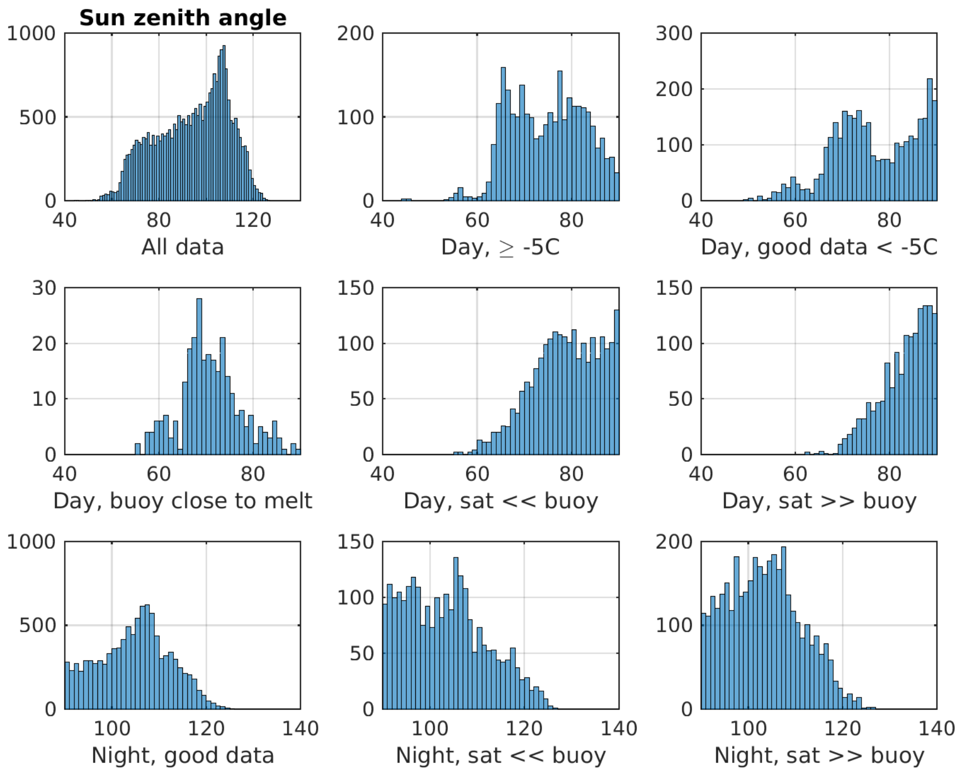

Figure E23 *as figure E16 but for sun zenith angle. Note the varying x-axis.*

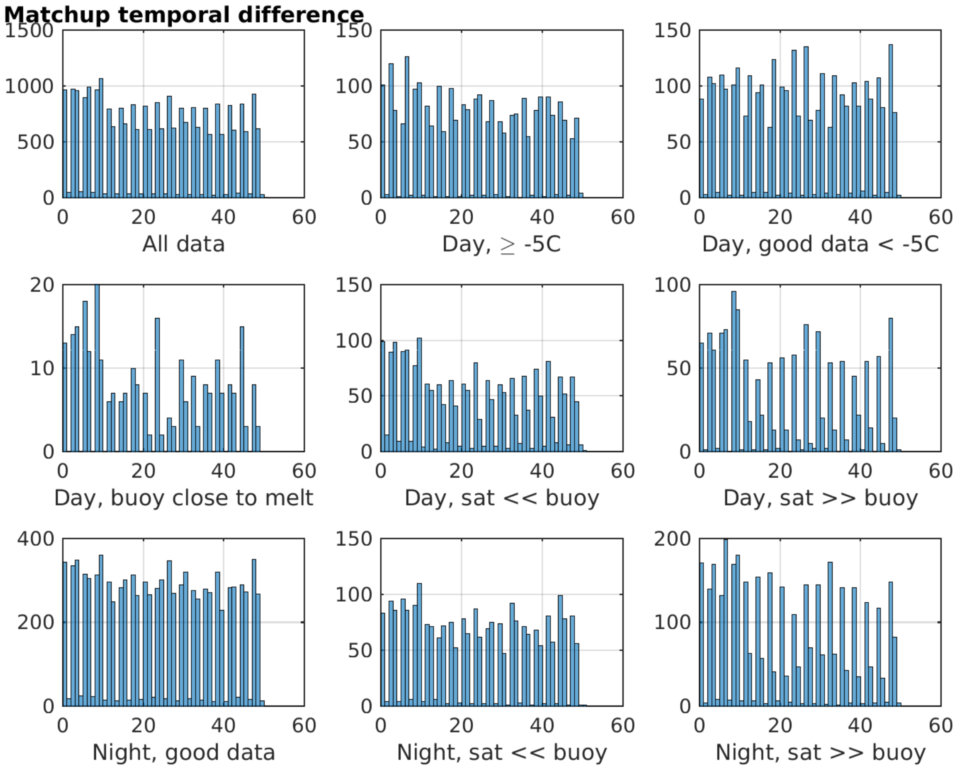

Figure E24 *as figure E16 but for matchup absolute temporal difference.*

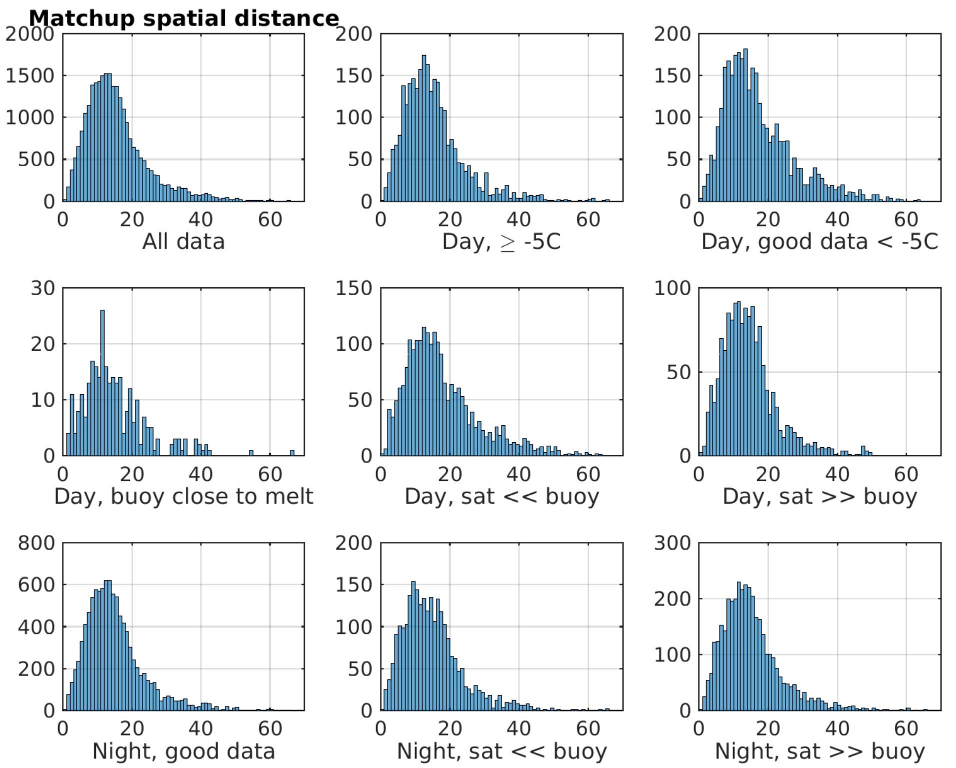

Figure E25 *as figure E16 but for matchup spatial difference.*

Appendix F: Satellite inter-comparison, including ERA-Interim

The figures below shows the manually selected regions, where the four satellite IST products have been inter-compared and where ERA-Interim has also been included. Note that the ERA-Interim values are temporal snapshots and not averages as for the satellite products, which may explain the larger variability. See section 7.3 for more details.

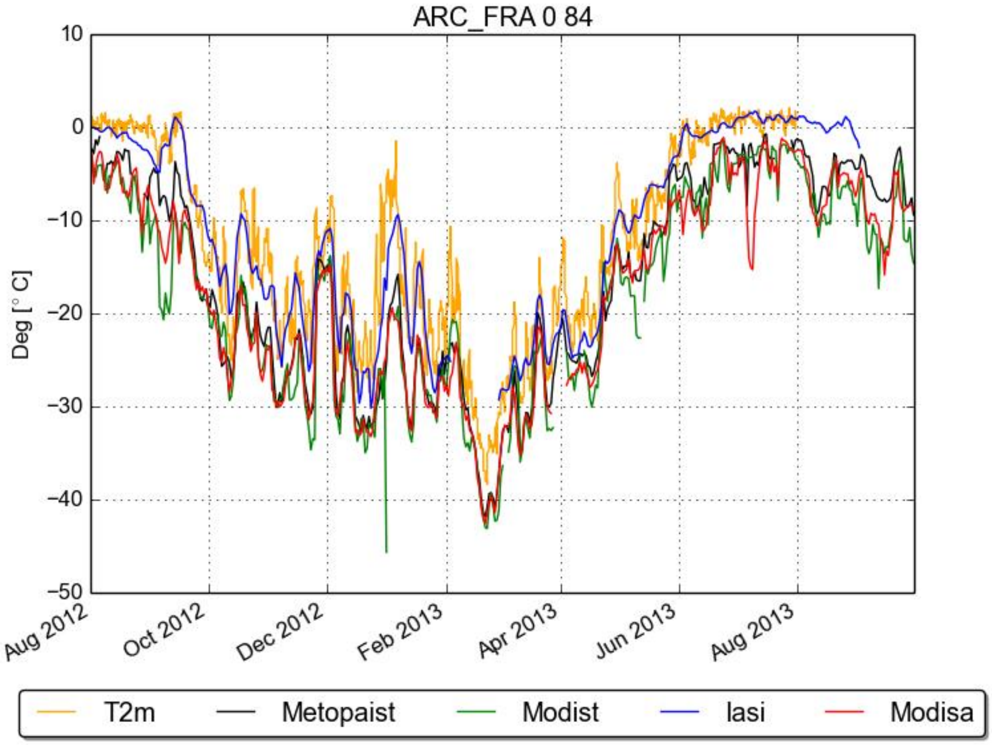

Figure F1 *Averaged Surface temperature and T2m from ERA-Interim from manually selected regions. The central positions (longitude, latitude) of the regions are listed in the title of each figure.T2m is the 3 hourly snapshot from the ERA-Interim and Metopaist is the Metop AVHRR SST/IST product.*

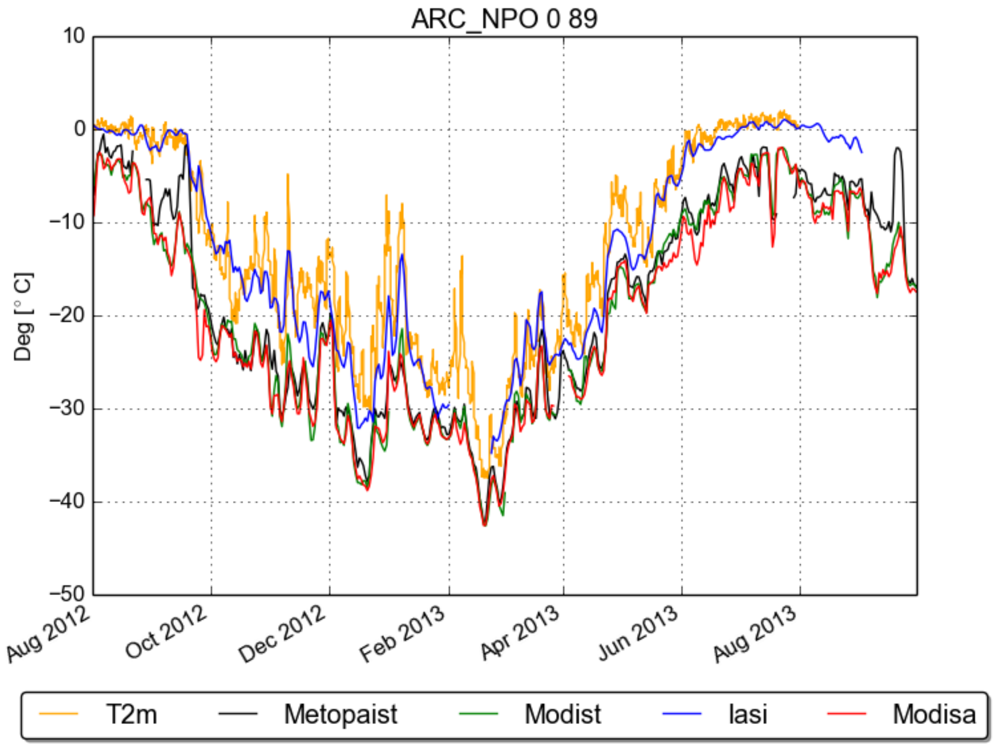

Figure F2 *Averaged Surface temperature and T2m from ERA-Interim from manually selected regions. The central positions (longitude, latitude) of the regions are listed in the title of each figure.T2m is the 3 hourly snapshot from the ERA-Interim and Metopaist is the Metop AVHRR SST/IST product.*

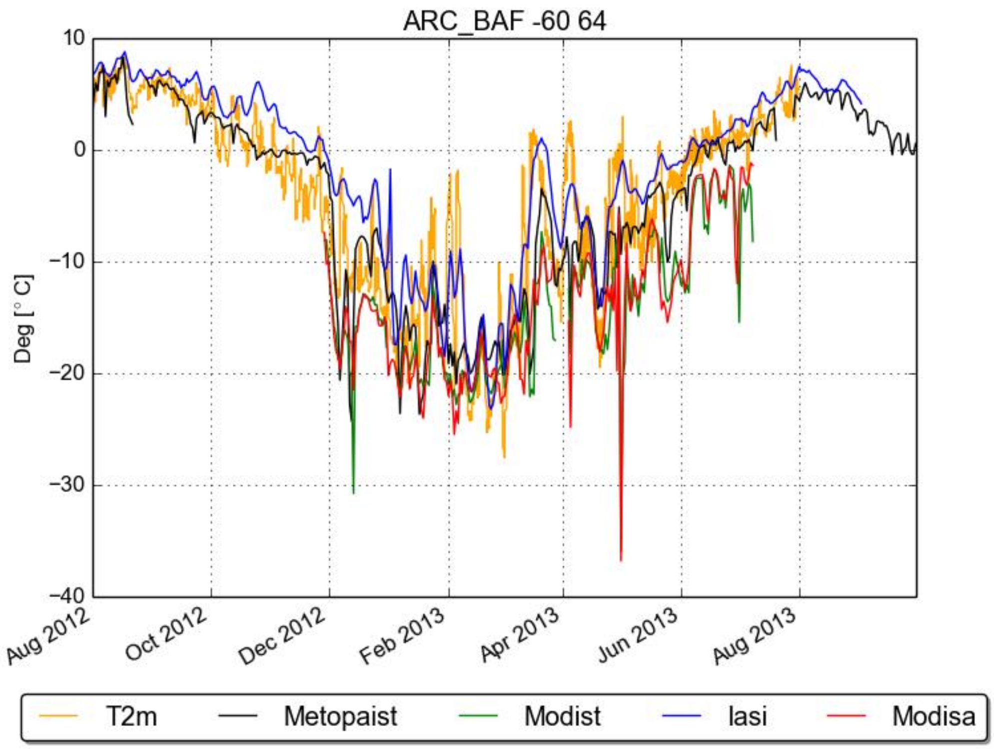

Figure F3 *Averaged Surface temperature and T2m from ERA-Interim from manually selected regions. The central positions (longitude, latitude) of the regions are listed in the title of each figure.T2m is the 3 hourly snapshot from the ERA-Interim and Metopaist is the Metop AVHRR SST/IST product.*

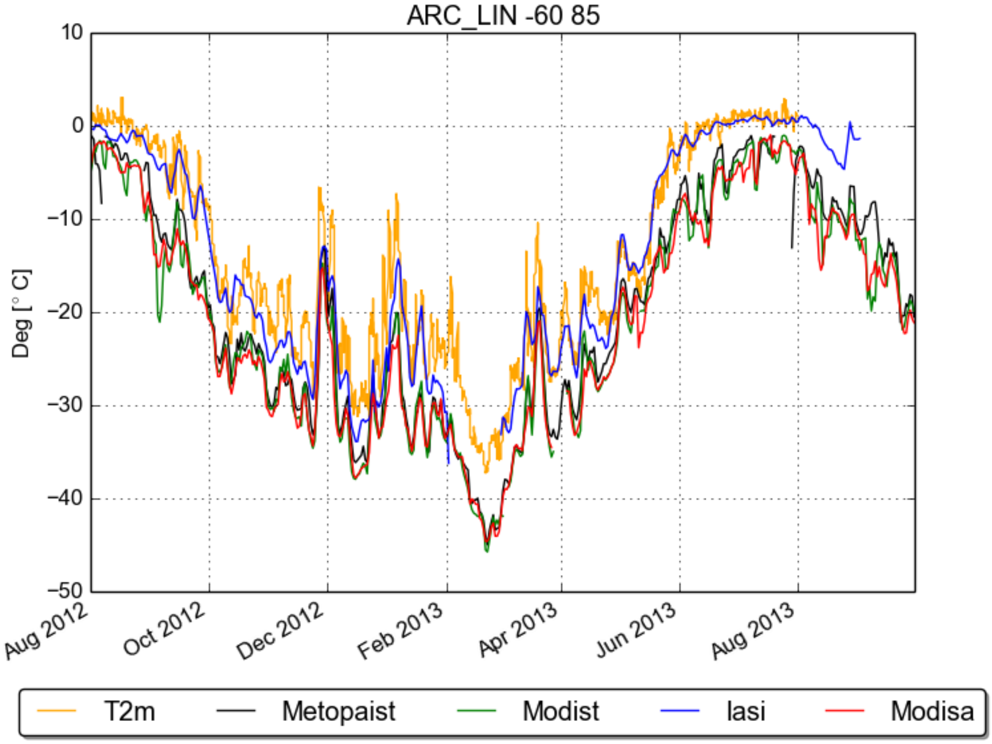

Figure F4 *Averaged Surface temperature and T2m from ERA-Interim from manually selected regions. The central positions (longitude, latitude) of the regions are listed in the title of each figure.T2m is the 3 hourly snapshot from the ERA-Interim and Metopaist is the Metop AVHRR SST/IST product.*

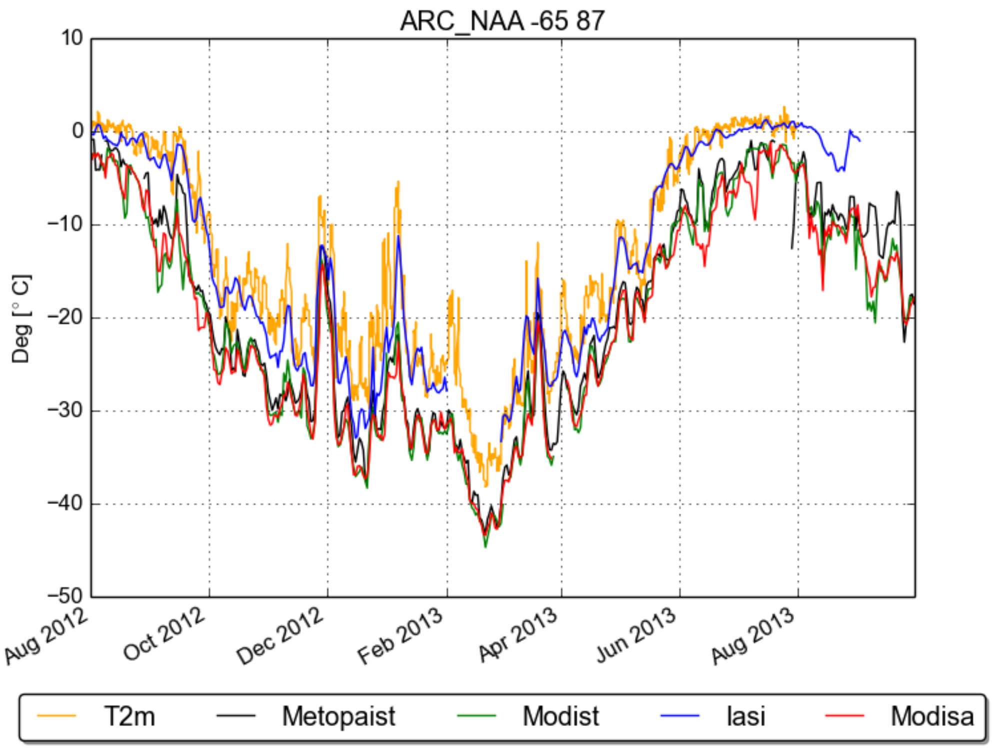

Figure F5 *Averaged Surface temperature and T2m from ERA-Interim from manually selected regions. The central positions (longitude, latitude) of the regions are listed in the title of each figure.T2m is the 3 hourly snapshot from the ERA-Interim and Metopaist is the Metop AVHRR SST/IST product.*

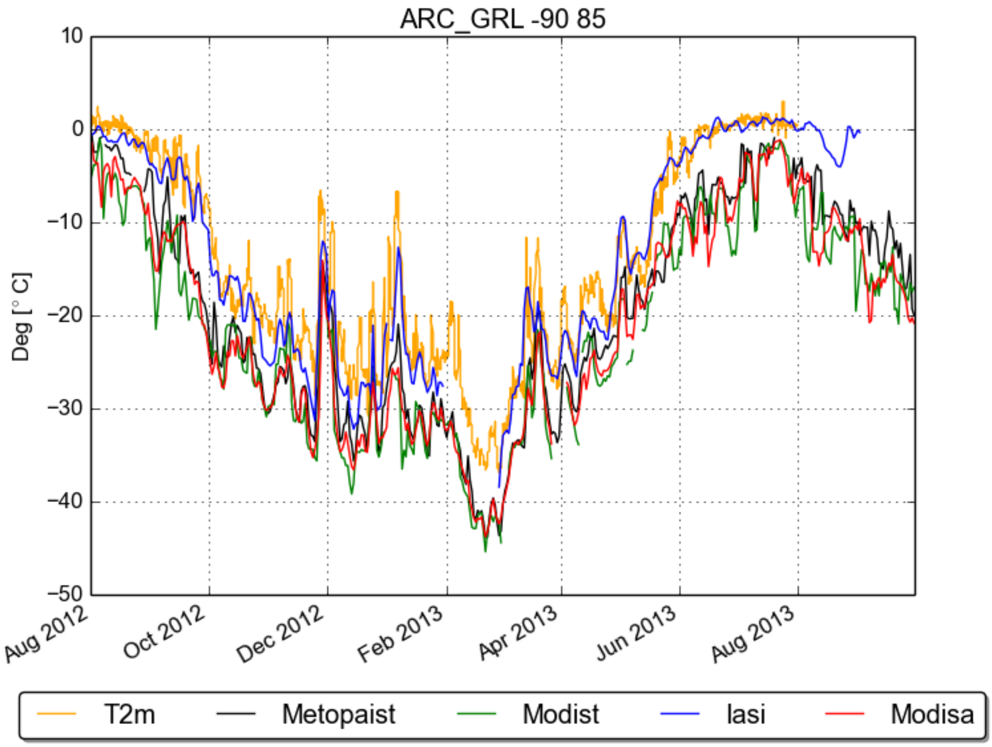

Figure F6 *Averaged Surface temperature and T2m from ERA-Interim from manually selected regions. The central positions (longitude, latitude) of the regions are listed in the title of each figure.T2m is the 3 hourly snapshot from the ERA-Interim and Metopaist is the Metop AVHRR SST/IST product.*

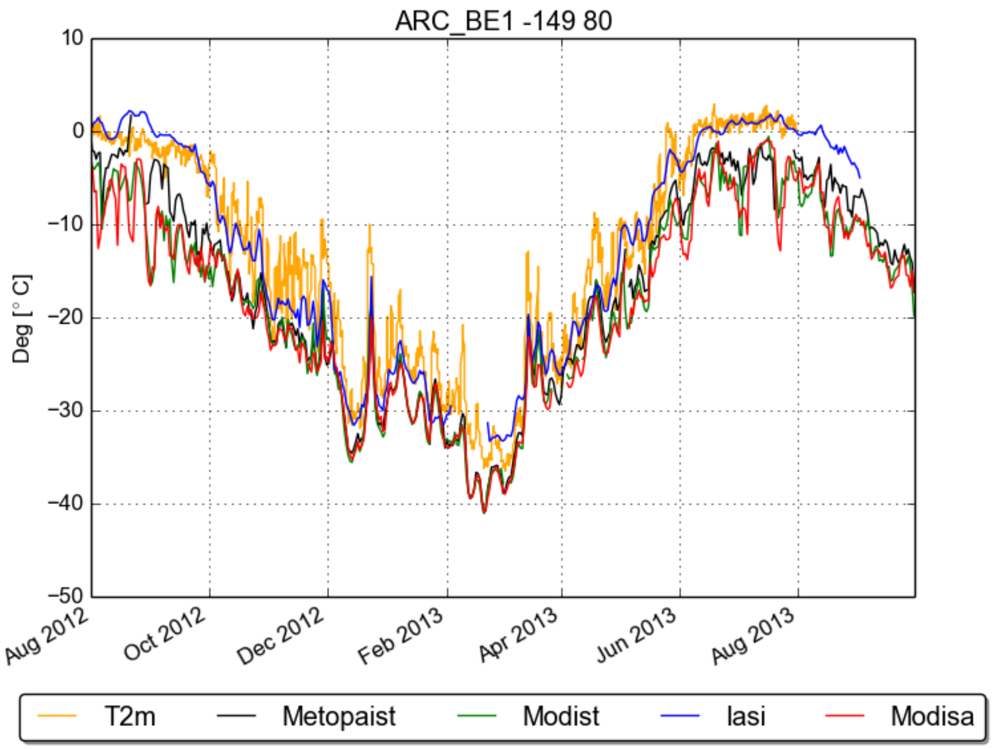

Figure F7 *Averaged Surface temperature and T2m from ERA-Interim from manually selected regions. The central positions (longitude, latitude) of the regions are listed in the title of each figure.T2m is the 3 hourly snapshot from the ERA-Interim and Metopaist is the Metop AVHRR SST/IST product.*

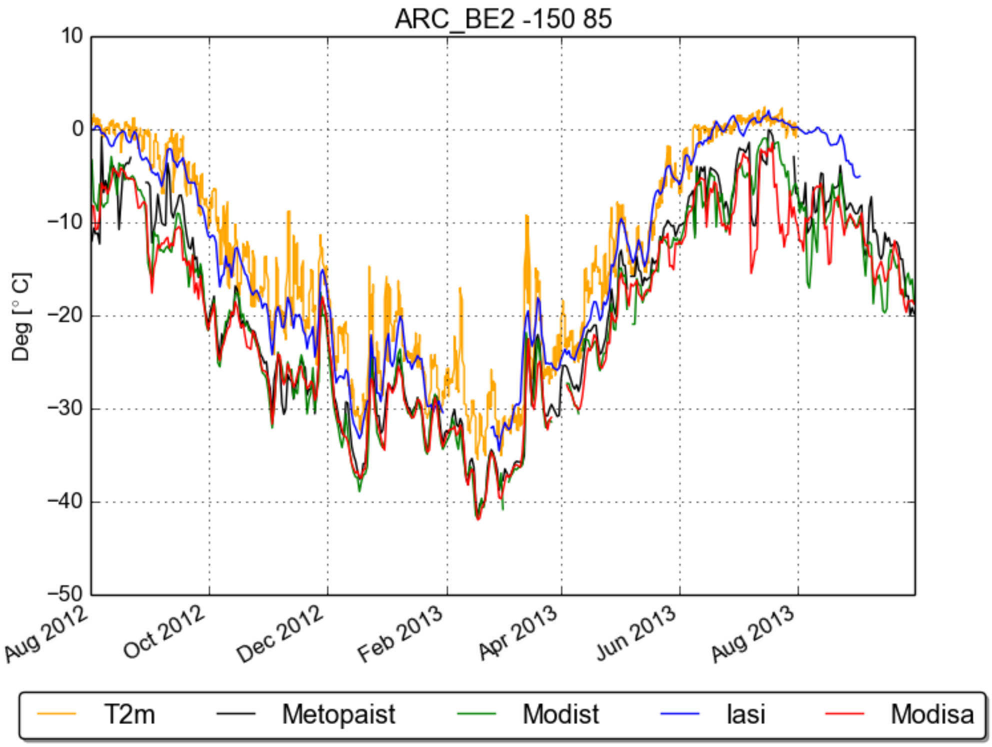

Figure F8 *Averaged Surface temperature and T2m from ERA-Interim from manually selected regions. The central positions (longitude, latitude) of the regions are listed in the title of each figure.T2m is the 3 hourly snapshot from the ERA-Interim and Metopaist is the Metop AVHRR SST/IST product.*

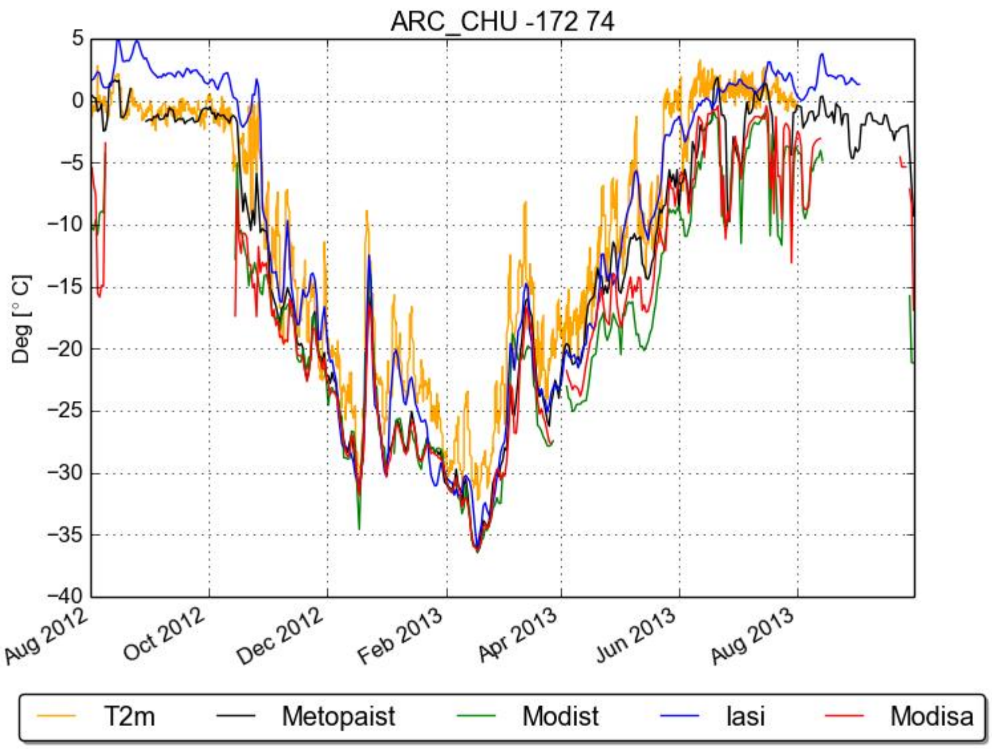

Figure F9 *Averaged Surface temperature and T2m from ERA-Interim from manually selected regions. The central positions (longitude, latitude) of the regions are listed in the title of each figure.T2m is the 3 hourly snapshot from the ERA-Interim and Metopaist is the Metop AVHRR SST/IST product.*

Appendix G: Look-Up table for General and filtered IASI IST performance

Tabel: General IASI IST Validation table, including STD and Bias for selected levels of data quality, i.e. best **x**% is the corresponding performance for the best x percent of the data, as filtered by the IST quality indicator. Qi lim. **X**% is the upper limit of IASI IST quality indicator that includes **x** percent of the data.

		Qual lim 33%	Qual lim 10%	STD all	STD best 33%	STD best 10%	Bias all	Bias best 33%	Bias best 10%	Corr. all	Counts all
land nh	IASI IST - airTobs	2.4	1.7	5.4	4.3	3.9	-2.5	-0.2	0.4	0.9	315140
	IASI IST - surfTobs	2.4	1.8	5.3	4.3	3.8	-0.8	1.0	1.3	0.9	298816
	IASI IST - airTnwp	2.4	1.7	5.3	4.0	3.6	-3.2	-0.9	-0.3	0.9	333885
	IASI IST - surfTnwp	2.4	1.7	6.2	4.5	3.9	0.3	0.7	1.0	0.9	333885
land sh	IASI IST - airTobs	1.1	0.8	5.1	5.3	4.2	3.8	5.2	8.8	0.9	8889
	IASI IST - surfTobs	1.8	1.6	6.8	5.7	4.0	4.3	7.3	6.5	0.4	694
	IASI IST - airTnwp	1.1	0.7	2.9	2.9	3.1	-2.2	-1.6	0.1	1.0	10790
	IASI IST - surfTnwp	1.1	0.7	2.9	3.3	3.3	-0.1	0.7	2.7	1.0	10774
Sea nh	IASI IST - airTobs	2.0	1.4	7.5	6.8	4.7	0.4	1.1	1.1	75%	26268
	IASI IST - surfTobs	2.2	1.7	8.9	8.7	7.9	-7.7	-5.0	-2.5	53%	12252
	IASI IST - airTnwp	2.0	1.5	2.8	2.2	1.8	-0.6	0.0	-0.3	96%	34468
	IASI IST - surfTnwp	2.0	1.5	2.9	2.3	1.9	-0.3	0.1	-0.3	96%	34468
Sea sh	IASI IST - airTobs	1.9	1.5	2.8	2.3	2.3	-2.3	-2.8	-2.5	76%	722
	IASI IST - surfTobs	-	-	-	-	-	-	-	-	-	0
	IASI IST - airTnwp	1.9	1.5	2.5	2.0	1.5	-0.9	-1.3	-1.6	72%	728
	IASI IST - surfTnwp	1.9	1.5	2.3	1.7	1.5	-1.4	-1.7	-1.7	76%	728